Contributions to Drilling, Completion and Workover Technology

Beiträge zur Bohr-, Komplettierungs- und Aufarbeitungstechnik

HABILITATIONSSCHRIFT

zur Erlangung der Lehrbefugnis

für das Fachgebiet Drilling, Completion and Workover

vorgelegt von

Dr. Dr.-Ing. Catalin Teodoriu

aus PLOIESTI, Rumänien

genehmigt von der

Fakultät für Energie- und Wirtschaftswissenschaften

der Technischen Universität Clausthal

11.06.2011

Für Lavinia

Content

Preamble

Publishing is the key in characterizing and defining the academic development of a faculty member. The author's peer-reviewed and conference papers are listed in Appendix 1. They can be grouped into two primary categories: papers dealing with investigations in the areas of drilling and completions, and papers with a focus on production and workover operations. Each category is then subdivided into the following topics:

Drilling and completions

- Equipment, processes, special procedures (i.e. horizontal drilling)
- Critical equipment and components
- Analysis and modeling of operational procedures, well control methods
- Drilling and cementing fluids
- Health, Safety and Environment (HSE) aspects
  (thread compounds, fluid rheology, formation damage)
- Advanced drilling technology
- Geothermal technology
- Advanced teaching methods and tele-teaching

Production operations and workover

- Equipment to improve recovery efficiency, multiphase flow in pipelines
- Tubular stress and strain, tubular integrity over field life,
  sealability of tubular components, temperature effects, corrosion issues
- Liquid loading in gas wells
- Recovery of hydrocarbons
- Optimization of geothermal energy recovery

The full list of papers, organized according to the scheme presented above, is presented in Appendix 2. From the total number of publications listed in Appendix 1 (94 in total, plus 2 pending peer-revision), only those publications listed in Appendix 3 were chosen for the application for habilitation at Clausthal University of Technology.

1. Introduction

Drilling and production are at the heart of the petroleum engineering discipline. Together, they cover fundamental hardware and operational aspects of the upstream sector of the Exploration and Production (E&P) business. Several advanced technologies have been developed since the onset of hydrocarbon exploitation in 1859, both in the USA (Titusville, Pennsylvania) and Germany (Wietze, Niedersachsen).

Drilling technology and hydrocarbon production operations have remained key areas in the education and training of petroleum engineers for more than 100 years.

With a specialization in mechanical and process engineering within petroleum engineering, the author is convinced that there is still a strong need to further improve components and systems in drilling and production operations. Figure 1 gives an example of the continued development of drilling technology (specifically with respect to mechanization of pipe handling at the rig floor) throughout the years, starting from the 1970s.

All drilling and production operations require a thorough understanding of the associated environmental aspects. Traditionally, the majority of accidents take place close to where drilling operations are carried out and in particular where heavy hardware components are to be maneuvered during tripping or make-up of downhole assemblies.

A few years back, Norway initiated an investigation of situations where personnel safety was endangered. It was concluded that human work should be replaced by machines wherever the majority of accidents were proven to take place, e.g. in the vicinity of the borehole. This theory soon spread worldwide, first to deep-sea drilling rigs, and later to other drilling installations. Experience with automated systems quickly showed that not only safety is increased, but also the overall drilling time is reduced compared to manual operations. Additionally, automated systems to make-up Rotary shouldered connections are much more accurate than the traditional make-up with chains and rig tongs, thus reducing connections damage. State-of-the-art automated make-up devices also provide sufficient data to analyze the quality of the connection make-up, which can be used to increase the connections lifetime and reduce drill string failures.

Drilling as well as production operations are an integral part of hydrocarbon exploitation as a whole, and therefore can not be studied in isolation. This is the reason behind the broad range of topics covered by the selected papers and reports.

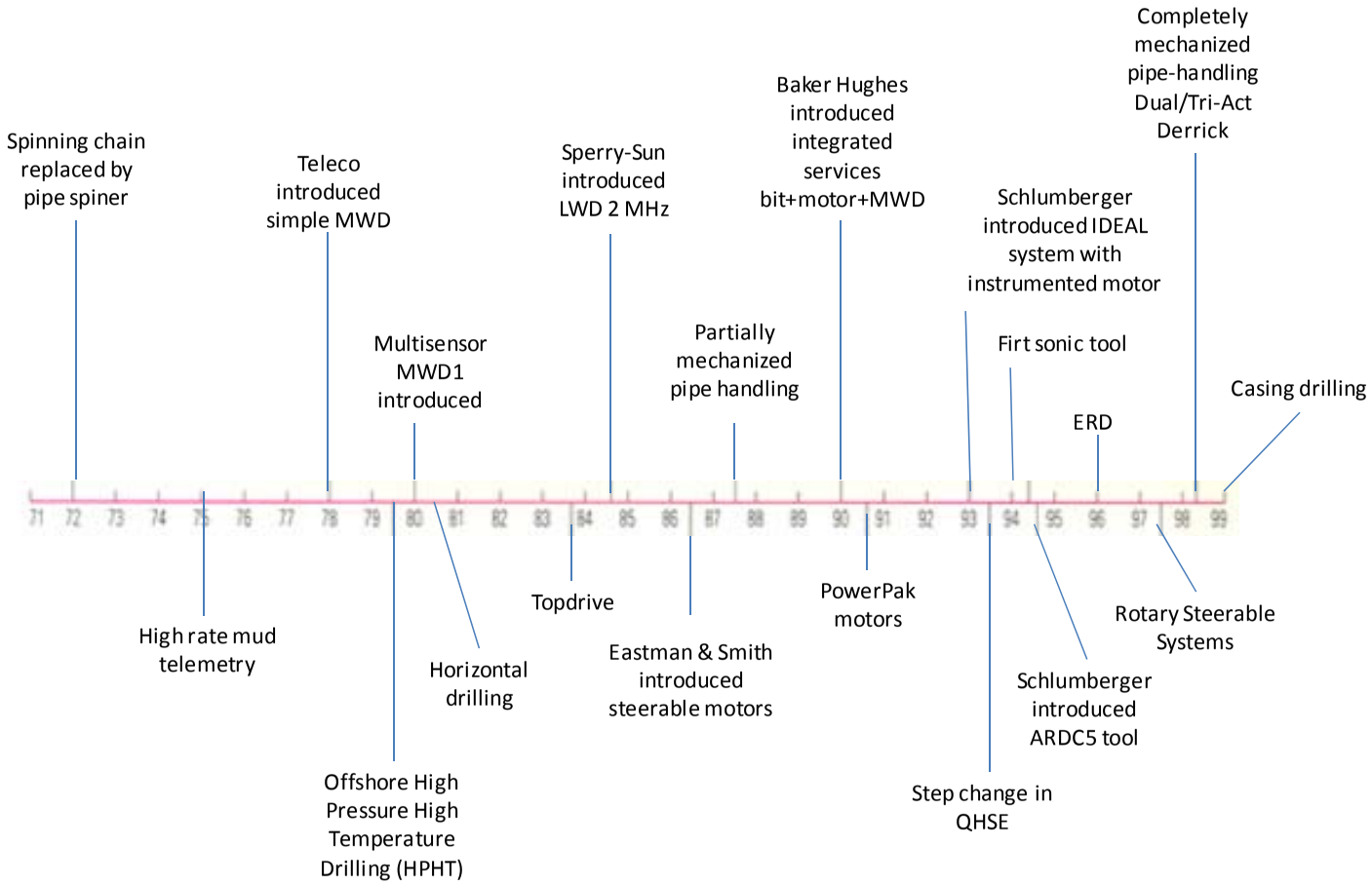
Spinning chain replaced by pipe spiner
Teleco introduced simple MWD
Multisensor MWD1 introduced
Sperry-Sun introduced LWD 2 MHz
Partially mechanized pipe handling
Baker Hughes introduced integrated services bit+motor+MWD
Schlumberger introduced IDEAL system with instrumented motor
Firt sonic tool
ERD
Completely mechanized pipe-handling Dual/Tri-Act Derrick
Casing drilling
71 72 73 74 75 76 77 78 79 80 81 82 83 84 85 86 87 88 89 90 91 92 93 94 95 96 97 98 99
High rate mud telemetry
Offshore High Pressure High Temperature Drilling (HPHT)
Horizontal drilling
Topdrive
Eastman & Smith introduced steerable motors
PowerPak motors
Step change in QHSE
Schlumberger introduced ARDC5 tool
Rotary Steerable Systems

2. Selected contributions to drilling, completion and workover

The following topics have been selected for this habilitation synopsis. These topics cover drilling, completion and workover aspects of petroleum engineering with a special focus on equipment.

- Evaluation of wire line drill pipe with double shoulder connections and suggestions for further improvements.
- Study of the influence of contact pressure within the threaded turns and shoulder part of tool joints
- Determination of the lifetime of casing couplings and development of an analytical solution
- Testing of thread lubricants to enhance the seal capacity of API connections
- Study of excessive loads on large size anchor pipe underneath the casing well head
- Discussions of new developments in deep drilling
- Multiphase flow with sand transport in horizontal pipes
- Development of advanced testing facilities for multiphase flow investigations
- Close view on the low recovery factor in many oil fields and discussions on possible improvements

In what follows, an insight into the author's work on stress/strain state in tubular goods, deep drilling technology and multiphase flow is presented.

2.1. Advanced modeling of the stress/strain state in tubular goods

The advances in petroleum technology are linked to advances in the fundamental sciences, such as mathematics, physics and material engineering. For example, the need to develop more resistant downhole tools (stronger threaded connections in particular) led to the need for the petroleum discipline to implement mathematical techniques (e.g. numerical solvers) and materials characterization techniques (e.g. the Finite Element Method (FEM)). A brief overview of these developments is presented below.

In the analysis of shouldered connections, analytical methods offer, in comparison to other types of investigation (DMS, FEM, photo-elasticity), the advantage of reduced computing time and great flexibility in varying influencing parameters. Thus, these methods allow easy change of input parameters and/or geometry (configuration of shoulder area, thread shape and cone angle) in the calculations workflow. A time scale of key developments in the area of stress distribution in threaded connections, including analytical models and make-up torque criteria, is presented in figure 2.

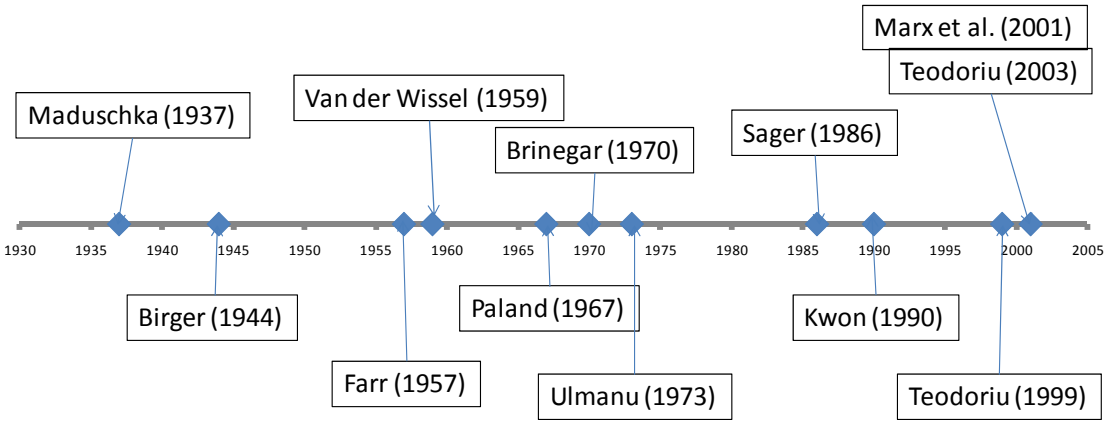

Figure 2: Milestones in the developments of analytical models for stress distribution in threaded connections

Finite element analysis and other experimental research are applied specifically to a given type of threaded connection, and therefore not of general applicability, but they can accurately define local stress distribution and help to improve thread features.

All the analytical models available to compute stress distribution in threaded connections assume that the thread flank stress distribution is uniform. Thus, the resulting forces are considered as acting on the mid-axis of the thread tooth. Usually, the mid-axis of the thread tooth is considered to be identical to the pitch radius. As presented in several papers (Marx et al., 2001; Sager, 1986; Teodoriu, 2003; Birger, 1944; Ulmanu, 1973) the thread tooth deflection strongly influences the stress distribution computation. Figure 3 shows a qualitative comparison between a connection with elastic thread teeth and one with rigid teeth. The thread tooth rigidity changes the stress distribution in the connection and the tooth loading, which may have a negative influence on the connection reliability. To compute the connection deformation induced by the tooth deflection, Paland used in its paper (Sager, 1986) a beam model with distributed load (see figure 4). A few years later, Marx et al. (2001), Sager (1986) and Teodoriu (2005) initiated the first discussion group related to the force position on loaded flank. It was stated that the force position may be the key to understand the stress distribution in threaded connections.

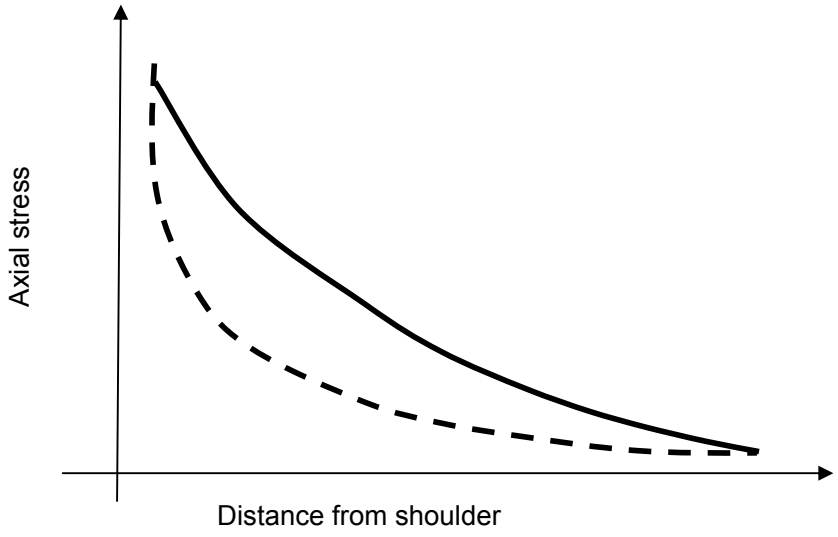

Figure 3: Stress distribution for a connection with rigid teeth (dotted line) and with elastic teeth (continuous line)

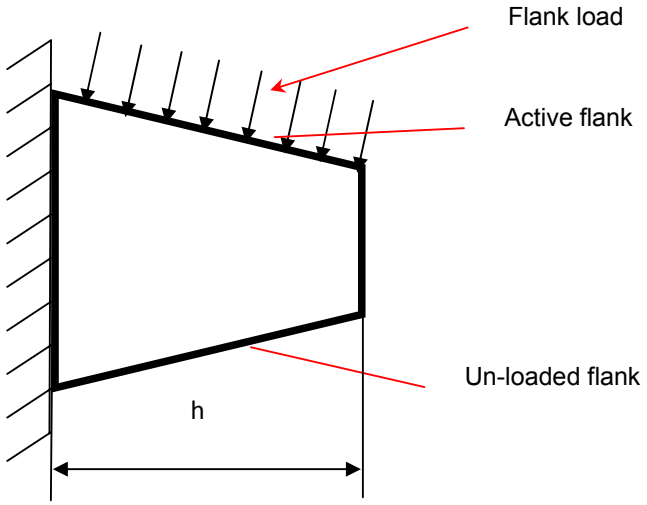

Figure 4: Schematic simplification of a loaded flank

The casing strings are made of pipes of a certain length (e.g. 10 m) which are connected by means of a threaded coupling. Actual standards only account for static loads for the casing string. Special cases are represented by steam injection and geothermal wells, where variable loads are applied to the casing string due to temperature and internal pressure variations. Due to movement restriction (i.e. cement ring around the casing) temperature variations will induce thermal stresses inside the casing string. The value of induced thermal stresses may overcome the material's yield strength, and the fatigue behavior of the casing material can be classified as low cycle fatigue. The presence of geometry changes in the casing body (i.e. threads) will amplify the local stress distribution, and will reduce the low cycle

fatigue resistance. The local stress concept permits the evaluation of low cycle fatigue resistance of such casing connection using the experimental results on uniaxial small-scale specimens and reduces the time and costs needed for classic statistical evaluation on full-scale specimens. The implementation of this concept makes use of analytical and numerical methods. FEMs are intensively used to quantify the local stress distribution and the local concentration factors. Once these parameters are determined, they will be used in a semi-analytical method to determine the fatigue resistance of the casing and its couplings.

The same analytical and numerical methods can also be used to provide new insights into connection resistance. For instance, the numerical methods can be used to validate the analytical solutions, hence reducing the need for full-scale testing.

2.2. New developments in deep drilling technology

Rotary drilling became the preferred deep drilling method for oil and gas wells during the mid- and late 20th century. It is described as the method where the rock is crushed by simultaneously developing a continuous circular motion of the bit (rotational speed), pumping a drilling fluid down the drill pipe to flush out the debris (flow rate), and exerting a downward force on the drill bit to enforce the rock breakage (Weight On Bit (WOB)). The drilling system used to achieve this can be either a Kelly/Rotary Table or a Top Drive system. Prior to the 1980's, drilling with the Kelly was a common trend, both onshore and offshore, therefore the actual technology was called: Rotary drilling = drilling using a Rotary table system. The Kelly was basically used to transmit the rotational motion given by the Rotary table to the drill pipes, and the fluid circulation was performed by means of mud pumps connected to the Kelly through a swivel that allowed free rotation of the Kelly itself. Moreover, drilling using a Kelly allowed only drilling with singles (i.e. only one drill pipe length at a time was made). After the 1980s, the introduction of the Top Drive system revolutionized the way of drilling wells. This system enabled the simultaneous tripping of the drill string and circulation of the drilling fluid. In this case, the making up of doubles, triples and quadruples was made possible, which radically increased drilling speed (but not necessarily the rate of penetration) and allowed for deeper wells. In both systems, downhole motors could be used and WOB was applied statically by the drill collar (representing two thirds of the DC length) and dynamically by raising and lowering the Drilling Assembly. Top Drive systems became the preferred technology for offshore drilling activities.

The impact of mechanized rig operations on work efficiency is proven by many papers (Teodoriu, 2005). A wide spectrum of power tongs can allow mechanized operations at the rig floor. Mechanized rig operations improve the reliability of oilfield tools. When Rotary drilling is used, the most important components to characterize this process are the tubular goods and their connections, which can be achieved by using power tongs. The main purpose of a power tong is to perform an optimum

make-up of the threaded connection between two tubulars. Accurate make-up of Rotary Shouldered Connections (RSC) is of greatest importance towards achieving the best torque and axial force transmission through the connection, which optimizes the connection's lifetime under downhole conditions. The make-up torque value of RSCs depends on the friction coefficient between the threads and the parts of the shoulder that are connected during the make-up procedure. This friction coefficient normally cannot be individually measured or determined; this is why the API Recommended Practice 7G gives an average recommended make-up torque based upon an assumed friction coefficient, adding a certain safety margin. Thus, the majority of RSCs are being made-up with a torque value that differs from the connection optimum torque. This has two consequences: the lifetime of each connection is not maximized, and the torque and axial force values that can be transferred through the connection are different from the technical maximum, which the connection would be able to transfer if it was made-up with the optimum make-up torque. The make-up of drill string components (such as Drill Pipe, Heavy Weight, Drill Collars and Bottom Hole Assemblies) is a key task in the drilling process, which requires significant non-productive time.

2.3. Experimental investigation of multiphase flow

The reservoir fluids produced from oil wells are rarely pure liquid or gaseous hydrocarbon mixtures. Most often, the fluid emerges as a multiphase mixture of natural gas and oil, but, in many systems, water is present as well as a variety of solid phases (sand, hydrates, and asphaltenes). Traditionally, the flow rates of well fluids have been measured by separating the phases and measuring the outputs of the separated fluids by conventional single-phase techniques (Falcone, 2009). However, the economics of offshore oil recovery have moved towards subsea completions with multiphase pipelines over long distances to either the shore or to existing platforms. The problems of multiphase production through wellbores and pipelines require therefore an in depth understanding through fundamental research.

As tubular guarantee the flow from the reservoir to surface, they must be designed based not only on loads (axial load, internal pressure, etc.), but also on the flow regime that is expected through them. Multiphase flow modeling requires extensive experimental investigations in order to validate analytical and numerical models. Such investigations can be performed in dedicated experimental testing facilities capable of mimicking multiphase flow phenomena.

At the onset of the petroleum industry, oil and gas reservoirs were discovered on land. However, at the end of the 19^{th} century, reserves discovered near shore initiated the offshore petroleum industry. In more recent times, economics and demand have justified exploration and development of fields offshore in the Gulf of Mexico, the North Sea, West Africa, the northeast coast of Brazil, Australia and other regions around the world. For each field, there are several development options to bring production to the market. The successful design of an offshore development option depends on many factors, such as water depth, surface/underwater conditions

and available infrastructure, which lead to the choice of a fixed platform, a floating vessel, a floating structure or a subsea system. For the final hydrocarbons to be placed on the market, phase separation is necessary to remove unwanted water or solids and provide the right specifications for the oil (e.g. API gravity) and for the gas (e.g. calorific value). A production system must be configured so as to guarantee flow assurance from the reservoir to the point of sale.

Sand management and multiphase production technology has become conventional for the exploitation of a vast amount of petroleum resources trapped in unconsolidated formations located in offshore, deep water and ultra deep water environments. Increased water depths create a requirement for reliable subsea wells and flowlines to minimize flow assurance issues. Modeling of three-phase gas-oil-sand flow in horizontal wells remains a challenge to the petroleum industry. One effect of the increased frictional pressure losses in horizontal wells is the reservoir performance. The effect of increasing pressure loss in horizontal wellbore translates to an increase in reservoir pressure drawdown.

The advantages of sand management have been identified by a large number of investigators (Salama, 1998; Dusseault et al., 1998; Dusseault and El-Sayed, 2001; Dusseault et al., 2000; Geilikman and Dusseault, 1997; Bratli et al., 2000; Tronvoll et al., 2001; Dusseault et al., 2002; Bello and Fasesan, 2003; Bello and Fasesan, 2004). A major challenge in sand management during production is the understanding of solid particle hydrodynamic behavior, which is related to the profile of sand velocity, the interaction between the suspended solid phase and other phases, and the gas-liquid turbulent slug flow structure. The understanding of the behavior of the suspended sand particles during gas-liquid multiphase production and transfer operations enables the assessment of the severity or risk of potential sand deposition. It also helps to identify the parameters that would need to be controlled in order to check sand deposition and optimize production.

Inefficient sand transport by the gas-liquid flow can lead to numerous problems, including sand deposition and accumulation in the well and in the production lines, increased pressure loss, increased erosion risk, frequent and expensive cleaning operations, and increased downtime (Oudeman, 1993; Appah and Ichara, 1994; Appah et al., 1997).

Although many studies have been performed on the transport velocity of various solid particles during production of manganese nodules (Sakaguchi et al., 1987a; Sakaguchi et al., 1987b; Sahara and Saibe,1991; Sakaguchi et al., 1992; Sakaguchi et al., 2000). However, the behavior of solid particles during production of manganese nodules is essentially different from oil-gas-sand multiphase production and pipeline transportation. The oil-gas-sand multiphase pipeline transportation consists of fine particles while in manganese nodules production coarse particles are contained. The size of the fine particles is usually less than 0.7 mm and that of course particle is about 5 mm. These particularities require a rethinking of testing

facilities and measurement concepts, which have been implemented in the ITE Multiphase Flow Loop system.

To efficiently design and operate gas-liquid-sand flows in wells and pipelines, the degree of the distribution of the solid phase in the tubular must be quantified and controlled. Because it is crucial to understand the influence of various operating and system conditions on the solid velocity profile, a measuring technique capable of probing the internal flow structure without being invasive to it is highly desirable. The implementation of digital image techniques is an established method for multiphase flow visualization and analysis (Caicedo et al., 1993; Sam et al., 1995; Kundakovic and Vunjak-Novaakovie, 1995; Kaftori et al., 1995a; Kaftori et al., 1995a; Nino and Garcia, 1996; Aloui and Souhar, 1996; Gopal and Jepson, 1997; Marques et al., 2002; Leifer et al., 2003; Shen et al., 2004). It has advantage over other existing solutions for solid velocity and hold-up measurements because of its non-invasive character. The fast response of the technique justifies its likely application to multiphase process control. Hence, the development of a non-intrusive measuring technique that can provide reliable information on the solid phase flow structure appears to be key towards the development of a mechanistic and hydrodynamic approach to sand transport in multiphase production. This may improve operations and safety, and reduce capital costs.

To respond these new challenges new flow loops have been re-designed and built. A thorough investigation and ranking of world-wide flow loops for multiphase flow experiments should include all of the following factors: loop geometry, dimensions, operating pressure and temperature, range of phase flow rate, equipment and instrumentation, piping material, fluid properties, data acquisition and information processing systems. However, the objective of the research task is to illustrate how to approach such an investigation and to identify future needs for niche experimental investigations. The outcomes of the performed review show that there is a need for a dedicated flow loop to mimic the dynamic interactions between reservoir and wellbore. Furthermore, a dedicated flow loop to understand sand transport phenomena in multiphase flows is also required.

2.4. The importance of the recovery factor

Why investing so much time in research? The oil and gas business is constructed around the amount of fluids stored in the reservoir. The actual recovery factors are rather low for oil (average of 35%) and they can be increased through new technology and extraction concepts. Research activities performed within academia allow, through technology transfer, a better exploitation of our finite resources, and will also lead to smooth transition to renewable and environment friendly energy resources.

High-pressure and high-temperature (HPHT) gas reservoirs are defined as having pressures greater than 10,000 psia and temperatures over 300ºF. Modeling the performance of these unconventional reservoirs requires the understanding of gas

behavior at elevated pressure and temperature. An important fluid property is gas viscosity, as it is used to model the gas mobility in the reservoir that can have a significant impact on reserves estimation during field development planning. Accurate measurements of gas viscosity at HPHT conditions are both extremely difficult and expensive. Thus, this fluid property is typically estimated from published correlations that are based on laboratory data. Unfortunately, the correlations available today do not have a sufficiently broad range of applicability in terms of pressure and temperature, and so their accuracy may be doubtful for the prediction of gas viscosity at HPHT conditions. Ehsan et al. (2009) performed a sensitivity analysis to assess the effect of gas viscosity estimation errors on the overall gas recovery from a synthetic HPHT reservoir, using numerical reservoir simulations. The result shows that a -10% error in gas viscosity can produce an 8.22% error in estimated cumulative gas production, and a +10% error in gas viscosity can lead to a 5.5% error in cumulative production. These results indicate that the accuracy of gas viscosity estimation can have a significant impact on reserves evaluation.

Experimental investigations on gas viscosities at HPHT conditions is not an easy task and require development of laboratory equipment and testing procedure that ensure first of all the safety of the experimental work. Ehsan et al. (2009) show an example of the work performed on gas viscosity measurements where a falling body viscometer was used to measure the HPHT gas viscosity in the laboratory. The instrument was calibrated with nitrogen and then, to represent reservoir gas behavior more faithfully, pure methane was used. The subsequent measured data, recorded over a wide range of pressure and temperature, were then used to evaluate the reliability of the most commonly used correlations in the petroleum industry. The results of the comparison suggest that at pressures higher than 8,000 psia, the laboratory measurements drift from the National Institute of Standards and Technology (NIST) values by up to 7.48%.

3. Comments on selected categories of peer-reviewed papers and comparable contributions

In what follows, a summary of the selected papers based on the categories shown in chapter 2 is presented.

3.1. Evaluations and proposals for further product improvements on wire line drill pipe with double shoulder connections

The wire line technology uses drill pipes having threaded connections with no external or internal upsets. These connections are usually weaker than the pipe body and require high make-up torque values. To achieve this, double shoulder connections are used because they have the advantage of improving the stress distribution on thread turns.

The paper in question shows the analytical, numerical and experimental work performed on a double shoulder connection in order to understand the effect of the internal shoulder as well as the shoulder load distribution. To solve this, the existing equation for shoulder connection calculation was extended to incorporate the internal shoulder effect. The results showed a good comparison of the analytical, experimental and numerical results. The extended equation to calculate the make-up torque can be easily generalized for any double shoulder connection.

The technology of double shoulder connection has a high impact on the future of drilling technology, especially when deep drilling activities like HPHT and geothermal are involved.

Untersuchung zur Belastbarkeit von SLIMHOLE-Bohrgestängen mit Doppelschulter, Erdöl, Erdgas, Kohle, 125 Jg. 2009, Heft 7/8.

3.2. Study of the influence of contact pressure within the threaded turns and shoulder part of tool joint

The previous work showed the importance of combining numerical and experimental work in order to better describe the load envelope of a given connection, in particular double shoulder connections. The research work is related to the second selected paper is enhancing the fundamental studies on threaded connections by analyzing the influence of contact pressure within the thread turns and shoulder part of a tool joint.

Drill pipe connections are a primary component of the drill string, and the entire “well security” depends upon tool joint performance reliability. An adequate connection between two drill pipes depends on the quality of the assembly process, which is significantly affected by thread compound performance. Since the variety of thread

compounds is large, standards have been developed to determine thread compound performance and to define minimum thread compound properties. Thread compound frictional performance is normally defined by its friction coefficient (COF) in the standard American Petroleum Institute (API) Rotary shouldered connection (RSC), or the friction factor (FF) relative to a standard API friction coefficient, which is accepted to be 0.08. The 0.08 value was determined by the API after multiple tests utilizing standard API RSCs and metal-based thread compounds, primarily 40% zinc and 60% lead. The friction coefficient of a thread compound has been generally considered to be constant. Although the API defines a constant coefficient for a given load range, recent studies indicate that the friction coefficient can vary considerably depending on connection geometry, contact stress and thread compound composition.

As stated by Farr (1956), the make-up torque of a connection is a function of its geometry, the pre-defined buck-up force and the friction coefficient between the two members of the connection (pin and box):

$$M = F_v \cdot \left(\frac{P}{2 \cdot \pi} + \frac{R_p}{\cos \beta} \cdot \mu_{th} + R_s \cdot \mu_s \right). \qquad (1)$$

Typically, under field conditions, the applied make-up torque M can be measured, while the buck-up force F_v can only be estimated. As equation (1) shows, knowing the applied torque M and the parameters within the brackets, the Farr formula can be used for reverse calculation of the induced buck-up force in the connection. Since a better understanding of the friction process and consequently an accurate make-up torque calculation allow optimizing the load resistance of the connection, more research must be focused on friction coefficient behavior under real conditions (e.g. temperature, contact pressure, composition, etc). Based on the findings presented in this paper as well as in previous work, a DGMK Project was initiated.

Rotary-Shouldered Connections Make-up Torque Calculation Considering the Effect of Contact Pressure on Thread Compound's Friction Coefficient; OIL GAS European Magazine 4/2009.

3.3. Determination of lifetime for casing couplings and development of a method for an analytical solution

The success of any drilling operation is to drill the well to the target depth (TD) in a safe manner. This includes the integrity of the drill string (i.e. drill pipes and their threaded connections) as well as the integrity of the wellbore, especially of the casing string. Well lifetime definition has changed during the history from few years to as long as 50 years. This generates new research areas, one of them being the topic presented in the following.

Any well drilled deeper than 3 km would present temperatures in line with those typical of higher enthalpy geothermal resources. However, this paper focuses on well integrity issues for hot wells, independent of their depth. In Europe, the majority of the geothermal wells, which have been drilled to depths greater than 4000m, are completed with surface casing diameters of 18−5/8in. (473mm) or larger. The large diameter of production casings is a consequence of the amount of fluids that needs to be produced from geothermal wells. For large installed power systems, production diameters of 13−3/8 in. (340mm) are required, but such diameter requirements strongly affect well costs. Over the operating life of a well, its casing string is generally subject to external loads that can be considered as static or quasi-static. Current industry design standards, such as those issued by the American Petroleum Institute (API), consider the casing string to be statically loaded, yet it can be subject to variable loads due to changes in temperature or internal pressure during geothermal operations. As the movement of the casing is restricted by the presence of a cement sheath, temperature variations induce thermal stresses in the casing string, which may exceed the yield strength of the casing material. Thus, the fatigue behavior of the casing material during the operational life of a well can be classified as low-cycle fatigue (LCF). The presence of geometrical variations in the casing body such as the connection threads will amplify the local stresses and reduce the LCF resistance of the casing. The surface casings of deep geothermal wells are exposed to significant temperature variations during drilling, which may affect their subsequent integrity. The size of the surface casing depends on that of the production casing and also on the drilling challenges presented by that particular well. The theoretical and experimental work focuses on the fatigue resistance of an 18−5/8in. (473mm) diameter casing with Buttress thread connections, which is a common size for surface casing in geothermal wells, as reported by several authors.

Extensive Finite Element runs have been used to determine the local stress values due to stress concentration effects. Figure 5 shows the stress distribution for two different load types (tension and compression). It shows a slightly different behavior of the connection between the two load scenarios.

Based on the FEM analysis, it was found that for a buttress connection the stress concentration factor, K, differs from tension to compression. This variation can be explained by the more aggressive bending on the thread turn for the tensile load and also by the asymmetric geometry of the Buttress thread that has different flank angles. The following results were obtained: K = 3.51 for tension, K = 2.73 for compression. In reality, the incomplete thread turns present sharp edges and therefore higher stress concentration factors may be expected.

Comparing completion design in hydrocarbon and geothermal wells: the need to evaluate the integrity of casing connections subject to thermal stresses, submitted to the Geothermics journal in April 2008.

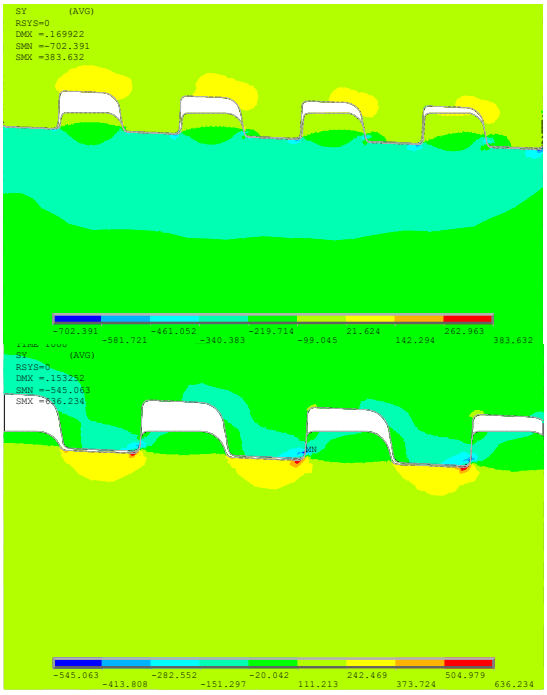

Figure 5: Stress distribution at the thread root for the compression (top) and tension (bottom) load cases, as simulated with FEM. High stresses at the thread root are shown in red.

3.4. Study of excessive loads on large size anchor pipe underneath the casing well head

Since modern wells are drilled to reach complex purposes, loads considered for casing design are in some cases extreme. HPHT wells are known for their extreme environment and therefore the acting loads on the casing string. The casing design under axial compression was learn from steam injection projects. For these cases there was found that pre-stressing the casing string may reduce the negative effect of axial compression. During more than 40 years of steam injection it has been found that Buttress connections have a good loading capacity under high axial tension loads. The advantage of a Buttress connection is given by its simplicity and low costs comparing to premium connections. Therefore, it is usual for some casing strings like anchor casing to have Buttress connections, which are cheaper, especially for large casing diameters. Concerning anchor casing the acting loads are typically low, but at the surface the entire casing strings are hanging on it. It is necessary to investigate the compression resistance of such casings. The threaded connections are mostly designed to have a maximum tension resistance. There are some new connections on the market especially designed for high compressive loads, but for special purposes like drilling with casing or high temperature wells. This special condition makes the price for such connections high. The paper presents a method to quantify the compression resistance of Buttress connections based on experimental and

analytical results. Experimental, numerical and analytical methods have been combined.

Figure 6 shows a comparison of the full scale test versus Finite Element results. Both methods pointed out that the system will fail due to a local buckling of the last engaged threads.

Buttress Connection Resistance under Extreme Axial Compression Loads, Oil and Gas Magazine, 4/2005, Volume 31, ISSN 0342-5622.

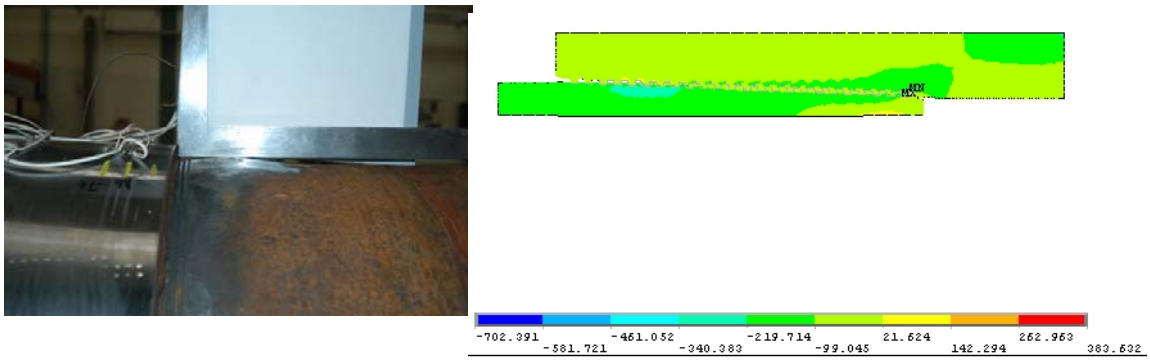

Figure 6: Measured and estimated failure modes for a Buttress connection.

3.5. Testing thread lubricants to enhance seal capacity of API connections

This paper presents a combination of “near praxis” and laboratory development. Petroleum Institute are generally criticized for their lack of “fundamental research” due to their praxis-oriented approach. This work presents the experimental results of tests carried out on four different compounds using the improved “grooved-plate” method. The tests have shown a large variation of the tested-thread-compounds sealing capacity. Starting from the experimental results and the theoretical analysis of the American Petroleum Institute (API) connection, a useful chart was built to determine the real connection resistance, based on its initial make-up torque, see figure 7. The chart offers to engineers involved in the design of a fracturing process the possibility to estimate the maximum pressure that may lead to a connection leak. The paper combines experimental and numerical approaches to solve an industry-known problem: thread compound characterization.

The tests performed on four different types of compounds have shown that the API compound has the lowest leak resistance in conjunction with the API-thread type. The Buttress leak resistance has an asymptotic behavior. At contact pressures higher than 100 MPa, the leak resistance is constant.

The difference between API-round and Buttress leak resistance consists in the contact-pressure dependency of the API-round leak resistance. It is recommended for API-round connections to be made-up with optimum make-up torque or higher.

As a result of this study, we recommend that research focused on the relationship between dope-rheological properties, time, and flow behavior should be performed.

Sealing Capacity of API Connections - Theoretical and Experimental Results, SPE 106849, March 2009 SPE Drilling and Completion Journal.

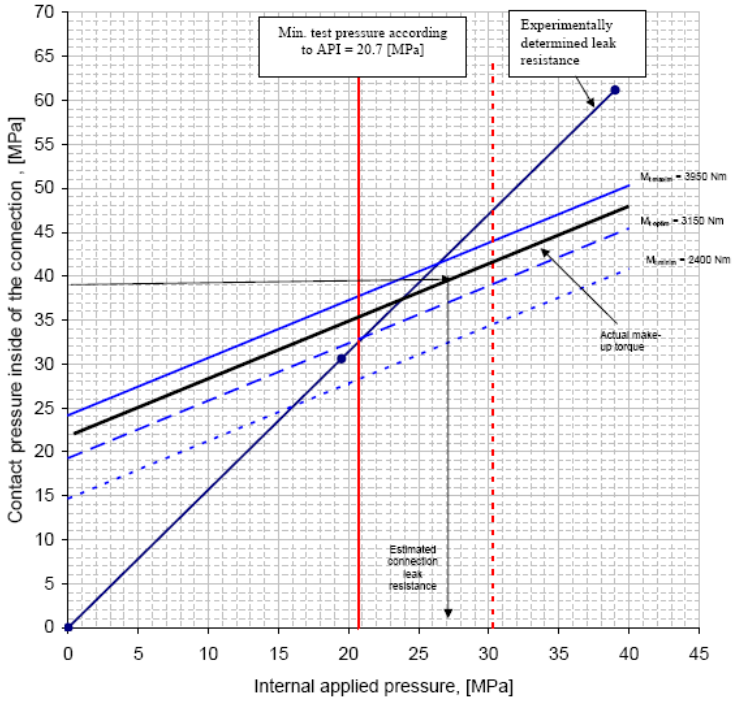

Figure 7: Chart for API connection leak resistance estimation knowing the thread compound leak resistance.

3.6. Discussion of new developments in deep drilling

It has already been presented above that focal research points are moving throughout the history of drilling. This is why reviews must be performed in order to identify new tendencies in the drilling business.

Such developments are to a large extend related to the complexity of the reservoirs that have to be drilled. New drilling rigs are introduced onto the market to enhance safety and working conditions, while downhole technology becomes more complex. Nevertheless, new developments include some improvements, especially in the area of threaded connections. Two papers shall be mentioned here with respect to the discussion upon new developments:
Neue Entwicklungen in der Bohrtechnik, Akademie der Geowissenschaften zu Hannover Veröffentlichungen, 2005, Heft 25, ISBN 3-510-95943-4
and
Increasing Geothermal Energy Demand: the Need for Urbanization of the Drilling Industry, Bulletin of Science, Technology & Society 2008, Volume 28, No. 3, Special

Issue, Part 2: The Age of Alternative Energy: Is the Future Renewable?, DOI:10.1177/0270467608315531, 16 April 2008.

Current drilling practices are based on the principle of Rotary drilling, where a dedicated rotating system drives a cutting tool (i.e. drill bit) in order to break the rock. A continuous weight is applied to the bit to provide the necessary cutting force. The weight on the bit is controlled via the hoisting system, which is also used to lift and trip the well tubular in and out of the well. The cuttings are removed from downhole and transported to surface by a drilling fluid (air, foam or drilling mud). Cuttings removal is the main function of the circulating system that allows the drilling fluid to be pumped downhole (via the drill pipe) and returned to surface (via the annular space between drill pipe and hole), where it is reconditioned. Until recently, the oil and gas drilling industry portrayed an image using equipment and working environment that was "large, dirty and downright ugly". Nowadays this is unacceptable and the industry pays close attention to making drilling rigs clean, safe and environmentally friendly. Consequently, modern oil and gas drilling rigs have become ergonomic and tailored to the driller's need for a safe and adequate working space. Modern drilling rigs rely on integrated mechanized equipment and ergonomic working space. Figure 8 shows an example of a highly computerized control system used to operate a modern rig, as opposed to the high level of labor required for a conventional rig.

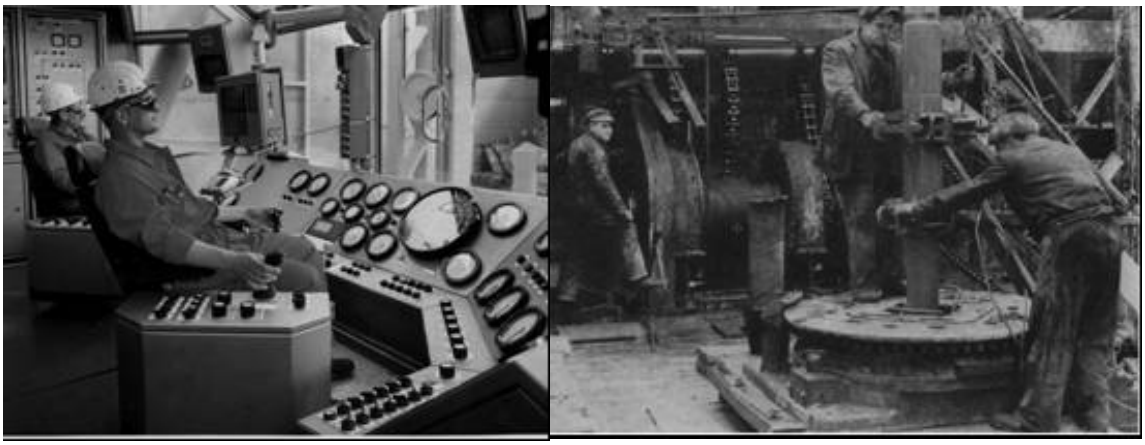

Figure 8: Driller's cabin on a modern drilling rig (Reinicke, 2005) compared to a driller's working location in 1942.

Moreover, the paper "*Increasing Geothermal Energy Demand: the Need for Urbanization of the Drilling Industry*", *Bulletin of Science, Technology & Society 2008, Volume 28, No. 3, Special Issue, Part 2: The Age of Alternative Energy: Is the Future Renewable?, DOI:10.1177/0270467608315531, 16 April 2008."* shows the new trends in rig development and presents the future rig design from the authors point of view. To accommodate the future needs of drilling in urban environments, the new breed of drilling rigs will have the following design characteristics:

- Modular construction for easier mobilization and transportation through narrow city streets. Being modular will mean that most of the rig equipment will be mounted in small containers of small size, which has the added benefit of reducing noise emissions by sound insulation of the containers' walls.

- Low noise emissions outside the drill site. One of the mandatory changes to rig design to reduce noise levels is to lower the rig's height by using single drilling rigs instead of triple rigs. Noise reduction is also obtained by using non-conventional hoist systems (e.g. rack and pinion system, linear hydraulic motors)

- High hook load capacity, despite the small size of the drilling rig, which can be achieved by means of non-conventional technologies.

- Easily camouflage for long term drilling projects.

- Smart power supply using on-site diesel generators or tapping into the city electrical power grid, and having low emissions of noise, vibrations and exhaust gases.

- Closed loop spill and mud processing unit to avoid any contamination of the rig site.

- Small size of drilling rig, which will be achieved through integrating the automated processes and computer controlled rig floor equipment.

3.7. Multiphase flow with sand transport in horizontal pipes

All the above presented work requires a good understanding of the conditions existing downhole. This can be done by experimental and theoretical studies which sometimes are not directly linked to drilling technology. This explains the rather wide subjects in the selected papers and reports. Another interesting subject in the oil industry is the multiphase flow aspects of drilling and production fluids.

A crucial point, still to be established in the prediction of oil-gas-sand multiphase production and transfer system performance, is the identification of relevant mechanisms describing sand particle transport. To resolve this issue, experimental investigations are made on the behavior of suspended sand particles in simulated oil-gas-sand multiphase pipe flows paying attention to the time-averaged local and global sand velocity and holdup. Simultaneous measurements of the time-averaged local and global sand velocity are made by digital imaging technique for better understanding of the oil-gas-sand multiphase flow hydrodynamics and sand transport mechanisms. The results show that flow regimes of the multiphase flows significantly influence sand transport in the pipe flow. The shape of the local and global sand particle velocity and holdup profiles are also strongly modified by flow regimes. Furthermore, the experimental results indicate that the transport effect of the

suspended sand particles can be enhanced by operating the multiphase flows under slug flow conditions. It is concluded that a new mechanism based on bubble-particle interaction needs to be considered in the modeling of sand transport behavior during oil-gas-sand multiphase production and transfer operations. This work is based on extensive experimental investigations that were performed on a state-of-the-art testing facility. Figure 9 shows the schematic of the experimental facility. The developed testing facility can be successfully used for simulation of drilling and production well conditions. This facility will also be used as part of the research effort to improve the cuttings transport in geothermal wells as a part of the 2009 started project gebo (Forschungsverbund gebo – Geothermie und Bohrtechnik).

Particle Holdup Profiles in Horizontal Gas-Liquid-Solid Multiphase Flow Pipeline, Chemical Engineering &Technology, Volume 28, No. 12, December 2005, ISSN 0930-7516.

3.8. Development of advanced testing facilities for multiphase flow investigations

This paper is an example of the author's efforts to perform fundamental research on "near praxis" environment. The need of such facility was shown through an SPE Journal published paper (*Multiphase Flow Modelling Based on Experimental Testing: A Comprehensive Overview of Research Facilities Worldwide and the Need for Future Developments, (original SPE 110116) SPE Projects, Facilities & Construction, Volume 3, Number 3, September 2008, pp.1-10)*, that dealt with the current testing facilities worldwide and their applicability to specific research outcomes. Once the niche had been identified, a team has been built and the results are shown as follows.

Existing models to predict and analyze liquid loading in gas wells are based on steady-state flow. Even when transient multiphase wellbore models are employed, steady-state or pseudo steady-state inflow performance relationships are used to characterize the reservoir. A more reliable approach consists of modeling the dynamics in the near-wellbore region with its transient boundary conditions for the wellbore. The development of new models to mimic these dynamics requires a purpose-built flow loop. A design to construct such a facility has been developed.

This facility is the first to integrate pipe representing the wellbore with a porous medium that fully mimics the formation surrounding the wellbore. This design accounts not only for flow into the wellbore, but for any reverse flow from the pipe into the medium. Integrated wellbore/reservoir system analysis was used to screen the parameters required to recreate liquid loading under laboratory conditions. Once the range in operating conditions was defined, the equipment and mechanical components for the facility were selected and designed. The results showed that three reciprocating compressors working in parallel provide the smallest, most economic, and most flexible configuration for the Tower Lab facility at Texas A&M

University. The design of the pressure vessel hosting the porous medium requires a cylindrical body with top- and bottom-welded flathead covers with multiple openings to minimize weight. The required superficial velocities for air and water indicate that the system needs independent injection into the porous medium through two manifolds. Optimally, the system uses digital pressure gauges, coriolis or vortex technology to measure airflow and turbine meters for water flow. The new facility significantly improves the ability to mimic the physics of multiple phase flow for the development of liquid loading models and leads to better optimization of gas fields.

Design of a High-Pressure Research Flow Loop for the Experimental Investigation of Liquid Loading in Gas Wells, SPE-122786-MS, presented at the 2009 SPE Latin American & Caribbean Petroleum Engineering Conference to be held 31-May-09 to 03-Jun-09 in Cartagena, Colombia.

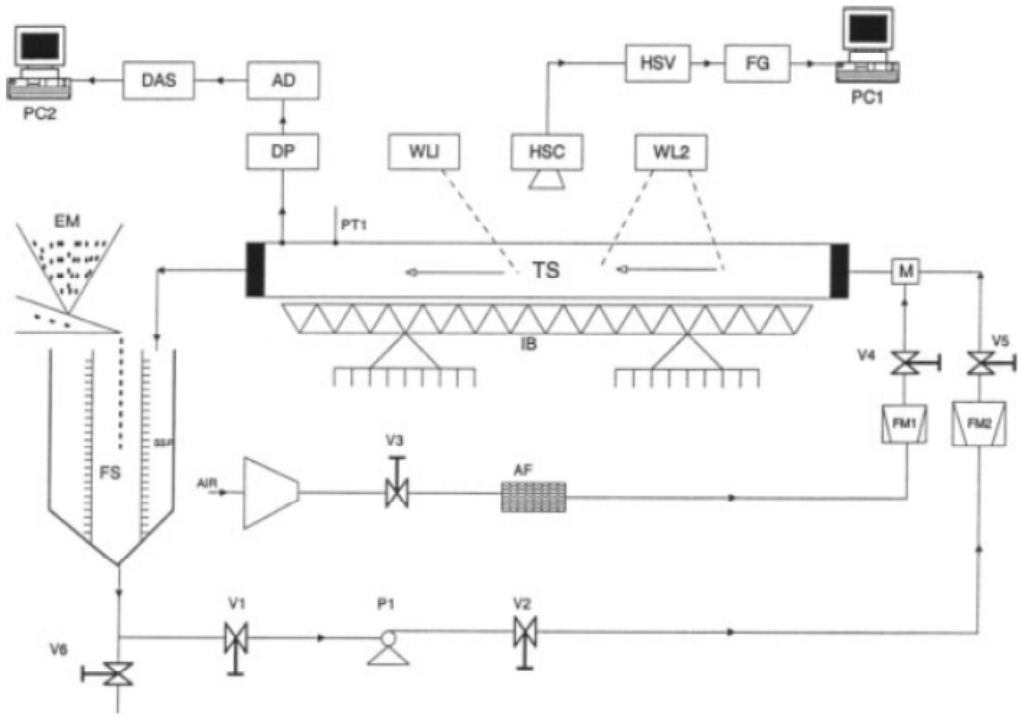

Figure 9: Schematic diagram of the experimental setup as shown in the paper: *Particle Holdup Profiles in Horizontal Gas-Liquid-Solid Multiphase Flow Pipeline, Chemical Engineering &Technology, Voume 28, No. 12, December 2005, ISSN 0930-7516.*

3.9. Close view on the low recovery factor in many oil fields and discussions of possible improvements

Technological developments and the decision to use high technology (HighTech) strongly depend on the reserves and resources which are to be found. This is why, drilling and production operation researchers have to look in the aspects of recovery factors and definition of reserves. This will enhance the capacity of generating applicable research, thus the fundamental aspect is preserved.

Accepted wisdom suggests that the higher an oil or gas fields' value of recovery factor (RF), the more efficient the hydrocarbons have been produced from the reservoir. Optimizing the recovery from a hydrocarbon field should be the common goal of both governments and operators, although increasing production levels at the right economic and political moment may prove too tempting to some. Hence, the use of RF as a yardstick to measure the performance of a reservoir (or the management of that reservoir) has some serious shortcomings. In order to use RF appropriately, it is important to understand what it is, how it is calculated and the uncertainty inherent to the parameters from which it is derived. The value of RF is defined as the ratio of the recoverable volume to the hydrocarbons originally in place (HOIP) over the course of a field's economic life. Yet this seemingly trivial calculation has inherent uncertainty and can vary due to many reasons.

Table 1: Template for what production data should be provided by government agencies. [WHP=Well Head Pressure; WHT=Well Head Temperature; GOR=Gas-Oil Ratio; WOR=Water-Oil Ratio; EOR=Enhanced Oil Recovery; PVT=Pressure-Volume-Temperature; FVF=Formation Volume Factor; CGR=Condensate-Gas Ratio; STOIIP=Stock Tank Oil Initially In Place]

	Item to be Reported	**Reported Variables for Item**	**Outputs Derived from Variables**
1a	Monthly well producer records	gas-oil-water volumes, days online, WHP, WHT, choke %	Producer Uptime, Well producing GOR-WOR-Water Cut, Well Decline Curve, Reserves per well, Field Reserves
1b	Monthly well injector records	gas, water volumes, days online, WHP, WHT	Injector Uptime, Injectivity model, Producer:Injector Ratio
1c	Well Technology	Artificially lifted? Stimulated? Water shut-offs? Horizontal or vertical? Completion details	Aids selection of appropriate analogue fields
3a	Monthly Field production records	gas-oil-water volumes	Field producing GOR-WOR-Water Cut, Field Decline Curve, Field Reserves
3b	Monthly Field injection records	gas, water volumes	Field Injectivity model (aquifer strength)
3c	Field Technology	Gas compression? Multiphase pumping? EOR?	Aids selection of appropriate analogue fields
4	Bottom hole Surveys	average reservoir pressure & temperature history (date and depth datum)	Material balance for HOIP
5	Top & Base reservoir structure maps	depth contours, scale, well locations, fluid contacts, major faults	Gross rock volume, Field area, Hydrocarbon fill factor
6	Field Geological description	sandstone or carbonate, matrix porosity or naturally fractured, massive or thin-bedded	Aids selection of appropriate analogue fields
7	Field Petrophysical parameters	porosity, water saturation, gross thickness, net-to-gross	Hydrocarbon pore volume (at reservoir conditions) [Combining Items 5 & 7]
8	Field PVT properties (Oil)	API gravity, solution GOR, viscosity, bubble point, FVF	STOIIP (at surface conditions) [Combining Items 5, 7 & 8]
9	Field PVT properties (Gas)	Gas gravity, condensate gravity, CGR, viscosity, dew point, H2S-CO2-N2, FVF	GIIP (at reservoir conditions) [Combining Items 5, 7 & 9]
10	**Recovery Factor**	**Field Reserves (from 1a or 3a), HOIP (from 8 or 9), with date reference**	

This paper critically reviews the concept of the recovery factor of oil and gas fields. Although this simple parameter is used throughout the oil and gas industry, it is subject to misunderstanding and misuse. Besides changing continually through the producing life of a field, the estimate of RF is affected by geological uncertainty, inappropriate reserves reporting, technological shortcomings, commercial practices and political decisions. At present, the information necessary to fully evaluate RF is not unequivocally determined, audited or reported, which makes it impossible to produce consistent global field statistics. Based on the authors' experience, the paper outlines the shortcomings of RF and suggests how they may be overcome. To

promote clarity and transparency in RF calculations, a template for an open worldwide production database is proposed. Table 1 shows the minimum structure of such data base.

Can We Be More Efficient in Oil and Gas Exploitation? A Review of the Shortcomings of Recovery Factor and the Need for an Open Worldwide Production Database, Scientific Journals International, Journal of Physical and Natural Sciences, Volume 1, Issue 2, 2007.

References

Aloui, F. and Souhar, M. (1996): Experimental study of a two-phase bubbly flow in a flat duct symmetric sudden expansion — Part II: liquid and bubble velocities, bubble sizes, International Journal of Multiphase Flow, Vol. 22, No. 5, 849-861.

Appah, D. and Ichara, M. 1994 Empirical model determines energy required to clean Sand from wellbores, Oil and Gas Journal, Feb. 1994, 36-38.

Appah, D.; Ichara, M. and Bouhroun, A. 1997 Aerated wash over technique in sand producing wells, Oil and Gas European Magazine, Vol. 4, 1997, 29-33.

Bello, O. O. and Fasesan, S. O. 2003 Improved Profitability in Nigerian Hydrocarbon Production through Application of Sand Management Technology, Proceedings of the 33rd Annual Conference and Meeting of Nigerian Society of Chemical Engineers, Abeokuta, Nigeria, 19th to 21st Nov. 2003.

Bello, O. O. and Fasesan, S. O. 2003 Sand Management Technology for Improved Oil Recovery in Nigeria" NAFTA Oil and Gas Scientific Journal, Year 55, Number 7-8, July-August, 2003.

Birger, I. A. 1944, Spannungsverteilung auf die Gewindeanzeiger des Maschinen-baues, Moskau, Heft 11.

Bratli, R. K.; Dusseault, M. B.; Santarelli, F. J. and Tronvoll, J. 2000, Sand Management Protocol Increases Production Rate, Reduces Completion Costs, Proc. Trinidad and Tobago Biennial SPE Conf., Port-of-Spain.

Caicedo, G. R.; Marques, J. J.; Ruiz, M. G. and Soler, J. G. 2002, A study on the behaviour of bubbles of a 2D gas-liquid fluidized bed using digital image analysis, Chemical Engineering and Processing, Vol. 42, 2002, 9-14.

Dusseault, M. B. and El-Sayed, S. 2001, Heavy Oil Production Enhancement by Encouraging Sand Production, Proceedings 2001 SPE/DOE Improved Oil Recovery Symposium, Tulsa, Oklahoma, 3-5 April 2001.

Dusseault, M. B.; Geilikman, M. B. and Spanos, T. J. T. 1998 Mechanism of Massive Sand Production in Heavy Oils, Proc. 7th UNITAR Int. Conf. Heavy Oils and Tar Sands, Beijing.

Dusseault, M. B.; Tronvolli, J.; Santilippo, F and Santarelli, F. J. 2000, Sand-Self Cleaning in High Rate Oil Wells Using Sand Management, SPE 58786, Int. Conf. on Formation Damage.

Dusseault, M. B.; Chun, X. L.; Yiqiu, M. and Wu, G. 2002, CHOPS in Jilin Province, China, Proceeding of SPE International Horizontal Well Technology Conf., Calgary, Alberta, Canada, 4-7 November 2002.

Ehsan, D.; Kegang, L.; Teodoriu, C.; William, D.; McCain, Jr.; and Falcone, G. 2009, More Accurate Gas Viscosity Correlation for Use at HPHT Conditions Ensures

Better Reserves Estimation, SPE 124734, This paper was prepared for presentation at the 2009 SPE Annual Technical Conference and Exhibition held in New Orleans, Louisiana, USA, 4–7 October 2009.

Falcone, G.; Hewitt, G. F.; Alimonti, C. 2009, Multiphase Flow Metering: Principles and Applications, Elsevier, Textbook for the Developments of Petroleum Science series. Elsevier, October 2009.

Geilikman, M. B. and Dusseault, M. B. 1997, Fluid-rate Enhancement from Massive and Production in Heavy oil Reservoirs, J. of Petr. Science and Engineering, 17, 5-8. Special Issue: Near Well bore Formation Damage and Remediation, 1997.

Gillies, R. G.; Hill, K. B.; Mckibben, M. J. and Shook, C. 1999, Solids transport by laminar Newtonian flows, Powder Technology, Vol. 104, 1999, 269-277.

Gillies, R. G.; Mckibben, M. J. and Shook, C. 1997, Pipeline flow of gas, liquid and sand mixture at low velocity, J. Can. Petro. Tech. 36, 1997, 36-42.

Gillies, R. G.; Mckibben, M. J. and Shook, C. 1995, Oil, water and sand flow experiments in a model horizontal well, J. Can. Petro. Tech. 34, No. 9, 1995, 56-63.

Gopal, M. and Jepson, W.P. 1997, Development of digital image analysis techniques for the study of velocity and void profiles in slug flow, International Journal of Multiphase Flow, Vol. 23, No. 5, 1997, 945-965.

Jepson, W. P. 1987, The flow characteristics in horizontal slug flow, Proc. 3rd Int. Conf. on Multiphase Flow, B.H.R. Group, The Hague, Netherlands 18-20 May, 1987.

Kaftori, D.; Hetstroni, G. and Banerjee, S. 1995, Particle behaviour in the turbulent layer: motion, deposition and entrainment, Physics of Fluid, Vol. 7, No. 5, 1995,1095-1106.

Kaftori, D.; Hetstroni, G. and Banerjee, S. 1995, Particle behaviour in the turbulent layer: velocity, flux and concentration distribution, Physics of Fluid, Vol. 7, No. 5, 1995, 1107-1121.

King, M. J. J.; Fairhurst, C. P. and Hill, T. J. 2001, Solids transport in multiphase flows: applications to high viscosity systems, Journal of Energy Resources, Vol. 123, 2001. 200-204.

Kundakovic, L. and Vunjak-Novaakovie, G. 1995, Mechanics of Particle Motion in Three-phase flow, Chemical Engineering Science, Vol. 50, No. 20, 1995, 3285-3295.

Leifer, I.; Leeuw, G-d.; Kunz, G. and Cohen, L. H. 2003, Calibrating optimal bubble size by the displaced-mass method, Chemical Engineering Science, Vol. 58, 2003, 5211-5216.

Marx, C. Teodoriu, C., Pupazescu, Al., 2001, A New Method to Determine the Stress Distribution in Conical Shouldering Thread Connections, DGMK-Frühjahrstagung, 2001.

Oudeman, P. 1993, Sand Transport and Deposition in Horizontal Multiphase Trunk lines of Sub-sea Satellite Developments, SPE 25142.

Sager, J. A 1986, Contribution to the Determination of the Stress Distribution in Shouldered Threaded Connections under Axial Load, ITE.

Sakaguchi, T.; Minagawa, H. and Tomiyama, A. 1997, Slug characteristics and slug modelling of the gas-liquid-solid three-phase slug flow in vertical pipes, Proceedings of the Experimental Heat Transfer, Fluid mechanics and Thermodynamics, Giot, M., Mayinger, F. and Celata, G. P. (editors), 1997, 1137-1144.

Sakaguchi, T.; Minagawa, H.; Sahara, K.; Kato, Y.; Kuroda, N. and Matsumoto, T. 1987, Estimation of volumetric fraction of each phase in gas-liquid-solid three-phase flow, Proceedings of the JSME/ASME Thermal Engineering Joint International Conference, Honolulu, Hawaii, March, 1987.

Sakaguchi, T.; Minagawa, H.; Saibe, T. and Sahara, K. 1988, Estimation of volumetric fraction of each phase in gas-liquid-solid three-phase slug flow, Proceedings of the Japan-US Seminar on Two-phase Flow Dynamics, Ohtsu, Japan, July, 1988.

Sakaguchi, T.; Minagawa, H.; Tomiyama, A. and Shakutshi, H. 1992, Gas-liquid-solid three-phase flow in a vertical pipe, International Video Journal of Engineering Research, Vol. 2, 1992, 37-45.

Sakaguchi, T.; Shakutsui, H.; Tomiyama, A.; Minagawa, H. and Takahashi, H. 1991, Flow characteristics of gas-liquid-solid three-phase bubbly flow in vertical pipes, proceedings of the 1st JSME/ASME Joint International Conference on Nuclear Engineering, Tokyo, Japan, November, 1991.

Salama, M. M. 1998, Sand Production Management", OTC 8900, Houston, 4-7 May 1998.

Shen, I.; Johnson, F. and Leckner, B. 2003, Digital image analysis of hydrodynamic two-dimensional bubbling fluidized beds, Chemical Engineering Science, Vol. 59, 2003, 2607-2617.

Stevenson, P. 2001, Particle transport in pipes by two-phase flows, Ph.D. Thesis, University of Cambridge, Cambridge, United Kingdom.

Stevenson, P. and Thorpe, R. B. 1999, Towards understanding sand transport in oil flowlines, Proc. 9th Int. Conf. on Multiphase Flow, B.H.R. Group, Cannes,France 16-18 June, 1999.

Stevenson, P. and Thorpe, R. B. 2002, Method calculates sand velocity, hold-up in flowlines, Oil and Gas Journal, 100 (30), 47-50.

Stevenson, P. and Thorpe, R. B. 2003, Energy dissipation at the slug nose and the modeling of solids transport in intermittent flow, Can. J. Chem. Engineering, 81, 271- 278.

Stevenson, P., Kennedy, J.E. and Thorpe, R. B. Prediction of sand behaviour in intermittent flow using the long slug approximation, Proc. 12th Int. Conf. on Multiphase Technology, B.H.R. Group, Bantif, Canada, 2002

Stevenson, P.; Thorpe, R. B.; Kennedy, J. E. and McDermott, C. 2001, The transport of particles at low loading in near-horizontal pipes by intermittent flow, Chemical Engineering Science, 56, 2149-2159.

Stevenson, P.; Thorpe, R. B.; Kennedy, J. E. and McDermott, C. 2001, The similarity of sand transport by slug flow and hydraulic conveying, Proc. 10th Int. Conf. on Multiphase Flow, B.H.R. Group, Cannes, France 13-15 June 2001.

Teodoriu, C. 2003, Analysis of the make-up procedure and evaluation of conical shouldered connections, Ph.D. Thesis, Institute of Petroleum Engineering, Technical University Clausthal.

Tronvoll, J.; Dusseault, M. ; Sanfilippo, F. and Santarelli, F. J. 2001, The Tools of Sand Management, Annual Tech. Conf. and Exhibition, New Orleans, Louisiana, 30 Sept. -3 Oct. 2001.

Wicks, M. 1971, Advances in solid-liquid flow in pipes and its application. Ed. Zandi, I. Pergamon Press, 101-124.

Ulmanu, V. 1973, Ph.D. Thesis, Universitatea Petrol-Gaze, Ploiesti.

***, API RECOMMENDED PRACTICE 7A1 (RP 7A1) Recommended practice for testing of thread compound for rotary connections, American Petroleum Institute, first edition , 1992

***, API RECOMMENDED PRACTICE 7G (RP 7G), 1992

Appendix 1:

List of papers and other publications

Chapters in Books

1. Delgado, J. C.; Schubert, J. J.; **Teodoriu, C.** — OFFSHORE DRILLING AND PRODUCTION, prepared for ENCYCLOPEDIA OF LIFE SUPPORT SYSTEMS (EOLSS) by UNESCO, online since 2010.

Journal Papers

2. **Teodoriu, C.**; Reichetseder, P.; Marx, C.; Kinzel, H. — An introduction to Intelligent Make-up facilities: Analysis of Torque-Turn Recordings to make-up Rotary-Shouldered-Connections (RSC), Oil and Gas Magazine, 4/2002, ISSN 0342-5622.

3. Ulmanu, V.; **Teodoriu, C.** — Fatigue Life prediction and Test Results of Casing Threaded Connection, Mecanica Ruperii, Buletinul ARMR, No. 17, July 2005, ISSN14538148.

4. Reinicke, K. M.; **Teodoriu, C.** — Neue Entwicklungen in der Bohrtechnik, Akademie der Geowissenschaften zu Hannover Veröffentlichungen, Heft 25, 2005, ISBN 3-510-95943-4.

5. **Teodoriu, C.** — Buttress Connection Resistance under Extreme Axial Compression Loads, Oil and Gas Magazine, 4/2005, Volume 31, ISSN 0342-5622.

6. Bello, O. O.; Reinicke, K. M.; **Teodoriu, C.** — Particle Holdup Profiles in Horizontal Gas-Liquid-Solid Multiphase Flow Pipeline, Chemical Engineering &Technology, Vol 28, No. 12, November 2005, ISSN 0930-7516.

7. Falcone, G.; Harrison, B.; **Teodoriu C.** — Can We Be More Efficient in Oil and Gas Exploitation? A Review of the Shortcomings of Recovery Factor and the Need for an Open Worldwide Production Database, Scientific Journals International, Journal of Physical and Natural Sciences, Volume 1, Issue 2, 2007.

8. Falcone, G.; **Teodoriu, C.**; Reinicke, K. M.; Bello, O. O. — Multiphase Flow Modeling Based on Experimental Testing: A Comprehensive Overview of Research Facilities Worldwide and the Need for Future Developments, (original SPE 110116) SPE Projects, Facilities & Construction, Volume 3, Number 3, September 2008, pp.1-10.

9. **Teodoriu, C.**; Falcone, G. — Increasing Geothermal Energy Demand: the Need for Urbanization of the Drilling Industry, Bulletin of Science, Technology & Society 2008, volume 28, No. 3, Special Issue, Part 2: The Age of Alternative Energy: Is the Future Renewable?, DOI:10.1177/0270467608315531, 16 April 2008.

10. Surendra, M.; Falcone, G.; **Teodoriu, C**. — Investigation of Swirl Flows Applied to the Oil and Gas Industry, (original SPE 115938), accepted in August 2008 for publication in the SPE Projects, Facilities & Construction Journal.

11. **Teodoriu, C.**; — Comparing completion design in hydrocarbon and geothermal

Falcone, G. wells: the need to evaluate the integrity of casing connections subject to thermal stresses, Geothermics journal, doi:10.1016/ j.geothermics.2008.11.006, 9 January 2009.

12. **Teodoriu, C.**; Badicioiu, M. Sealing Capacity of API Connections - Theoretical and Experimental Results, SPE 106849, SPE Drilling and Completion Journal, March 2009.

13. Ulmanu, V.; **Teodoriu, C.**; Marx, C.; Pupazescu, A. Untersuchung zur Belastbarkeit von SLIMHOLE-Bohrgestänge mit Doppelschulter, Erdöl, Erdgas, Kohle, Heft X, 125 Jg. 2009.

14. Park, H. Y.; Falcone, G.; **Teodoriu, C.** Decision matrix for liquid loading in gas wells for cost/benefit analyses of lifting options, Journal of Natural Gas Science and Engineering, June 2008.

15. **Teodoriu, C.** Rotary-Shouldered Connections Make-up Torque Calculation Considering the Effect of Contact Pressure on Thread Compound's Friction Coefficient; OIL GAS European Magazine 4/2009.

16. Falcone, G.; Chava, G.; **Teodoriu. C.** "Plunger Lift Modeling Toward Efficient Liquid Unloading in Gas Wells", SPE Projects, Facilities & Construction Journal, March 2010.

17. Fernandez, J.; Falcone, G.; **Teodoriu, C.** "Design of a High-Pressure Research Flow Loop for the Experimental Investigation of Liquid Loading in Gas Wells", SPE Projects, Facilities & Construction Journal, June 2010.

18. Zhang, H.; Falcone, G.; **Teodoriu, C.** "Modeling Fully-Transient Two-phase Flow in the Near-Wellbore Region During Liquid Loading in Gas Wells", accepted in April 2010 for publication in the Journal of Natural Gas Science & Engineering.

19. Limpasurat, A.; Falcone, G.; **Teodoriu, C.**; Barrufet, M. A.; Bello, O. O. "Artificial Geothermal Energy Potential of Steam-Flooded Heavy Oil Reservoirs", accepted in February 2010 for publication in the Int. J. Oil, Gas and Coal Technology.

20. Davani, E.; Ling, K.; **Teodoriu, C.**; McCain, W. D.; Falcone, G. "Accurate Gas-Viscosity Correlation for Use at HP/HT Conditions Ensures Better Reserves Estimation", Journal of Petroleum Technology (JPT), April 2010.

Full Peer-reviewed Conference Papers

21. Bello, O.; Reinicke, K. M.; **Teodoriu, C.** — Measurement of sand velocity and hold-up distributions in multiphase pipeline flow using digital image analysis techniques, Proceeding of the BHRI Multiphase Production Technology Conference 2005, Barcelona, Spain, Volume 1, May 25-27, 2005, pp. 171-189.

22. Bello, O. O.; Reinicke, K. M.; **Teodoriu, C.** — Experimental Study on Particle Behavior in a Simulated Gas-Oil-Sand Multiphase Production and Transfer Operation. Proceedings of the 2006 ASME Joint US - European Fluids Engineering Division Summer Meeting and Exhibition, FEDSM2006-98353, Miami, FL, USA, July 17-20 2006.

23. **Teodoriu, C.**; Ohla, K.; Nielsen, W. — The future of environmental riserless drilling: dope free drill pipe connections using thread saver technology, OMAE-29459, The 26th International Conference on Offshore Mechanics and Arctic Engineering, San Diego, California, USA, June 10-15, 2007.

24. **Teodoriu, C.;** Kinzel, H.; Schubert, J. — Evaluation of Real Time Torque-Turn Charts with Application to Intelligent Make-up Solutions, OMAE2007-29518, The 26th International Conference on Offshore Mechanics and Arctic Engineering, San Diego, California, USA, June 10-15, 2007.

25. **Teodoriu, C.**; McDonald, H.; Bolfrass, C. — Friction Considerations in Rotary Shouldered Threaded Connections, OMAE2007-29583, The 26th International Conference on Offshore Mechanics and Arctic Engineering, San Diego, California, USA, June 10-15, 2007.

26. Bello, O. O.; Falcone, G.; **Teodoriu, C.** — Experimental Validation of Multiphase Flow Models and Testing of Multiphase Flow Meters: a Critical Review of Flow Loops Worldwide, International Multiphase Flow Conference and Exhibition 2007, Bologna, 2007.

27. **Teodoriu, C.**; Falcone, G.; Espinel, A. — Letting Off Steam and Getting Into Hot Water – Harnessing the Geothermal Energy Potential of Heavy Oil Reservoirs, World Energy Congress 2007, ROME 2007.

28. Solomon, F.; Falcone, G.; **Teodoriu, C.** — The Need to Understand the Dynamic Interaction Between Wellbore and Reservoir in Liquid Loaded Gas Wells, 27th International Conference on Offshore Mechanics and Arctic Engineering (OMAE 2008), Estoril, Portugal, 15-20 June 2008.

29. **Teodoriu, C.**; Falcone, G. — Investigation of Drilling Problems in Gas Hydrate Formations, 27th International Conference on Offshore Mechanics and Arctic Engineering (OMAE 2008), Estoril, Portugal, 15-20 June 2008.

Conferences

30. **Teodoriu, C.**; Dinulescu, V. — Study of Casing Loads in Steam Stimulated Wells, ICPT Campina, 1997.

31. **Teodoriu, C.**; Dinulescu, V. — A Discussion about Casing Performance Under Thermal Cycling Conditions, The first Huf'n'Puff Project in Romania, ICPT Campina, 1997.

32. Ene, C. D.; **Teodoriu, C.**; Arvunescu, M. — About Kinematics of Reciprocal Pumps without Pulsation, Bul. Universitatii „Petrol-Gaze" Ploiesti, Vol. XLVII, Nr. 6, 1998.

33. Popovici, A.; Ene, C. D.; Olteanu, M.; **Teodoriu, C.** — Developing a Dynamical Model of a Sonic Pump Unit, Bul. Universitatii „Petrol-Gaze" Ploiesti, Vol. XLVII, Nr. 6, 1998.

34. Marx, C.; **Teodoriu, C.**; Pupazescu, A. — A new method to determine the stress distribution in conical shouldering thread connections, DGMK, Frühjahrstagung, 22./23. April 2002, Band 1, ISBN 3-931850-90-0, ISSN 1433-9013.

35. **Teodoriu, C.**; Reichetseder, P. — A review of analytical calculation of shouldered connections, DGMK, Frühjahrstagung, 28./29. April 2003, Band 1, ISBN 3-936418-03-9, ISSN 1433-9013.

36. **Teodoriu, C.**; Reichetseder, P.; Marx, C.; Kinzel, H. — Analysis of Torque-Turn Recordings to make-up Rotary-Shouldered-Connections (RSC), DGMK, Frühjahrstagung, 28./29. April 2003, Band 1, ISBN 3-936418-03-9, ISSN 1433-9013.

37. Popa, A.; **Teodoriu, C.**; Reichesteder, P. — Data management for small research network, SPC-2003, "Petroleum-Gas" University of Ploiesti, 8th- 9th October 2003.

38. **Teodoriu, C.**; Popa, A.; Reichetseder, P. — Data Acquisition system for real-time strain gauge, measurement using DASYLab, SPC-2003,"Petroleum-Gas" University of Ploiesti, 8th- 9th October 2003.

39. **Teodoriu, C.** — Contact pressure distribution on the thread flank of shouldered threaded connections using finite element analysis, DGMK Tagungsbericht 2004-2, Frühjahrstagung, 29./30. April 2004, ISBN 3-936418-17-9, ISSN 1433-9013.

40. **Teodoriu, C.**; Marx, C.; Reichetseder, P. — Analytical method to determine stress distribution in rotary shouldered connections, DGMK Tagungsbericht 2004-2, Frühjahrstagung, 29./30. April 2004, ISBN 3-936418-17-9, ISSN 1433-9013.

41. Ghofrani, R.; **Teodoriu, C.**; Stekolschikov, K. — Swelling cement induced forces and experimental swelling pressure, DGMK Tagungsbericht 2004-2, Frühjahrstagung, 29./30. April 2004, ISBN 3-936418-17-9, ISSN 1433-9013.

42. Pisarski, P.; Reichetseder, P.; **Teodoriu, C.**; Lieser, D. — Die Simulation des nicht-isothermen Gasdurchflusses in Pipelines mit der Berücksichtigung des Wärmespeichereffekts der Rohrumgebung, DGMK Tagungsbericht 2004-2, Frühjahrstagung, 29./30. April 2004, ISBN 3-936418-17-9, ISSN 1433-9013.

43. Ulmanu, V.; **Teodoriu, C.** — Experimental Stress Analysis on a Double Shoulder Connection, 10th International Symposium on experimental Stress Analysis and Material Testing, Sibiu, Romania, 22-23 OCTOBER 2004.

44. **Teodoriu, C.**; Kinzel, H. — The Application of an Analytical model for the Controlled Make-up of Rotary Shouldered Connections in the Field, SPE Asia-Pacific Conference 2005, SPE 93777.

45. Bello, O. O.; Reinicke, K. M.; **Teodoriu C.** — Evaluation of the modes of transporting sand under conditions analogous to oil-gas multiphase pipeline system, DGMK Tagungsbericht 2005-1, Frühjahrstagung, 29./30. April 2005, ISBN 3-936418-17-9, ISSN 1433-9013.

46. Popa, A.; **Teodoriu, C.** — Sistem de ceasuri dinamice pentru cronometrarea experimenttelor multiple, SPC-2005,"Petroleum-Gas" University of Ploiesti, 11th- 13th May 2005.

47. **Teodoriu, C.**; Popa, A.; Reinicke, K. M.; Rothfuss, M. — Implementation of an online monitoring system for the ITE Center for testing oilfield country tubular goods, SPC-2005, "Petroleum-Gas" University of Ploiesti, 11th- 13th May 2005.

48. **Teodoriu, C.**; Popa, A.; Klaws, M. — Optical system for leak measurement of PREMIUM threaded connections, SPC-2006,"Petroleum-Gas" University of Ploiesti, 17th- 19th May 2006.

49. **Teodoriu, C.**; Patil, P**.** — Evaluation of Surface Casing Resistance having Corrosion Damage, DGMK Tagungsbericht 2006-1, Frühjahrstagung, 29./30. April 2006, ISBN 3-936418-48-9, ISSN 1433-9013.

50. Ulmanu, V.; Badicioiu, M.; **Teodoriu, C.** — Laboratory for Testing Full Scale Oil Country Tubular Goods Subjected to Complex Loads, UPG Bulletin, 2006.

51. Badicioiu, M.; **Teodoriu, C.** — Sealing Capacity of API Connections - Theoretical and Experimental Results, SPE 106849, 2007 SPE Production and Operations Symposium held in Oklahoma City, Oklahoma, U.S.A., 31 March – 3 April 2007.

52. **Teodoriu, C.**; Schubert, J. — Redefining the OCTG Fatigue – A Theoretical Approach, 2007 Offshore Technology Conference held in Houston, Texas, U.S.A., 30 April – 3 May 2007.

53. **Teodoriu, C.**; Falcone, G. — How real-time monitoring technology will change the future of laboratory classes, Teaching with Technology Conference 2007, Held at Texas A&M University, College Station, 2007.

54. Falcone, G.; **Teodoriu, C.**; Reinicke, K. M.; Bello, O. O. — Multiphase Flow Modeling Based on Experimental Testing: a Comprehensive Overview of Research Facilities Worldwide and the Need for Future Developments, ATCE 2007.

55. **Teodoriu, C.**; Reinicke, K. M.; Holzmann, J.; Klaws, M. — Testing of Tubular Goods – a Critical Review of Past and Actual Testing Procedures, DGMK Tagungsbericht 2005-1, Frühjahrs-tagung, 28./29. April 2007.

56. **Teodoriu, C.**; Falcone, G. — Low cost completion for steam injections wells: theoretical and experimental results, 150 Years of the Romanian Petroleum Industry: Tradition & Challenges, Bucharest, 14-17 October 2007.

57. **Teodoriu, C.**; Ulmanu, V.**;** Badicioiu, M. — Casing Fatigue Life Prediction using Local Stress Concept: Theoretical and Experimental Results, 150 Years of the Romanian Petroleum Industry: Tradition & Challenges, Bucharest, 14-17 October 2007.

58. Haghshenas, A.; Amani, M.; **Teodoriu, C.** — Feasibility Study of Steam Injection in one of Iranian Naturally Fractured Heavy Oil Fields, 150 Years of the Romanian Petroleum Industry: Tradition & Challenges, Bucharest, 14-17 October 2007.

59. Paknejad, A.; Schubert, J.; **Teodoriu, C.**; Amani, M. — Sensitivity Analysis of Key Parameters in Foam Drilling Operations, 150 Years of the Romanian Petroleum Industry: Tradition & Challenges, Bucharest, 14-17 October 2007.

60. **Teodoriu C.**; Falcone, G. — Fatigue Life Prediction of Buttress Casing Connection Exposed to Large Temperature Variations, 33rd Stanford Workshop on Geothermal Reservoir Engineering, Fisher Conference Center on the Stanford University campus, 28-30 January 2008.

61. **Teodoriu, C.**; Falcone, G. — Comparison of Well Completions used in Oil/Gas Wells and Geothermal Wells: a New Approach to Technology Transfer, 33rd Stanford Workshop on Geothermal Reservoir Engineering, 28-30 January 2008, Fisher Conference Center on the Stanford University campus.

62. **Teodoriu, C.**; Ulmanu, V.; Badicioiu, M. — Casing Fatigue Life Prediction Using Local Stress Concept: Theoretical and Experimental Results, SPE 110785, 2008 SPE Western Regional Meeting held 31-MAR to 02-APR-08 in Los Angeles, CA., 2008.

63. **Teodoriu, C.**; Falcone, G. — Low-Cost Completion for Steam Injections Wells: Theoretical and Experimental Results, SPE 110454, 2008 SPE Improved Oil Recovery Symposium to be held 21 to 23 APR 2008 in Tulsa, OK., 2008.

64. **Teodoriu C.**; Falcone, G. — Oil and Gas expertise for Geothermal Exploitation: the Need for Technology Transfer", SPE 113852, SPE EUROPEC Conference, ROME 2007.

65. Ibeh, C.; Schubert, J.; **Teodoriu, C.** — Methodology for Testing Drilling Fluids under Extreme HP/HT Conditions, AADE 2008 conference held April 8-9, 2008 at the Hilton (formerly Wyndham) Greenspoint Hotel in Houston, Texas, 2008.

66. Ibeh, C.; **Teodoriu, C.**; Schubert, J.; Gusler, W.; Harvey, F. — Investigation on the Effects of Ultra-High Pressure and Temperature on the Rheological Properties of Oil-Based Drilling Fluids, AADE 2008 conference to be held April 8-9, 2008 at the Hilton (formerly Wyndham) Greenspoint Hotel in Houston, Texas, 2008.

67. **Teodoriu, C.**; Schubert, J.; Vivek, G,; Ibeh, C. — Investigations to Determine the Drilling Fluid Rheology Using Constant Shear Rate Conditions, presented at the SPE IADC conference, held in Berlin, Germany, June, 2008.

68. Chava, G.; Falcone, G.; **Teodoriu, C.** — Development of a New Plunger-Lift Model Using Smart Plunger Data, SPE 115934, presented at the 2008 SPE Annual Technical Conference and Exhibition, Denver, Colorado, U.S.A., 21-24 September 2008.

69. Surendra, M.; Falcone, G.; **Teodoriu, C.** — Investigation of Swirl Flows Applied to the Oil and Gas Industry, SPE 115938, presented at the 2008 SPE Annual Technical Conference and Exhibition, Denver, Colorado, U.S.A., 21-24 September 2008.

70. Solomon, F.; Falcone, G.; **Teodoriu, C.** — Critical Review of Existing Solutions to Predict and Model Liquid Loading in Gas Wells, SPE 115933, presented at the 2008 SPE Annual Technical Conference and Exhibition, Denver, Colorado, U.S.A., 21-24 September 2008.

71. Fernandez, J.; Falcone, G.; **Teodoriu, C.** — Design of a High-Pressure Research Flow Loop for the Experimental Investigation of Liquid Loading in Gas Wells, SPE-122786-MS, presented at the 2009 SPE Latin American & Caribbean Petroleum Engineering Conference to be held 31-May-09 to 03-Jun-09 in Cartagena, Colombia, 2009.

72. Zhang, H.; Falcone, G.; Valko, P.; **Teodoriu, C.** — Numerical Modeling of Fully-Transient Flow in the Near-Wellbore Region During Liquid Loading in Gas Wells, SPE-122785-MS, presented at the 2009 SPE Latin American & Caribbean Petroleum Engineering Conference to be held 31-May-09 to 03-Jun-09 in Cartagena, Colombia, 2009.

73. Ehsan, D.; Kegang, L.; **Teodoriu, C.**; McCain, W. D.; Falcone, G. — Inaccurate Gas Viscosity at HP/HT Conditions and its Effect on Unconventional Gas Reserves Estimation, SPE-122827-MS, presented at the 2009 SPE Latin American & Caribbean Petroleum Engineering Conference to be held 31-May-09 to 03-Jun-09 in Cartagena, Colombia, 2009.

74. **Teodoriu, C.**; Reinicke, K. M.; Falcone, G. — Real-Time Long Distance Teaching: An Overview of Two Years of Tele-Teaching between Texas and Germany, SPE 124748, paper was prepared for presentation at the 2009 SPE Annual Technical Conference and Exhibition held in New Orleans, Louisiana, USA, 4–7 October 2009.

75. Ehsan, D.; Kegang, L.; **Teodoriu, C**.; McCain, W. D. Jr.; Falcone, G. — More Accurate Gas Viscosity Correlation for Use at HPHT Conditions Ensures Better Reserves Estimation, SPE 124734, This paper was prepared for presentation at the 2009 SPE Annual Technical Conference and Exhibition held in New Orleans, Louisiana, USA, 4–7 October 2009.

76. Chava, G.; Falcone, G.; **Teodoriu, C.** — Plunger Lift Modeling Towards Efficient Liquid Unloading in Gas Wells, SPE 124515, This paper was prepared for presentation at the 2009 SPE Annual Technical Conference and Exhibition held in New Orleans, Louisiana, USA, 4–7 October 2009.

77. Chava, G.; Falcone, G.; **Teodoriu, C.** — Use of Integrated Electronic and Sensors to Improve Plunger Lift Modeling Towards Efficient Liquid Unloading in Gas Wells, DGMK/ÖGEW-Frühjahrstagung 2009, 27./28. April 2009.

78. **Teodoriu, C.**; Falcone, G.; Fichter, C. — Drilling Beyond Oil and Gas: a Discussion about How Technology will Change to Enhance Drilling in Urban Areas, DGMK/ÖGEW-Frühjahrstagung 2009, 27./28. April 2009.

79. Ling, K.; **Teodoriu, C**.; Ehsan, D.; Falcone, G. — "Measurement of Gas Viscosity at High Pressures and High Temperatures", International Petroleum Technology Conference, Doha, Qatar, 7–9 December 2009.

80. Reinicke, K. R.; Ostermeyer, G. P.; Overmeyer, L.; **Teodoriu C.**; Thomas, R. — Der Niedersächsische Forschungsverbund Geothermie und Hochleistungsbohrtechnik (gebo), Energie und Rohstoffe 2009, Goslar, 2009.

81. Popa, A.; **Teodoriu, C.** — Automatic Test Facility for the Wellbore Cement Integrity, 6th International Symposium on Process Control, SPC-2009, Ploiesti, June 1 – 3, 2009.

82. Popa, A.; **Teodoriu, C.**; Popa, C. — Analysis of the Nonlinearities in the Hydraulic Actuators 6th International Symposium on Process Control, SPC-2009, Ploiesti, June 1 – 3, 2009.

83. Fichter, C.; Reinicke, K. M.; **Teodoriu, C.** — Tiefbohrtechnik – Erschließung von tiefgeothermischen Wärmespeichern, GeoTHERM 2009, Offenburg, April 2009.

84. **Teodoriu, C.**; Fichter, C.; Falcone, G. — Drilling Deep Geothermal Reservoirs: the Future of Oil and Gas Business, Beitrag "Der Geothermiekongress 2009" Bochum, Germany, 17.-19. November 2009.

85. Fichter, C.; Reinicke, K. M.; **Teodoriu, C.**; Wang, Y.; Lotz, U. — Influences and limiting parameters of casing design on the success of hydrogeothermal projects - a new approach for the design of geothermal wells, Beitrag "Der Geothermiekongress 2009" Bochum, Germany, 17.-19. November 2009.

86. **Teodoriu, C.**; Reinicke, K. M.; Fichter, C.; Wehling, P. — Investigations on Casing-Cement Interaction with Application to Gas and CO_2 Storage Wells, SPE 131336, EUROPEC/EAGE Annual Conference and Exhibition held in Barcelona, Spain, 14–17 June 2010.

87. **Teodoriu, C.**; Ugwu, I.; Schubert, J. — Estimation of Casing-Cement-Formation Interaction using a new Analytical Model, SPE131335, SPE EUROPEC/EAGE Annual Conference and Exhibition held in Barcelona, Spain, 14–17 June 2010.

88. Khabibullin,T.; Falcone, G.; **Teodoriu, C.**; Bello, O. O. — "Drilling through Gas Hydrate Sediments: Managing Wellbore Instability Risks", SPE EUROPEC/EAGE Annual Conference and Exhibition held in Barcelona, Spain, 14–17 June 2010.

89. **Teodoriu, C.**; Fichter, C. — Anpassung der Tiefbohrtechnik aus der Erdöl-/Erdgasindustrie an die Tiefengeothermie, 3. Fachtagung, Geothermische Technologien – Technologien zur Nutzung der tiefen Geothermie und ihre Integration in Energieversorgungssysteme, 23./24. März 2010.

90. Gedzius, I.; **Teodoriu, C.**; Fichter, C.; Reinicke, K. M. — Betrachtung von Korrosionsschäden an Casings im Primärkreislauf geothermischer Anlagen, DGMK/ÖGEW-Frühjahrstagung 2010, Fachbereich Aufsuchung und Gewinnung, Celle, 12./13. April 2010.

91. Pilisi,N.; — An Advisory System for Selecting Drilling Technologies and

	Teodoriu, C.	Methods with Application for Tight Gas Reservoirs, DGMK/ÖGEW-Frühjahrstagung 2010, Fachbereich Aufsuchung und Gewinnung, Celle, 12./13. April 2010.
92.	Bai, M.; Fichter, C.; **Teodoriu, C.**; Reinicke, K. M.	Development of a Novel Testing Method to Perform Investigations on Rock-Fluid Interaction under Geothermal Hot Dry Rock Conditions, DGMK/ÖGEW-Frühjahrstagung 2010, Fachbereich Aufsuchung und Gewinnung, Celle, 12./13. April 2010.
93.	**Teodoriu, C.**; Baruffet, M.; Epps, M.L.; Falcone, G.; Reinicke, K. M.	Real-Time Long Distance Teaching: The Texas A&M DL Experience, ATCE 2010, Florence, Italy, Sept. 2010.
94.	**Teodoriu, C.**	Hands-on Teaching as Part of Petroleum Engineers Education: An International Experience, ATCE 2010, Florence, Italy, Sept. 2010.
95.	Reinicke, K. M.; Oppelt, J.; Ostermeyer, G. P.; Overmeyer, L.; **Teodoriu, C.**; Thomas, R.	Enhanced technology transfer for geothermal exploitation through a new research concept: The Geothermal Energy and High Performance Drilling Research Program – gebo, ATCE 2010, Florence, Italy, Sept. 2010.
96.	Bello, O. O.; Falcone, G.; **Teodoriu, C.**; Udong, I.	“Hydraulic Analysis of Gas-Oil-Sand Flow in Horizontal Wells”, SPE 136874 to be presented at the SPE Latin American & Caribbean Petroleum Engineering Conference, Lima, Peru, 1–3 December 2010.
97.	Zhang, H.; Falcone, G.; Valko, P.; **Teodoriu, C.**	"Relative Permeability Hysteresis Effects in the Near-Wellbore Region During Liquid Loading in Gas Wells", SPE 139062 to be presented at the SPE Latin American & Caribbean Petroleum Engineering Conference, Lima, Peru, 1–3 December 2010.
98.	Limpasurat, A.; Falcone, G.; **Teodoriu, C.**; Barrufet, M.	“Unconventional Heavy-Oil Exploitation for Waste Energy Recovery”, SPE 139054 to be presented at the SPE Latin American & Caribbean Petroleum Engineering Conference, Lima, Peru, 1–3 December 2010.

Submitted papers, currently under review

99.	Bello, O. O.; Falcone, G.; **Teodoriu, C.**; Udong, I.	“Optimizing Two-Phase Oil-Sand Flow through a Horizontal Well”, submitted to the Oil & Gas Science and Technology - Revue de l'IFP in December 2009.

100. Khabibullin,T.; Falcone, G.; **Teodoriu, C.**; Bello, O. O. — "Drilling through Gas Hydrate Sediments: Managing Wellbore Instability Risks", submitted to the SPE Drilling & Completion journal in March 2010.

101. Limpasurat, A.; Falcone, G.; **Teodoriu, C.**; Barrufet, M. A.; Bello, O. O. — "Artificial Geothermal Energy Potential of Steam-Flooded Heavy Oil Reservoirs", accepted in February 2010 for publication in the Int. J. Oil, Gas and Coal Technology.

Invited Speaker and Presentations to Industry Boards

102. **Teodoriu, C.** — Formation damage and stimulation, held at the "Industry meets University" Workshop, Institute of Petroleum Engineering, TU-Clausthal, Germany, 06.02.2004.

103. **Teodoriu, C.** — Introduction to Intelligent Make-up Facilities, German Section of SPE, ITE, TU Clausthal, 25. June 2004.

104. **Teodoriu, C.** — Tiefpumpen, eine Übersicht über Bauarten und Anwendungen, presentation at the Tiefpumpen Workshop, held in Karlsruhe, 06.07.2005.

105. **Teodoriu, C.** — Use of Analytical Models for the Development of Intelligent Make-up Machines, held at Texas A&M, Department of Petroelum Engineering, J. L. "Corky" Frank '58 Graduate Seminar Series, 14 Nov. 2006.

106. **Teodoriu, C.**; Falcone, G. — The future of laboratory classes: virtual and remote controlled experiments using real-time monitoring and web integrated approaches, held at Texas A&M, Department of Petroleum Engineering, J. L. "Corky" Frank '58, Graduate Seminar Series, 13 Feb. 2007.

107. **Teodoriu, C.** — Well Construction 2020+, SPE 2008 Forum Series, held in Dubrovnik, Croatia, invited as discussion leader for Cultural Changes and Human Resources Session, 14-19 September 2008.

108. Reinicke, K. M.; Ostermeyer, G. P.; Overmeyer, L.; **Teodoriu C.**; Thomas, R. — Der Niedersächsische Forschungsverbund Geothermie und Hochleistungsbohrtechnik (gebo), HotSpot Geothermietag, Hannover, 29.10.2009.

109. **Teodoriu, C.** Intelligent Oil Country Tubular Goods Make-up: An Alternative to Increase Tubular Reliability, BERG- UND HÜTTENMÄNNISCHER TAG, Freiberger Forschungsforum „Ressourcen für die Zukunft“ 17.-19.06.2009.

Industry Seminars and short-courses

1. Reichetseder, P.; **Teodoriu, C.** Kurz-Seminar, Petroleum Production Engineering, at J. H. Bornemann GmbH, Obernkirchen, 9. Sept. 2003.
2. **Teodoriu, C.** Kurz-Seminar, Oil Production Systems, at BASF, Ludwigshafen, May 2006.
3. **Teodoriu, C.** Short Seminar, Drill String mechanics, Perforator GmbH, Walkenried, Germany, April 2006.
4. **Teodoriu, C.** Short Seminar, Drill String mechanics, Weatherford Oil Tools GmbH, Germany, April 2006.
5. **Teodoriu, C.** Stuck pipe course, on behalf of NExT Training Center for PETROM S.A., Ploiesti, Romania, June and Nov. 2007.
6. **Teodoriu, C.** Drilling Hydraulics, on behalf of NExT Training Center for PETROM S.A., Ploiesti, Romania, May 2008.
7. **Teodoriu, C.** Casing Design, on behalf of NExT Training Center for PETROM S.A., Ploiesti, Romania, May 2008.
8. **Teodoriu, C.** Directional and Horizontal drilling, on behalf of NExT Training Center for PETROM S.A., Ploiesti, Romania, May 2008.
9. **Teodoriu, C.** Drill string Mechanics, on behalf of NExT Training Center for PETROM S.A., Ploiesti, Romania, June 2008.
10. **Teodoriu, C.** Drilling Summer School, held at TU Clausthal, 2005 to 2010.

Appendix 2:

List of Papers grouped by Subject

Drilling and completion

Equipment, processes, special procedures (i.e. horizontal drilling)

Peer-reviewed Journals

1. **Teodoriu, C.** — Rotary-Shouldered Connections Make-up Torque Calculation Considering the Effect of Contact Pressure on Thread Compound's Friction Coefficient; OIL GAS European Magazine 4/2009.

Conferences

2. Paknejad, A.; Schubert, J.; **Teodoriu, C.**; Amani, M. — Sensitivity Analysis of Key Parameters in Foam Drilling Operations, 150 Years of the Romanian Petroleum Industry: Tradition & Challenges, Bucharest, 14 -17 October 2007.

3. **Teodoriu, C.**; Kinzel, H. — The Application of an Analytical model for the Controlled Make-up of Rotary Shouldered Connections in the Field, SPE 93777, SPE Asia-Pacific Conference 2005.

4. **Teodoriu, C.**; Reichetseder, P.; Marx, C.; Kinzel, H. — An introduction to Intelligent Make-up facilities: Analysis of Torque-Turn Recordings to make-up Rotary-Shouldered-Connections (RSC), Oil and Gas Magazine, 4/2002, ISSN 0342-5622.

5. Pilisi, N.; **Teodoriu, C.** — An Advisory System for Selecting Drilling Technologies and Methods with Application for Tight Gas Reservoirs, DGMK/ ÖGEW-Frühjahrstagung 2010, Fachbereich Aufsuchung und Gewinnung, Celle, 12./13. April 2010.

6. Bai, M.; Fichter, C.; **Teodoriu**, **C.**; Reinicke, K. M. — Development of a Novel Testing Method to Perform Investigations on Rock-Fluid Interaction under Geothermal Hot Dry Rock Conditions, DGMK/ÖGEW-Frühjahrstagung 2010, Fachbereich Aufsuchung und Gewinnung, Celle, 12./13. April 2010.

Critical equipment and components

Peer-reviewed Journals

7. Reinicke, K. M.; **Teodoriu, C.** — Neue Entwicklungen in der Bohrtechnik, Akademie der Geowissenschaften zu Hannover Veröfentlichungen, Heft 25, 2005, ISBN 3-510-95943-4.

8. **Teodoriu, C.** — Buttress Connection Resistance under Extreme Axial Compression Loads, Oil and Gas Magazine, Volume 31, 4/2005, ISSN 0342-5622.

Conferences

9. **Teodoriu, C.**; Schubert, J. — Redefining the OCTG Fatigue – A Theoretical Approach, 2007 Offshore Technology Conference held in Houston, Texas, U.S.A., 30 April–3 May 2007.

10. **Teodoriu, C.**; Reinicke, K. M.; Holzmann, J.; Klaws, M. — Testing of Tubular Goods – a Critical Review of Past and Actual Testing Procedures, DGMK Tagungsbericht 2005-1, Frühjahrstagung, am 28./29. April 2007.

11. **Teodoriu, C.**; Popa, A.; Klaws, M. — Optical system for leak measurement of PREMIUM threaded connections, SPC-2006,"Petroleum-Gas" University of Ploiesti, 17th- 19th May 2006.

12. **Teodoriu, C.**; Patil, P. — Evaluation of Surface Casing Resistance having Corrosion Damage, DGMK Tagungsbericht 2006-1, Frühjahrstagung, 28./29. April 2006, ISBN 3-936418-48-9, ISSN 1433-9013.

13. Ulmanu, V.; Badicioiu, M.; **Teodoriu, C.** — Laboratory for Testing Full Scale Oil Country Tubular Goods Subjected to Complex Loads, UPG Bulletin, 2006.

14. **Teodoriu, C**.; Popa, A.; Reinicke, K. M.; Rothfuss, M. — Implementation of an online monitoring system for the ITE Center for testing oilfield country tubular goods, SPC-2005,"Petroleum-Gas" University of Ploiesti, 11th- 13th May 2005.

15. **Teodoriu, C.** — Contact pressure distribution on the thread flank of shouldered threaded connections using finite element analysis, DGMK Tagungsbericht 2004-2, Frühjahrstagung, 29./30. April 2004, ISBN 3-936418-17-9, ISSN 1433-9013.

16. **Teodoriu, C.**; Marx, C.; Reichetseder, P. — Analytical method to determine stress distribution in rotary shouldered connections, DGMK Tagungsbericht 2004-2, Frühjahrstagung, 28./29. April 2004, ISBN 3-936418-17-9, ISSN 1433-9013.

17. **Teodoriu**, **C.**; Reinicke, K. M.; Fichter, C.; Wehling, P. — Investigations on Casing-Cement Interaction with Application to Gas and CO_2 Storage Wells, SPE 131336, EUROPEC/EAGE Annual Conference and Exhibition to be held in Barcelona, Spain, 14–17 June 2010.

18. **Teodoriu, C.**; Ugwu, I.; Schubert, J. — Estimation of Casing-Cement-Formation Interaction using a new Analytical Model, SPE131335, SPE EUROPEC/EAGE Annual Conference and Exhibition held in Barcelona, Spain, 14–17 June 2010.

Analysis and modeling of operational procedures, well control methods

Peer-reviewed Journals

19. Ulmanu, V.; **Teodoriu, C.**; Marx, C.; Pupazescu, A. — Untersuchung zur Belastbarkeit von SLIMHOLE-Bohrgestänge mit Doppelschulter, Erdöl, Erdgas, Kohle, Heft X, 125 Jg. 2009.

Conferences

20. **Teodoriu, C.**; Ohla, K.; Nielsen, W. — The future of environmental riserless drilling: dope free drill pipe connections using thread saver technology, OMAE-29459, The 26th International Conference on Offshore Mechanics and Arctic Engineering, San Diego, California, USA, June 10-15, 2007.

21. **Teodoriu, C.**; Kinzel, H.; Schubert, J. — Evaluation of Real Time Torque-Turn Charts with Application to Intelligent Make-up Solutions, OMAE2007-29518, The 26th International Conference on Offshore Mechanics and Arctic Engineering, San Diego, California, USA, June 10-15, 2007.

22. **Teodoriu, C.**; McDonald, H.; Bolfrass, C. — Friction Considerations in Rotary Shouldered Threaded Connections, OMAE2007-29583, The 26th International Conference on Offshore Mechanics and Arctic Engineering, San Diego, California, USA, June 10-15, 2007.

23. Ulmanu, V.; **Teodoriu, C.** — Fatigue Life prediction and Test Results of Casing Threaded Connection, Mecanica Ruperii, Buletinul ARMR, No. 17, July 2005, ISSN14538148.

Drilling and cementing fluids
Health, Safety and Environment (HSE) aspects
Thread compounds, fluid rheology, formation damage

Conferences

24. Ibeh, C.; Schubert, J.; **Teodoriu, C.** — Methodology for Testing Drilling Fluids under Extreme HP/HT Conditions, AADE 2008 conference held April 8-9 at the Hilton (formerly Wyndham) Greenspoint Hotel in Houston, Texas, 2008.

25. Ibeh, C.; **Teodoriu, C.**; Schubert, J.; Gusler, W.; Harvey, F. — Investigation on the Effects of Ultra-High Pressure and Temperature on the Rheological Properties of Oil-Based Drilling Fluids, AADE 2008 conference to be held April 8-9 at the Hilton (formerly Wyndham) Greenspoint Hotel in Houston, Texas, 2008.

26. **Teodoriu, C.**; Schubert, J.; Vivek, G.; Ibeh, C. — Investigations to Determine the Drilling Fluid Rheology Using Constant Shear Rate Conditions, presented at the SPE IADC conference, held in Berlin, Germany, June, 2008.

27. Ghofrani, R.; **Teodoriu, C.**; Stekolschikov, K. — Swelling cement induced forces and experimental swelling pressure, DGMK Tagungsbericht 2004-2, Frühjahrstagung, 28./29. April 2004, ISBN 3-936418-17-9, ISSN 1433-9013.

Advanced drilling technology
Geothermal technology

Peer-reviewed Journals

28. **Teodoriu, C.**; Falcone, G. — Increasing Geothermal Energy Demand: the Need for Urbanization of the Drilling Industry, Bulletin of Science, Technology & Society 2008, volume 28, No. 3, Special Issue, Part 2: The Age of Alternative Energy: Is the Future Renewable?, DOI:10.1177/0270467608315531, 16 April 2008.

29. **Teodoriu, C.**; Falcone, G. — Comparing completion design in hydrocarbon and geothermal wells: the need to evaluate the integrity of casing connections subject to thermal stresses, Geothermics journal, doi:10.1016/ j.geothermics.2008.11.006, 9 January 2009.

Conferences

30. **Teodoriu, C.**; Falcone, G.; Fichter, C. — Drilling Beyond Oil and Gas: a Discussion about How Technology will Change to Enhance Drilling in Urban Areas, DGMK/ÖGEW-Frühjahrstagung 2009, Fachbereich Aufsuchung und Gewinnung Celle, 27./28. April 2009.

31. Fichter, C.; Reinicke, K. M.; **Teodoriu, C.** — Tiefbohrtechnik – Erschließung von tiefgeothermischen Wärmespeichern, GeoTHERM 2009, Offenburg, April 2009.

32. **Teodoriu, C.**; Fichter, C.; Falcone, G. — Drilling Deep Geothermal Reservoirs: the Future of Oil and Gas Business, Beitrag “Der Geothermiekongress 2009” Bochum, Germany, 17.-19. November 2009.

33. Fichter, C.; Reinicke, K. M.; **Teodoriu, C.**; Wang, Y.; Lotz, U. — Influences and limiting parameters of casing design on the success of hydrogeothermal projects - a new approach for the design of geothermal wells, Beitrag “Der Geothermiekongress 2009” Bochum, Germany, 17.-19. November 2009.

34. Reinicke, K. M.; Ostermeyer, G. P.; Overmeyer, L.; **Teodoriu, C.**; Thomas, R. — Der Niedersächsische Forschungsverbund Geothermie und Hochleistungsbohrtechnik (gebo), Energie und Rohstoffe 2009, Goslar, 2009.

35. **Teodoriu, C.**; Falcone, G. — Investigation of Drilling Problems in Gas Hydrate Formations, 27th International Conference on Offshore Mechanics and Arctic Engineering (OMAE 2008), Estoril, Portugal, 15-20 June 2008.

36. **Teodoriu, C.**; Falcone, G. — Oil and Gas expertise for Geothermal Exploitation: the Need for Technology Transfer", SPE 113852, SPE EUROPEC Conference, ROME, 2007.

37. **Teodoriu, C.**; Falcone, G. — Fatigue Life Prediction of Buttress Casing Connection Exposed to Large Temperature Variations, 33rd Stanford Workshop on Geothermal Reservoir Engineering, Fisher Conference Center on the Stanford University campus, 28-30 January 2008.

38. **Teodoriu, C.**; Falcone, G. — Comparison of Well Completions used in Oil/Gas Wells and Geothermal Wells: a New Approach to Technology Transfer, 33rd Stanford Workshop on Geothermal Reservoir Engineering, Fisher Conference Center on the Stanford University campus, 28-30 January 2008.

39. **Teodoriu, C.**; Fichter, C. — Anpassung der Tiefbohrtechnik aus der Erdöl-/Erdgasindustrie an die Tiefengeothermie, 3. Fachtagung, Geothermische Technologien, – Technologien zur Nutzung der tiefen Geothermie und ihre Integration in Energieversorgungssysteme, 23./24. März 2010.

40. Gedzius, I.; **Teodoriu, C.**; Fichter, C.; Reinicke, K. M. — Betrachtung von Korrosionsschäden an Casings im Primärkreislauf geothermischer Anlagen, DGMK/ÖGEW-Frühjahrstagung 2010, Fachbereich Aufsuchung und Gewinnung, Celle, 12./13. April 2010.

Advanced teaching and tele-teaching

Conferences

41. **Teodoriu, C.**; Reinicke, K. M.; Falcone, G. — Real-Time Long Distance Teaching: An Overview of Two Years of Tele-Teaching between Texas and Germany, SPE 124748, paper was prepared for presentation at the 2009 SPE Annual Technical Conference and Exhibition held in New Orleans, Louisiana, USA, 4–7 October 2009.

42. **Teodoriu, C.**; Falcone, G. — How real-time monitoring technology will change the future of laboratory classes, Teaching with Technology Conference 2007, Held at Texas A&M University, College Station, 2007.

43. **Teodoriu**, **C.**; Baruffet, M.; Epps, M. L.; Falcone, G.; Reinicke, K. M. — Real-Time Long Distance Teaching: The Texas A&M DL Experience, SPE, paper was accepted for presentation at the 2010 SPE Annual Technical Conference and Exhibition held in Florence, Italy, Sept. 2010.

44. **Teodoriu, C.** — Hands-on Teaching as Part of Petroleum Engineers Education: An International Experience, SPE, paper was accepted for presentation at the 2010 SPE Annual Technical Conference and Exhibition held in Florence, Italy, Sept. 2010.

Production Operations and Workover

Equipment to improve recovery efficiency, multiphase flow in pipelines

Peer-reviewed Journals

45. Falcone, G.; **Teodoriu, C.**; Reinicke, K. M.; Bello, O. O. — Multiphase Flow Modeling Based on Experimental Testing: A Comprehensive Overview of Research Facilities Worldwide and the Need for Future Developments, (original SPE 110116) SPE Projects, Facilities & Construction, Volume 3, Number 3, September 2008, pp.1-10.

46. Bello, O. O.; Reinicke, K. M.; **Teodoriu, C.** — Experimental Study on Particle Behavior in a Simulated Gas-Oil-Sand Multiphase Production and Transfer Operation. Proceedings of the 2006 ASME Joint US - European Fluids Engineering Division Summer Meeting and Exhibition, Miami, FL, USA, July 17-20 2006.

47. Surendra, M.; Falcone, G.; **Teodoriu, C.** — Investigation of Swirl Flows Applied to the Oil and Gas Industry, (original SPE 115938), SPE Projects, Facilities & Construction Journal, August 2008.

48. Bello, O. O.; Reinicke, K. M.; **Teodoriu, C.** — Particle Holdup Profiles in Horizontal Gas-Liquid-Solid Multi-phase Flow Pipeline, Chemical Engineering &Technology, Vol 28, No. 12, November 2005, ISSN 0930-7516.

Conferences

49. Solomon, F.; Falcone, G.; **Teodoriu, C.** — The Need to Understand the Dynamic Interaction Between Wellbore and Reservoir in Liquid Loaded Gas Wells, 27th International Conference on Offshore Mechanics and Arctic Engineering (OMAE 2008), Estoril, Portugal, 15-20 June 2008.

50. **Teodoriu, C.**; Falcone, G. — Low-Cost Completion for Steam Injections Wells: Theoretical and Experimental Results, SPE 110454, 2008 SPE Improved Oil Recovery Symposium to be held 21-APR-08 to 23-APR-08 in Tulsa, OK.

51. Bello, O. O.; Falcone, G.; **Teodoriu, C.** — Experimental Validation of Multiphase Flow Models and Testing of Multiphase Flow Meters: a Critical Review of Flow Loops Worldwide, International Multiphase Flow Conference and Exhibition 2007, Bologna, 2007.

52. Falcone, G.; **Teodoriu, C.**; Reinicke, K. M.; Bello, O. O. — Multiphase Flow Modeling Based on Experimental Testing: a Comprehensive Overview of Research Facilities Worldwide and the Need for Future Developments, ATCE 2007.

53. Ene, C. D.; **Teodoriu, C.**; Arvunescu, M. — About Kinematics of Reciprocal Pumps without Pulsation, Bul. Universitatii „Petrol-Gaze“ Ploiesti, Vol. XLVII, Nr. 6, 1998.

54. Popovici, A.; Ene, C. D.; Olteanu, M.; **Teodoriu, C.** — Developing a Dynamical Model of a Sonic Pump Unit, Bul. Universitatii „Petrol-Gaze“ Ploiesti, Vol. XLVII, Nr. 6, 1998.

Tubular stress and strain, tubular integrity over field life, sealability of tubular components, temperature effects, corrosion issues

Peer-reviewed Journals

55. **Teodoriu, C.**; Ulmanu, V.; Badicioiu, M. — Casing Fatigue Life Prediction Using Local Stress Concept: Theoretical and Experimental Results, SPE 110785, 2008 SPE Western Regional Meeting held in Los Angeles, CA., 31 March to 02 April 2008.

56. **Teodoriu, C.**; Badicioiu, M. — Sealing Capacity of API Connections - Theoretical and Experimental Results, SPE 106849, SPE Drilling and Completion Journal, March 2009.

57. **Teodoriu, C.**; Dinulescu, V. — Study of Casing Loads in Steam Stimulated Wells, ICPT Campina, 1997.

58. **Teodoriu, C.**; Dinulescu V. — A Discussion about Casing Performance Under Thermal Cycling Conditions, The first Huf'n'Puff Project in Romania, ICPT Campina, 1997.

Liquid loading in gas wells

Peer-reviewed Journals

59. Zhang, H.; Falcone, G.; Valko, P.; **Teodoriu, C.** — Numerical Modeling of Fully-Transient Flow in the Near-Wellbore Region During Liquid Loading in Gas Wells, SPE-122785-MS, presented at the 2009 SPE Latin American & Caribbean Petroleum Engineering Conference held in Cartagena, Colombia, 31 May to 03 June 2009.

60. Park, H. Y.; Falcone, G.; **Teodoriu, C.** — Decision matrix for liquid loading in gas wells for cost/benefit analyses of lifting options, submitted to the Journal of Natural Gas Science and Engineering in June 2008.

Conferences

61. Chava, G.; Falcone, G.; **Teodoriu, C**. — Plunger Lift Modeling Towards Efficient Liquid Unloading in Gas Wells, SPE 124515, This paper was prepared for presentation at the 2009 SPE Annual Technical Conference and Exhibition held in New Orleans, Louisiana, USA, 4–7 October 2009.

62. Solomon, F.; Falcone, G.; **Teodoriu, C.** — Critical Review of Existing Solutions to Predict and Model Liquid Loading in Gas Wells, SPE 115933, presented at the 2008 SPE Annual Technical Conference and Exhibition, Denver, Colorado, U.S.A., 21-24 September 2008.

Recovery of hydrocarbons
Optimization of geothermal energy recovery

Peer-reviewed Journals

63. Falcone, G.; Harrison, B.; **Teodoriu, C.** — Can We Be More Efficient in Oil and Gas Exploitation? A Review of the Shortcomings of Recovery Factor and the Need for an Open Worldwide Production Database, Scientific Journals International, Journal of Physical and Natural Sciences, Volume 1, Issue 2, 2007.

Conferences

64. Ehsan, D.; Kegang, L.; **Teodoriu, C.**; McCain, W. D. Jr.; Falcone, G. — More Accurate Gas Viscosity Correlation for Use at HPHT Conditions Ensures Better Reserves Estimation, SPE 124734, This paper was prepared for presentation at the 2009 SPE Annual Technical Conference and Exhibition held in New Orleans, Louisiana, USA, 4–7 October 2009.

65. Davani, E.; Kegang, L.; **Teodoriu, C.**; McCain, W. D.; Falcone, G. — Inaccurate Gas Viscosity at HP/HT Conditions and its Effect on Unconventional Gas Reserves Estimation, SPE-122827-MS, presented at the 2009 SPE Latin American & Caribbean Petroleum Engineering Conference be held in Cartagena, Colombia, 31 May to 03 June 2009.

66. Ehsan, D.; Ling, K.; **Teodoriu, C.**; McCain, W. D. Jr.; Falcone, G. — More Accurate Gas Viscosity Correlation for Use at HPHT Conditions Ensures Better Reserves Estimation, SPE 124734, This paper was prepared for presentation at the 2009 SPE Annual Technical Conference and Exhibition held in New Orleans, Louisiana, USA, 4–7 October 2009.

67. Fernandez, J.; Falcone, G.; **Teodoriu, C.** — Design of a High-Pressure Research Flow Loop for the Experimental Investigation of Liquid Loading in Gas Wells, SPE-122786-MS, presented at the 2009 SPE Latin American & Caribbean Petroleum Engineering Conference to be held in Cartagena, Colombia, 31 May to 03 June 2009.

68. **Teodoriu, C.**; Falcone, G.; Espinel, A. — Letting Off Steam and Getting Into Hot Water – Harnessing the Geothermal Energy Potential of Heavy Oil Reservoirs, World Energy Congress 2007, ROME, 2007.

69. Haghshenas, A.; Amani, M.; **Teodoriu, C.** — Feasibility Study of Steam Injection in one of Iranian Naturally Fractured Heavy Oil Fields, 150 Years of the Romanian Petroleum Industry: Tradition & Challenges, Bucharest, 14 -17 October 2007.

Appendix 3:

List of selected papers for this Habilitation
(Paper full length is presented)

Ulmanu, V.; **Teodoriu, C.**; Marx, C.; Pupazescu, A. — Untersuchung zur Belastbarkeit von SLIMHOLE-Bohrgestänge mit Doppelschulter, Erdöl, Erdgas, Kohle, Heft X, 125 Jg. 2009.

Teodoriu, C. — Rotary-Shouldered Connections Make-up Torque Calculation Considering the Effect of Contact Pressure on Thread Compound's Friction Coefficient; OIL GAS European Magazine 4/2009.

Teodoriu, C.; Falcone, G. — Comparing completion design in hydrocarbon and geothermal wells: the need to evaluate the integrity of casing connections subject to thermal stresses, Geothermics journal, doi:10.1016/j.geothermics. 2008.11.006, 9 January 2009.

Teodoriu, C. — Buttress Connection Resistance under Extreme Axial Compression Loads, Oil and Gas Magazine, 4/2005, Volume 31, ISSN 0342-5622.

Teodoriu, C.; Badicioiu, M. — Sealing Capacity of API Connections - Theoretical and Experimental Results, SPE 106849, SPE Drilling and Completion Journal, March 2009.

Teodoriu, C.; Falcone, G. — Increasing Geothermal Energy Demand: the Need for Urbanization of the Drilling Industry, Bulletin of Science, Technology & Society 2008, volume 28, No. 3, Special Issue, Part 2: The Age of Alternative Energy: Is the Future Renewable?, DOI:10.1177/0270467608315531, 16 April 2008.

Reinicke, K. M.; **Teodoriu, C.** — Neue Entwicklungen in der Bohrtechnik, Akademie der Geowissenschaften zu Hannover Veröffentlichungen, Heft 25, 2005, ISBN 3-510-95943-4.

Bello, O. O.; Reinicke, K. M.; **Teodoriu, C.** — Particle Holdup Profiles in Horizontal Gas-Liquid-Solid Multiphase Flow Pipeline, Chemical Engineering &Technology, Vol 28, No. 12, November 2005, ISSN 0930-7516.

Fernandez, J.; Falcone, G.; **Teodoriu, C.** — "Design of a High-Pressure Research Flow Loop for the Experimental Investigation of Liquid Loading in Gas Wells", SPE Projects, Facilities & Construction Journal, June 2010.

Falcone, G.; Harrison, B.; **Teodoriu C.** — Can We Be More Efficient in Oil and Gas Exploitation? A Review of the Shortcomings of Recovery Factor and the Need for an Open Worldwide Production Database, Scientific Journals International, Journal of Physical and Natural Sciences, Volume 1, Issue 2, 2007.

C 6183 E

ERDÖL ERDGAS KOHLE

Juli/August
HEFT 7/8, 2009
125. JAHRGANG
7/8

Aufsuchung und Gewinnung · Verarbeitung und Anwendung · Petrochemie · Kohlenveredlung

Untersuchungen zur Belastbarkeit von Slimhole-Bohrgestänge mit Doppelschulter

Investigations on Load Envelope of an Double Shoulder Slimhole Threaded Connection

*Von V. ULMANU, C. TEODORIU, C. MARX und A. PUPAZESCU**

Abstract

The WireLine technology uses drill pipes having threaded connections with no upsets. These connections are usually weaker then the pipe body and require high makeup torque values. To achieve this, double shoulder connections are having the advantage of improving the stress distribution on thread turns.

This article shows the analytical, numerical and experimental work performed on a double shoulder connection in order to understand the effect of the internal shoulder as well as the shoulder last distributions. To solve this, the existing equation for shoulder connection calculation was extended to incorporate the internal shoulder effect.

The results show a good comparison of the analytical, experimental and numerical results. The extended equation to calculate the makeup torque can be easily generalized for any double shoulder connection.

Kurzfassung

***Das Bohren** mit einem WireLine-Bohr**strang bed**ingt integrale Verbinder. Diese Gewindeverbinder sind schwächer als die entsprechenden Rohre. Um dies zu gewährleisten, werden Doppelschulterverbinder entwickelt, welche den Vorteil besitzen, eine bessere Verteilung der Lasten auf die Gewindeflanken zu haben.*

Dieser Artikel beschäftigt sich mit analytischen, numerischen und experimentellen Untersuchungen an einem ausgewählten Doppelschultergewindeverbinder, um die Vorteile einer Innerschulter zu bewerten. Die klassische Einschulterverbinder-Gleichung wurde hierzu modifiziert, um den inneren Schulter-Effekt zu beurteilen.

Die Ergebnisse zeigen, dass eine sehr gute Übereinstimmung der analytischen, numerischen und experimentellen Werte existiert. Die neu entwickelte Gleichung kann für jede Doppelschulterverbinderkonfiguration angewendet werden.

* Prof. Dr.-Ing. V. Ulmanu, Dr. Ing. A. Pupazescu, Universitatea »Petrol si Gaze« Ploiesti, Rumänien; Dr.-Ing. C. Teodoriu, Prof. Dr.-Ing. C. Marx, Institut für Erdöl- und Erdgastechnik, TU Clausthal, Deutschland (E-mail: catalin.teodoriu@tu-clausthal.de).

0179-3187/09/7-8

1 Einleitung

Das Slimhole-Bohrkonzept der Amoco baut auf dem Diamantkernbohrsystem und der Wireline-Technik (WL) auf: Die WL-Technik ist in den Größen 2 1/4″ bis 6″ verfügbar. Für das gerichtete Bohren werden Krümmungsradien entsprechend Dog-Leg-Severity-Werten DLS = 3 bis 12°/30,5 m angewendet. Für diese Untersuchung wurde ein Seilkern-Bohrgestänge aus dem WL-Gestänge der Serie Q entwickelt.

Das Bohren mit WL-Bohrstrang bedingt integrale Gewindeverbinder. Diese Gewindeverbinder sind schwächer als die entsprechenden Rohre. Bei Überschrauben der Verbindung im Bohrloch können die Stoßschultern nachgeben. Dadurch wird die Muffe aufgeweitet. Diese Auftulpungen können zu Längsrissen in der Muffe und zu Querrissen in den Zapfen führen. Um diese Nachteile zu vermeiden, wurde die Konstruktion eines Doppel-Schulter-Verbinders (DSV), 15° mit Schrägschultern einer inneren Stoßfläche und 3° Flankenwinkel für die lasttragende Gewindeflanke ausgelegt.

In der vorliegenden Arbeit wird die Spannungsverteilung in der Gewindeverbindung in Abhängigkeit von den äußeren Belastungen wie Drehmoment, Zug, Innendruck und Biegung rechnerisch und experimentell ermittelt. Die Lastverteilung auf die Außen- und Innenschulter doppelt schulternder Verbinder bedingt eine konstruktive Vorgabe über die Spaltweite zwischen Zapfenende und Innenschulter vor Beginn der Kraftverschraubung. Das weiterentwickelte Rechenverfahren nach Sager und Teodoriu erlaubt eine genaue Berechnung der Vorgabe [15].

2 Das untersuchte Slimhole-Bohrgestänge DSV

Das Bohrgestänge DSV ist ein Kompositgestänge, wobei der Gewindeverbinderbereich aus hochfestem Material der Qualität 34CrNiMo4v bzw. 42CrMo4v nach DIN 17000 besteht und durch Pressstumpfschweißen (Reibschweißen) mit dem Rohrkörper verbunden wird. Der Gewindeverbinder ist in Abbildung 1 dargestellt. Bei einer Rohrwanddicke von t = 7 mm beträgt die Wandstärke durch Innenverdickung im Gewindebereich t = 11 mm.

Das Gewinde ist schwach konisch ausgebildet. Das buttress-ähnliche Gewinde hat eine Steigung von h = 10 mm (2,5 tpi) und einen 3°-Flankenwinkel. Der Verbinder ist doppeltschulternd mit je einer 15°-Schräge im Innen- und Außenstoßbereich. Der Verbinder kann jedoch auch ohne inneren Schulterstoß ausgeführt und verwendet werden.

Die Schrägschultern und der Flankenwinkel von 3° haben den Zweck, eine Aufweitung der Muffe bei hohen Momenten zu vermeiden. Die zusätzliche Stossfläche am Zapfenende hat die Aufgabe, die Vorspannung des Zapfens zu reduzieren und eine gleichmäßigere Spannungsverteilung über die einzelnen Gewindegänge sicher zu stellen. Die Torsionsfestigkeit liegt um min. 40 % höher als die übliche Konstruktion mit nur einer Außenschulter.

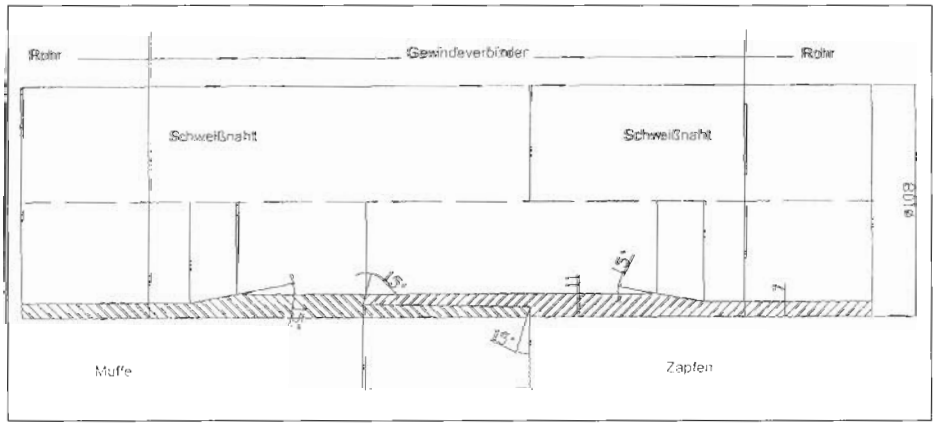

Abb. 1 Slimhole-Bohrgestänge DSV

Die Zapfenlänge ist um 0,2 mm kürzer als die entsprechende Muffenlänge. Damit soll sichergestellt werden, dass der Schulterkontakt zuerst außen erfolgt. Bei der Kraftverschraubung wird die Innenschulter aktiviert. Somit ist die Vorspannkraft auf der Außenschulter höher als auf der zusätzlichen Stossfläche des Zapfens.

3 Beanspruchung des Gewindeverbinders

3.1 Statische Beanspruchung

Das Bohrgestänge wird im praktischen Bohrbetrieb gleichzeitig auf Torsion, Längszug (bzw. Druck), Innendruck und Biegung beansprucht. Die Lage und Größe der Spannungshöchstwerte soll in Abhängigkeit von den Betriebsbelastungen berechnet werden. Für ein bestimmtes Gestänge des Bohrstranges werden die axiale Kraft (Stranggewicht), der effektive Innendruck und das Drehmoment als konstant angesehen. Mit der Gestaltänderungsenergie-Hypothese (GEH) können die Spannungen zu Vergleichsspannungen zusammengefasst werden.

Die Biegespannung S_b ergibt sich unter Längszug F in einem gekrümmten Bohrloch zu [8]:

$$S_b = \frac{E \cdot D \cdot c}{2} \cdot \frac{K \cdot L}{\tanh(K \cdot L)} \qquad (1)$$

mit

$$K = \sqrt{\frac{F}{E \cdot I}} = 4 \cdot \sqrt{\frac{S_z}{E \cdot (D^2 - d^2)}} \qquad (2)$$

E	Elastizitätsmodul
L	halbe Rohrlänge im Krümmungsbereich
c	Dog leg severity (DLS – direkt proportional der Bohrlochkrümmung 1/R) in Grad /30,5 m
I	Trägheitsmoment des Rohrquerschnittes
S_z	Axial- bzw. Zugspannung
D, d	Außen- bzw. Innendurchmesser des Rohres.

Biegung ohne Zug berechnet sich zu

$$S_b = 0{,}0607 \times \theta \times D, \qquad (3)$$

D in mm, c in °/30,5 m.

3.2 Dynamische Beanspruchung

Bei zusammengesetzter ruhender und wechselnder Beanspruchung ist der Einfluss von Kerbfaktoren zu berücksichtigen. Im Kerbgrund des Gewindes tritt eine Spannungspitze S_{max} auf, die ein Mehrfaches der Nennspannung S_n betragen kann.

Diese Spannungserhöhung wird durch die Einführung der Formzahl K_t berücksichtigt.

$$K_t = \frac{S_{max}}{S_n} \qquad (4)$$

Das Buttressgewinde kann als Flachkerbe betrachtet werden. Nach DIN 471 berechnet sich K_t zu

$$K_t = 1{,}14 + 1{,}08 \cdot \sqrt{\frac{w}{r}} \qquad (5)$$

w Nuttiefe (1,3 mm)
r Nutradius (0,1 mm).

Für den gefährdeten Zapfenquerschnitt des Gestänges DSV ergibt sich ein Wert von $K_t = 5$.

4 Lebensdauerabschätzung

Die Dauerfestigkeit eines Bauteiles unter betriebsbedingten Beanspruchungen wird neben der Werkstofffestigkeit stark durch die Bauteilgeometrie beeinflusst. Die Bauteilfestigkeit muss grundsätzlich experimentell überprüft werden. Die rechnerische Ermittlung des Dauerschwingverhaltens wurde mit Hilfe des sog. Örtlichen Konzeptverfahrens ermittelt, dazu wurden die mechanischen Eigenschaften des Verbindermaterials an vier Proben bestimmt.

Näherungsweise besteht ein linearer Zusammenhang zwischen der Werkstoffdauerfestigkeit und statischen Werkstoffkennwerten wie Zugfestigkeit oder 0,2-%-Dehngrenze:

$\sigma_w = 0{,}45\ Rm = 447{,}3\ N/mm^2$ bzw.
$\sigma_w = 0{,}436\ R0{,}2 + 77 = 447{,}6\ N/mm^2$

σ_w Dauerfestigkeit

4.1 Experimentelle Untersuchung zum zyklischen Materialverhalten

Für die Lebensdauerberechnung nach dem Örtlichen Konzept wurden stabilisierte, zyklische σ-ε-Kurven ermittelt. Das zyklische Werkstoffverhalten wird experimentell unter rein wechselnder dehnungskontrollierter Beanspruchung bestimmt.

Für die Gewindeverbindung erfolgt eine weitere Berechnung über einen Schädigungsparameter P_{SWT}. Nach Smith, Watson und Topper kann eine Wöhlerlinie mit P_{SWT} als Bestimmungsfunktion entwickelt werden. Bei der Übertragung auf den Gewindeverbinder DSV wird für den Zapfen eine Anrisslebensdauer berechnet, und zwar für verschiedene Biegespannungen entsprechend den tatsächlichen Bohrlochkrümmungen (Abb. 6).

Parallel zu den Berechnungen wurden die experimentellen Untersuchungen durchgeführt. Die Belastungen erfolgten durch Axialkraft 0 bzw. 100 kN, umlaufendes Biegemoment aus DLS = 9°/30,5 m oder S_b = 60 N/mm². Die Schwingfestigkeitsversuche konnten nach 1,82 Mio. Lastspielen abgebrochen werden, da keinerlei Anzeichen auf Anrisse zu erkennen waren. Ein Vergleich zwischen berechneten und experimentellen Ergebnissen ist gut. Dabei ist zu betonen, dass die Anrisswöhlerlinie grundsätzlich zu konservativen Werten führt.

5 Untersuchung des Spannungs- und Verformungszustandes

5.1 Versuchsprogramm

Die Ermittlung der Spannungsverteilung in der Gewindeverbindung in Abhängigkeit von den äußeren Belastungen erfolgt mit folgenden Untersuchungen:

- Messung der Verformungs- und Spannungsverteilung mit Dehnungsmessstreifen. Es wurden folgende Versuche durchgeführt:
  - Verschraubversuche mit 13 Verschraubmomenten zwischen 4 und 25 kNm
  - Verschraubversuche mit unterschiedlichem Schulterkontakt
    - nur Außenschulterkontakt
    - nur Innenschulterkontakt
    - Außen- und Innenschulterkontakt
- Bestimmung des Spannungsverlaufes kraftverschraubter Gewindeverbinder unter Zug, Innendruck und Biegung
- Finite-Elemente-Analyse zur Spannungsermittlung im Verbinderbereich, den örtlichen Spannungen im Gewindegrund und im Schulterbereich.

5.2 Messtechnische Untersuchungen

Zur Ermittlung der Spannungsverteilung in der Gewindeverbindung in Abhängigkeit von den äußeren Lasten wurden Verformungsmessungen mit Hilfe von Dehnungsmessstreifen (DMS) durchgeführt. Die DMS wurden entsprechend dem in Abbildung 2 dargestellten Klebeplan appliziert.

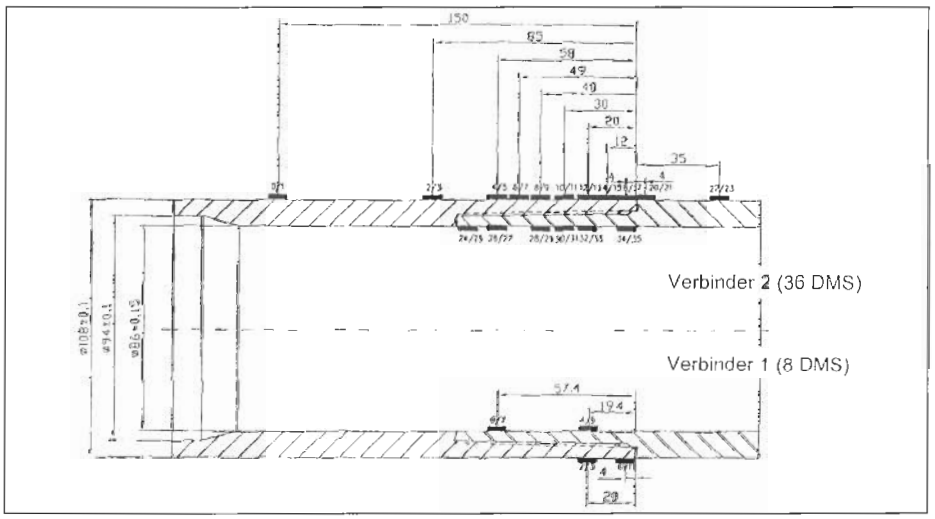

Abb. 2 Position der DMS

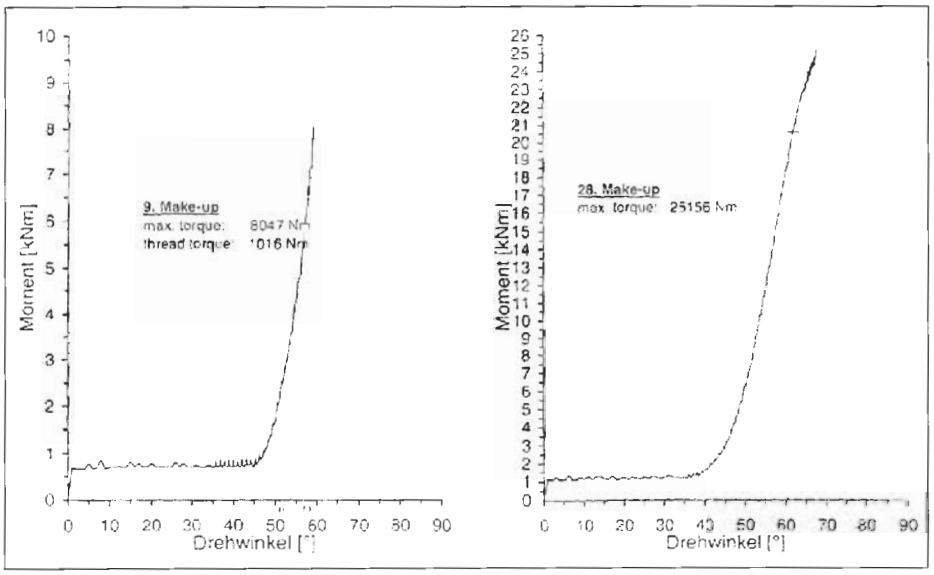

Abb. 3 Verschraubdiagramm; a) nominales Verschraubmoment 8.047 Nm; b) nominales Verschraubmoment 25.156 Nm

5.2.1 Verschraubversuche

Mit einer hydraulischen Verschraubzange wurden die Verbinder mit steigenden Momenten ver- und entschraubt. Abbildung 3a zeigt ein Verschraubdiagramm für eine Kraftverschraubung mit 8 kNm. Nach Handverschraubung wird in der Verschraubzange bei einem weiteren Verschraubwinkel von 45° die äußere Schulter erreicht und nach ca. 50° auch die Innenschulter. Abbildung 3b zeigt das Verschraubdiagramm für eine Kraftverschraubung mit ca. 25 kNm. Bei einem Verschraubmoment von ca. 28 kNm ist eine Änderung der Steigung des Diagramms (Fließbeginn) ersichtlich.

Für außenschulternde Gewindeverbinder wird der Zusammenhang zwischen Verschraubmoment und Belastung im gefährdeten Querschnitt nach einer Formel von API RP 7G, der sogenannten Farr'schen Formel, berechnet. Mit den Daten des untersuchten Verbinders ergibt sich:

$$M_{va} = F_{va}\left(\frac{p}{2\pi} + \frac{r_{Fl}\cdot\mu}{\cos\beta} + r_{Sch.a}\cdot\mu\right)$$

$$= A_z \cdot R_{p0,2}\cdot 9{,}72 = 11.540\ Nm$$

p Steigung
ß Flankenwinkel des Gewindezahnes
r_{Fl} mittlerer Radius des Gewindebereiches
μ Reibungszahl
F_{va} axiale Vorspannkraft
$R_{p0,2}$ 850 N/mm² – Fließgrenze des Werkstoffes
$r_{Sch.a}$ mittlerer Radius der Außenschulter.

Für Doppelschulterkontakt wird das Verschraubmoment mit folgender Gleichung berechnet:

$$M_v = (F_{va} + F_{vi})\cdot\left(\frac{p}{2\pi} + \frac{r_{Fl}\cdot\mu}{\cos\beta}\right) + \qquad (6)$$

$$+ F_{va}\cdot r_{Sch.a}\cdot\mu + F_{vi}\cdot r_{Sch.i}\cdot\mu$$

$r_{Sch.i}$ mittlerer Radius der Innenschulter
F_{vi} Vorspannkraft in der Innenschulter.

Die Abbildung 4 zeigt die mit DMS bestimmten Spannungen am Zapfeninnendurchmesser und dem Muffenaußendurchmesser für drei ausgewählte Positionen sowie verschiedene Verschraubmomente. Die Ergebnisse erlauben folgende Feststellungen:

- Die höchsten Axialspannungen (Zugspannungen) wurden an der Innenwand des Zapfens – etwa 19 mm von der Außenschulter entfernt – gemessen (Messstelle 4/5).
- In einer Entfernung von etwa 20 mm von dem Zapfenende (Messstelle 6/7) wurden Druckspannungen gemessen, die für 10 kNm Verschraubmoment etwa 210 N/mm² für den Zapfen betragen. Für die Muffe ebenfalls 20 mm von der Schulter entfernt werden Spannungen von 380 N/mm² ermittelt. Somit ist die äußere Schulter höher belastet als die innere Schulter. Dies resultiert daher, dass die Zapfenlänge konstruktiv 0,2 mm kürzer ist als die Muffenlänge.
- Die Axialspannungen an der Messstelle 0/1, die sich in der Nähe der Außenschulter befindet, sind wesentlich niedriger, als an der Messstelle 2/3, die 20 mm von der Schulter entfernt liegt. Dies ist die Folge der Konstruktion mit einer 15° Schrägschulter. Die druckspannungsbedingte radiale Aufweitung wird erst in einem gewissen Abstand von der Schrägschulter ermöglicht. Dort treten auch die höchsten Zugspannungen auf.
- Die höchsten Spannungen an der Innenwand des Zapfens (Abb. 4 DMS 6/7) steigen linear mit dem Verschraubmoment an. Durch Extrapolation wird die Fließgrenze des Werkstoffes bei etwa 16.000 Nm Verschraubmoment erreicht.

Man erkennt für Doppelschulterkonstruktion eine wesentliche Erhöhung (ca 56 %) des Drehmomentes beim Fließen gegenüber der ursprünglichen Konstruktion.

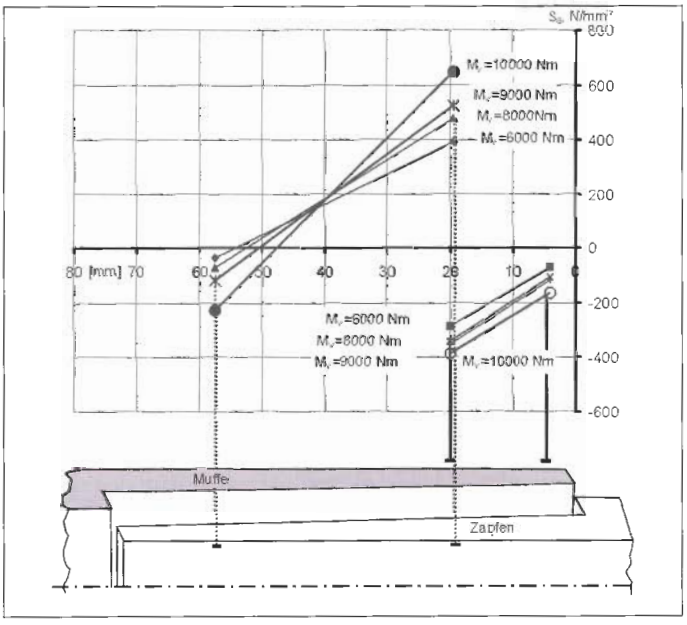

Abb. 4 Axialspannungswerte am ersten Verbinder

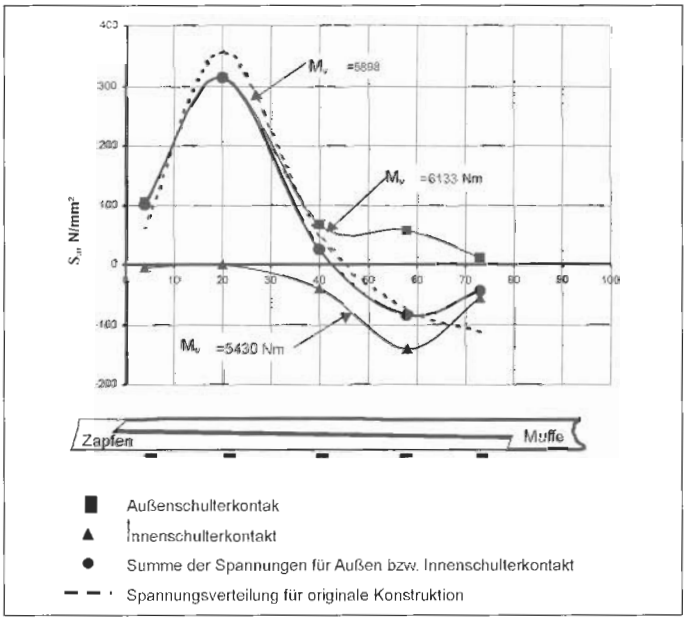

Abb. 5 Gegenüberstellung der Axialspannungsverteilung in dem Zapfen für verschiedene Konstruktionen

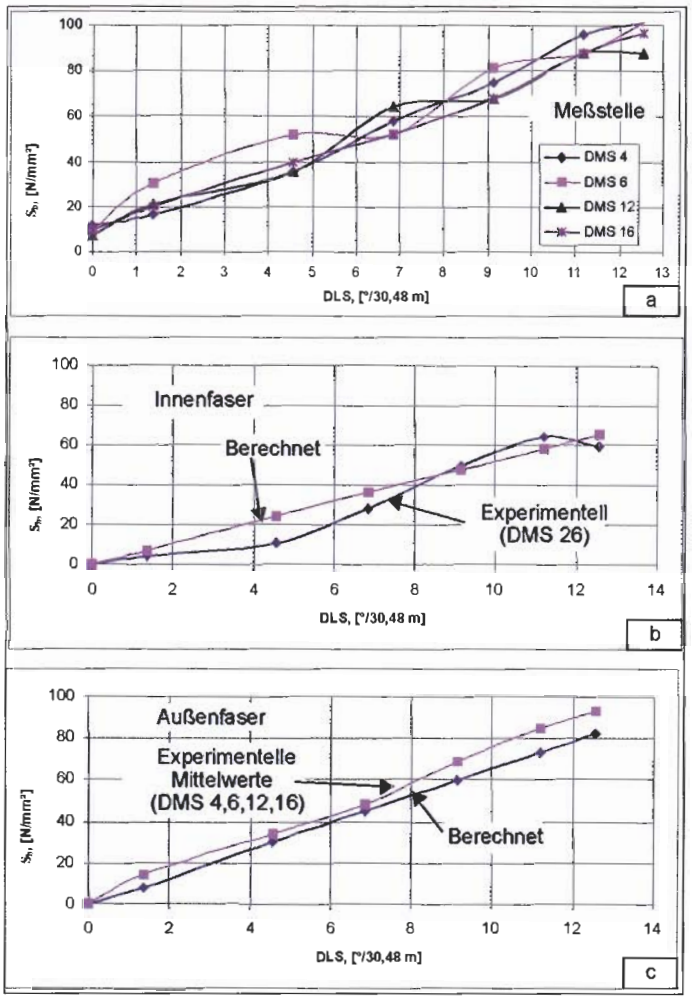

Abb. 6 Biegespannungen in Abhängigkeit von der Bohrlochkrümmung

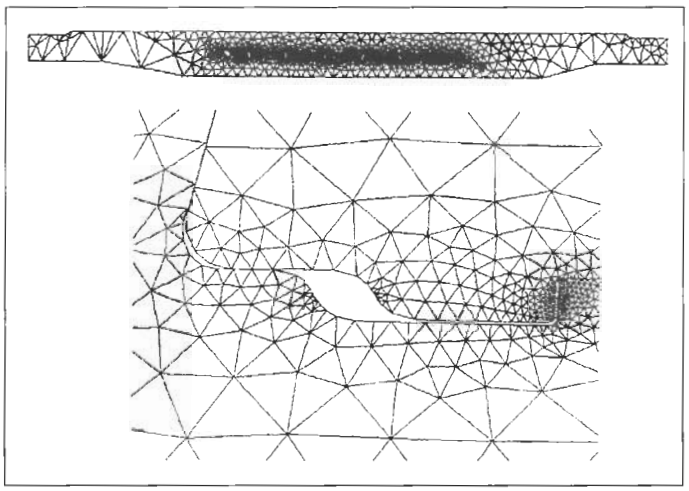

Abb. 7 FEA-Netzstruktur des Gewindemodells; oben: Gesamtnetz; unten: Detail der Schultern und Gewindeflanke

5.2.2 Verschraubung mit überlagerten Zug- bzw. Innendruck- und Biegebelastungen

Der Spannungsverlauf im Gewindeverbinder unter Belastung durch Zug, Innendruck, Torsion und Biegung führt zu folgenden Ergebnissen:

- Die gemessenen Zugspannungen im schulternahen Bereich von Zapfen und Muffe sind niedriger als die durch die äußeren Belastungen in den entsprechenden Querschnittsflächen errechneten Werte. Dies ist der Vorteil der Kraftverschraubung.
- Ein zusätzliches Torsionmoment bis 3.000 Nm führt zu keiner Veränderung der Axialspannungen.
- Innendruck. Durch den zusätzlichen Innendruck in Höhe von 150 bar tritt eine Erhöhung der Axialspannung von 40 N/mm² auf (Messstelle 4; 58 mm unterhalb der Muffenschulter).
- Biegung. Durch Biegung wird eine zusätzliche axiale Zugspannung an der Außenseite des Bogens hervorgerufen. An der Innenseite des Bogens entsteht eine entsprechende Druckspannung. Für die Erzeugung einer umlaufenden Biege-Wechsel-Beanspruchung wurde ein Rohrprüfstand eingesetzt. Durch einen verstellbaren Excenter wird eine umlaufende Biegespannung bewirkt, wie sie durch Bohrlochkrümmungen beim rotierenden Strang hervorgerufen wird. Die gemessenen und berechneten Werte für den Belastungsfall statische Biegung stimmen sehr gut überein (Abb. 6).

5.3 Finite-Elemente-Analyse (FEA)

Die Bestimmung des Spannungs- und Verformungs-Zustandes in der Gewindeverbindung unter Anwendung der Finite-Elemente-Analyse gestattet eine genauere Darstellung der Spannungsverteilung in Gewindeverbindungen als die messtechnische Untersuchung mit Dehnungsmessstreifen (DMS). Die DMS-Methode ist eine Spannungsermittlung an der Oberfläche der Testgewindeverbindung. Sie basiert auf Dehnungsmittelwerten über der Messstreifenlänge. Somit können die Dehnungsspitzen und die entsprechenden Spannungsspitzen in örtlichen kleinen Bereichen nicht erfasst werden.

Die Finite-Elemente-Analyse hatte folgende Ziele:

- Ermittlung der Axialspannungsverteilung an der Innenoberfläche des Zapfens und der Außenoberfläche der Muffe für verschiedene Verschraubmomente, um die Ergebnisse der DMS-Messungen zu validieren
- Bestimmung von lokalen Spannungsspitzen zur Erkennung des Fließbeginns und der bruchgefährdeten Zonen
- Untersuchung des Einflusses der Zapfenlänge auf die Spannungsverteilung. Durch Einstellung verschiedener Spaltweiten wird das Verhältnis zwischen der Vorspannkraft von Außen- und Innenschulter bestimmt.

Die Finite-Elemente-Analyse wurde mit dem Programmpaket ANSYS 5.6 durchgeführt.

Als Modell der Struktur der Verbindung wurden axialsymmetrische Ringelemente mit dreieckigem Querschnitt mit sechs Knoten (Plane 2 Elementtyp) gebildet.

5.3.1 Netzstruktur

Die Rechengenauigkeit bei Finite-Elemente-Analyse steigt mit der Feinheit der Vernetzung der Struktur, gleichzeitig wächst die Rechenzeit mit der Anzahl der Elemente. In der DSV-Gewindeverbindung sind Zapfen und Muffe nur über die Lastflanken und Schulterstöße in Kontakt. Deswegen kann die Elementeinteilung grober im Körper und

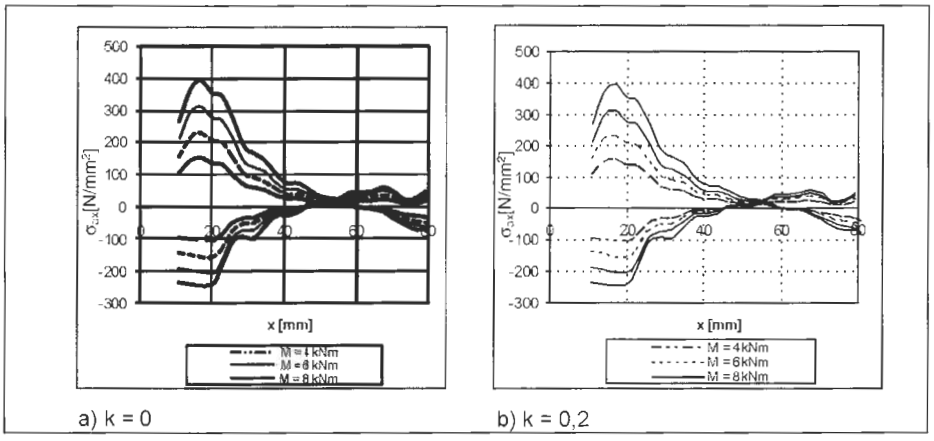

Abb. 8 Axialspannungsverlauf an der Außenoberfläche des Zapfens und der Muffe

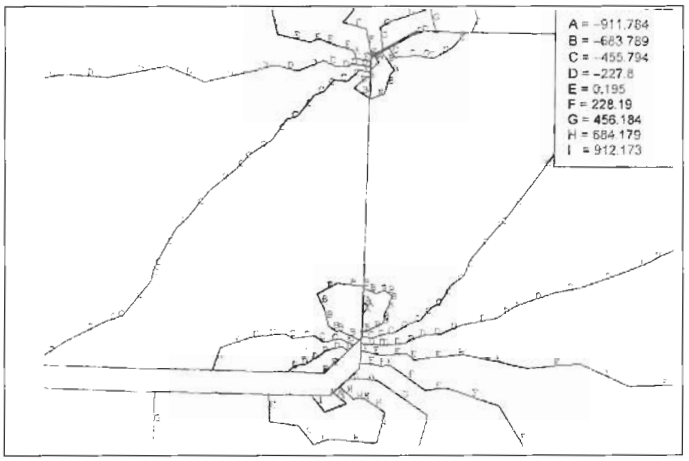

Abb. 9 Axialspannung-Isolinien an ersten tragenden Gewindeflanken des Zapfens und der Muffe (Verschraubmoment 6.000 Nm, k = 0,4)

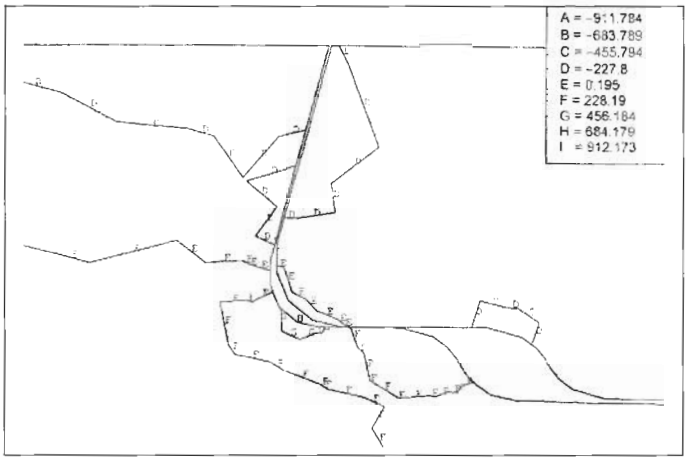

Abb. 10 Die Spannungsverteilung auf der Außenschulter (Verschraubmoment 6.000 Nm, k = 0,4)

feiner an Schulter- und Flankenstößen erfolgen. Die Spannungskonzentrationen in unmittelbarer Nähe der Lastflanke und Schulterstöße werden dadurch genauer ermittelt. Die Abbildung 7 zeigt einen Ausschnitt aus dem Finite-Elemente-Netz der Gewindeverbindung.

Zur Bestimmung der Schulterkräfte F_{va} und F_{vi} wird angenommen, dass die Vorspannkraft auf der inneren Schulter nur einen Anteil k der Vorspannkraft der äußeren Schulter beträgt, das heißt

$$\frac{F_{vi}}{F_{va}} = k.$$

Der Einfluss der Zapfenlänge wird über das Verhältnis k der Schulterkräfte F_{vi} und F_{va} modelliert. Für k = 0 besteht kein Innenschulterkontakt.

Unter der Annahme eines Reibfaktors μ = 0,08 wurden die Werte der Vorspannkräfte und die entsprechenden Schulterkontaktdrücke, sowie die k-Werte für verschiedene Verschraubmomente ermittelt (Tab. 1).

Die Beanspruchung durch das Verschraubmoment wurde folgenderweise modelliert: man beanspruchte die äußere Schulter (Muffenende) mit einer Axialkraft F_{va}, und die innere Schulter am Zapfenende mit der Axialkraft F_{vi}.

Bei einer Beanspruchung des Gewindeverbinders durch das Verschraubmoment wurden mit der Finite-Elemente-Analyse folgende Ergebnisse ermittelt:

- die Lage und Größe der Spannungsspitzen für verschiedene Verschraubmomente
- der Einfluss der inneren Stoßschulter auf die Spannungsverteilung in der Gewindeverbindung
- die Spannungsverteilung an der Oberfläche des Gewindeverbinders.

Der mit FEA erhaltene Axialspannungsverlauf an der Zapfeninnenoberfläche und an der Außenoberfläche der Muffe ist in Abb. 8 dargestellt. Man erkennt, dass der Verlauf und auch die Spannungswerte in guter Übereinstimmung mit DMS-gemessenen Spannungen stehen (Abb. 5).

Die Abbildung 9 zeigt die Axialspannung-Isolinien an den ersten tragenden Gewindeflanken des Zapfens bei einem Verschraubmoment von 6.000 Nm und k = 0,4.

Tabelle 1 **Werktabelle für verschiedene Verschraubmomente**

k	Mv = 4.000				Mv = 6.000				Mv = 8.000			
	Fva kN	pva MPa	Fvi kN	pvi MPa	Fva kN	pva MPa	Fvi kN	pvi MPa	Fva kN	pva MPa	Fvi kN	pvi Mpa
0	411,5	232	0	0	617,3	348	0	0	823,0	464	0	0
0,2	346,6	195	69,3	61,3	519,8	293	104,0	91,9	693,1	391	138,6	122,6
0,4	299,2	168,6	119,7	105,8	448,8	252,9	179,5	158,7	598,4	337,2	239,4	211,6
0,6	263,2	148,3	157,9	139,6	394,9	222,5	236,9	209,5	526,5	296,7	315,9	279,3

k	Mv = 10.000				Mv = 12.000			
	Fva kN	pva MPa	Fvi kN	pvi MPa	Fva kN	pva MPa	Fvi kN	pvi Mpa
0	1029,29	580,0	0	0	1235,15	696,0	0	0
0,2	866,42	488,3	173,28	153,2	1039,71	585,9	207,94	183,8
0,4	748,06	421,6	299,22	264,6	897,67	505,8	359,07	317,5
0,6	658,15	370,9	394,89	349,2	789,77	445,1	473,86	419,0

Die maximale Zugspannung, σ = 912 N/mm², tritt am Zapfenflankengrund auf (Isolinie I). Die größten Druckspannungen, σ = 912 N/mm², treten an aktiven Flanken des Zapfens und der Muffe auf (Isolinien A und B).

In Abbildung 10 sind die Bereiche der höchsten Axialspannungen an der Außenschulter bei einem Verschraubmoment von 6.000 Nm und k = 0,4 ersichtlich.

Die höchsten Zugspannungswerte, σ = 684 N/mm², treten aufgrund der Kerbwirkung im Schultergrund der Muffe (Isolinie H) auf, die etwa 75 % von der Zugspannung am Gewindegrund darstellt.

Die Spannungsverteilung am Zahngrund des Zapfens entlang des Gestängeverbinders für verschiedene k-Werte und zwei Verschraubmomente ist in Abbildung 11 a) dargestellt. An der ersten tragenden Lastflanke nehmen die Zugspannungen mit steigenden k-Werte nur wenig ab. Das heißt, dass der Innenschulterkontakt keinen entscheidenden Einfluss auf die Spannungswerte in der Nähe der Außenschulter hat. Die Steigerung der k-Werte verursacht eine gleichmäßigere Spannungsverteilung über die einzelnen Gewindegänge, besonders in der Muffe. Die Steigerung des Verschraubmomentes verursacht keine Spannungserhöhung, sondern eine Ausdehnung der plastifizierten Zone im Grund der ersten zwei Gewindeflanken. Eine ähnliche Spannungsverteilung für verschiedene k-Werte zeigt für die Muffe die Abbildung 11 b.

Schlussfolgerungen

Um den Einfluss einer zusätzlichen Zapfenstoßschulter der Gewindeverbindung auf die Spannungsverteilungen abzuleiten, werden gegenübergestellt:

- die gemessene Axialspanungsverteilung in der Original-Gewindeverbindung (Außen- und Innenschulter)
- die Axialspannungsverteilung die als Summe der gemessenen Spannungen bei alleinigem Innen- bzw. Außenschulterkontakt ermittelt wurde.

Der ausschlaggebende Vorteil einer doppelschulternden Verbindung liegt darin, dass bei der gleichen Höhe der Spannungsverteil-

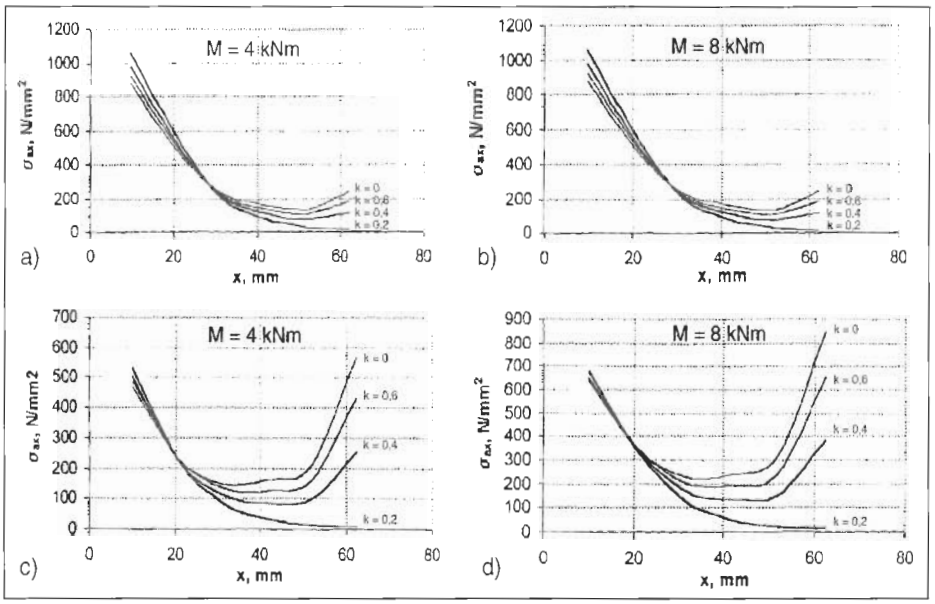

Abb. 11 Spannungsverteilung am Zahngrund des Zapfens und der Muffe entlang des Gestängeverbinders

lung die Belastbarkeit des Verbinders größer ist.

In allen Fällen ergibt sich eine gute Übereinstimmung der Gesamtspannungskurvenverläufe zwischen den berechneten und den gemessenen Werten.

Literatur

[1] FKM-Richtlinie Rechnerischer Festigkeitsnachweis für Maschinenbauteile. VDMA Verlag, 1988.

[2] Stahlbau Handbuch Für Studium und Praxis. Sonderdruck. Stahlbau-Verlagsgesellschaft mbH, Köln, 1996.

[3] Altmann, Th.: Umlaufbiegeversuche an Modell-Gewindeverbindern für Schwerstangen. Ergebnisse der Biegewechselversuche, Teil 1: Übersicht über die Versuchsergebnisse; 60 %-IF-Gewinde, Erdöl und Kohle, 13.Jg., April 1960.

[4] Hauk, V., Koehler H.: Untersuchungen an Gestängeverbindern. Verschraubversuche mit verschiedenen Konstruktionen. Erdoel-Zeitschrift 78 , Juli 1962.

[5] Herminghausen, J.: Untersuchungen zur dynamischen Belastung eines neuentwickelten, außenschulternden Gewindeverbinders für Bergbau-Bohrgestänge. Diplomarbeit, ITE, TU Clausthal, 1997

[6] Kessler, F.: Beanspruchungen in Gewindeteil von Bohrgestängen beim Bohren um Radien: ERDÖL ERDGAS KOHLE 112, Heft 7/8, August 1996.

[7] Knipp, H.: Inspektionserfahrungen mit Tool Joints und Schwerstangen. Erdöl-Erdgas-Zeitschrift 85, Jan. 1969, S. 18–20.

[8] Lubinski, A.: Maximum permissible dog legs in rotary boreholes. Journal of Petroleum Technology 13 (1961), S. 175–194.

[9] Lenz, E.: Verformungsmessungen an 3 ½"-API-IF-Gestängeverbindern. Erdoel-Zeitschrift 75, Juli 1962.

[10] Meyer, A.: Untersuchungen zur Gestaltung und Berechnung von hochbeanspruchten Wellen mit axialbelasteten Kerben. Dissertation, TU Berlin, 1995.

[11] Pöttingl, S.: Zum Einfluss der Mittelspannung auf die Schwingfestigkeit. Diplomarbeit, Institut für Maschinelleanlagentechnick und Betriebfestigkeit, TU Clausthal, 1998.

[12] Thomas, M.: Box OD stability of Double Shoulder Tool Joints at Catastrophic Failure. IADC/SPE 35035, Drilling Conference, New Orleans, 12–15 March 1996, S. 33–40.

[13] Ulmanu V.: Lebensdauerabschätzung der Bohrstrangkomponenten (1), Berechnungskonzepte und Werkstoffcharakteristiken. ERDÖL ERDGAS KOHLE 112, Heft 4, April 1996.

[14] API: Recommended Practice for Drill Stem Design and Operating Limits, API Recommended Practice 7G, Fifteenth Edition, January 1, 1995.

[15] Teodoriu, C.: Analysis of the Makeup procedure and evaluation of conical shouldered threaded connections. Ph.D. Thesis, TU Clausthal, 2003.

C 6183 E

ERDÖL ERDGAS KOHLE

OIL GAS

EUROPEAN MAGAZINE
INTERNATIONAL EDITION OF ERDÖL ERDGAS KOHLE

Dezember
HEFT 12, 2009
125. JAHRGANG
12

Aufsuchung und Gewinnung · Verarbeitung und Anwendung · Petrochemie · Kohlenveredlung

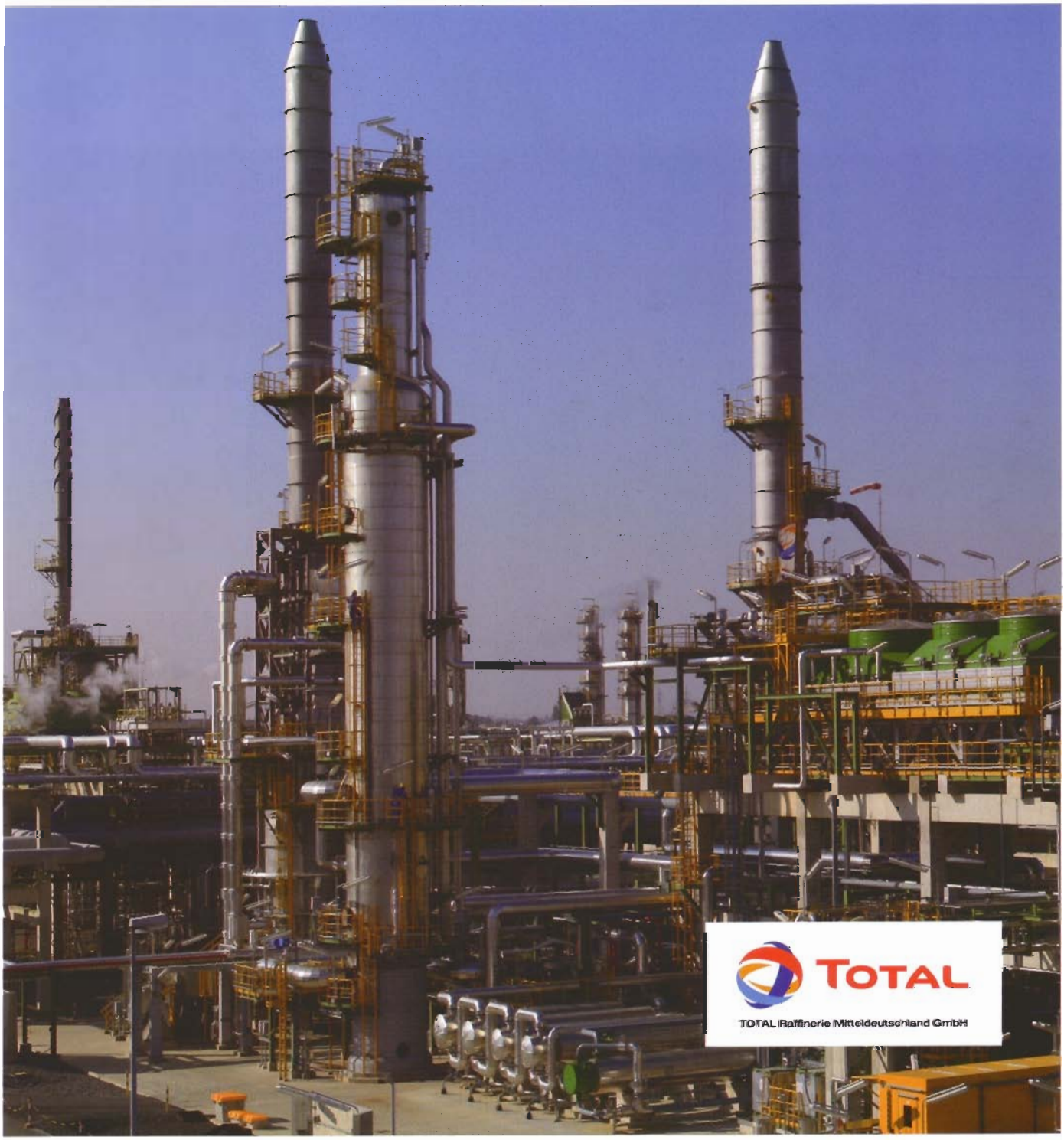

Rotary-Shouldered Connections Make-up Torque Calculation Considering the Effect of Contact Pressure on Thread Compound's Friction Coefficient

By C. TEODORIU*

Abstract

This article presents a new theoretical approach to enhance the equation used to calculate the optimum make-up torque by using the latest research on thread compound frictional properties. For the first time, the thread turn load, hence thread flank contact stress, will be related to the optimum make-up torque. The new equation developed herein, based on published experimental results, demonstrates that the newly developed equation helps to make a better estimation of proper make-up torque, especially for used rotary shouldered connections.

1 Introduction

The new connection designs introduced by drill pipe manufacturers (double shoulder connections, intelligent drill pipes or any new design with increased torque resistance) make the use of the Farr equation for calculating proper assembly torque more problematic, since the equation has been developed for external shoulder connections, specifically API Rotary Shouldered Connections (RSC) [9, 12]. Additionally, severe drilling conditions like High-Pressure High-Temperature (HPHT), directional drilling and extreme environments are affecting thread compound performance properties, which can make it impossible to attain the optimum make-up torque for the connection. Especially the exposure to high temperature changes generates problems in estimating the proper make-up torque. Even more, the RSC optimum make-up torques are different under static and cyclic conditions [10]. Another paper [11] shows that increased uncontrolled make-up torque will lead to a reduction of fatigue resistance of the RSC. On the contrary, a lower friction coefficient will lead to an equivalent high make-up torque, again with negative influence on RSC resistance. Many authors [9–11, 14] have pointed out that the make-up process is the only way to control and achieve the maximum tool joint loading capacity; therefore it becomes important to understand the effect of friction on optimum make-up torque calculation.

Drill pipe connections are a primary component of the drill string, and the entire "well security" depends upon tool joint performance reliability. An adequate connection between two drill pipes depends on the quality of the assembly process, which is significantly affected by thread compound performance. Since the variety of thread compounds is large, standards have been developed to determine thread compound performance and to define minimum thread compound properties. Thread compound frictional performance is normally defined by its friction coefficient (COF) in the standard American Petroleum Institute (API) rotary shouldered connection (RSC), or the friction factor (FF) relative to a standard API friction coefficient, which is accepted to be 0.08. The 0.08 value was determined by the API after multiple tests utilizing standard API RSCs and metal-based thread compounds, primarily 40% zinc and 60% lead. The friction coefficient of a thread compound has been generally considered to be constant. Although the API defines a constant coefficient for a given load range, recent studies indicate that the friction coefficient can vary considerably depending on connection geometry, contact stress and thread compound composition [3, 14, 15].

Baryshnikov [9] mentions that most of the new connections are designed for drilling in an extreme environment or in other words to drill deeper and faster and therefore are loaded up to their envelope limits. Since the make-up of the connection should induce an optimal stress – strain state in the connection that will maximize its resistance, it is evident why accurate calculation of the applied make-up torque must be performed.

Based on the Farr formula [12], a sensitivity analysis was performed to determine the primary influencing factors that characterize the final assembly (make-up) of the connection. Results of this analysis, concerning the influencing factors involved in Farr's formula, are presented in Figure 1. The variation of the friction coefficient may significantly influence the make-up torque value. Because the pitch influence is less than 2%, it will be considered constant for the purpose of this discussion.

As stated by Farr [12], the make-up torque of a connection is a function of its geometry, the pre-defined buck-up force and the friction coefficient between the two members of the connection (Pin and Box):

$$M = F_v \cdot \left(\frac{P}{2\pi} + \frac{R_p}{\cos\beta} \cdot \mu_{th} + R_s \cdot \mu_s \right) \qquad (1)$$

Typically, under field conditions, the applied make-up torque M can be measured,

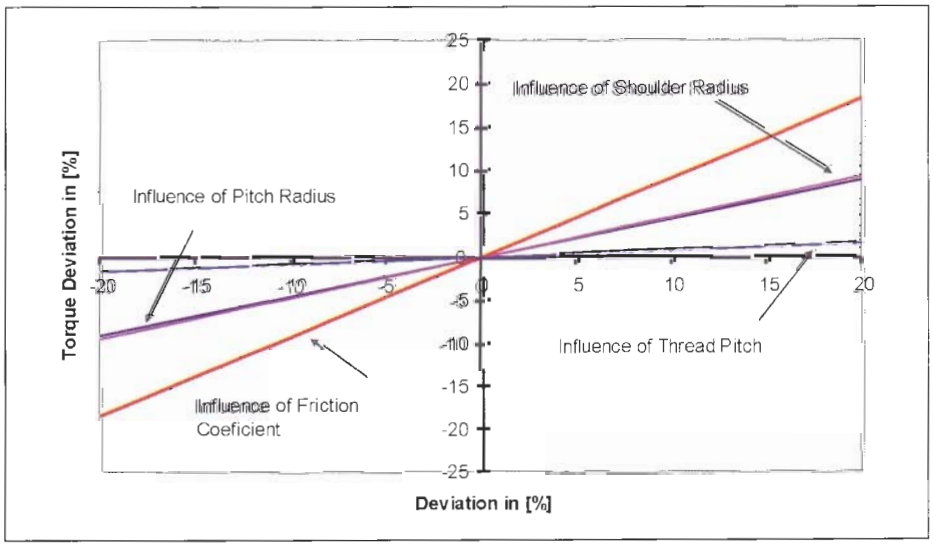

Fig. 1 Influence of factors involved in the Farr formula

*Catalin Teodoriu, TU Clausthal, Clausthal-Zellerfeld/Germany (E-mail: Catalin.Teodoriu@tu-clausthal.de).

0179-3187/09/IV

while the buck-up force F_v can only be estimated. As Eq. (1) shows, knowing the applied torque M and the parameters within the brackets, the Farr formula can be used for reverse calculation of the induced buck-up force in the connection.

Since a better understanding of the friction process and consequently an accurate make-up torque calculation allows optimizing the load resistance of the connection, more research must be focused on friction coefficient behaviour under real conditions (e. g. temperature, contact pressure, composition, etc).

2 The Friction Process

Friction is characterized by a coefficient of friction (COF), which is defined as the ratio of the frictional resistance force to the normal force between contacting surfaces [8]. A significant difference exists between the coefficients of static friction and kinetic friction. The static friction coefficient does not characterize the static friction in general, but represents the condition at the threshold of motion only [8]. Static frictional forces developed by the interlocking of irregularities of two surfaces will increase to prevent any relative motion, up to the limit condition where motion occurs. It is that threshold of motion which is characterized by the coefficient of static friction. The coefficient of static friction is larger than the coefficient of kinetic friction. When coefficients of friction are quoted for specific surface combinations, they are generally referenced to the kinetic coefficient. Thus, the static coefficient of friction exists as long as no relative motion occurs between the two bodies. This situation exists when Tool Joint (TJ) »make-up« or »break-out« is imminent [14].

Three basic assumptions are generally considered to characterize a model for friction between contact surfaces [7]:

1. The frictional force is independent of the area of contact
2. The frictional force is proportional to the normal force
3. The frictional force is independent of the velocity of motion

For a wide range of applications these assumptions are valid. For some complex applications, as in bearings and threaded connections, these assumptions are not adequate to define all cases. For example, in the case of pressure-lubricated bearings the hydrodynamic lubrication prevents the contact between bearing elements and therefore, the friction coefficient becomes more a function of the lubrication fluid shear stresses. A second example will be presented in this article that refers to the extreme contact pressure situation in which the friction coefficient becomes a function of thread compound composition and contact pressure.

In the early days of drilling very little attention was paid to the friction coefficient. Usually, it was considered being equal to 0.2 [9]. Later investigations showed that the friction coefficient without dope has a value of 0.133, while the common dope used at that time (60% lead powder and 40% grease base) showed a friction coefficient equal to 0.08 [9]. The experimental tests conducted by Farr showed that the 0.08 value is a practical choice, since it was matching the relationship between make-up torque, buck-up force and connection geometry.

3 The Thread Compounds

The thread compound provides the following functions: to assure lubrication between pin and box, to avoid adhesive wear (galling), to facilitate optimum make-up and break-out torque, and, in most cases, to seal fluids within the connection. A suitable compound must provide a consistent and predictable value for its friction coefficient. According to ISO 13678 [5], the general performance requirements of thread compounds include consistent frictional properties, adequate lubrication properties, adequate sealing properties, physical and chemical stability both in service and in storage conditions, and properties that allow the effective application of the compound on the connection surfaces. In addition, for RSC thread compounds they should lubricate the connection during the make-up runs to achieve proper bearing stresses (buck-up force), form an effective seal between connection shoulders to prevent wash-out, provide resistance to down-hole make-up and help to distribute bearing stresses evenly in the shoulder contact area.

API SPEC 7 [6] as well as ISO 10407 [7] recommend two main compound types for RSC: 40% to 60% zinc-based for tool joints and 40% to 60% zinc-based or 60% lead-based for drill collars. The API Reference Compound, a lead-based compound, is used only for laboratory testing. The accepted friction coefficient for the API Reference Compound is 0.08. The API Modified Compound, a multi-component compound containing 30 wt.% lead (Table 1), provides a similar friction coefficient to the API Reference Compound ($\mu = 0.08$) at typical tool joint (NC-46) contact stress. Because the loads on RSCs are increasing substantially, the demand for reliable and predictable thread compound properties is also increasing. Several types of drilling compounds have been developed and tested under extreme conditions. Compounds, such as copper-based or green (metal free) compounds are being used today for RSCs. Because the composition of many compounds is proprietary and can be changed by the producer, new methods were created to compare and measure their friction coefficient. The results of such methods are a general (global) friction coefficient or, according to API, a correction factor FF [2]. This correction factor represents the ratio between the API friction coefficient ($\mu_{API} = 0.08$) and another friction coefficient.

The friction coefficient for compounds may vary as a function of the contact force. For dry friction (non-lubricated surfaces or metal-to-metal friction) the friction coefficient is a constant value. It is known that, by interlaying a single-phase lubrication material between the contact surfaces, the friction coefficient becomes a function of the relative speed between surfaces. When a multi-phase lubrication material such as a thread compound is used, the friction coefficient is a complex function of different factors that include not only the compound composition but also the connection geometry, material and contact surface finish. It should be noted that what this paper defines is an "apparent" COF of the complete compound/connection "system".

Table 1 **Various thread compound compositions**

Product Specification	API Mod. Compound	Copper-Based Compound	50% Zn
Grease Base	36%	60%	50%
Powdered Graphite	18%	10–15%	–
Lead Powder	30.5%	–	–
Zinc Dust	12.2%	–	50%
Copper Flake	3.3%	10–15%	
Fluid Type	Petroleum	Petroleum	Petroleum
Density	1900 kg/m³	1200 kg/m³	1750 kg/m³
Colour	black/brown	brown	gray

4 Published Experimental Data Related to Friction Coefficients

In the last 15 years, several investigations dealt with friction phenomena in threaded connections. Sawitzky [13] stated in his thesis that the friction coefficient at the shoulder differs from the friction coefficient in the thread. His tests were performed on an apparatus based on a previous API 7A1 test machine. Because of low contact pressure, the results were not conclusive for shouldered threaded connections, where high contact pressure exists. Investigations on thread compound friction coefficient have been paralleled by an expansion in the variety of thread compound compositions. Investigations done by Farr and Brinegar [11] showed that a value of 0.08 is a practical choice when RSC thread compounds are used. Sawitzky reported the same values for low contact pressures. Although Sawitzky did not extend his investigations to higher

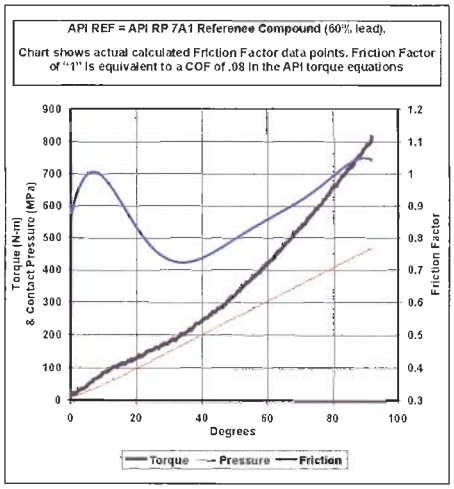

Fig. 2 Torque-turn results with API Reference Compound [3]

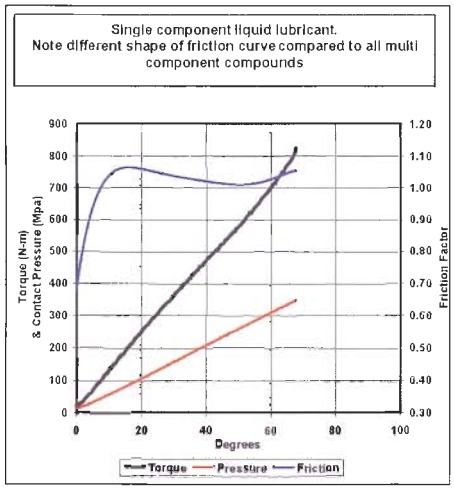

Fig. 3 Torque-turn results with single component Lubricant (fluid lubricant with small percentage of PTFE) [3]

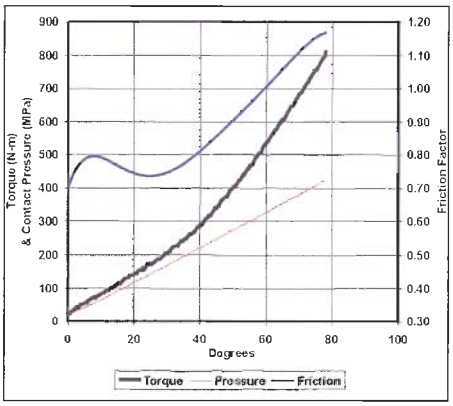

Fig. 4 Torque-turn results with copper based compound [3]

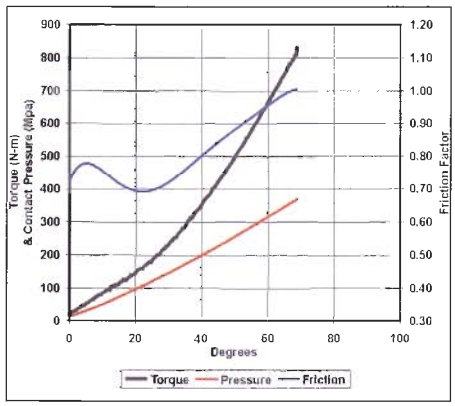

Fig. 5 Torque-turn results -turn results with API Modified Compound [3]

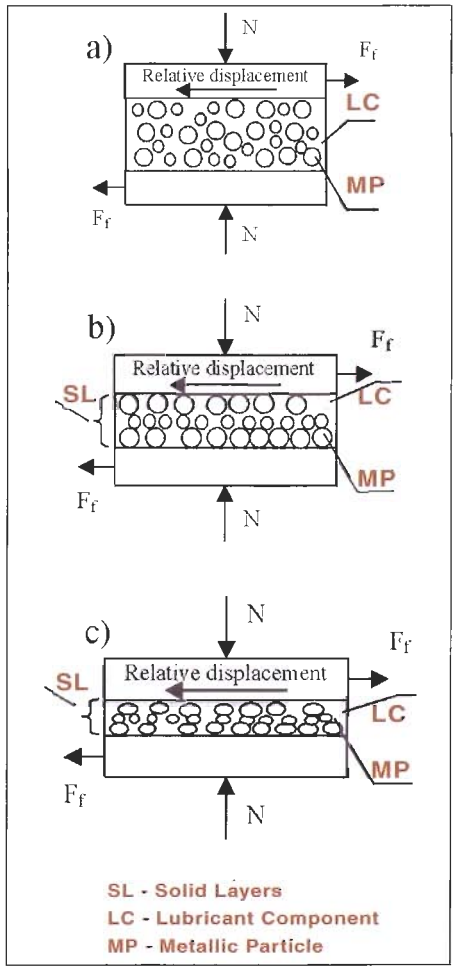

Fig. 6 Compound behaviour as a function of normal force

contact pressures, all his data points showed a decrease of friction coefficient once the contact pressure exceeds 1.4 MPa.

Earlier tests showed a discrepancy between full scale tests (Tool Joint) and small scale setup (Nut and Bolt machine) in which friction coefficients measured on the Nut and Bolt machine showed lower values than for the full scale tests [11]. Although this aspect was not explained at that time, the only logical answer is that the thread flank load distribution in the samples may affect the results. The contact pressure for RSCs at the shoulder, however, reaches values up to 800 MPa. The friction coefficients of various compounds were tested at high contact pressures (300–500 MPa) in an API sponsored project [3] and are presented in Figures 2 to 5.

API performed this series of tests to achieve reliable friction coefficients for different compounds and contact pressures [3]. For the project a new test machine to measure the friction coefficient has been developed, based on the small-scale test machine presented in API RP 7A1. The new design allows the direct measurement of shoulder contact stress, and models the relative contact surface movement in a full-scale RSC. In most cases, the COF results differed from the accepted API value of 0.08 considerably. Figures 2, 3, 4, and 5 show the friction factors measured for the API Reference Compound, a special lubrication fluid, a copper-based compound, and API Modified. Results revealed that the friction coefficient is a function of the contact pressure (a FF of 1.0 = a COF of 0.08) for higher pressures. For low contact pressures the friction coefficient variation seems to be a function of thread compound only. With different sizes and types of solid components, the shape of the friction coefficient vs. contact pressure curve changes. This behaviour can be seen by comparing Figure 3 with Figures 4, or 5. Figure 3 shows the friction factor for a fluid lubricant containing a small percentage (<5 wt.%) of finely divided PTFE. Its frictional behaviour above very low contact stress is relatively constant.

For lubricants containing a large percentage of solid particles of varying type, size, and shape, the FF becomes a function of contact pressure. Note that the tribological behaviour of copper based and API modified compounds is similar. A theoretical background for this phenomenon is presented in more detail in the following section.

5 The Influence of Compound Composition during Make-Up

A simple scheme will be used to describe the compound behaviour during make-up conditions. Consider two plates with a given volume of compound between them, as presented in Figure 6. The normal force N on both plates will create a friction force F_f when the plates start moving relative to each other. If the pressing force N is low, then the lubricant phase within the compound creates the friction, while the metallic particles are able to move in parallel layers without creating a noticeable resistance. By increasing the force N, the solid particle layers come closer to each other and their resistance will increase up to a greater, measurable value. When the force N becomes even higher, the metallic particles are plastically deformed and the friction force becomes a function of the normal force N and tribological properties of the metallic particles. When the particles are deformed into the shape of flakes (small plates), localized friction occurs between these layers. This global, friction coefficient is in transition to some function of metal-on-metal friction.

If the solid particles are not ductile or deformable the change in the COF can be even more dramatic. An example would be ceramic particles in spherical form or amorphous graphite. In the case of the ceramic spheres, the measured friction can be quite low initially, as the particles roll between the contact surfaces like bearings and then becomes extremely high, as the contact pres-

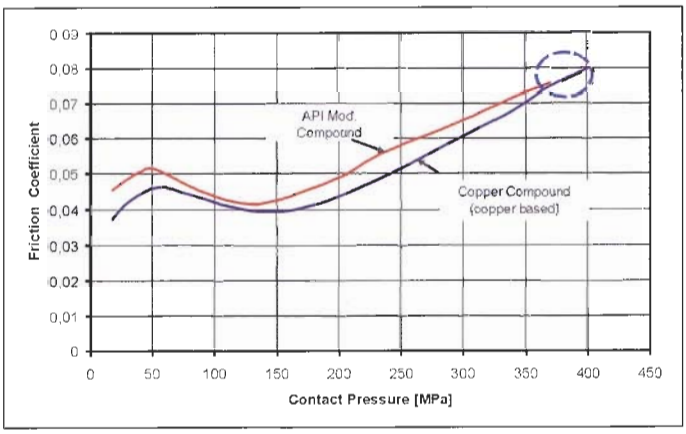

Fig. 7 Friction coefficient as a function of contact pressure (red – API Mod.; blue – copper base)

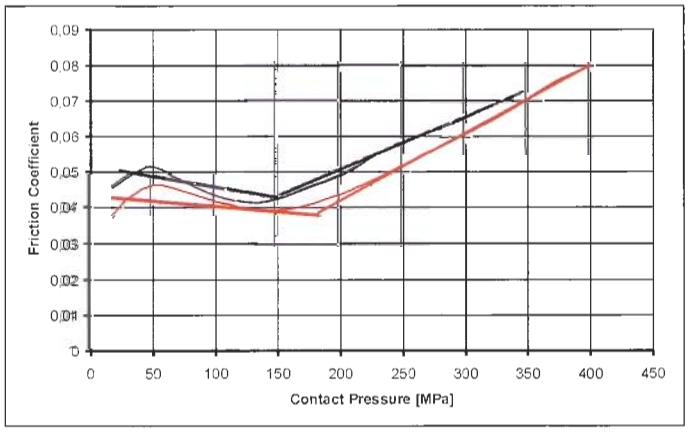

Fig. 8 Schematic representation of friction coefficient behaviour (linear interpolation)

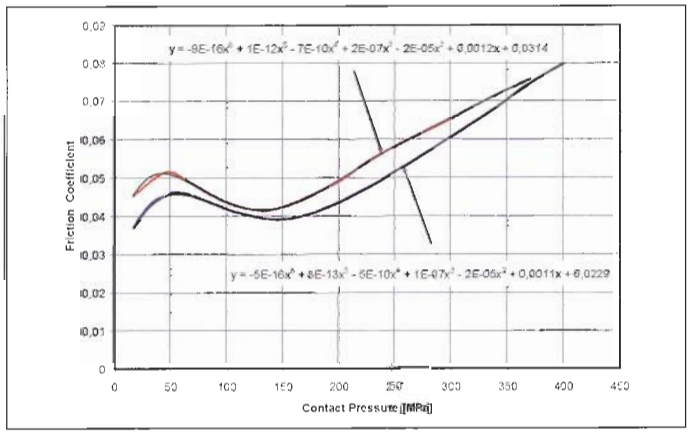

Fig. 9 Simulation of Friction coefficient behaviour using a 6th grade fitting polynomial

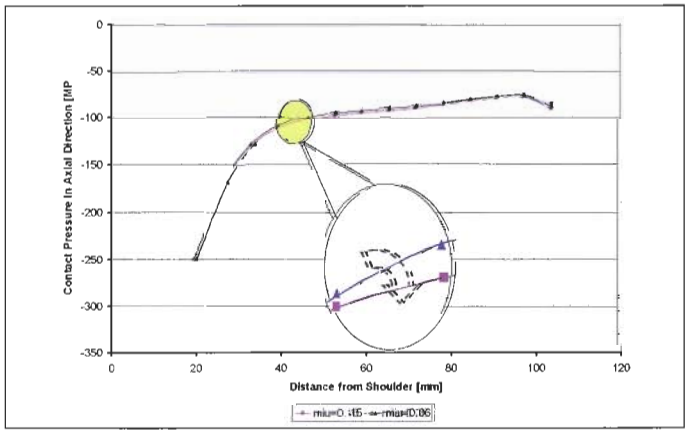

Fig. 10 Contact stress on flanks as a function of friction coefficient

sure increases and the particles fracture and become abrasive.

Figure 7 was prepared using test data collected in the API test programme [3] and shows these phenomena. The chart shows the friction coefficient of an API Modified Compound (red line) which contains primarily lead and graphite powder, and that of a commercially available copper-based compound having copper as the primary solid component (blue line).

Note that at pressures lower than 350 MPa the friction coefficient for API Modified Compound is higher than that for copper based compound. At higher contact pressures the friction coefficients are the same. The API prescribed value of 0.08 is achieved only for higher contact pressure. A schematic description (approximated by straight lines) for friction factor as a function of contact pressure is presented in Figure 8. For both compounds the friction coefficient decreases from a value μ_0 to a minimum μ_1 at 150 MPa. The second range represents an increasing friction coefficient from μ_1 up to the highest measured value, μ_2.

To describe the friction coefficient behaviour more accurately, the function of contact pressure was expressed using a polynomial function of 6th grade, see Figure 9. For example, the following equation demonstrates computed coefficients for the API Modified Compound:

$$y = 9.949\ 10^{16}\ x^6 \quad 1.3\ 10^{12}\ x^5 \quad 7.03\ 10^{10}\ x^4 \quad 1.83\ 10^{7}\ x^3 \quad 2.28\ 10^{5}\ x^2 \quad 1.15\ 10^{3}\ x \quad 0.0314$$

Table 1 provides a comparative description for three types of compounds: API Modified, copper-based and zinc-based.

6 The Influence of Connection Geometry and Load Distribution on the Farr Formula

The API formula for computing assembly torque for RSC is called the Farr formula. More than 200 experimental tests were made to confirm the validity of this equation [12]. However, under field conditions the results do not always confirm the Farr formula. The terms in this equation are not constants as assumed, but are variable to some degree. When the friction coefficient is regarded as a function of the contact pressure, as presented before, the Farr formula can be improved. The Farr formula is composed of two terms: thread torque and shoulder torque.

$$M = F_v \cdot \left(\frac{P}{2\pi} + \frac{R_p}{\cos\beta} \cdot \mu_{th} + R_s \cdot \mu_s \right)$$

$$= F_v \cdot \left(\frac{P}{2\pi} + \frac{R_p}{\cos\beta} \cdot \mu_{th} \right) + F_v \cdot R_s \cdot \mu_s \quad (2)$$

F_v, the buck-up force developed on the shoulder face, is equal to the sum of the flank loads:

$$F_v = Q_0 + Q_1 + \ldots + Q_n = \sum_{i=1}^{n} Q_i \quad (3)$$

Replacing the equation (3) in (2) we obtain:

$$M = \frac{P}{2\pi} \cdot \sum_{i=1}^{n} Q_i + \frac{1}{\cos\beta} \cdot \mu_{th} \cdot \sum_{i=1}^{n} (R_i \cdot Q_i) + F_v \cdot R_s \cdot \mu_s \quad (4)$$

Introducing the friction coefficient as a function of contact pressure, the equation (4) can be written as:

$$M = \frac{P}{2\pi} \cdot \sum_{i=1}^{n} Q_i + \frac{1}{\cos\beta} \cdot \sum_{i=1}^{n} (R_i \cdot Q_i \cdot \mu_{th,i}) + F_v \cdot R_s \cdot \mu_s \quad (5)$$

If we define the ratio between load of the turn and the buck-up force as follows:

$$k_i = \frac{Q_i}{F_v} \quad (6)$$

then: $Q_i = k_i \cdot F_v \quad (7)$

The thread turn load ratio k_i can be determined using finite element (FE) simulations or analytically using existing models. Although the friction coefficient seems to slightly affect the contact pressure and through this the thread turn ratio, this influ-

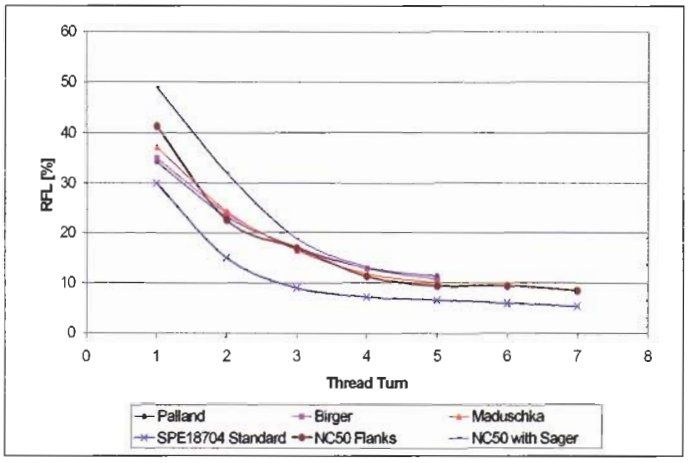

Fig. 11 Relative thread flank load (RFL) distribution for a NC50 connection determined using different approaches

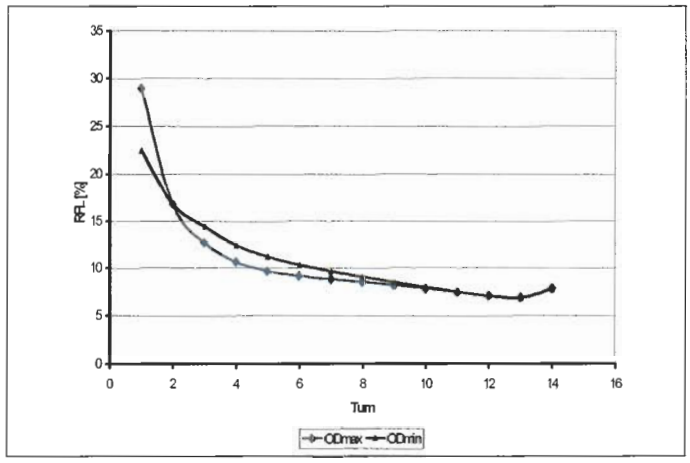

Fig. 12 Relative thread flank load for new and used NC50 connection

ence is small as shown in Figure 10 for the case of a NC50 Tool Joint. The increase of friction coefficient has the effect of lowering the stress distribution inside the connection slightly without affecting the load for the first thread turn.

Figure 11 shows the relative thread flank load distribution for an NC50 connection based on different authors' models [14]. To highlight the importance of load distribution, Figure 12 shows the thread flank load distribution for two practical cases: a new connection and one used to maximum limit. It can be seen that the distribution becomes more uniform in the case of a used connection (minimum OD), which, somehow, confirms the API approach to increase the optimum stress in the critical area to 60% of material yield strength. Using figure 12 it is possible to determine the value of k_i for each thread turn. For example, k_i for the first thread turn in the case of a new tool joint will be 0.28, while for the second thread turn it is 0.16. When the thread geometry is known, a predefined data base and diagrams can be generated to help engineers with their calculation.

By replacing the equation (7) in (5) we obtain:

$$M = F_v \cdot \left(\frac{P}{2\pi} + \frac{1}{\cos\beta} \cdot \sum_{i=1}^{n} \left(k_i \cdot R_t \cdot \mu_{th,i} \right) + R_s \cdot \mu_s \right) \quad (8)$$

According to API, the K_{up} coefficient is defined as:

$$K_{up} = \frac{M}{F_v} \quad (9)$$

The recalculated K_{up} coefficient is:

$$K_{up} = \frac{P}{2\pi} + \frac{1}{\cos\beta} \cdot \sum_{i=1}^{n} \left(k_i \cdot R_t \cdot \mu_{th,i} \right) + R_s \cdot \mu_s \quad (10)$$

A non-uniform load on the thread will create an increase of the calculated pitch radius for tapered connections. The modified pitch radius is given as follows:

$$R_t = \frac{\sum_{i=1}^{n} \left(k_i \cdot R_t \cdot \mu_{th,i} \right)}{\mu_{th}} \quad (11)$$

With equation (10) one may calculate the K_{up} coefficient as a function of thread load flank. It takes into account any changes in the friction coefficient. It is obvious that for constant radius and friction coefficient formula (10) will give K_{up} as presented in API standards:

$$K_{up} = \frac{P}{2\pi} + \frac{R_t}{\cos\beta} \cdot \mu_{th} \cdot \sum_{i=1}^{n} \left(k_i \right) + R_s \cdot \mu_s \quad (12)$$

and because: $\sum_{i=1}^{n} k_i = 1$ then

$$K_{up} = \frac{P}{2\pi} + \frac{R_t}{\cos\beta} \cdot \mu_{th} + R_s \cdot \mu_s = K_{up,API} \quad (13)$$

7 Discussion of the Results

As Figure 12 shows, the thread flank load is a function of connection geometry or state (new or used). Therefore, the newly defined K_{up} will become a function of connection geometry. The primary geometric parameters that influence flank load distribution for the same thread form are the ID and the OD of the Tool Joint. Any change in ID or OD leads to a redistribution of the flank load, which, as shown by the eq. (14), will modify the value of K_{up}. Finite Element models along with theoretical analyses have confirmed this observation.

As $\mu_{th,i}$ and k_i are functions of connection geometry, the newly defined K_{up} will be formulated on realistic parameters. According to API, the given K_{up} is considered to be constant for the full range of connections. Table 2 shows the calculated values for the two NC50 connections under consideration of OD_{max} – new connections with maximum OD and OD_{min} – class 2 with minimum admissible OD. The overall coefficient for a used tool joint has a comparable value with the API given K_{up}.

Because the contact pressure on the shoulder may vary considerably, as presented before, the higher values for shoulder contact pressure lead to a higher shoulder friction coefficient. For example, in case of an RSC NC50 with 69 mm ID the shoulder contact pressure is about 800 N/mm² [14]. Therefore, the friction coefficient at the shoulder is higher than the friction coefficient in the thread (see Fig. 9 by comparing the friction coefficient values at 100 MPa and 400 MPa).

Table 3 shows the value of K_{up} as calculated according to API and using equ. (10), considering the friction coefficient as a function of thread flank load. Figure 13 shows possible deviations from the API calculated value of make-up torque, in the case of new connections (OD_{max}) and class 2 (OD_{min}). It can be seen that all situations will require a higher make-up torque than the API recommended one. For practical values of COF, the deviation is within 10%, except for the case number 2, in which the deviation for new connections is 20%. In case of severe loads, API recommends increasing the make-up torque by 10%, a recommendation which is fully explained by the results using the newly developed equation. We must not forget that some connections generate high contact pressure on shoulders which, as depicted by the Figure 11, may lead to COF between 0.1 and 0.2 at contact pressures beyond 450 MPa. This aspect is shown in the Figure 13 in the fourth case, in which an extreme value of 0.2 has been assumed for COF on the shoulder. For this particular case the deviation is more than 70% and will dramatically affect the connection reliability and performance.

As other authors [9, 14] have pointed out, the

Table 2 K_{up} values for new connections (OD_{max}) and class 2 (OD_{min}) NC50 tool joints

	OD_{max}	OD_{min}
Calculated K_{up} (variable μ in thread, 0.08 on Shoulder)	13.3362	12.6683
$K_{up,API}$ (μ = 0.08)	12.3251	

Table 3 **K_{up} values for different friction coefficient values and combinations**

	K_{up} mm		Make-up Torque, kNm	
	OD_{max}	OD_{min}	OD_{max}	OD_{min}
Variable μ in thread, 0.08 on shoulder	13.34	12.67	47.25	44.88
Constant μ in thread and on shoulder, μ = 0.1	14.78	14.11	52.36	50.00
Constant μ in thread, μ = 0.05 and on shoulder, μ = 0.1	13.27	13.25	47.03	46.97
Constant μ in thread, μ = 0.08 and on Shoulder, μ = 0.2 (slight galling on shoulder)	22.00	21.33	77.95	75.59
$K_{up,API}$, μ = 0.05	8.08		28.63	
Reference $K_{up,API}$, μ = 0.08	12.3251		43.66	
$K_{up,API}$, μ = 0.1	13.77		48.78	
$K_{up,API}$, μ = 0.2 (metal on metal with light galling)	22.22		78.72	
$K_{up,API}$, μ = 0.5 (galling)	71.72		254.11	

Table 4 **Friction factor calculation for different compounds**

Compound type	Friction Factor (FF)			Friction Coefficient (COF)		
	Exp. 1	Exp. 2	Exp. 3	Exp. 1	Exp. 2	Exp. 3
API Mod. Compound	1.000	1.000	1.000	0.080	0.080	0.080
Kopr Kote	1.213	1.167	1.310	0.097	0.093	0.105
	1.231*	1.182*	1.219*	0.099*	0.095*	0.097*
	1.231**	1.182**	1.219**	0.099**	0.095**	0.099**
No Dope (metal on metal)	1.550	1.527	1.512	0.124	0.122	0.121

* values are computed using the same end make-up torque
** values are computed using a higher end make-up torque but the slope is calculated for the same make-up torque value as for *

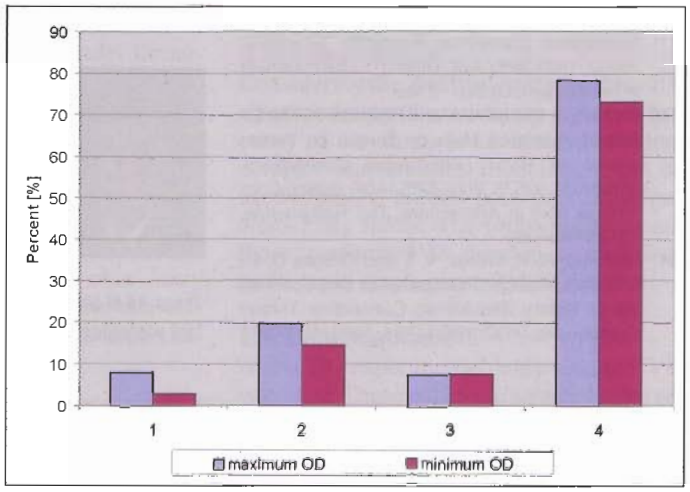

Fig. 13 Make-up torque deviation calculated by equation (10) compared to API recommended make-up torque. 1: Variable μ in thread, 0.08 on Shoulder; Constant μ in thread and on Shoulder, μ = 0.1; 3: Constant μ in thread, μ = 0.05 and on Shoulder, μ = 0.1; 4: Constant μ in thread, μ = 0.08 and on Shoulder, μ = 0.2

API calculation of make-up torque is based on the estimation of K_{up} values determined using lab tests on thread compounds and RSCs commonly used at that time. The new suggested equation to determine K_{up} is a step forward in understanding the make-up process and allows better determination of the make-up torque of a single shouldered connection by taking into account the COF dependence on contact pressure and true tapered geometry of the connection. As mentioned in the introduction and then showed in Table 3, the understanding of COF is the key to allow the correction of the API recommended make-up torque value with up to 10–15% increase. The development of computer controlled power tongs will permit the implementation of equation (10) for direct field application, when COF behaviour versus contact pressure is known.

Using a series of full-scale tests (NC50) and the API Mod. Compound as a reference, the friction factor was also determined experimentally. According to the manufacturer's information the API Mod. Compound has a friction coefficient equal to 0.08. The friction coefficients for the copper based compound and no dope experiments can be then computed. Table 4 shows the results using three methods to calculate the slope. Three different methods have been used to interpret the torque–turn plots to extract the Friction Factor. All these methods are presented in paper [14].

8 Conclusions

The friction coefficient for multi-component thread compounds is a function of the contact pressure intensity. When the friction coefficient is a function of the contact pressure between thread flanks, the Farr formula may lead to errors.

The formula developed herein demonstrates that the new K_{up} factor may differentiate between used and new connections. This can help improving the connection performance in the field by correcting the API recommended make- up torque value.

The new equation demonstrates that the API recommendation to increase the make-up torque by 10% in the case of difficult drilling conditions is justified and more over can be applied, in general, to all new connections.

All published data as well as laboratory experiments have shown that the tested thread compounds have a COF that is strongly affected by the contact pressure. Extrapolations of the existing results lead to values of COF close to 0.133, as initially assumed by several authors. Thus, the thread flank load distribution in a RSC requires the introduction of a different COF for thread and shoulder.

Nomenclature

A_b, A_p	cross sectional area of box, respectively pin
A_{sh}	contact area on shoulder
β	half of flank angle
D_r	bevel diameter of pin and box shoulder
F_s	buck-up force or shoulder load
F_t	friction force
K_{up}	overall connection coefficient
k_i	thread turn load ratio
M	make-up torque
M_{out}	break-out torque
n	maximum number of fully engaged threads
P	thread pitch or lead of thread
R_t	averaged thread radius
$R_{t,i}$	radius of current thread turn
R_s	averaged shoulder radius
Q_i	acting load on thread turn i
Q_s	Box Counterbore
μ_{API}	API friction coefficient
μ_{fi}	friction coefficient on thread flanks
$\mu_{fi,i}$	friction coefficient on thread flanks corresponding to the load level of thread flank i
μ_s	friction coefficient on shoulder
μ_{test}	friction coefficient of tested compound
COF	Coefficient of Friction
TJ	Tool Joint
RSC	Rotary Shouldered Connection
FF	Friction Factor
OCTG	Oil Country Tubular Goods
API	American Petroleum Institute

References

[1] ***, API RECOMMENDED PRACTICE 7G (RP 7G), Recommended practice for drill stem design and operating limits, 1998.

[2] ***, API RECOMMENDED PRACTICE 7A1 (RP 7A1) Recommended practice for testing of thread compound for rotary connections, *first edition*, 1992.

[13 ***, Test data from API E&P SC5 Work Item 1033 – "Thread Compound Research".

[4] ***, Ansys User Manual, 2006.

[5] ***, ISO13678:2000(E), Petroleum and natural gas industries – Evaluation and testing of thread compounds for use with casing, tubing and line pipe.

[6] ***, API SPECIFICATION 7 (SPEC 7), Specification for rotary drill stem elements, 1999.

[7] ***, ISO 10407, Petroleum and natural gas industries – Drilling and production equipment – Drill stem design and operating limits, 2000.

[8] ***, Dubbel, 1999, Taschenbuch fur den Maschinenbau, Springer Verlag, Berlin, 1999.

[9] Baryshnikov, A., Ferrara, P., Schenato, A., Adn Curioni E., 1995, Make-up Torque and Rotary Shouldered Connection Reliability, SPE/IADC 29352, 1995 SPE/IADC Drilling Conference held in Amsterdam, 28 Feb.–2 Mar.

[10] Breihan, J., Muradov, A. and Shepard, J., The Effect of Increased Make-up Torque on Performance of Rotary Shouldered Connections. SPE/IADC 92575, 2005 SPE/IADC Drilling Conference held in Amsterdam, The Netherlands, 23–25 February.

[11] Holcomb, R. T., Wilcox, V. T. and Oldiges D. A., The Performance Characteristics and Economics of Rotary Shouldered Connection Thread Compounds. IADC/SPE 14794, 1986 IADC/SPE Drilling Conference held in Dallas, TX, February 10–12.

[12] Farr, A. P., 1976, Tool Joint Design and Operation Torque, *IADC Rotary Drilling Conference*, Dallas, 1976.

[13] Sawitzki, 1987, Untersuchungen der Reibungsverhältnisse beim Verschraubvorgang und Analyse der daraus resultierenden Beanspruchungen hochbelasteter Gewindeverbinder, Doktorarbeit, 1987.

[14] Teodoriu, C., 2003, Analysis of the Make-up procedure and evaluation of conical shouldered threaded connections, Ph.D. Thesis, TU Clausthal, 2003.

[15] Teodoriu, C., Reichetseder, P., Marx, C., Kinzel, H., 2003, Analysis of Torque-Turn Recordings to make-up Rotary-Shouldered-Connections (RSC), *DGMK, Frühjahrstagung, am 28 und 29 April, 2003*, Band 1, ISBN 3-936418-03-9.

[16] Teodoriu, C., Kinzel, H., 2005, The Application of an Analytical model for the Controlled Make-up of Rotary Shouldered Connections in the Field, *SPE 93777, SPE Asia-Pacific Conference, 2005.*

Catalin Teodoriu *is Head of Drilling, Completion and Workover sub-department Institute of Petroleum Engineering of TU Clausthal and an Adjunct Assistant Professor in the Harold Vance Department of Petroleum Engineering at Texas A&M University since 2009. He was an Assistant professor in the Harold Vance Department of Petroleum Engineering at Texas A&M University between 2006 and 2009. Dr. Teodoriu has an equivalent M.S. (1996) from "Oil and Gas" University of Ploiesti, Romania, and two Ph.D.s (2003 Technical University of Clausthal and 2005 – "Oil and Gas" University of Ploiesti). Dr. Teodoriu has worked as a R&D Engineer for two years with R&D Center of Petrom, Romania, over six years as researcher and later on as Research Supervisor with the Technical University of Clausthal. Dr. Teodoriu was involved in teaching graduate and undergraduate drilling, production and completion courses.*

Related research activities that Dr. Teodoriu has been involved with are casing resistance under extreme loads, swelling cements for gas wells, drillstring components makeup procedures, underbalanced drilling and formation damage, evaluation of the casing fatigue and fatigue of casing connectors, and development of laboratory testing devices and facilities. His activity also includes finite element analysis and optimization of OCTG and drilling related tools, data acquisition systems and integrated data possessing systems.

He has published more than 50 papers, from which more than 12 are peer-reviewed and more than 6 are ISI indexed.

Fuzzy Logic Prediction of Dew Point Pressure of Selected Iranian Gas Condensate Reservoirs

*By S. NOWROOZI, M. RANJBAR, H. HASHEMIPOUR and M. SCHAFFIE**

Abstract

The experimental determination of dew point pressure in a window PVT cell is often difficult especially in the case of lean retrograde gas condensate. Besides all statistical, graphical and experimental methods, the fuzzy logic method can be useful and more reliable for estimation of reservoir properties. Fuzzy logic can overcome uncertainty existent in many reservoir properties. Complexity, non-linearity and vagueness are some reservoir parameter characteristics, which can be propagated simply by fuzzy logic. The fuzzy logic dew point pressure modeling system used in this study is a multi input single output (MISO) Mamdani system. The model was developed using experimentally constant volume depletion (CVD) measured samples of some Iranian fields. The performance of the model is compared against the performance of some of the most accurate and general correlations for dew point pressure calculation. Results show that this novel method is more accurate and reliable with an average absolute deviation of 1.33% and 2.68% for developing and checking, respectively.

* S. Nowroozi, M. Ranjbar, H. Hashemipour, M. Schaffie, Shahid Bahonar University of Kerman (E-mail: M.Ranjbar@web.de).

0179-3187/09/IW

1 Introduction

Efficient production of Gas condensate reservoirs is very important and crucial in the petroleum industry. High rate gas production will decrease reservoir pressure below the dew point pressure (DPP). Liquid drop out around the well bore will decrease gas relative permeability and gas production rate consequently. So, accurate determination of dew point pressure is vital.

The experimental determination of DPP is expensive and time consuming and often not available. During recent decades some empirical correlations [1–4], statistical [5] and graphical [6] models have been proposed to predict DPP of gas condensate reservoirs. Although empirical correlations are simple, yet accurate to some extent, they have not been able to reliably duplicate the temperature behavior of constant composition fluids [7]. Using equations of state to calculate DPP is an alternative method. However, the convergence problem and

Geothermics xxx (2009) xxx–xxx

Contents lists available at ScienceDirect

Geothermics

journal homepage: www.elsevier.com/locate/geothermics

Comparing completion design in hydrocarbon and geothermal wells: The need to evaluate the integrity of casing connections subject to thermal stresses

Catalin Teodoriu, Gioia Falcone*

Department of Petroleum Engineering, Texas A&M University, 3116 TAMU, College Station, TX 77843, USA

ARTICLE INFO

Article history:
Received 25 April 2008
Accepted 14 November 2008
Available online xxx

Keywords:
Geothermal
Well completion design
Well integrity
Casing fatigue
Low-cycle fatigue

ABSTRACT

Tapping for geothermal energy very often requires deep drilling in order to access high-temperature resources. This type of drilling is expensive and is financed by the operator with a long period of debt service before costs can be recovered from the energy sale (heat, electricity or a combination of both). Drilling costs are only a part of the total well expenditure. Tubulars can double the total well cost, especially when complex well completions are required. Together, drilling and well completions can account for more than half of the capital cost for a geothermal power project. A comparison is made of the different completions used for oil, gas and geothermal wells, and geothermal well completion requirements are discussed. Special attention is given to the thermal stresses induced by temperature variations in the casing string of a geothermal well. When the induced thermal stresses exceed the yield strength of the casing material, the fatigue behavior of the latter can be defined as low-cycle fatigue (LCF). The connection threads in the casing body amplify the local stresses and lower the LCF resistance. A theoretical approach is presented to evaluate that parameter, and calculations are compared with preliminary results from experiments on large-diameter Buttress connections, which are commonly used in geothermal well completions. It is shown that under extreme loads the LCF resistance of the Buttress thread connection can be as low as 10 cycles.

1. Introduction

For about 100 years, deep drilling has been associated with the oil and gas industry. With the advent of geothermal energy development, the drilling of deep wells has also become a requirement. While drilling for hydrocarbons leads to a fast cash return, thanks to the revenues from the sale of oil and gas, geothermal projects may only break even many years after the wells have been completed. Geothermal drilling costs can be "2–5 times greater than oil and gas wells of comparable depths" and can "account for 42–95% of total power plant costs" (Augustine et al., 2006).

Today's drilling processes for the exploitation of oil and gas have been optimized to achieve affordable drilling costs (dollar per meter), though they are only part of the total well cost. The tubulars (i.e. casings and tubings) used in the completion of an oil well may double its total cost in the case of a complex well design. The diameter of the last casing string in a geothermal well, often termed the production casing, is commonly 9 – 5/8 in. (244 mm) (Teodoriu, 2005). Such a large diameter pipe requires a correspondingly larger surface casing and a 13 – 3/8 in. (340 mm) diameter is commonplace in the USA and Japan (Bohm, 2000; Jotaki, 2000; Williamson et al., 2001).

Any well drilled deeper than 3 km would present temperatures in line with those typical of higher enthalpy geothermal resources (Tenzer, 2001). However, this paper focuses on well integrity issues for hot wells, independently of their depth. In Europe, the majority of the geothermal wells which have been drilled to depths greater than 4000 m are completed with surface casing diameters of 18 – 5/8 in. (473 mm) or greater (Tenzer, 2001). The large diameter of production casings is a consequence of the amount of fluids that needs to be produced from geothermal wells. For large installed power systems, production diameters of 13 – 3/8 in. (340 mm) are required, but such diameter requirements strongly affect well costs.

Over the operating life of a well, its casing string is generally subject to external loads that can be considered as static or quasi-static. Current industry design standards, such as those issued by the American Petroleum Institute (API), considers the casing string to be statically loaded, yet it can be subject to variable loads due to changes in temperature or internal pressure during geothermal operations. As the movement of the casing is restricted by the presence of a cement sheath, temperature variations induce thermal stresses in the casing string, which may exceed the yield strength of the casing material. Thus, the fatigue behavior of the casing material during the operational life of a well can be classified as low-cycle

* Corresponding author. Tel.: +1 979 847 8912; fax: +1 979 845 1307.
E-mail address: gioia.falcone@pe.tamu.edu (G. Falcone).

0375-6505/$ – see front matter © 2008 Elsevier Ltd. All rights reserved.
doi:10.1016/j.geothermics.2008.11.006

Nomenclature

a_M	correlation coefficient [$a_M = (M+1)^2 - 1$]
b	fatigue strength exponent
c	fatigue ductility exponent
e	average strain
E	Young's modulus (MPa)
K'	cyclic hardening coefficient
K	total intensity factor
K_{ts}	intensity factor for stress
K_{te}	intensity factor for strain
M	factor depending on material characteristics
n'	cyclic hardening exponent
$2N$	number of cycles to failure (N—semicycles)
P_{SWT}	damage parameter
S	average stress (MPa)
S_0	thermal induced stress (MPa)

Greek letters

α	expansion coefficient [m/(m °C)]
ΔT	differential temperature to which casing is exposed (°C)
ε_a	total strain amplitude
$\varepsilon_{a,e}$	elastic strain amplitude
$\varepsilon_{a,p}$	plastic strain
ε'_f	fatigue ductility coefficient
ε_l	local strain
σ_a	total stress amplitude (MPa)
σ'_f	fatigue strength coefficient
σ_l	local stress (MPa)
σ_m	median stress (MPa)

fatigue (LCF). The presence of geometrical variations in the casing body such as the connection threads will amplify the local stresses, and reduce the LCF resistance of the casing.

The surface casings of deep geothermal wells are exposed to significant temperature variations during drilling, which may affect their subsequent integrity. The size of the surface casing depends on that of the production casing and also on the drilling challenges presented by that particular well. The following theoretical and experimental work focuses on the fatigue resistance of an 18 – 5/8 in. (473 mm) diameter casing with Buttress thread connections, which is a common size for surface casing in geothermal wells, as reported by several authors (Brunetti and Mezzetti, 1970; Carden et al., 1983; Chiotis and Vrellis, 1995; Tenzer, 2001).

2. Geothermal resources

Fig. 1 shows the geothermal temperature gradient for selected world regions, with an average of 3 °C/100 m. As electricity generation using flash technology requires temperatures in excess of 180 °C; binary technology can be used for fluid temperatures between about 100 and 180 °C. The depth range for an economic geothermal project can be inferred from Fig. 1. According to Grimsson (2007), the temperature at depths of 4–5 km could range between 200 and 300 °C in Europe, 300 and 400 °C in the USA and be greater than 500 °C in Japan. This paper addresses areas with a geothermal gradient in the region of 3 °C/100 m, corresponding to a maximum of 250 °C of temperature variation seen by the casing.

The completions of deep geothermal wells are extremely demanding because of the high pressure imposed on the well if subjected to hydraulic fracturing operations, the need for one or more intermediate casings to reach the target, the high temperature at depth and the large temperature variations along the well. In the next section, the complexity of geothermal well completions will be discussed *vis-à-vis* some typical oil and gas completion designs.

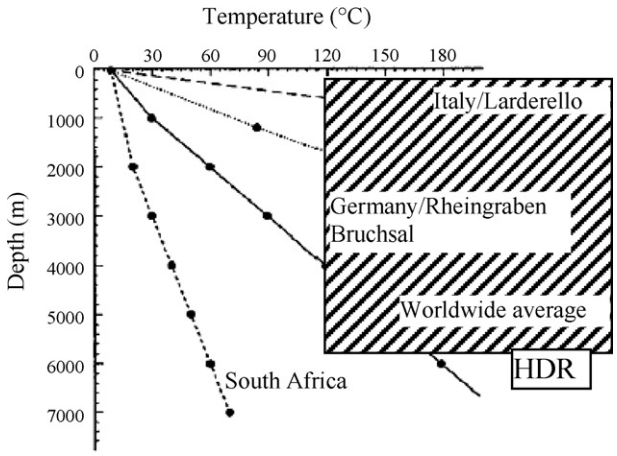

Fig. 1. Geothermal gradient in different regions (modified after Rogge, 2004). HDR: hot dry rock systems.

3. Comparison of completions used in oil/gas producers and geothermal wells

It is difficult to classify geothermal wells, as most of the existing geothermal projects are custom-designed to accommodate the local conditions. However, a classification may be attempted on the basis of the type of geothermal energy resources. It has been suggested that they should be classified by temperature (Dickson and Fanelli, 1990) or in a way that reflects their ability to do thermodynamic work (Lee, 2001).

The authors have chosen the following criteria to perform a comparison of well completions used in oil/gas and in geothermal fields:

- Wellhead and surface equipment are excluded.
- Tubulars, connections, and well integrity factors are accounted for.
- Three typical well completions are assumed, representative of a geothermal producing well, a deep gas well and a heavy oil producer.

The large diameter of production casings in geothermal wells is a consequence of the high volume and elevated enthalpy of the fluids being extracted. Large, high flow rate pumps (line shaft pumps or electrical submersible) must be accommodated in geothermal wells that require external energy to extract the hot water from the reservoir. This is true for binary wells (temperature < 180 °C) and also for deep Enhanced Geothermal Systems (EGS), where induced flow circulation of an external fluid is necessary. Fig. 2 shows an example of completions diagram for a geothermal producing well requiring pumping, based on the analysis of several geothermal projects worldwide. The setting depth of the 9 – 5/8 in. (244 mm) casing is calculated so that the downhole pump is completely submerged at maximum flow rate. This depth may vary depending on the characteristics of the specific geothermal reservoir. The main challenges for this type of completions are: the quality and long-term behavior of the cement, the selection of the appropriate casing hanger (able to withstand high temperatures) and the evaluation of thermally induced loads. Casing fatigue and cement integrity are the key issues for geothermal wells since the desired lifetime is higher than for oil and gas. For example, Carden et al. (1983) pointed out that despite the continuous casing design improvements, there still remain unknown factors related to casing fatigue and cement

Please cite this article in press as: Teodoriu, C., Falcone, G., Comparing completion design in hydrocarbon and geothermal wells: The need to evaluate the integrity of casing connections subject to thermal stresses. Geothermics (2009), doi:10.1016/j.geothermics.2008.11.006

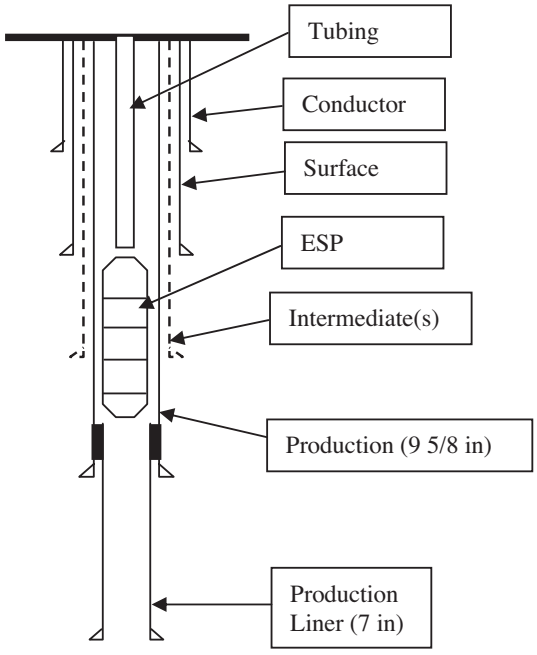

Fig. 2. Example of a completion diagram for a geothermal well requiring pumping. ESP: electrical submersible pump.

integrity that could potentially cause problems in long-term production operations.

The following thread types are used in geothermal well completions: API Round (Brunetti and Mezzetti, 1970; Ragnars and Benediktsson, 1981; Chiotis and Vrellis, 1995), virtually discontinued today; API Buttress (Brunetti and Mezzetti, 1970; Nicholson et al., 1982; Carden et al., 1983; Chiotis and Vrellis, 1995), which is known for its high axial tensional strength, but low compressive strength; premium connections (Carden et al., 1983), which are mostly used for production casing only, due to the associated high costs.

The following casing grades have been reported as commonly used in geothermal applications: J-55 (Brunetti and Mezzetti, 1970; Carden et al., 1983; Chiotis and Vrellis, 1995), usually replaced by K-55 for deep applications; N-80 (Brunetti and Mezzetti, 1970; Ragnars and Benediktsson, 1981; Carden et al., 1983; Chiotis and Vrellis, 1995; Witcher, 2001), usually replaced by L-80 in the presence of H_2S (Lazzarotto and Sabatelli, 2005.); C-95, which has recently been replaced by T-95, though some authors also report S-95 (Carden et al., 1983) and rarely P-110, in the absence of H_2S. For extreme environments, 9 Chrome L-80 and 13 Chrome L-80 can be utilized. Despite the often prohibitive costs, titanium (Beta-C Titanium) has been used for severe conditions (Pye et al., 1989). Casing pre-tensioning is reported by many authors as a common practice for geothermal well completions (Brunetti and Mezzetti, 1970; Carden et al., 1983; Chiotis and Vrellis, 1995).

Fig. 3 shows the completion of a typical gas well, where a 7 in. (178 mm) production casing is used to ensure good downhole accessibility and high well productivity. The first difference between geothermal and gas wells and is that, in the latter, the completion may have the same diameter from bottomhole to surface. The gas well uses production tubing string to transport the reservoir fluids to surface, so the casing string is not in direct contact with the reservoir fluids, nor is it directly exposed to the reservoir pressure. Generally, completion fluids containing corrosion inhibitors are placed into the annulus between tubing and casing to protect the tubulars. It should be noted that the conventional gas well completion illustrated in Fig. 3 is not representative of a high-pressure-high-temperature (HPHT) gas well, where completion can be 5–10 times more expensive.

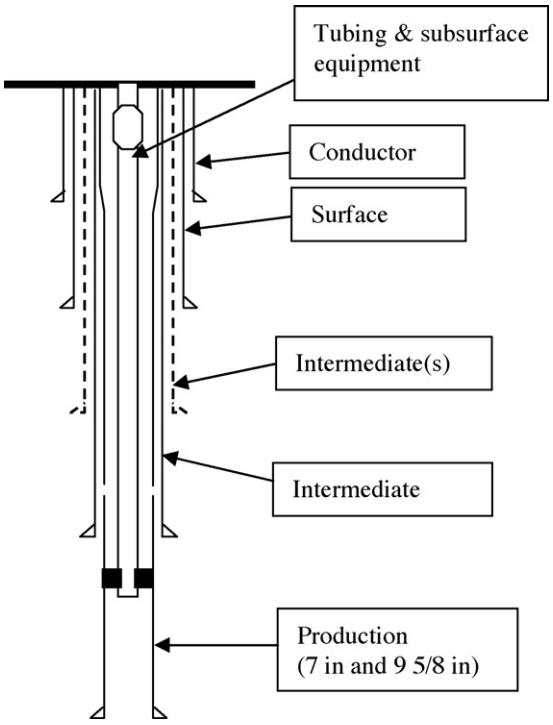

Fig. 3. Schematic completion diagram for a typical gas well.

A typical completion diagram for a heavy oil producer is presented in Fig. 4. The main feature of these wells is the need for casing string pre-tension, which limits the effects of axial compressive forces due to thermal expansion. Despite many reports (Brunetti and Mezzetti, 1970; Ellis, 1979; Allen et al., 2000) of casing failures for high-temperature applications, the importance of casing fatigue analysis for these wells is still not widely recognized. The production of heavy oils usually requires the injection of steam,

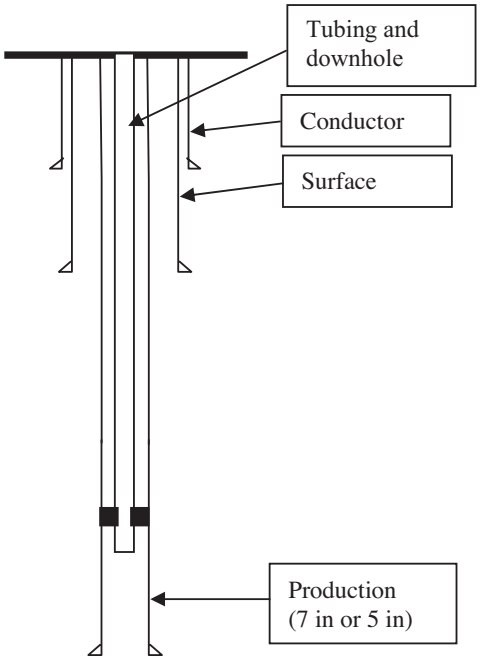

Fig. 4. Schematic completion diagram for a heavy oil producer.

Please cite this article in press as: Teodoriu, C., Falcone, G., Comparing completion design in hydrocarbon and geothermal wells: The need to evaluate the integrity of casing connections subject to thermal stresses. Geothermics (2009), doi:10.1016/j.geothermics.2008.11.006

Table 1
Key completions parameters for geothermal, gas, and heavy oil wells.

Parameter	Geothermal	Gas	Heavy oil
Temperature (°C)	80–250	60–150	60–350[a]
Depth (m)	1000–5000 (or more)	3000-6000	300–1200
Production casing OD[b]	9 – 5/8 in. and 7 in. liner	9 – 5/8 in. with crossover to 7 in.	5 or 7 in.
Connection type[c]	API Buttress	Premium	API long/Buttress

[a] The high-temperature values correspond to the injected steam in thermal oil recovery processes.
[b] Larger casing outer diameters (OD's) are reported for high power generation geothermal installations.
[c] With the development of oil country tubular goods (OCTG), market premium connections tend to be extensively used for production casing in geothermal applications.

which is used to reduce the in situ oil viscosity, thus making the oil more mobile. Steam injection increases the temperature of the reservoir fluids to be produced, which may represent an operational constraint from the well completion point of view. As heavy oil reservoirs tend to be found at relatively shallow depths, the completions for heavy oil wells have different requirements from those for deep hydrocarbon wells.

Table 1 shows a selection of well completions parameters for the three well completion types that have been discussed above. The above classification has shown that the common casing diameters for geothermal well are larger than 9 – 5/8 in. (244 mm), sometime exceeding 13 – 3/8 in. (340 mm). Surface casings are generally larger than 18 – 5/8 in. (473 mm) for such applications. It has also been shown that temperature variation may exist and therefore the casing string is subjected to variable tension/compression loads.

4. Thermally induced fatigue

In order to determine the influence of temperature on casing fatigue, the following assumptions were made:

- the casing cannot move in the cement sheath,
- there are no radial constraints as they would increase the average stress, and
- the induced average stresses remain in the elastic domain, but the local stress values are in the plastic domain.

The induced thermal stresses (S_0) are given by

$$S_0 = \alpha E \, \Delta T \tag{1}$$

If the casing string is pre-tensioned, the total stress becomes an algebraic sum of thermally induced stresses and the existing pre-stress state in the casing. Commonly, the pre-tensioning is intended to reduce or eliminate axial compressive loads. However, a section of the casing must be cemented without any pre-stress state in order to obtain the pre-tensioning state. For example, Carden et al. (1983) reported that the best option for their casing design was to cement the first 300 m prior to exposing the casing to a successive pre-tensioning and cementing sequence. Thus, Eq. (1) is applicable for non pre-stressed sections. Additionally, fatigue becomes more severe in symmetric alternating cycles and the effect of cement around the casing is to increase the thermal stresses. Although many authors have investigated this problem, it is not easy to quantify these effects, especially when cement quality is not measurable. Thus, it is not unreasonable to use Eq. (1) to determine the thermal stresses.

Material properties such as the yield strength change with temperature. This implies that, at elevated temperatures, the resistance of a casing is lower than at ambient temperature. Fig. 5 shows the yield strength variation with temperature for different grades of oil country tubular goods (OCTG) (Lari, 1997).

Table 2 shows the temperature variation that induces thermal stresses equal to material yield strength for commonly used grades of steel pipe. The values presented in the table were calculated using Eq. (1) and the following values for steel expansion coefficient (α) and steel Young's modulus (E): $\alpha = 12.5 \times 10^{-6}\,°C^{-1}$, $E = 2.05 \times 10^5$ MPa. The table shows that the temperatures in any higher enthalpy geothermal well will cause plastic deformation even in casing strings made of high-grade steel. It is also important to note that, for low-enthalpy geothermal wells with temperatures below 120 °C, a J55 steel-grade pipe is adequate. In the latter case, the well depth and the required collapse resistance are the parameters that will dictate the appropriate selection of steel grade.

A geothermal well is subjected to cooling and heating sequences during its life. The thermal expansion of the casing occurs when hot fluids start flowing up the well. Repeated cooling of the wellbore for logging or other remedial activities has long been known to cause well integrity problems. Cyclic cooling and heating exposes the casing string to cyclic tension–compression loading that may lead to casing failure. The following section presents a study that attempts to evaluate casing fatigue using the local stress–strain concept (LSSC), a method widely used in civil engineering and aeronautics (Ulmanu and Ghofrani, 2001).

5. Casing fatigue: theoretical background

Fatigue represents any effect on materials due to repeated cycles of stress. The material shows no obvious sign or warning prior to failure. It is known that cracks are produced at a later stage of fatigue, but more likely those cracks do not affect the total system deformation. In some cases, like drill pipe, intensive non-destructive inspection allows the avoidance of catastrophic failures by detecting the small cracks. Casings are normally cemented into a well and allow no control after being set in place. Fatigue may be classified as low-cycle fatigue and multi- or high-cycle fatigue. A typical high cycle fatigue is represented by drill pipe fatigue in deviated wells. Unlike drill pipe, the casing may be exposed both to low-cycle as well as to high-cycle fatigue. Low-cycle fatigue is a common type of failure when the applied loads induce high stresses in the metallic material, greater than material yield strength. The number of cycles may vary from as low as 10 up to 100. High-cycle fatigue will require a large number of cycles to failure. Usually for a minimum of 10^6 cycles, fatigue resistance is considered to be sufficient for metallic components in order to avoid catastrophic failures. Tubular fatigue is not an unknown failure mode, but for a long time it was considered as being unimportant for well casings and tubings.

The LSSC method uses the local stress state to determine the fatigue resistance of materials. It allows the evaluation of LCF resistance of components having notches (which act as stress concentration zones) using the results of uniaxial tests performed on

Table 2
Temperature at which the induced stress is equal to the yield strength of the material.

Grade	J55	N80	P105	P110
Temperature change, ΔT (in °C)	157	222	286	310
Temperature-corrected yield strength (in MPa)	392	553	712	771

Please cite this article in press as: Teodoriu, C., Falcone, G., Comparing completion design in hydrocarbon and geothermal wells: The need to evaluate the integrity of casing connections subject to thermal stresses. Geothermics (2009), doi:10.1016/j.geothermics.2008.11.006

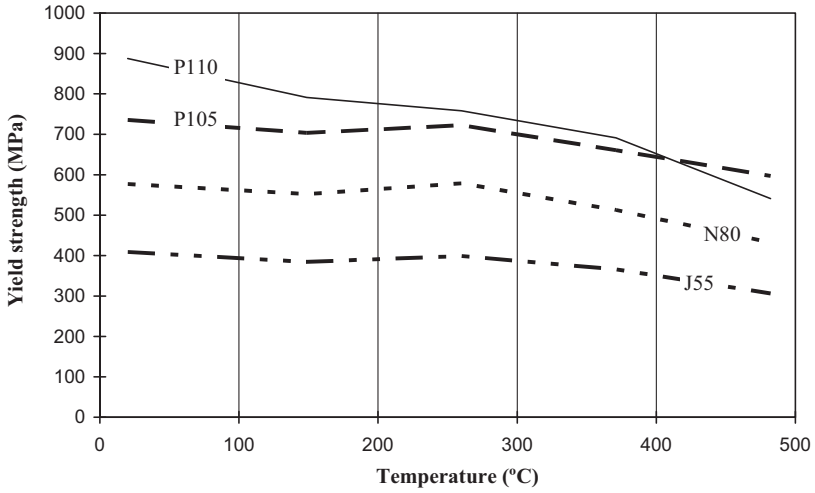

Fig. 5. Yield strength of different oil country tubular goods (OCTG) grades as a function of temperature (after Lari, 1997).

small-scale specimens whose dimensions are specified by current norms and standards. Casing connections are known to have stress concentration zones due to thread geometry. Classic fatigue estimation requires intensive full-scale testing. The application of the local stress concept reduces the time and cost needed for a traditional statistical evaluation using full-scale specimens. Two input data are required for the application of the LSSC: the experimental determination of the stress–strain curve (σ/ε curve) and an evaluation of the local stress distribution.

The stress–strain curve is measured using pure uniaxial load, with constant deformation cycles. A constant deformation cycle exposes the specimen to constant amplitude deformation instead of constant amplitude stress. The results can be represented as a stress–strain diagram or a Wöhler diagram, also known as stress-cycle curve (S–N curve) (Teodoriu, 2005), and is a way to represent the cyclic behavior of materials. The higher the magnitude of the stress is, smaller the number of semicycles (N) to failure. A flattened curve (almost horizontal) at higher N values is characteristic of ferrous materials (steels) and it is called the fatigue limit or endurance limit. For high stress values there is no endurance limit. This is also characteristic of casing loads in which the induced stresses are higher then the material yield strength.

The stress vs. strain dependency can be written using the Ramberg-Osgood correlation (Ulmanu and Ghofrani, 2001):

$$\varepsilon_a = \varepsilon_{a,e} + \varepsilon_{a,p} = \frac{\sigma_a}{E} + \left(\frac{\sigma_a}{K'}\right)^{1/n'} \quad (2)$$

where K', n', and E are empirically determined parameters.

The Wöhler-type diagram (Ulmanu and Ghofrani, 2001; Teodoriu, 2005) can be drawn using the following equation:

$$\varepsilon_a = \varepsilon_{a,e} + \varepsilon_{a,p} = \frac{\sigma'_f}{E}(2N)^b + \varepsilon'_f(2N)^c \quad (3)$$

The experimental determination of σ'_f, ε'_f, b and c is required because the stress–strain curve differs from static to cyclic loading. The b and c parameters in Eq. (3) are material constants and are experimentally evaluated, or estimated based on casing material characteristics determined by a tensile test. When the external load variation is slow, the static stress–strain load may be used without introducing large errors. For example, Fig. 6 shows a comparison between static and cyclic stress–strain curve for 42 CrMo4 steel. A detailed description of how the various parameters are to be determined is presented by Ulmanu and Ghofrani (2001) and Teodoriu (2005).

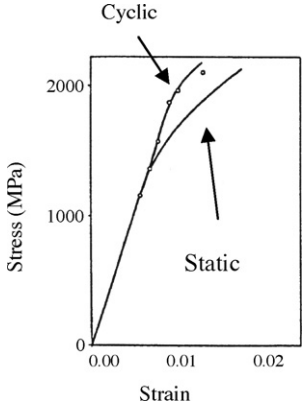

Fig. 6. Static vs. cyclic stress–strain diagrams for 42CrMo4/SAE 4142, hardened steel (Teodoriu, 2005).

Fatigue determination using the local stress–strain method is based on the cyclic behavior of materials, on the relationship between external loads and local stress, and on the evaluation of the stress–strain curve. The result is represented as a Wöhler diagram or stress–strain curve for a crack having a length of 0.5–1.0 mm.

The relationship between local and average stresses and strains is given by the Neubert equation (Ulmanu and Ghofrani, 2001):

$$K^2 = K_{ts}K_{te} = \frac{\sigma_l}{S}\frac{\varepsilon_l}{e} \quad (4)$$

Using the notation $e = S/E$, Eq. (4) can be rewritten as

$$\sigma_l \varepsilon_l E = (KS)^2 \quad (5)$$

The left-hand term of the equation represents a parameter that, for different loads, describes the corresponding damage. According to Ulmanu and Ghofrani (2001), the damage parameter (noted as

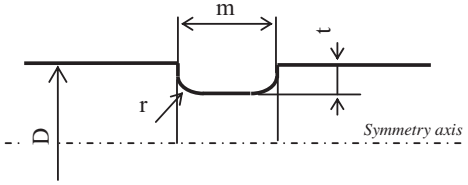

Fig. 7. Typical U-type notch that mimics a threaded connection (based on DIN 471, 1990). D: external diameter (mm); r: notch root fillet radius (mm); m: notch width (mm); t: notch depth (mm).

Please cite this article in press as: Teodoriu, C., Falcone, G., Comparing completion design in hydrocarbon and geothermal wells: The need to evaluate the integrity of casing connections subject to thermal stresses. Geothermics (2009), doi:10.1016/j.geothermics.2008.11.006

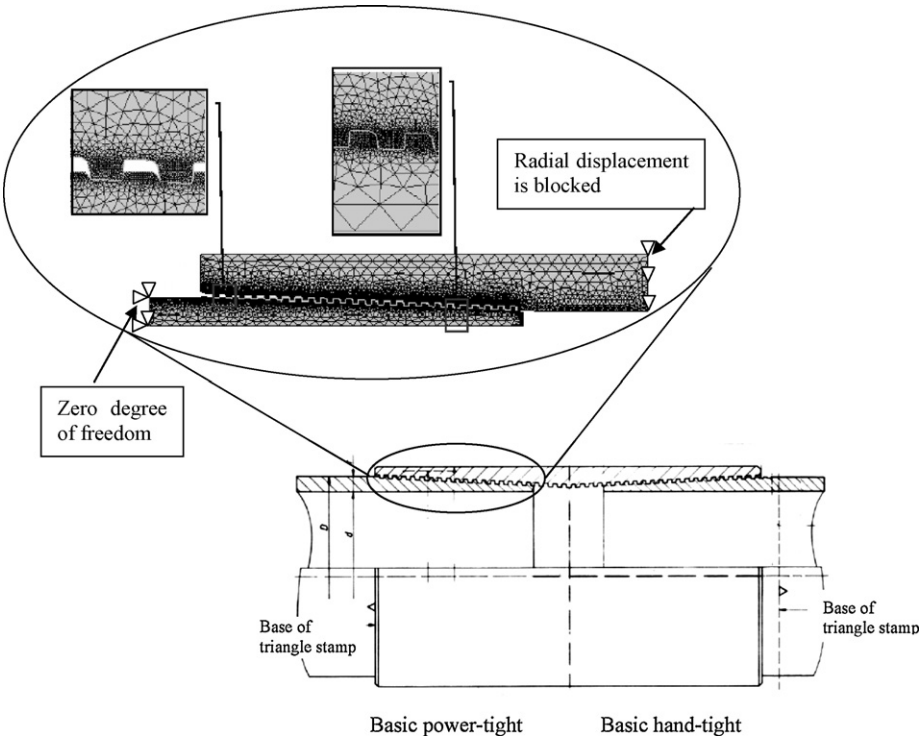

Fig. 8. Geometry and mesh of a two-dimensional finite element method model of an 18 – 5/8 in. diameter casing connection.

P_{SWT}) is given by

$$P_{SWT} = \sqrt{\sigma_1 \varepsilon_1 E} \tag{6}$$

The so-called modified Wöhler curve of P_{SWT} can be determined using the following equation:

$$P_{SWT} = \sqrt{\sigma_f'^2 (2N)^{2b} + \sigma_f' \varepsilon_f' E (2N)^{b+c}} \tag{7}$$

By solving Eqs. (3) and (5), it is possible to determine the local stress and strain for a given load. Given σ_1 and ε_1, parameter P_{SWT} and the number of semicycles, N, can be calculated using Eqs. (6) and (7).

The influence of the average tension on the damage process must also be considered. The following equation can be used for this purpose:

$$S = a_M(\sigma_m + \sigma_a) \tag{8}$$

For specific notch geometries, the stress concentration factor can be calculated using empirical formulae. The equivalent notch of a casing connection thread can be modeled by using the so-called V- or U-type notch. For the U-type notch (see Fig. 7), the German standard DIN 471 (1990) provides the following formula (assuming a bending stress state):

$$K = 1.14 + 1.08\sqrt{\frac{t}{r}} = 1.14 + 1.08\sqrt{\frac{1.57}{0.2}} = 4.17 \tag{9}$$

For standard threaded connections (nut and bolt) the stress concentration factor is considered to be between 4 and 10 (Buch, 1988).

6. Casing fatigue: numerical investigations

The finite element method (FEM) was used to better understand the stress state in the threaded connection of a casing. The ANSYS Version 11.0 (University License) software package (Lethbridge, 2008) was used to investigate the stress induced in the threaded connection during axial tension and compression.

The first goal was to estimate the stress concentration factors within the complete and incomplete thread turns. Changes in material properties due to high temperature were not initially considered, as it was assumed that these factors are a function of geometry only.

A two-dimensional model of a N80 grade, 18 – 5/8 in. (473 mm) casing with 11.05 mm wall thickness was built (see Fig. 8), which provided fast and reliable results. The connection is considered to be axially restrained at the ends, with free radial displacement. One end has zero degrees of freedom, while the other end has only the radial displacement blocked. This ensures a pure axial load due to the applied force. The different way in which the connection responds to the loads was evaluated using a three-dimensional model, as presented in Fig. 9.

The stress concentration factor, K, is defined as the maximum stress that occurs in the connection (commonly at the thread root) vs. the average stress in the casing body. Based on the FEM analysis, it was found that, for a Buttress connection K differs from tension to compression. This variation can be explained by the more aggressive bending on the thread turn for the tensile load and also by the asymmetric geometry of the Buttress thread that has different flank angles. For Buttress threads, the flank angles are 3° for

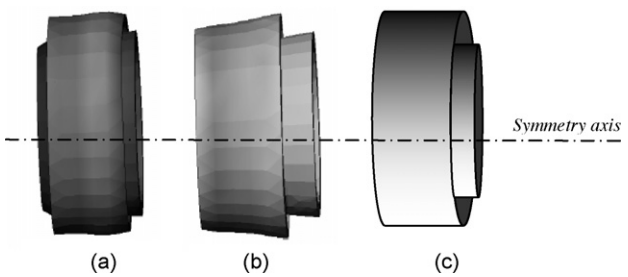

Fig. 9. Qualitative representation of the deformation of a compression loaded (a) and tension loaded (b) threaded connection compared to the non-deformed status (c).

Please cite this article in press as: Teodoriu, C., Falcone, G., Comparing completion design in hydrocarbon and geothermal wells: The need to evaluate the integrity of casing connections subject to thermal stresses. Geothermics (2009), doi:10.1016/j.geothermics.2008.11.006

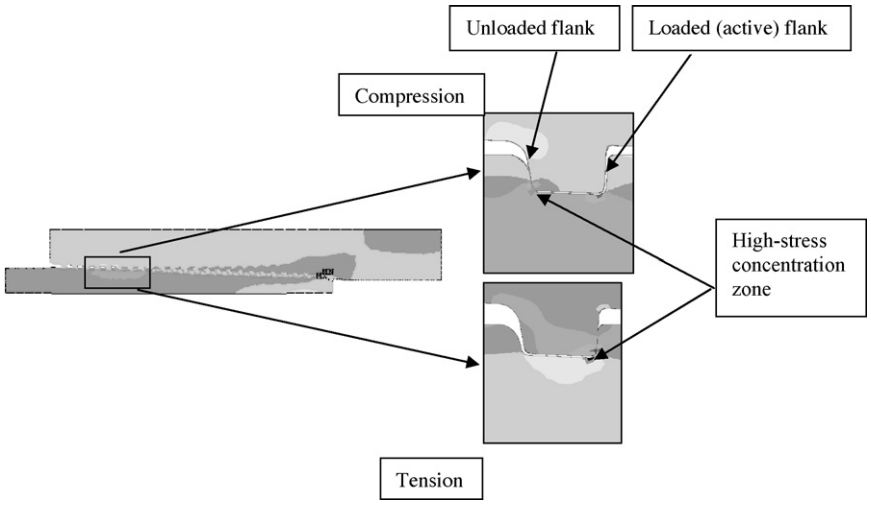

Fig. 10. Stress distribution at the thread root for the compression (top) and tension (bottom) load cases, as simulated using the finite element method model.

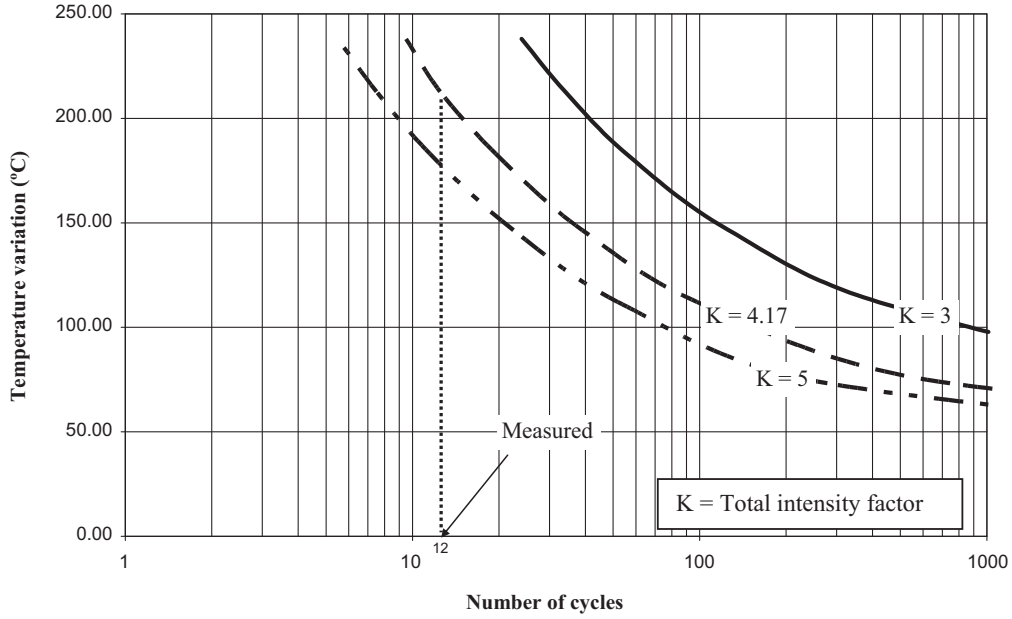

Fig. 11. Temperature vs. number of cycles for an 18 – 5/8 in. (473 mm) Buttress connection, grade N80.

the loaded (or active) flank and 10° for the unloaded flank. Fig. 10 shows the loaded and unloaded flanks' positions, and thread turns under compression and tension loads, with high resulting stresses at the thread root. In reality, the incomplete thread turns present sharp edges and therefore higher stress concentration factors may be expected.

The deformation of the thread turns under a tension load is different from that under a compression load; we obtained: $K = 3.51$ for tension and $K = 2.73$ for compression.

7. Discussion

The modified stress-cycle curve (S–N curve) obtained from the LSSC theoretical model is given in Fig. 11. The y-axis represents the maximum differential temperature to which the casing is subjected. Table 3 presents the parameters used for the casing fatigue estimation, which appear in Eq. (7).

Fig. 11 shows that, for extreme temperature variations, the fatigue resistance of the connections is as low as 10 cycles. It took 12 cycles to reach fracture with the full-scale experimental tests, corresponding to a stress concentration factor of 4.17. The experimental tests were conducted with a grade $N - 80$, 18 – 5/8 in. (473 mm) casing. The specimens were axially loaded in a testing frame, and exposed to alternating cycles of tension and compression until fracture occurred. The applied axial load was calculated so that the average stress inside the specimen body was equal to the material's minimum yield strength (550 MPa). A more detailed description of the testing procedure is presented by Teodoriu (2005).

Table 3
Parameters used for casing fatigue calculations.

Parameter	Notation	Value
Constant	b	−0.079
Constant	c	−0.869
Young's modulus	E	182 GPa
Maximum strain	ε_f	1.78
Tension strength	σ_f	720 MPa

Please cite this article in press as: Teodoriu, C., Falcone, G., Comparing completion design in hydrocarbon and geothermal wells: The need to evaluate the integrity of casing connections subject to thermal stresses. Geothermics (2009), doi:10.1016/j.geothermics.2008.11.006

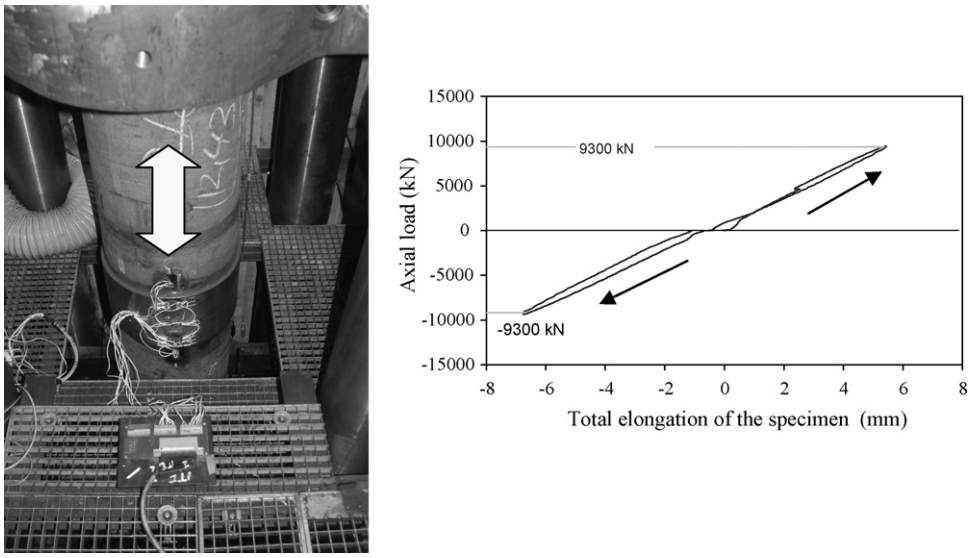

Fig. 12. Full-scale testing of an 18 – 5/8 in. (473 mm) Buttress connection, grade N80 (Teodoriu, 2005).

Several 18 – 5/8 in. (473 mm) specimens representing a Buttress connection of Grade N80 casing were tested under alternating axial tension and compression loads with slow variation (one cycle per hour). The applied loads were ±9300 kN, corresponding to an induced axial load equal to the yield strength of the pipe body. A plot of the applied cycles is shown in Fig. 12, which also shows the specimen mounted in a full-scale testing frame. The first specimen failed (by rupture) at the last engaged thread of the pipe after 10 cycles. The wall thickness in the failure area varied across the pipe circumference. A cross-section of the failed specimen showed that the pipe thickness in the threaded area was only 91.5% of that of the rest of the pipe, leading to a nominal stress in the failure area of 581 MPa, which was approximately 9% greater than the stress in the pipe body. No fractures or cracks appeared in two other specimens exposed to about six cycles each.

The stress concentration factor varies from one type of connection to another, as it is a function of connection geometry and its manufacturing process. The fracture obtained during the experimental investigations on Buttress thread was located at the zone of imperfect thread turns, suggesting that more attention must be paid during the thread manufacturing process.

For a high-enthalpy geothermal wells with fluid production temperatures between 100° and 250 °C the fatigue resistance of the tested N80 Buttress connections varies between 10 and 110 cycles. This information should be considered when evaluating the minimum project lifetime and optimizing well operations. The thread geometry, especially the incomplete thread turns, strongly affect the value of K. For example, a lower K will increase the lifetime of the casing over 1000 cycles, as shown in Fig. 11. Large temperature variations should be avoided by limiting well cooling. Maximum allowable temperature difference can be calculated using fatigue criteria as presented here or plastic deformation criteria discussed by Chiotis and Vrellis (1995).

8. Conclusions and recommendations

Drilling and well completions can account for more than half of the capital cost for a geothermal power project. The lessons learnt from oil and gas wells may be helpful in geothermal wells completions, both from the technical and the economic point of views.

The paper presented the theoretical and experimental work carried out to evaluate the low-cycle fatigue (LCF) resistance of an 18 – 5/8 in. (473 mm) diameter casing with Buttress thread connections (typically used in geothermal well completions). The results showed that, under extreme loads, the LCF resistance of this type of connections could be as low as 10 cycles. More full-scale experimental work is required to extend the validity of the results obtained by this study to other types of threaded connections. Also, as considerable geothermal field experience (>2000 wells) with Buttress threads is available, the results presented here need to be evaluated in light of field experience.

We consider that temperature variations in geothermal wells during drilling, testing, repair and other operations should be kept to a minimum. For example, as it can be deduced from Fig. 11, a temperature variation of less than 80 °C is required to ensure that the total number of cycles to failure remains higher than 100. This would minimize the risk of casing failure for the average life of a geothermal well.

Significant care should be taken when cyclic water injection/production (huff 'n' puff) operations are performed, like the ones discussed by Wessling et al. (in press). In addition, when considering reservoir stimulation procedures one should try to minimize the injection of cold water into the (hot) geothermal wells.

References

Allen, D.M., Ghomshei, M.M., Sadler-Brown, T.L., Dakin, A., Holtz, D., 2000. The current status of geothermal exploration and development in Canada. In: Proceedings of the 2000 World Geothermal Congress, Kyushu-Tohoku, Japan, pp. 55–58.

Augustine, C., Tester, J.W., Anderson, B., Petty, S., Livesay, B., 2006. A comparison of geothermal with oil and gas well drilling costs. In: Proceedings of the 31st Workshop on Geothermal Reservoir Engineering, Stanford University, Stanford, CA, USA, pp. 5–19.

Bohm, B., 2000. Drilling geothermal well ISO. Geo-Heat Center Quarterly Bulletin 21 (4), 12–19.

Brunetti, V., Mezzetti, E., 1970. On some troubles most frequently occurring in geothermal drilling. Geothermics Special Issue 2 (Part I), 751–756.

Buch, A., 1988. Fatigue Strength Calculation. TransTech Sa, Aedermannsdorf, Switzerland, 256 pp.

Carden, R.S., Shursen, G., Nicholson, R.W., Pettitt, R.A., Rowley, J.C., 1983. Unique aspects of drilling and completing hot dry rock geothermal wells. In: Proceedings of the IADC/SPE 1983 Drilling Conference, New Orleans, LA, USA, 20–23 February, pp. 123–140.

Chiotis, E., Vrellis, G., 1995. Analysis of casing failures of deep geothermal wells in Greece. Geothermics 24, 695–705.

Dickson, M.H., Fanelli, M. (Eds.), 1990. Small Geothermal Resources. UNITAR/UNDP Centre for Small Energy Resources. Rome, Italy, pp. 1–29.

DIN 471, 1990. German Standard DIN 471, Sicherungsringe (Halteringe) für Wellen. Regelausführung und schwere Ausführung, 29 pp.

Please cite this article in press as: Teodoriu, C., Falcone, G., Comparing completion design in hydrocarbon and geothermal wells: The need to evaluate the integrity of casing connections subject to thermal stresses. Geothermics (2009), doi:10.1016/j.geothermics.2008.11.006

Ellis, P.F., 1979. Failure Analysis Report: Well Production Casing Brady No. 5 Well. Geothermal Food Processors, Inc., Fernley, Nevada. Radian Corporation report DCN 79-212-003-04 prepared for the U.S. Department of Energy, Chicago Operations and Regional Office, Argonne, IL, USA, 17 pp.

Grimsson, O.R., 2007. A Clean Energy Future for the United States: the Case of Geothermal Power. Testimony by the President of Iceland Olafur Ragnar Grimsson at a Senate Hearing Committee on Energy and Natural Resources, US Senate, September, 31 pp.

Jotaki, H., 2000. High angle directional drilling at Takigami geothermal field. In: Proceedings of the 2000 World Geothermal Congress, Kyushu-Tohoku, Japan, pp. 2347–2352.

Lari, I., 1997. Rezistenta Coloanelor de Bulrane Tubate in Sondele Supuse Procesului de Injectioe de Abur. ICPT internal Report, Campina, Romania, 55 pp.

Lazzarotto, A., Sabatelli, F., 2005. Technological developments in deep drilling in the Larderello Area. In: Proceedings of 2005 World Geothermal Congress, Antalya, Turkey, p. 6.

Lee, K.C., 2001. Classification of geothermal resources by exergy. Geothermics 30, 431–442.

Lethbridge, P., 2008. An overview of ANSYS academic products at release 11.0. http://www.ansys.com/academic/downloads/academic_article_pdf_1.pdf.

Nicholson, R.W., Pettit, R.A., Sims, J., 1982. Production casing for hot dry rock wells EE-2 and EE-3. Geothermal Resources Council, Transactions 6, 219–222.

Pye, D.S., Holligan, D., Cron, C.J., Love, W.W., 1989. The use of beta-C titanium for downhole production casing in geothermal wells. Geothermics 18, 259–267.

Ragnars, K., Benediktsson, S., 1981. Drilling of a 2000 m (6562 ft) borehole for geothermal steam in Iceland. In: Proceedings of the International Geothermal Drilling and Completions Technology Conference, Albuquerque, NM, USA, 21 January, pp. 4.1–14.1.

Rogge, S., 2004. Geothermische Stromerzeugung in Deutschland Ökonomie, Ökologie und Potenziale. Ph.D. Thesis. Technichen Universität Berlin, Germany, 119 pp.

Tenzer, H., 2001. Development of hot dry rock technology. Geo-Heat Center Quarterly Bulletin 22 (4), 14–22.

Teodoriu, C., 2005. Cercetari privind comportarea materialelor sa imbinarilor filetate in sondele supuse procesului de injectie de abur. Ph.D. Thesis. Universitatea "Petrol-Gaze", Ploiesti, Romania, 155 pp.

Ulmanu, V., Ghofrani, R., 2001. Verfahren zur Lebensdauerabschätzung der Tiefpumpgestänge nach dem Ortlichen Konzept (Fatigue life prediction method for sucker rods based on local concept). Erdöl, Erdgas, Kohle 117 (4), 189–195.

Wessling, S., Junker, R., Rutqvist, Silin, D., Sulzbacher, H., Tischner, T., Tsang, C.F., in press. Pressure analysis of the hydromechanical fracture behaviour in stimulated tight sedimentary geothermal reservoirs. Geothermics.

Williamson, K.H., Gunderson, R.P., Hamblin, G.M., Gallup, D.L., Kitz, K., 2001. Geothermal power technology. Proceedings of the IEEE 89, 1783–1795.

Witcher, J.C., 2001. Geothermal direct-use well for commercial greenhouses radium springs, New Mexico. Geo-Heat Center Quarterly Bulletin 22 (4), 1–7.

Please cite this article in press as: Teodoriu, C., Falcone, G., Comparing completion design in hydrocarbon and geothermal wells: The need to evaluate the integrity of casing connections subject to thermal stresses. Geothermics (2009), doi:10.1016/j.geothermics.2008.11.006

OIL GAS

EUROPEAN MAGAZINE

INTERNATIONAL EDITION OF
ERDÖL ERDGAS KOHLE

Dezember, 4/05

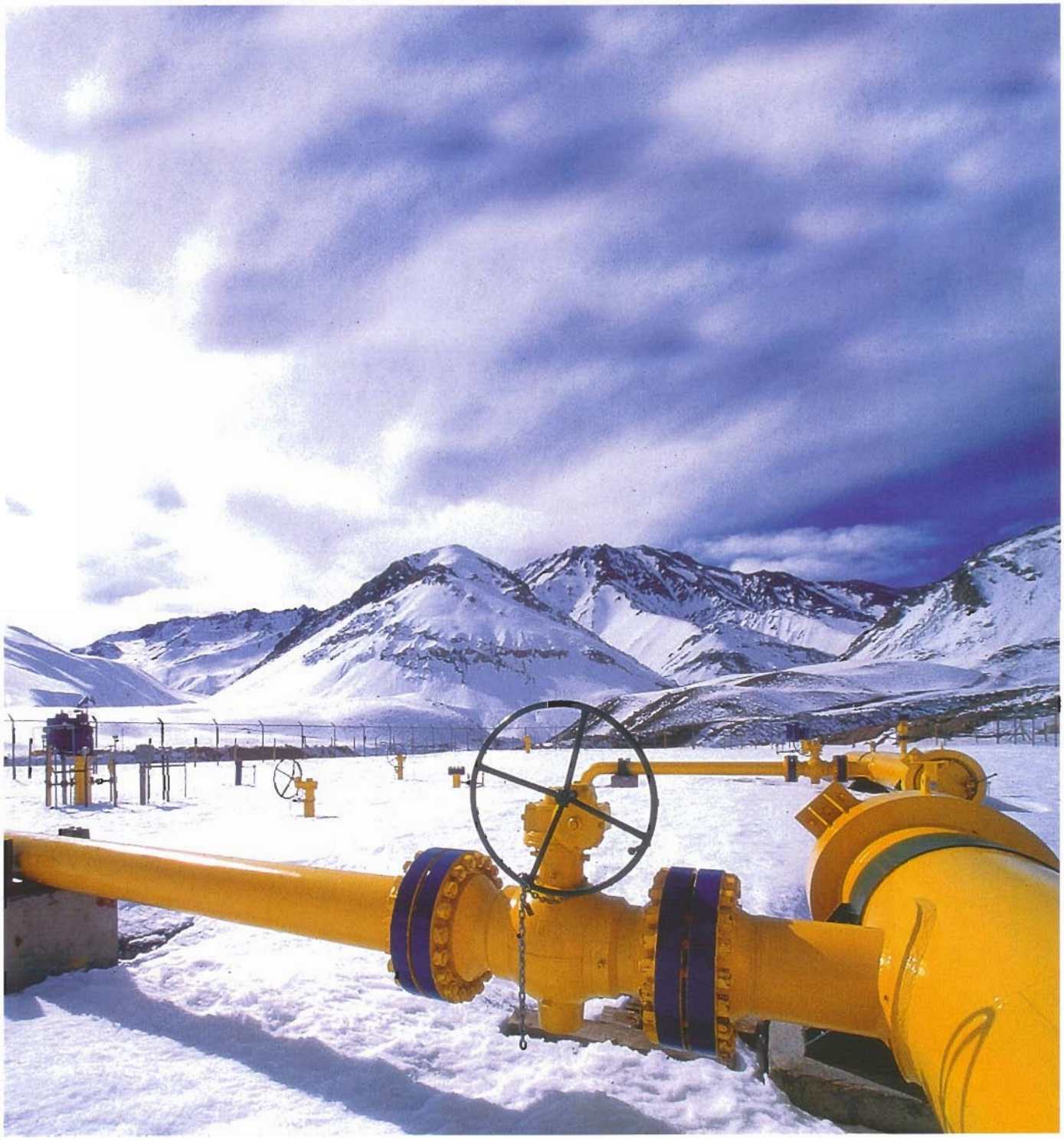

[18] Asquith, G., Krygowski, D.: Basic Well Log Analyses. 2nd edition, AAPG Methods in Exploration, Series 16, AAPG, Tulsa (2004).
[19] DePavia, L. et al.: A Next-Generation Wireline NMR Logging Tool. Paper SPE 84482 presented at the 2003 SPE Annual Technical Conference Denver, USA.
[20] Lowden, B. and Strobel, J: Maximising NMR Log Interpretations in Thinly Bedded Reservoirs. AAPG Annual Meeting, Barcelona, September 2003.
[21] Hertzog, R. C.: Geochemical Logging with Spectrometry Tools. Proc., paper SPE 16792 presented at the 62nd Annual Technical Conference and Exhibition, Society of Petroleum Engineers, Richardson, TX, USA (1987).
[22] Herron, S. L., and Herron, M. M.: Quantitative Lithology: An Application for Open- and Cased Hole Spectroscopy. Transactions, 32nd Annual SPWLA Logging Symposium (1996), June 16–19, paper E.
[23] Proett, M. et al.: Formation Testing in the Dynamic Drilling Environment. SPWLA 45th Annual Logging Symposium (2004); SPE/IADC Drilling Conference Amsterdam, The Netherlands (2005).
[24] Strobel, J. et al.: Comparison of Formation Pressure and Mobility Data Derived During Formation Testing While Drilling with a Mud Motor with Production Data and Core Analysis. Paper SPE 92492 presented at the 2005 SPE/IADC Drilling Conference, Amsterdam, Feb. 23–26.
[25] Dake, L. P.: Fundamentals of Reservoir Engineering. Elsevier Science B. V., Amsterdam (1978).
[26] Volokitin, Y. et al.: A Practical Approach to Obtain Primary Drainage Capillary Pressure Curves from NMR Core and Log Data. Petrophysics (2001) **42**, No.4.
[27] Bryan, J, et al.: Oil-Viscosity Predictions From Low-Field NMR Measurements. SPE Reservoir Evaluation & Engineering (Feb 2005) **8**, No 1.

Thies Dose *is a reservoir engineer with RWE Dea AG, Hamburg. His recent professional focus is on integrated 3D modeling. He owns a Diplom (equivalent to M. E.) in Petroleum Engineering from Technical University of Clausthal.*

Joachim Strobel *is head of Formation Evaluation Department with RWE Dea AG, Hamburg. Previously, he worked Schlumberger as wireline engineer and petrophysicist in africa and europe. He owns a Diploma from University College of Swansea and Diplom (equivalent to M. Sc.) from Munich University, both in Geology.*

Jason A. McLennan *is a second year PhD student at the Center for Computational Geostatistics within the University of Alberta. Prior to graduate studies, Jason has been involved in geostatistical research for 4 years. He owns a B. Sc. in Mining Engineering and a M. Sc. in Geostatistics, both from University of Alberta.*

Buttress Connection Resistance under Extreme Axial Compression Loads

*By C. TEODORIU**

Abstract

This paper presents the results of the analytical and experimental work on buttress connections tested under extreme tension and compression loads. Current standards do not give direct information on the compression resistance, and for this reason the following paper presents the method to calculate the compression strength of Buttress connections.

Introduction

The main load on the casing string is assumed to be given by the axial tension load resulting from its own weight. Basically, the assumption holds for a standard well. There are special wells where complementary loads in addition to axial tension could result in axial compression (i. e. steam injection wells, deviated wells, etc.). For such special wells the casing design program takes into consideration the axial compression load or measures to avoid high loading for compression. Typically the lower part of the casing string is considered to be compressed due to buoyancy or casing launching, but these loads are considered to be negligible in comparison with axial loads. Because of the high number of non-API connections, mostly Premium termed, the connection owners are given information regarding the compression resistance of their connections. Available standards give no recommended values.
Since modern wells are drilled to achieve complex purposes, the loads considered for casing design are in some cases extreme. HP/HT wells are known for their extreme environment and the resultant acting loads on the casing string. The casing design under axial compression was derived from steam injection wells. For these applications it was found that pre-stressing the casing string could reduce the negative effect of axial compression. During more than 40 years of steam injection it has been found that the Buttress connections have a good loading capacity under high axial tension loads. The advantage of a Buttress connection is given by its simplicity and costs compared with Premium connections.
Therefore for some casing strings, e. g. anchor casing, it is usual to have Buttress connections, which are cheaper, especially for large casing diameters. For anchor casing the acting loads are typically low, but at the surface the entire casing string hangs on it. Therefore it is necessary to investigate the compression resistance of such casings. The threaded connections are mostly designed to have a maximum tension resistance. There are some new connections on the market especially designed for high compressive loads, but for special purposes like drilling with casing or high temperature wells. This special condition makes the price for such connections high.
In the following a method to quantify the compression resistance of Buttress connections is presented. Experimental results are used for a comparison with the calculated values.

*Dr.-Ing. C. Teodoriu, ITE, TU-Clausthal, Clausthal-Zellerfeld, Germany (E-mail: Catalin.Teodoriu@tu-clausthal.de)

0179-3187/05/IV

Analytical Calculation of Compression Resistance of Buttress Connections

The failure modes of a threaded connection are:
– thread shear
– stripping
– fracture (under tension)
– local buckling (under compression).
Thread shear may occur in very special cases, where the thread length is too short or if the thread turn loading has not been optimized.
The stripping failure mode is given by the radial deformation caused by axial force deflection on the thread flank. Fracture is the most common failure mode and it is caused by exceeding the material resistance in the critical area.
To improve the threaded connection behavior some geometrical parameters were changed regarding the Buttress geometry: the flank angle was reduced to 3° which increases the stripping resistance. The shear strength was improved by using a minimum number of turns.
The first three failure modes presented above are defined for tension load only. The last failure mode was found during the tests carried out in the Institute of Petroleum Engineering of the TU Clausthal and presented in [6].
The tension resistance of API connections, based on catalogue information, is shown in Figure 1. The pipe body resistance was used

as a reference. Since the Buttress connection has a tension resistance similar to the pipe body it becomes obvious why the presented article gives much attention to this connection.

The literature contains sufficient information regarding the analytical calculation of Buttress resistance under tension loading. According to API the tensile resistance (fracture) is given by the following equation [1]:

$$F_{lim} = 0.95 \cdot A_b \cdot R_m \cdot [1.008 - 1.56 \cdot 10^{-3} \cdot (1.08 - R_{p0.2} / R_m) \cdot D] \quad (1)$$

where:

A_b	pipe cross sectional area, mm²;
D	pipe outer diameter, mm;
$R_{p0.2}$, R_m	yield strength and ultimate strength of the material, MPa.

The stripping force is computed based on the following equation [2]:

$$F_s = \pi \cdot \left(t - \frac{h}{2}\right) \cdot \left[R_{p0.2} \cdot d_m + 2 \cdot \Delta \cdot E_1 + \frac{2 \cdot h_t \cdot E \cdot t}{D} \right] \quad (2)$$

where:

β	flank angle (3° for Buttress's active flank)
Δ	thread interference
E	Young modulus
t	wall thickness
h_t	thread height.

The stripping force is computed as the axial force producing a radial deformation of the pin – box system which is higher than the thread height. As presented in the equation (2) the stripping force depends on the thread height, thread diameter and the pre-stress state. Equation (2) can also be used for the compression case, by replacing β with 11°, which is the value of the second (unloaded) flank angle.

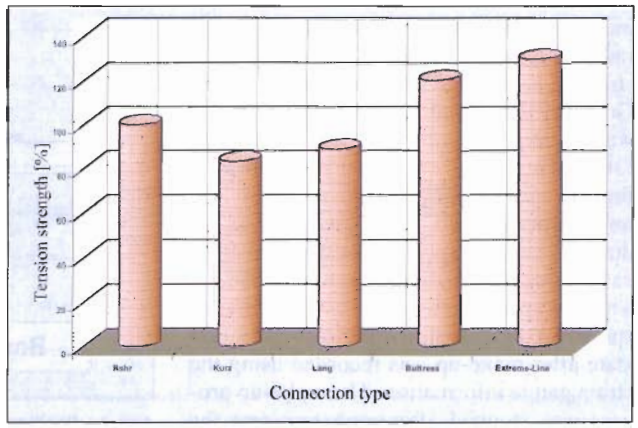

Fig. 1 Axial tension resistance for different API connections

The force needed to shear the thread turns is calculated as follows [2]:

$$F_{shear} = \frac{0.577 \cdot \pi \cdot d_1 \cdot b \cdot l \cdot R_m}{p} \quad (3)$$

with

b	thread turn length
l	length of total engaged threads
d_1	thread root diameter
p	thread pitch
R_m	ultimate strength.

Experimental Tests on Buttress-Connection (18 5/8″)

The experimental tests program consists of making up, tension and compression of three specimens having a diameter of 18 5/8″. The connections are standard buttress. The investigations were conducted in two steps: experimental stress analysis to determine the thread stress distribution and compression to failure tests.

52 strain gauges were applied on the first specimen as presented in Figure 2. The strain gauges were positioned in series along the connection axis. The results were later compared with those obtained by finite element analysis.

The specimen was subjected to axial tension and compression in seven load steps. First, the specimen was subjected to axial tension load up to 80% of its catalogue recom-

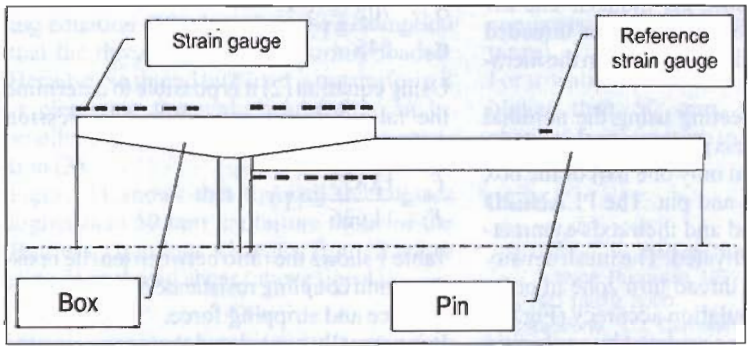

Fig. 2 Strain gauge positions for the specimen No. 1

Fig. 3 The reference specimen mounted in the ITE OCTG Testing Frame

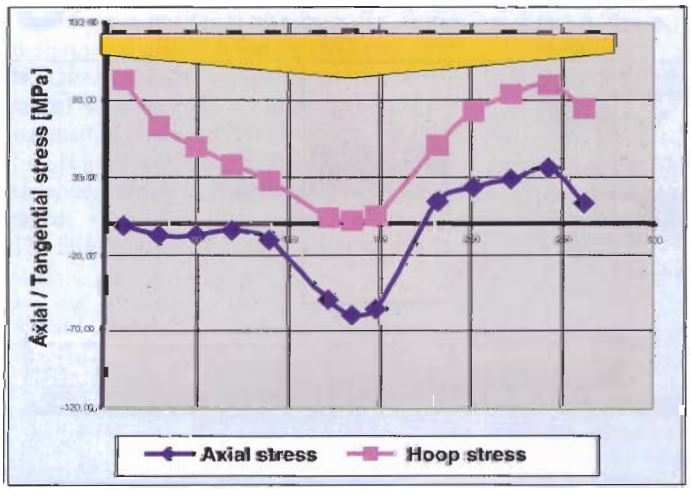

Fig. 4 Axial and tangential stress distribution for specimen No.1

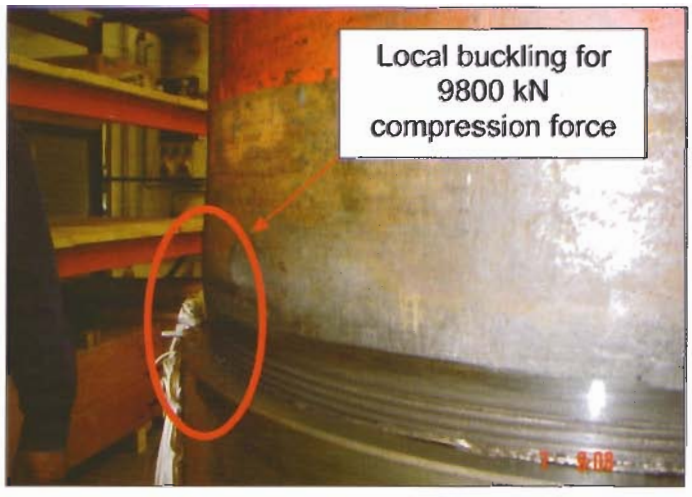

Fig. 5 View of the local buckling of the specimen No. 1

mended load. During each step the axial and radial stresses were recorded using a 60 strain gauge amplifier produced by HBM, Germany. The final compression load step was conducted until the connection had failed. The second specimen was tested using the same procedure, whereby only the number of applied strain gauges was reduced. The third specimen was tested up to catalogue recommended maximum load.

The first specimen was used as the reference specimen and therefore the stress and strain state after make-up was recorded using the strain gauge information. The make-up process was stopped after each turn and the strain gauge data were recorded. The axial and tangential stress distribution after the final make-up is presented in Figure 3. The stress distribution shows that after the make-up, only tangential stresses are acting in the connection. No significant axial stresses were recorded. After make-up the specimen was mounted in the ITE OCTG testing facility number 5 (Fig. 4).

The specimen was loaded under axial tension up to an axial force of 7900 kN, which represents about 80% of the catalogue recommended Buttress coupling resistance of 9670 N. Subsequently the load was decreased down to 0. The zero point was used to verify the accuracy of the strain gauges. No deviation was observed and therefore the specimen was subjected to axial compression stepwise up to 7900 and then continuously up to failure. The specimen fails due to local buckling of the pin below the last engaged thread turn at a load of 9800 kN. The failure zone is shown in Figure 5.

For the second specimen 18 strain gauges were used. The strain gauge position was calculated based on the finite element analysis results and is shown in Figure 6. Because both finite element analysis and the first failure test showed that the zone of last engaged threads and incomplete threads is the critical zone under compression load, the strain gauges were applied especially at this position. The load steps for the second specimen were the same as for the first specimen. The failure test of the second specimen shows the same failure mode as for the first one: local buckling at the last thread turns region, see Figure 7.

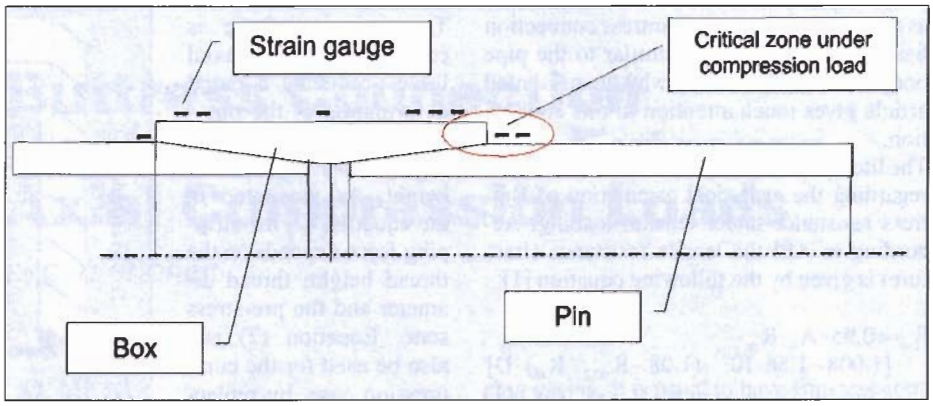

Abb. 6 Position of strain gauges for specimen No. 2

Because the API – 5CT gives only information about the Buttress coupling resistance under tension load, the last specimen was subjected to axial loading at maximum catalogue values. The test showed that the buttress connection has comparable resistance under tension and compression load as long as the load is smaller or equal to maximum recommended values according to API. No deformations were observed on the specimen, both on threaded connection and, respectively pipe body after testing.

Finite Elements Analysis of Buttress Connection

The program ANSYS 5.7 was used for the finite elements analysis. The analysis was carried out using 2D models. The 2D models have a good accuracy for threaded connection simulations as shown in the literature [4, 5].

The model was creating using the nominal values of the Buttress geometry. Due to symmetry of the system only one half of the box was modeled: box and pin. The PLANE2D elements were used and their axis-symmetric function was activated. The mesh density was refined in the thread turn zone in order to improve the simulation accuracy (Fig. 8). The axial force was simulated by applying a constant pressure on the pin free end. Figure 9 shows a comparison between stress distribution due to axial tension and compression load.

A comparison between radial deformation due to axial tension and compression shows that the radial deformation is higher in case of compression load having the same force value. The larger deformation is produced by the unloaded flank (having 11°) which becomes active under compression load. Figure 10 shows the radial deformation of the box for different values of the axial load.

Comparison Between Tension and Compression Resistance of Buttress Connection

Based on the maximum calculated stress values using finite element analysis, we can define the behaviour between axial stresses under compression, respectively tension:

$$\frac{\sigma_C}{\sigma_T} = \frac{702}{545} = 1.29$$

Using equation (2) it is possible to determine the ratio between maximum compression and tension stripping force:

$$\frac{F_c}{F_i} = \frac{13{,}835}{11{,}636} = 1.19$$

Table 1 shows the ratio between tensile resistance and coupling resistance or coupling resistance and stripping force.

It is normally considered that increasing the wall thickness will result in an increase of coupling resistance. However for large wall

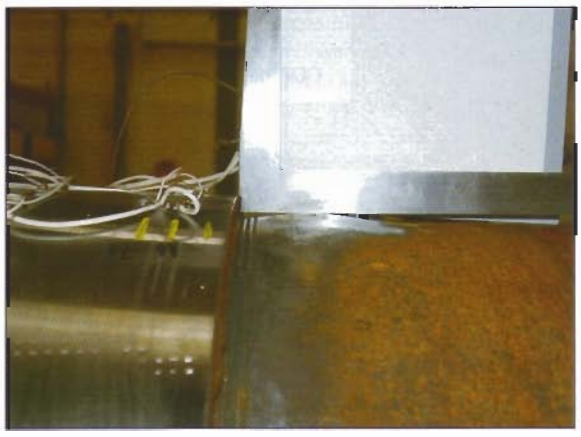

Fig. 7 View of the local buckling zone for specimen No. 2

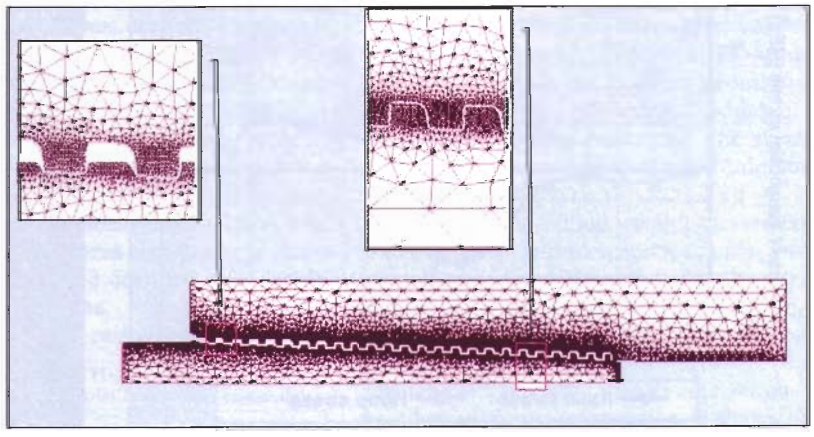

Fig. 8 Model meshing and details for finite element model

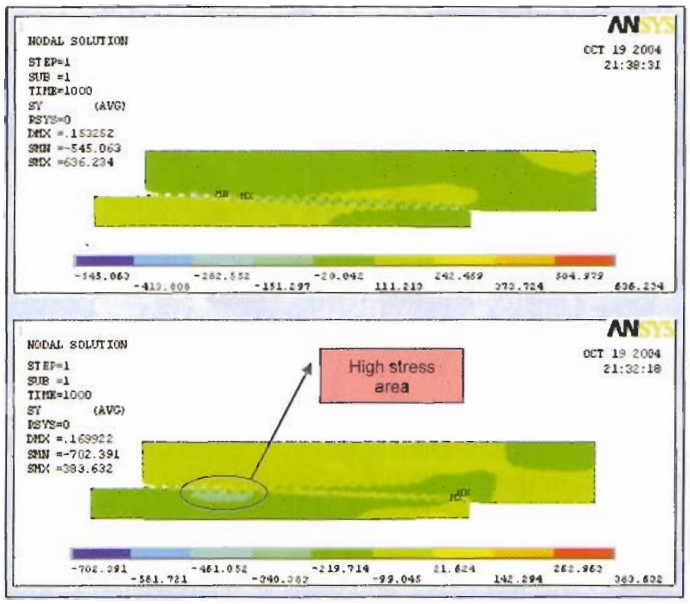

Fig. 9 **Stress state under axial tension (top) and axial compression load (bottom) for buttress thread**

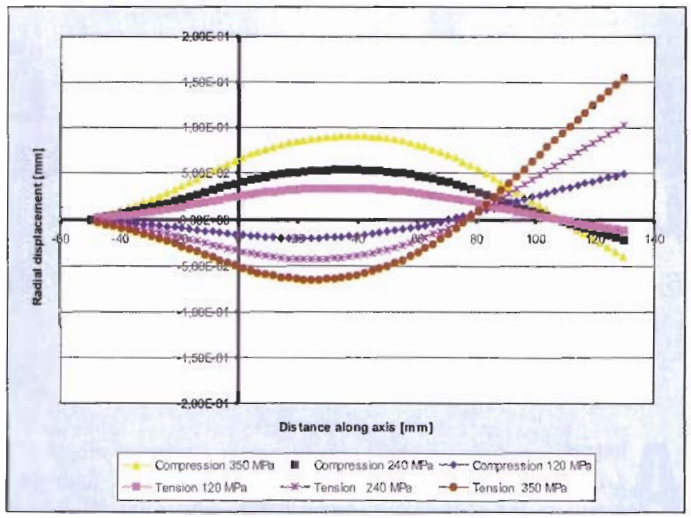

Fig. 10 **Radial displacement as a function of load level and load type**

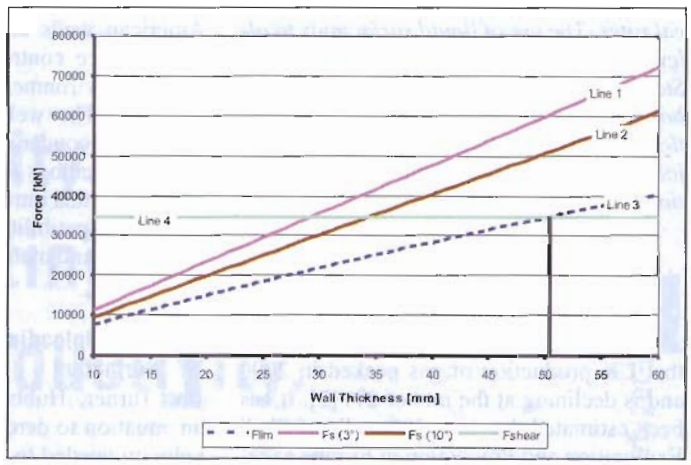

Fig. 11 **Buttress connection resistance as function of wall thickness**

thicknesses the failure mode may change from local buckling to thread shear. Figure 11 shows the variation of stripping force under tension (line 1), stripping force under compression (line 2), maximum tensile resistance (line 3) and shear force (line 4) for a Buttress connection as a function of wall thickness. The shear force does not depend on the wall thickness. The geometrical parameters involved in this equation are only the thread geometry data. Therefore the shear force is shown as constant in the Figure 11 (line 4). The shear force computed using equation (3) is based on the assumption that the thread turns are uniformly loaded. Because the thread turn load is not uniform it is clear that the real shear force can be smaller than the value computed using equation (3).

Figure 11 shows that for wall thicknesses higher than 50 mm the failure mode of the Buttress couplings changes from fracture (line 3) to thread shear (above line 4).

Conclusions

It is recommended to use the catalogue tension resistance as a basis for casing design, since at loads below the catalogue value both resistances (tension or compression resistance) are comparable. The compression resistance of an 18 5/8″ N80 Buttress connection is not much smaller than its tension resistance, but higher than the pipe body resistance.

The failure mode for compression load is local buckling below the last engaged thread turn. Under this type of failure the compression resistance could be very strongly influenced by time dependent factors like corrosion (e. g. corrosion may reduce the wall thickness, thus reducing the compression resistance).

For a wall thickness higher than 50 mm, the failure mode changes from fracture to thread shear.

Table 1 **Ratios**

	Compression	Tension
Eq. 1 and 2	1.26	1.56
Eq. 2 and tensile resistance	1.43	1.77

Literature

[1] API 5CT, 1990.

[2] Ulmanu, V.: Material Tubular Petrolier, Editura Tehnica, Bucuresti, 1992.

[3] ISO 13679, 2000.

[4] Teodoriu, C.: Cercetari privind solicitarile si comportarea materialului tubular in sondele cu injectie de abur, (Study of loads and behavior of tubular goods used in steam injection wells), 2nd Ph. D. Thesis, Universitatea »Petrol-Gaze« Ploiesti, 2005.

[5] Teodoriu, C.: Analysis of the make-up procedure and evaluation of conical shouldered threaded connections, 1st Ph. D. Thesis, TU Clausthal, 2003.

[6] Teodoriu, C., Karsch, H., Reinicke, K. M.: Untersuchungen an 18 5/8" Buttress-Verbindern unter extremen Druckbelastungen, DGMK-Tagungsbericht 2005-1, Frühjahrstagung am 28. und 29. April, 2005, ISBN 3-936418-17-9, ISSN 1433-9013.

The author would like to thank Dr. Kurt M. Reinicke, Head of Department Drilling, Production and Gas Supply for his support and encouragement in producing this paper. He also thanks Mr. H. Karsch and his company RWE DEA for making it possible to perform the tests and for allowing publication of the tests results. Finally he would like to thank the fine ITE team for their help in test preparation.

Catalin Teodoriu is research coordinator for petroleum engineering at the Technical University of Clausthal. After graduating in Mechanical Engineering for Oil and Gas Industry at the University "Petrol- Gaze" Ploiesti, Romania, he completed his first Ph.D. studies at the Technical University of Clausthal, Germany, in 2003. Between 1996–1998 he was employed in the Oil and Gas Company (PETROM) in Romania. In 1998 he joined Institute of Petroleum Engineering, TU Clausthal and has worked in various research projects related to oil and gas tubular goods, drilling fluids and field equipment development. In 2005 he received his second Ph. D. at the University "Oil&Gas" Ploiesti, Romania.

SPE 106849

Sealing Capacity of API Connections - Theoretical and Experimental Results

Marius Badicioiu/UPG Ploiesti, Catalin Teodoriu/Texas A&M

This paper was prepared for presentation at the 2007 SPE Production and Operations Symposium held in Oklahoma City, Oklahoma, U.S.A., 31 March–3 April 2007.

Abstract

Hydraulic fracturing has become a state of the art stimulation technique. It has been proved over the years that significant production increase can be obtained by applying the right fracturing technique. Nowadays, the most advanced techniques of geothermal energy recovery systems widely use hydraulic fracturing.

The following paper presents the experimental results of the tests carried out on four different compounds using the improved “grooved plate” method. The tests have showed a large variation of the tested thread compounds sealing capacity. Starting from the experimental results and the theoretical analysis of the API connection a useful chart was built to determine the real connection resistance, based on its initial makeup torque. The chart offers to engineers involved in the design of a fracturing process the possibility to estimate the maximum pressure that may lead to a connection leak.

Introduction

Most of the published data show that a long fracture is the key to well optimum stimulation. The desired length of the fracture can be achieved using equipment capable to deliver the right pressure and fluid volume. Since the hydraulic fracturing technique can be also applied to old wells, equipped with standard API connections, the high pressures that are achieved during the pumping phase require the understanding of leak resistance of API connections. It has been also proven that during the injection phase the high pump rate may lead to additional pressure increase into the well tubulars. The time and pressure values are two key parameters that may affect the sealing capacity of the API connection.

Testing the sealing capacity of a casing connection is not an easy task since it depends on many factors like: thread type and form, thread compound, ageing of the thread compound, make-up induced stresses, etc. Actually, there are no standards to evaluate the seal capacity of a thread compound. To date, three approaches have been found in the literature:

- the fixture designed during the project PRAC 88-51 that consists of two circular steel plates having spiral grove from the center to the exterior [1];
- full scale testing of threaded assembly using high load press [2] in which not only the thread compound but the entire sealing capacity of the assembly is tested;
- small size connections as described in paper [3]

There are many pros and cons for each one of the methods, but testing thread compounds separately require getting off all inconsistent parameters that may affect the evaluation process. The main parameters that may affect the thread compound evaluation are the stress-strain state induced due to make-up and thread tolerances.

The fixture proposed by the project PRAC 88-51 offers the advantage of comparing the threaded compounds only, by neglecting the make-up and tolerances induced errors. This is why it has been considered the use of the same experimental setup as the one described in paper [1]. The experimental setup will be presented in detail later in this paper.

Thread Compounds for Oil Country Tubular Goods (OCTG)

Typical threaded compounds for OCTG are formed using base grease in which solid particles are dispersed. The grease is standard lubricating grease made of mineral oil having a metal soap as thickener (i.e. aluminum stearate). In very low amount, additives are added to the compound to improve the following properties: high pressure resistance, wear protection, corrosion protection, etc.

The role of solid particles is to provide anti-galling resistance and sealing properties of the compound. Powdered metals and non-metallic particles like graphite or ceramic spheres are used as solid ingredients. Typical metals used for threaded compounds manufacturing are: lead, copper, zinc. The common non-metallic solids used for compounds are graphite, PTFE, ceramics.

The so called “green dope” or environmental friendly compounds have a totally metal-free composition. **Figure 1** shows a classification scheme of thread compounds after [3]. **Table 1** shows the composition of some common threaded compounds used in the oil industry, including the tested thread compounds described in this paper.

According to [4] the performance general requirements of threaded compounds include: consistent frictional properties, adequate lubrication properties, adequate sealing properties, physical and chemical stability both in service and in storage conditions, and properties that allow the efficient application of the compound on the connection surfaces. In addition, for

RSC threaded compounds they should lubricate the connection during the make-up runs to achieve bearing stresses (buck-up force).
The sealing capacity or, according to some authors, leak tightness, is provided by the high viscosity of the threaded compound and the small free path inside of the threaded connection.

The API threads

The API round thread is one of the very first standardized thread type used for casing and tubing. Being cheap, simple and easy to manufacture the API round threads have been extensively used for "low cost" wells. A proof of their importance for the oil industry is given by the extensively tests carried out by a technical advisory committee in the 90s having Mr. Phil Pattillo as Chairman [5, 6, 7]. The tests were focused on the better understanding of the mechanical behavior of the API 8 Round casing connection when subjected to service loads of assembly interference, tension and internal pressure [8, 9, 10]
The API round thread is an open type thread, which means that if no other material is applied on thread prior its make-up no seal is provided. Between threads a small gap remains that must be filled in order to provide a leak tight connection. This space is filled by the thread compound that is applied on pin and box before make-up. The shape and dimensions of the API 8rd are given in **Figure 2**. As it can be seen in the **Figure 2** the leak path consists of two spiral spaces comprising the gaps between pin thread crest and box thread root and pin thread root and box thread crest, respectively.
The Buttress thread has been introduced later in order to offer a connection with a very good tension resistance. It was patented Nov. 27, 1956 by Mr. Samuel Webb and assigned to United States Steel Corporation. As stated in the patent the high leak resistance should not be expected unless the stab flank is closed. The shape of the Buttress has a different leak path than API round, usually much higher. Early API tests [8] showed no difficulties with the leak resistance, but it must be noted that at that time API compounds were used for tests only.
The leak path size depends on the thread manufacturing tolerances. In order to calculate the gap volume, the minimum and maximum tolerances have been considered as presented in Annexes A and B for API round, respectively, API Buttress.

The experimental setup

As it has been explained before the grooved plate setup has been chosen for thread compound analysis because it allows testing of thread compounds independent from thread tolerances and stress-strain state. Later, full scale specimens with controlled geometry have been used for reference.
The test was performed according to the following procedure: the grooved plate was completely filled with the dope to be tested, and then the grooved plate was assembled over the sealing plate into the hydraulic press. The center of the grooved plate was connected to the high pressure pump. Mineral hydraulic oil has been used as pressurizing medium. The pressure was slowly increased and the moment at which the dope was expelled was recorded.
To build the groove plates, the groove size has been calculated according to the real dimensions of a 5 ½" API short round thread, with a wall thickness of 7.72 mm with J55 grade. The calculated dimensions for the grooved plate are shown in **Table 2**. The grooved and seal plates are shown in **Figure 3 and 4**.

Finite element analysis of the threaded connection and experimental setup

In order to estimate the contact stress to be simulated between grooved plate and seal plate a finite element analysis was carried out, using ANSYS University program. The contact pressure between the thread turns plays an important role for the sealing capacity of the connections because as long as the contact pressure is higher then the pressure to be sealed the only leak path remains the spiral path between thread turns crest and roots. Same conditions must be achieved between the two plates of the experimental setup.
Firstly, the 5 ½" connection has been investigated by determining the thread turn contact pressure after make-up and under make-up and axial load case. The results were similar with those reported by Asbill and Pattillo in [5, 6, 7]. According to the finite element analysis the contact pressure after the connection make-up with recommended torque is between 30 to 45 MPa and depends on how the averaging is performed. Due to local contact problems within the incomplete thread turns zone, some spots with high contact pressure have been found, see **Figure 5**. These values will not be considered for the further analysis. It has been also observed that the pressure on the thread flank is not uniform, as reported by Asbill and Pattillo [6], but for the experimental setup an average value has been considered.
Same analysis was carried out on several Buttress connection sizes. **Figure 6** shows the flank contact pressure for an 18 5/8" connection. The average contact pressure was 65 MPa.
The third finite element analysis was performed on the grooved plate model in order to investigate the groove deformation due to axial load applied on the plate. The results have showed that the pressure distribution on the contact area is uniform, excepting the contact zones at the end of the groove walls (see **Figure 7**). Also, it has been found that the shape of the groove is changing, as presented in **Figure 8**. The total amount of area shrinkage for the contact pressures produced in a real connection is low. When the contact pressure increases the groove deformation becomes important, especially for the API round plate model. For a contact pressure of 50 MPa the grove area changes for the Buttress plate are of 0.85% and for the API plate of 7.3%, which represents a 9 time area change compared to Buttress. These changes justify the results and show that the API plate leak resistance increases almost linearly compared to Buttress plate leak resistance (see **Figure 9**).

Experimental results

The first experiments were focused on testing four thread compounds using the grooved plate that mimics the Buttress thread. The tested compounds are presented in **Table 3**. The first two thread compounds are proprietary types, therefore they will be called T1 and T2, the third one is an API Modified and the last one is an API type compound with polymers to increase the viscosity. The API Modified was

used as reference for all tests.

Figure 8 shows the leak pressure as a function of contact pressure between plates. The leak pressure is the pressure at which the thread compound is expelled from the free end of the groove. It can be seen that all tested compounds show a higher leak pressure than the API Modified. Also, it has been observed that at high contact pressures the leak pressure tends to behave asymptotic. The thread compounds T1 and T2 as well as the API with polymers show very little differences at high contact pressures between plates. This is explained by the slight deformation of the groove due to confine axial force applied to keep the plates together and the viscosity of the compounds.

The second set of tests was carried out on a grooved plate that mimics the API short round thread. For these tests only the thread compound T1 has been evaluated in order to compare the results with the full scale specimens that have been doped with this type of compound. **Figure 9** shows a comparison between the results obtained using Buttress type groove and the API round type groove. One explanation for the asymptotic behavior of the API Buttress leak resistance curve is the groove deformation due to axial load of the plate. As presented before, the groove deformation can reduce its volume up to 7% for API style groove and 0.8% for Buttress style groove. Since the API groove size becomes smaller and smaller with the increasing contact pressure, it is obviously why the API plate leak resistance is a direct function of contact pressure, and Buttress plate not.

Practical application of the method

It is a common practice to record the applied torque while running casing. Knowing the minimum value for the threaded connections applied torque, it will be easier to estimate the maximum pressure that may be applied without loosing the connection tightness. In many fracturing operations the part of the casing string that is subjected to internal pressure will have a low or zero axial tension. Therefore, the chart presented in **Figure 10** has been constructed using the contact pressure calculated for the make-up torque and internal pressure case. Comparing the contact pressure inside the threaded connection to the minimum contact pressure at which the thread compound has been expulsed form the small scale setup it is possible to identify the actual leak resistance of the connection. The method does not consider the effect of tolerances and thread compound ageing.

Conclusions

The tests performed on four different types of compounds have showed that the API compound has the lowest leak resistance in conjunction with the API thread type.

The Buttress leak resistance has an asymptotic behavior. At contact pressures higher than 100 MPa, the leak resistance is constant.

The difference between API round and Buttress leak resistance consists in the contact pressure dependency of the API round leak resistance.

It is recommended for API round connections to be made-up with optimum make-up torque or higher.

Acknowledgement

The authors will like to thank Professor Vlad Ulmanu for his standing support and valuable advices.

References

1. ***, Thread compound test being developed, Oil & Gas Journal, Spet 10, 1990
2. ISO 13678,
3. Hoenig, S. Oberndorfer M. Tightness Testing of Environmentally Friendly Thread Compounds, SPE 100220, SPE Europe/EAGE Conference, Vienna, Austria, 12-15 June 2006
4. ***, ISO13678:2000(E)
5. Report on API PRAC Project 88-51, “Investigation of Pipe Thread Compound”, June 1989
6. Report on API PRAC Project 86-51, “Investigation of Pipe Thread Compound”, May 1987
7. Report on API PRAC Project 84-51, “Investigation of Pipe Thread Compound”, December 1985
8. Report on API PRAC Project 86-53, “Investigation of Leak Resistance of API Buttress Connector”, January 1987

Table 1. Tested thread compounds composition

Product Specification	**API Mod. Compound**	**T1**	**T2**
Grease Base	36.0%	N/A	~46%
Powdered Graphite	18.0%	N/A	20%
Lead Powder	30.5%	0%	0%
Zinc Dust	12.2%	N/A	20%
Copper Flake	3.3%	0%	0%
Thickener	Al Stearate	Ca Stearate	Ca Stearate
Fluid Type	Petroleum	Oil	Oil
Density	1700 kg/m³	N/A	N/A
Colour	Black/Brown	Black	Black

Table 2. Size and dimensions of the grooved plate for two different connection types

	Area, [mm^2]		D, [mm]	Thread turn dimensions, [mm]		
	Total thread clearance	Groove area		h	b	p_s
API round	0.049	0.056	120	0.08	0.70	1.75
API Buttress	0.312	0.310	156	0.20	1.55	3.1

Table 3. Leak resistance of Buttress type plate

Thread compound	Contact pressure [MPa)					
	43.1	53.9	64.7	75.5	86.2	97
T1	33.2	38.8	42.0	43.8	45.0	45.2
T2	32.0	37.0	40.3	42.2	43.7	44.0
API 5A2	19.0	24.3	28.5	32.0	35.0	37.2
API with polymers	29.0	33.5	37.0	39.8	42.5	44.0

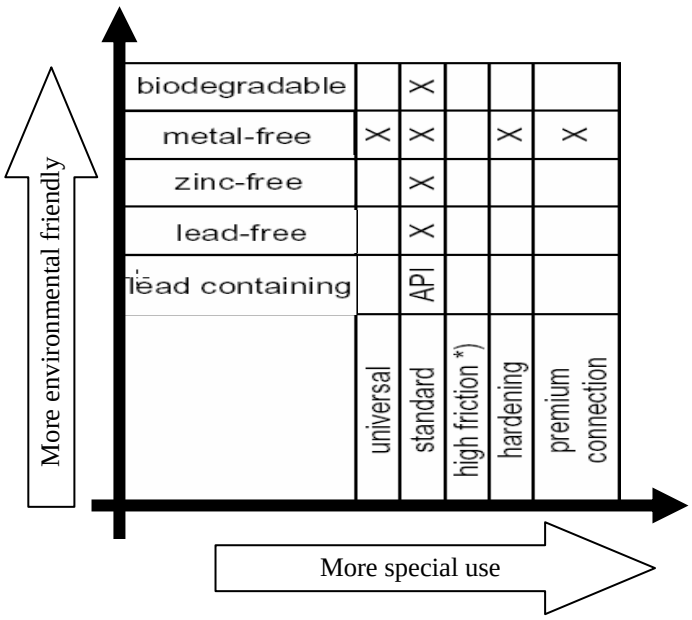

Fig. 1. Classification Scheme of Thread compounds, after [3]

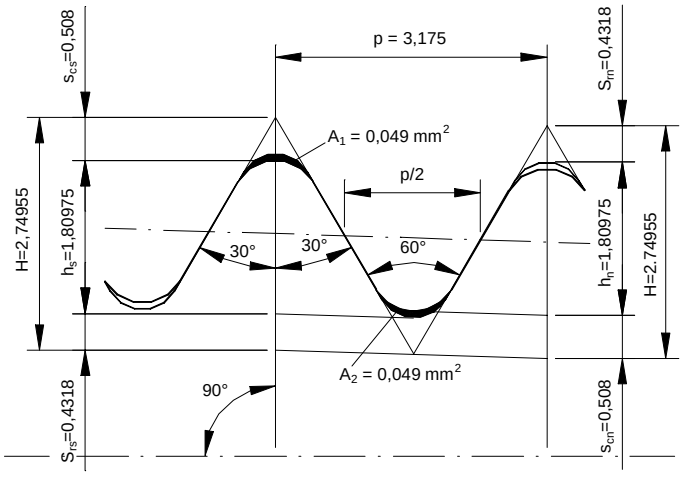

Fig. 2. API Round Thread Dimensions

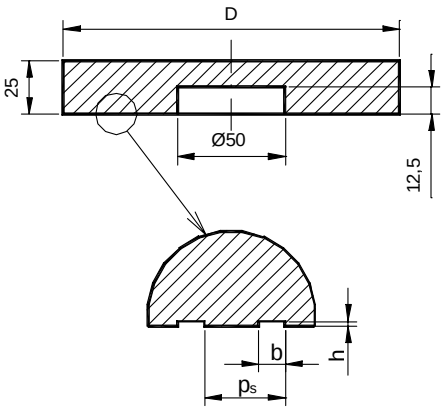

- b -

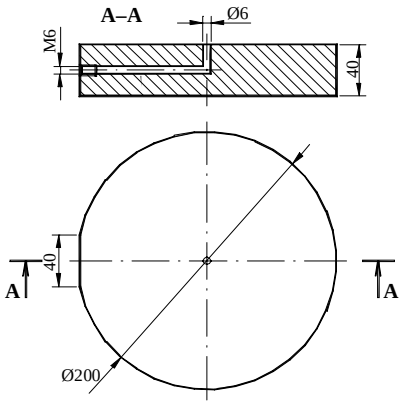

- a -

Fig. 3. Shape and dimensions of the grooved and seal plates used for the experiments

Fig. 4. Pictures of the grooved (top) and seal (bottom) plates

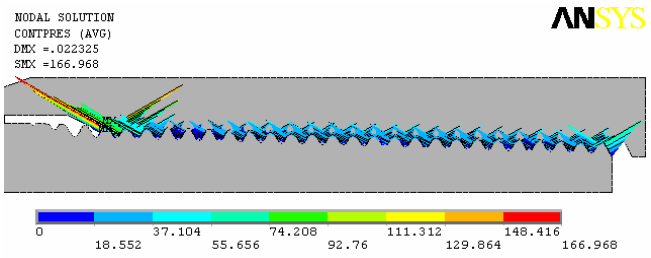

Fig. 5. Flank contact pressure of a 51/2" API round threaded connection after optimum make-up torque

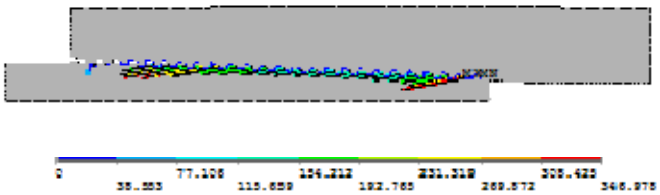

Fig. 6. Flank contact pressure of a 18 5/8" API Buttress threaded connection after optimum make-up torque and axial tension

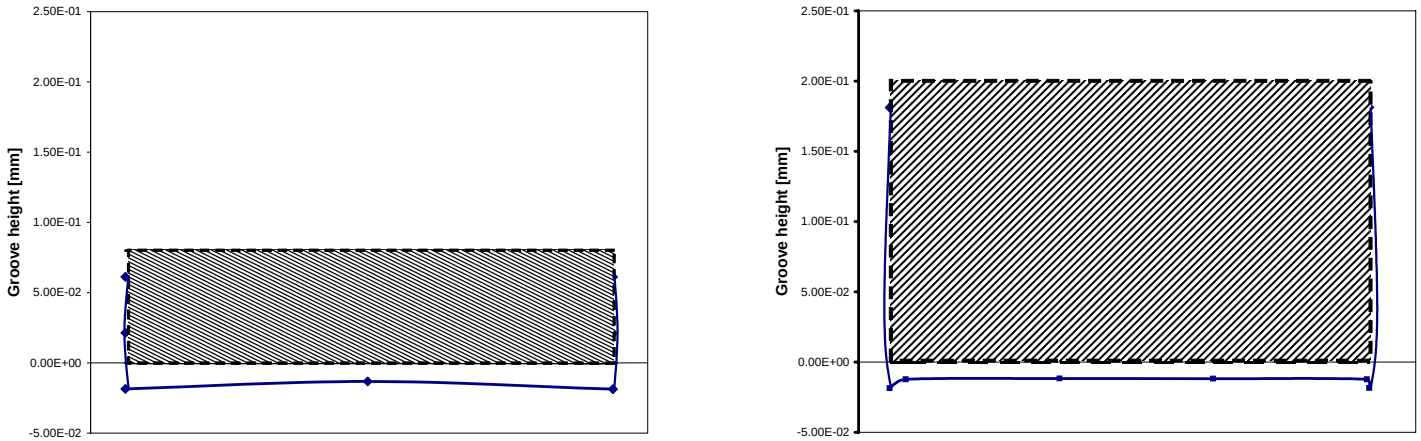

Fig. 7. Groove deformation at high contact pressure for API round type plate (left) and Buttress type plate (right)

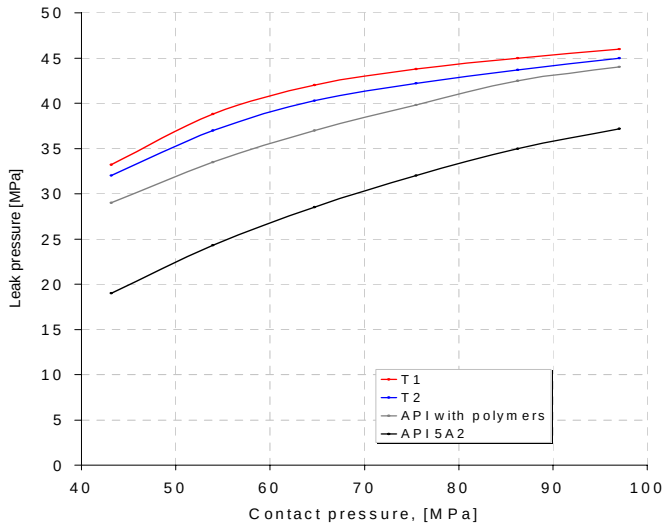

Fig. 8. Leak pressure curves for API Buttress type plate

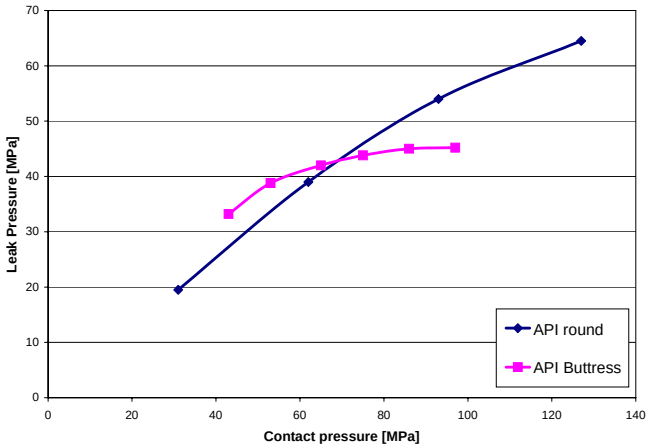

Fig. 9. Comparison of API round and Buttress leak resistance test results for thread compound T1

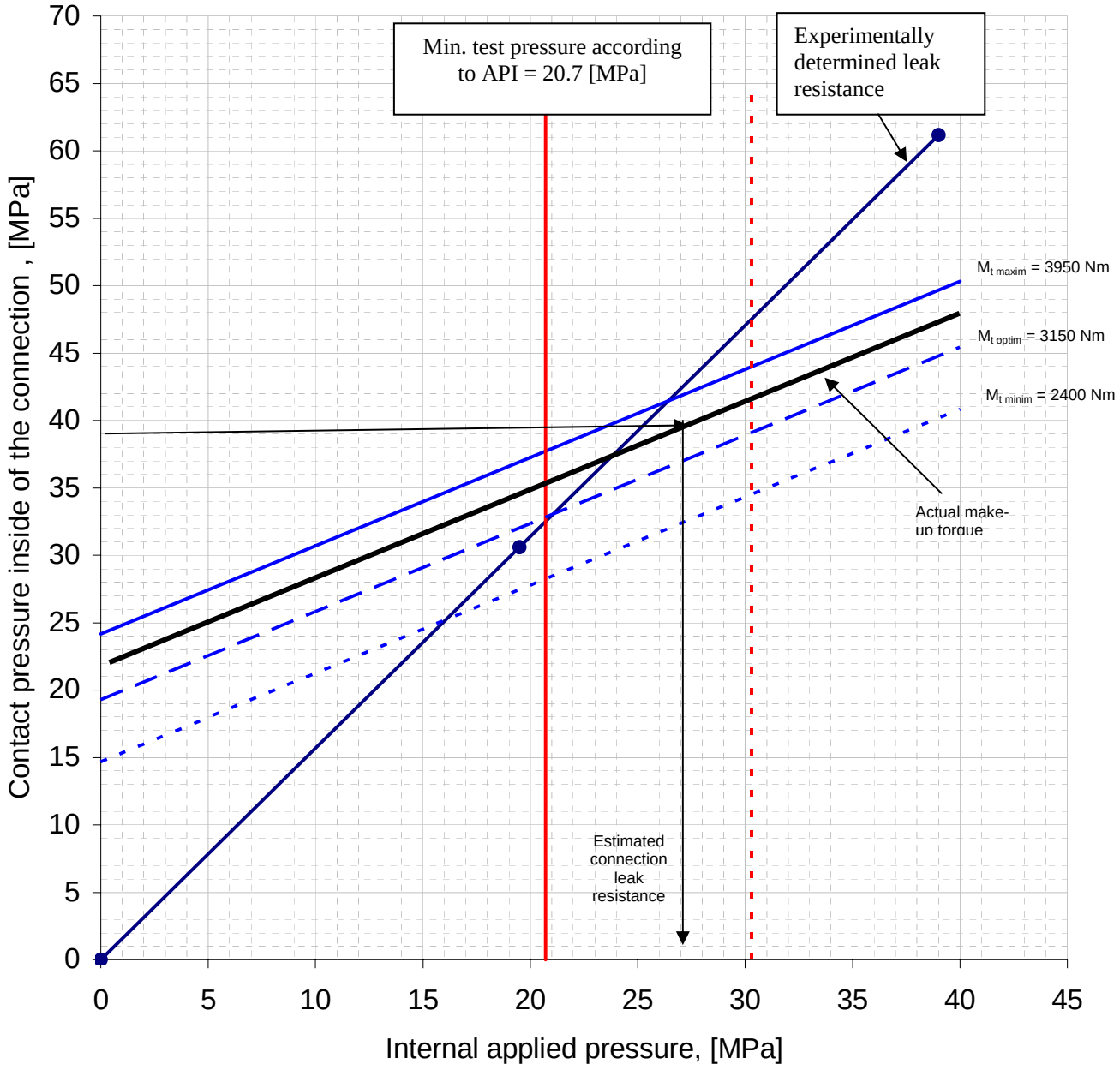

Fig. 10. Chart for API connection leak resistance estimation knowing the thread compound leak resistance

Appendix A

Leak path dimensions as a function of thread tolerances for API round thread

Case	Thread Height, [mm]	Leak path area, [mm^2]		Shape and dimensions of the thread gaps
		A_1	A_2	
1	h_s = 1.80975 h_n = 1.80975	0.0490	0.0490	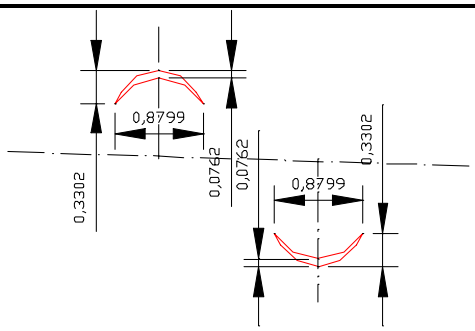
2	h_s = 1.80975 – 0.102 h_n = 1.80975 + 0.051	0.1555	0.1555	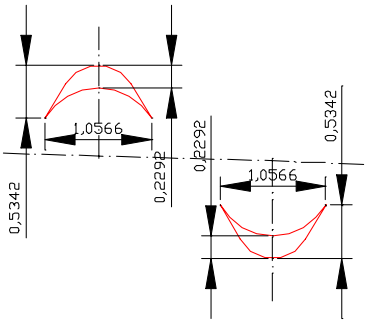
3	h_s = 1.80975 + 0.051 h_n = 1.80975	0.0153	0.0153	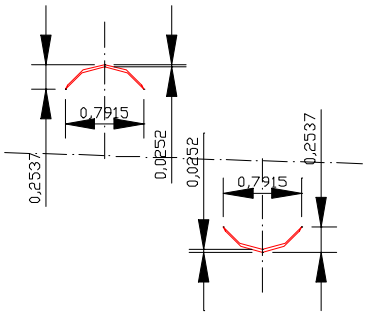
4	h_s = 1.80975 – 0.102 h_n = 1.80975 – 0.102	0.0597	0.0597	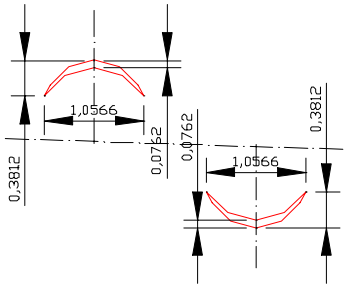

Appendix B

Leak path dimensions as a function of thread tolerances for API Buttress thread

Case	Tolerances	Leak path area, [mm^2]	Shape and dimensions of the thread gaps
1	*No tolerances*	0.0472	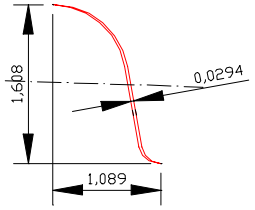
2	*Deviation from thread turn length and fillet radius*	A1: 0.3116 A2: 0.0036 A3: 0.0036	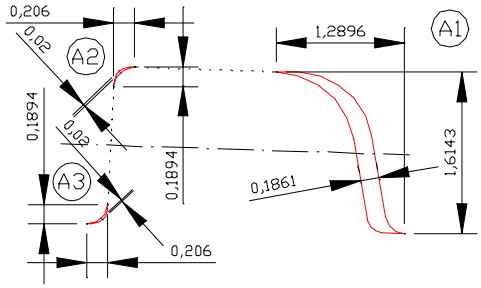
3	*Deviaiton from thread height*	0.1646	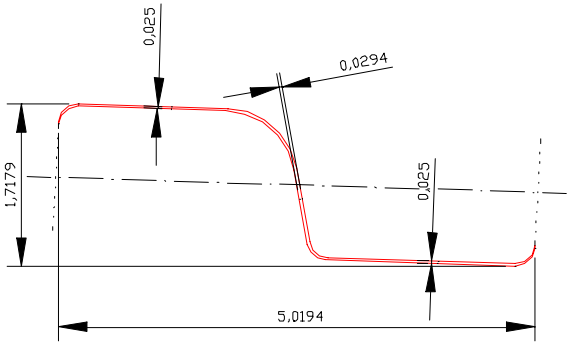

Increasing Geothermal Energy Demand: The Need for Urbanization of the Drilling Industry

Catalin Teodoriu
Gioia Falcone
Texas A&M University

Drilling wells in urban spaces requires special types of rigs that do not conflict with the surrounding environment. For this, a mutation of the current drilling equipment is necessary into what can be defined as an "urbanized drilling rig." Noise reduction, small footprint, and "good looking" rigs all help persuade the general public to accept the presence of drilling rigs in their neighborhood. This article reviews international projects that aim to integrate drilling with the urban infrastructures with a special focus on geothermal projects. Case studies are presented where tailored drilling rigs and new technology have already been implemented. The review aids the analysis of the main urban-related technical aspects of modern drilling rigs. Finally, the new trends in integrating architecture, urbanism, and drilling rig design are discussed.

Keywords: *geothermal; energy; drilling; rigs; urbanization; environment.*

Introduction to Well Drilling: Past and Present

History of Well Drilling

Drilling equipment is needed to penetrate underground reservoirs for water, oil, and natural gas, or into subsurface mineral deposits. Drilling systems are also required to exploit geothermal resources and for civil and mining engineering applications.

According to the American Ground Water Trust (2007), there are more than 15 million homes in America with their own water well. More than half of the nation's drinking water is from municipal and private wells. Some estimates suggest that 6,000 new wells are completed each week in the United States.

In 1848, the first modern oil well was drilled in Asia, on the Aspheron Peninsula northeast of Baku, by a Russian engineer named F.N. Semyenov (Talwan, Belopolsky, & Berry, 1998). In 1854, the first oil wells were drilled in Europe, at Bóbrka, Poland by Ignacy Lukasiewicz, who also designed the kerosene lamp (Arabas, 2005). In 1859, the most important U.S. oil well was drilled in northwestern Pennsylvania by Colonel Edwin Drake (Baker, 1996). This was one of the first successful oil wells that were drilled for the sole purpose of finding oil. Known as the Drake Well, after the man responsible for the well, it began an international search for petroleum, and in many ways eventually changed the way we live. The Spindle Top well, drilled by Anthony Lucas in Texas in 1901, was the first well to be drilled by rotary drilling, to overcome geological problems.

Geothermal resources for the production of electricity have been used since the beginning of the 20th century. The first successful experiment to produce energy from geothermal sources was carried out in 1904 by Prince Piero Ginori Conti at the Larderello dry steam field in Italy (Lungonelli & Migliorini, 2003). Today, Larderello provides 10% of the world's supply of geothermal electricity. In the United States, the first large-scale geothermal electricity-generating plant began operation in 1960, at The Geysers in Sonoma County, California (U.S. Department of Energy, 2006). 69 facilities are in operation at 18 resource sites around the country.

The depth that the well has to reach is one of the main criteria that dictate the size and the specifications required for a drilling rig. In the case of water

Bulletin of Science, Technology & Society Vol. XX, No. X, Month XXXX, xx-xx
DOI: 10.1177/0270467608315531

wells, for instance, the drilling depth will depend on where the water table is located. Also, drilling time and depth are usually directly related: The deeper the well, the longer it will take to drill it (although the type of formation to be drilled—hard or soft—will also have an impact on the overall drilling time).

Drilling Rigs

A drilling rig's sole purpose is to get a hole from a surface location to a subsurface target at a specified depth in a safe and controlled manner. All the equipment that makes up a drilling rig is designed and manufactured to this aim. Generally, a drilling rig consists of five main subsystems: pipe rotation, drilling fluid circulation, hoisting, power supply, and blow-out prevention. These subsystems are designed to work seamlessly together. Figure 1 shows a typical onshore drilling rig.

Current drilling practices are based on the principle of rotary drilling, where a dedicated rotating system drives a cutting tool (i.e., drill bit) to break the rock. A continuous weight is applied to the bit to provide the necessary cutting force. The weight on the bit is controlled via the hoisting system, which is also used to lift and trip the well tubulars in and out of the well. The cuttings are removed from downhole and transported to surface by a drilling fluid (air, foam, or drilling mud). Cuttings removal is the main function of the circulating system that allows the drilling fluid to be pumped downhole (via the drill pipe) and returned to surface (via the annular space between drill pipe and hole), where it is reconditioned.

Until relatively recently, the oil and gas drilling industry portrayed an image using equipment and working environment that was "large, dirty and downright ugly." This is unacceptable nowadays and the industry pays close attention to making drilling rigs clean, safe, and environmentally friendly. Consequently, modern oil and gas drilling rigs have become ergonomic and tailored to the driller's need for a safe and adequate working space.

Modern Drilling Rigs

Modern drilling rigs rely on integrated mechanized equipment and ergonomic working space. Figure 2 shows an example of a highly computerized control system used to operate the modern rig, as opposed to the high level of labor required for a conventional rig.

A major feature of a drilling rig, particularly when it is used in environmentally sensitive areas or urban

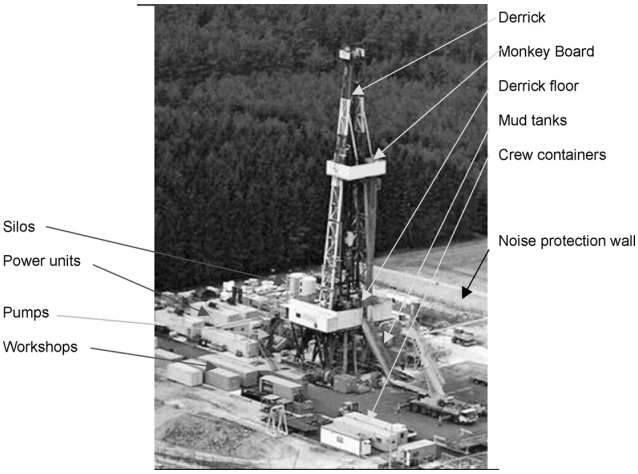

Figure 1. A Typical Onshore Drilling Rig and Its Main Components

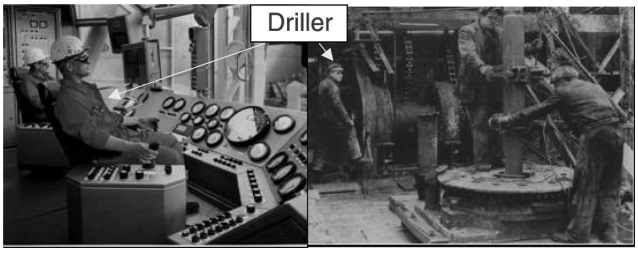

Figure 2. Driller's Cabin on a Modern Drilling Rig Compared to a Driller's Working Location in 1942
Source: Reinicke and Teodoriu (2005).

locations, is its footprint. The size of a rig's footprint depends on rig type (mobile vs. fixed) and well specification (which is a function of target depth and geology). Figure 3 shows the overall footprint of a typical onshore drilling rig.

The transition from traditional to modern drilling sites has required much closer collaboration between drilling engineers and architects. This has led to the design and construction of ergonomic and tailored drilling structures to meet the needs of today's energy industry. Examples of using modern rigs to drill in urban areas will be shown later in the article.

Drilling Deep Wells in Urban Areas

In some cases, wells must access reservoirs that are situated directly underneath or in close proximity to urban areas. In other cases, wells must be drilled to investigate the geology of an area prior to building on

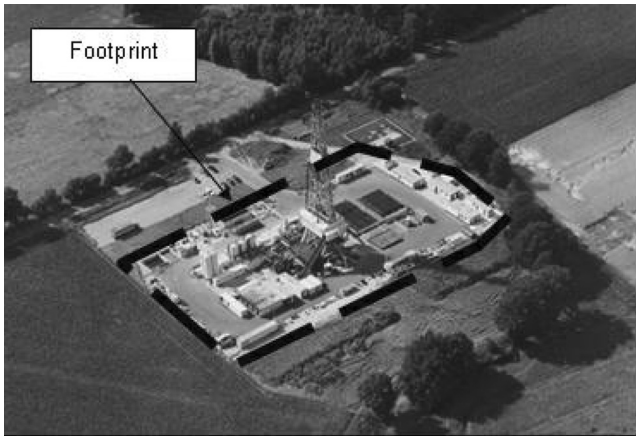

Figure 3. Aerial View of a Drilling Rig Footprint
Source: Reinicke and Teodoriu (2005).

Figure 4. Camouflaged Oil Rigs on Grissom Island, Long Beach, California
Source: California Department Of Conservation (2007).

or tunneling through the land. If the target depth is shallow, the rig will not remain in place long enough to disrupt the local "way of life." For example, an artesian well with a shallow water table may only take a couple of days to drill. However, for deeper wells, there are many issues that cause concern when drilling in urban areas, such as

- Risk of explosion
- Risk of pollution of air and potable water
- Noise level and vibrations
- Impact on the landscape
- Conformity with local environmental regulations
- Space taken away from urban development
- Length of time that the rig stays on site
- Footprint of the drilling site

There are numerous examples of urbanization of the drilling industry for hydrocarbon exploitation, which can be used as a reference for geothermal applications.

One is the THUMS Island project (Occidental Petroleum Corporation, 2007; Oxy Long Beach Inc, 2000) in Long Beach, California, which takes its name from the original consortium of Texaco, Humble, Unocal, Mobil, and Shell that operated the Wilmington field. THUMS is a model example of how drilling operations can be run in a sensitive environment.

It consists of four artificial islands, named Grissom, White, Chaffee, and Freeman, after the NASA astronauts who died in training accidents early in the U.S. space program. Built from boulders and sand, they mimic resort islands to blend in with the surrounding coastal environment of Long Beach Harbor.

THUMS is the largest crude oil producer in the Los Angeles area. Despite the high rate levels of the THUMS development, there has not been any pipeline leak since the beginning of production. Because of the unique successes that the THUMS project has achieved, it has already been awarded special recognition by local and national groups for environmental protection, community beautification, and outstanding design.

Figure 4 shows the architectural aspects of rig camouflage at THUMS.

Cases like THUMS make it possible to produce oil and gas without offending environmentally sensitive places and without interfering with the urban and tourist development of inhabited places.

The following examples of wells drilled in urban areas for geothermal energy recovery illustrate how and when it is possible for drilling rigs and urban life to coexist with one another.

There are two main types of geothermal energy: low temperature (less than 100°C) and high temperature (greater than 200°C). Although the high temperature sources are used for electrical energy generation, the low temperature sources become more attractive when they are coupled directly with on-site heat utilization (e.g., heating of buildings, hot houses, etc). In the latter case, it is not always possible to keep the drilling rigs outside the cities, so architects and engineers must work together to design the plant in conjunction with the infrastructure that will directly use the geothermal energy. Although the daily running costs of generating electricity are relatively low, large initial capital investments are usually necessary. With the latest energy conversion techniques,

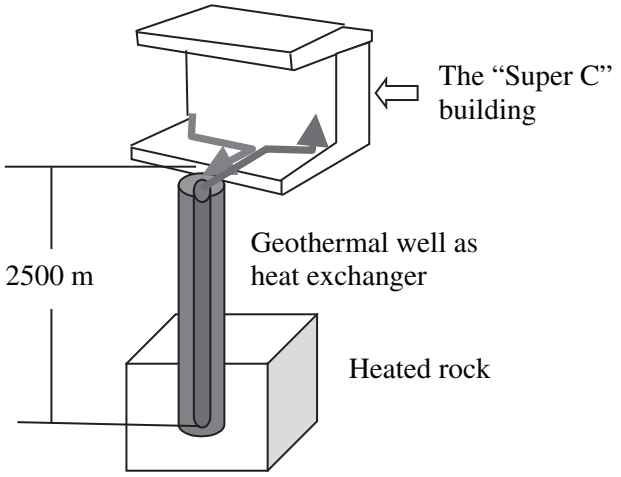

Figure 5. Schematic of a Well Used for Heat Mining as an Integral Part of a New Building Design
Source: Modified after Sanner (2005).

Figure 6. The SuperC Project of the RWTH Aachen University, Germany
Source: Superc (2006).

geothermal resources may become more attractive for areas where low underground temperatures are found. One such example is represented by the modern conversion techniques based on the "Rankin and Kalima cycle," which enables electric power generation at temperatures as low as 100°C (WEA, 2004).

The following is a review of worldwide projects in which the geothermal energy from a deep well is used to heat or cool buildings or districts. Projects of this type can be classified as those involving new buildings, for which the geothermal well is an integral part of the building (see Figure 5), or as projects that use district heat transport infrastructures to connect the geothermal facility (well plus heat exchangers) to buildings. Note that the injection and production wells can both be on location when directional drilling techniques are used.

When new buildings are designed, the well construction requirements are based on the heat capacity of the building. Well depths may vary, but the produced fluids' temperature range is typically between 45 and 80°C. Existing projects, which used mobile drilling rigs, reported that the major problems experienced were size of rig site, noise, and pollution (SuperC, 2006). Figure 6 shows the building of the so-called "SuperC" project in Germany, which uses geothermal energy to supply heat to the new "Student-Service-Center SuperC" at RWTH Aachen University. The center will be heated using a deep well, "RWTH-1," that is drilled adjacent to the RWTH main building (SuperC, 2006). The well temperature at 2,500 m is about 85°C and the well is expected to deliver hot water at a temperature of at least 70°C for the building's heating and cooling supply. It is a closed system, which means that it can be installed in any rock type. Because of the specific geology of the Aachen region, the chosen solution is very important as the hot springs must be protected from any possible contamination.

According to some authors (SuperC, 2006), "the project *Super C and geothermal energy* proves that geothermal heat supply for large buildings is technically feasible and economically efficient, although the initial costs are relatively high."

The projects that use geothermal energy to heat or cool existing buildings or districts face more complicated issues. As most of these projects are applied for large public buildings, often being tourist attractions, the rigs must be part the architectural environment. Drilling and completing a well for heat mining can take up to several months, but the area cannot be closed to the public or to tourists for this length of time.

Another major project from Germany, shown schematically in Figure 7, is considering using a geothermal source to heat and cool the German parliament using a pair of wells; one shallow (for cooling) and one deep (for heating) (Bussmann, 2007).

The deep heat mining project to produce electrical power and district heating in Basel, Switzerland, was initiated in 1996, being partially financed by the Federal Office of Energy and supported by private and public institutions. The drilling target is located at a depth of

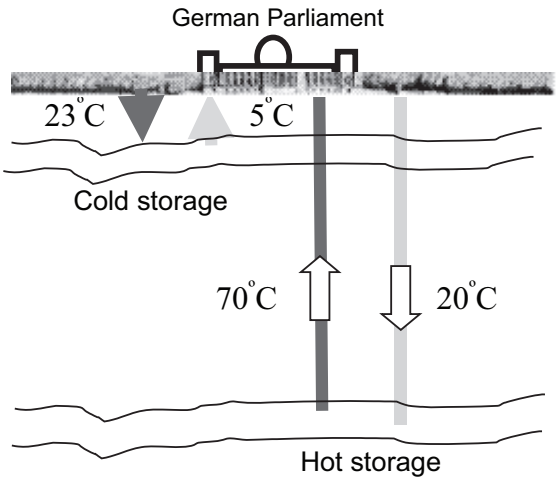

Figure 7. Geothermal Heating and Cooling of the German Parliament
Source: Modified after Bussmann (2007).

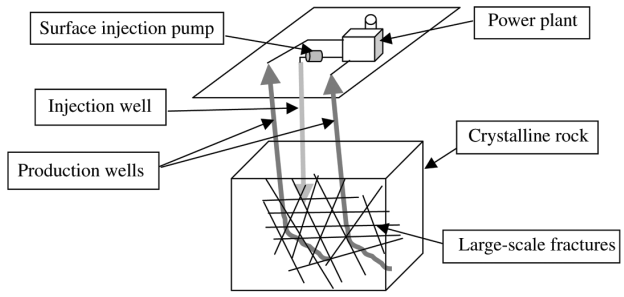

Figure 8. The Concept of the Deep Heat Mining Project System, Basel, Switzerland

5 km (3.125 miles) below the surface, where the expected average water temperature is about 200°C. Figure 8 shows a schematic diagram of the target well location according to the original plan. It must be noted that the first attempt at drilling this geothermal well failed because of geological complications and overloading of the drilling rig (Haering & Hopkirk, 2002). A new rig with higher hook load capacity was purchased and the well was successfully drilled at the second attempt.

Classification of Drilling Rigs Used to Drill in Urban Locations

The concept of modern drilling rigs was introduced earlier in this article. In what follows, a review of some of the main modern rig designs used specifically to drill wells in urban areas will be presented.

Figure 9. The New Generation of Light Land Drilling Rig That Can Be Used for Both Oil and Gas Wells and Deep Geothermal Wells
Source: Gutsche (2005). Copyright of ITAG Tiefbohr.

Conventional Drilling Rigs Used for Urban Drilling Activities

For deep heat mining projects (e.g., drilling through hot dry rocks), the drilling rigs normally adopted by the oil and gas industry have proved to be the best option as they can drill quickly to the target depth. Unfortunately, the recent rise in oil and gas prices has caused an increase in demand for rigs, triggering a corresponding increase in their day rates, which has made it uneconomic to use oil and gas drilling rigs for geothermal applications. Despite this, several services companies are designing their future rig fleet with the geothermal drilling capability. For example, ITAG's Rig 40 (Gutsche, 2005) shown in Figure 9, allows rig transportation and erection in a much shorter time than for any equivalent oil rig. The rig was originally conceived for transportation through the narrow streets of southern Germany and

Figure 10. Typical Small Roads Through French Villages

Figure 11. Conventional Drilling Rig Used for the Deep Mining Project in Basel, Switzerland

northern France (see Figure 10), hence its modular design. The low footprint of Rig 40 (3500 m^2) is comparable to that of conventional mobile rigs, but its maximum hook load and mud tank capacity are much higher.

Figure 11 shows the conventional drilling rig used to drill the deep geothermal well in Basel, discussed earlier. Although the well has proved to be a success from the point of view of recovering energy in an urban environment for district heating, the rig has caused obvious disruption to the local architecture. The only way to reduce the negative impact on the local architecture is to reduce the height of the drilling rig to ensure an easy camouflage. Figure 12 shows the height comparison between a conventional rig for deep drilling and a modern or unconventional drilling rig, which considerably reduces the overhead working space requirement.

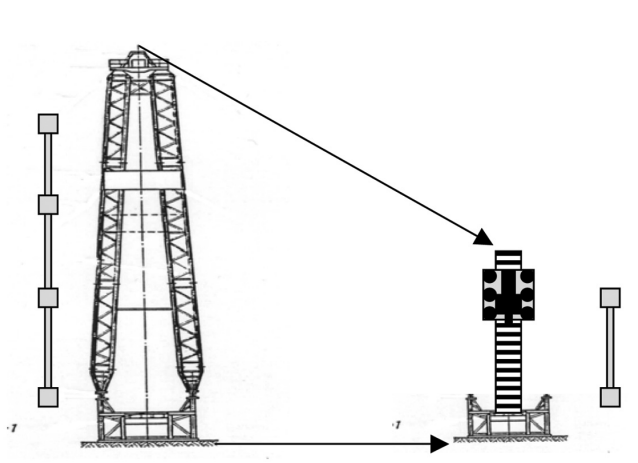

Figure 12. Conventional Drilling Rig (45 m to 55 m High, Can Accommodate Three Drill Pipes) on the Left Versus Unconventional Drilling Rig (15 m to 18 m High, Can Accommodate One Single Drill Pipe) on the Right
Note: One single drill pipe is approximately 9 m long.

Unconventional Drilling Rigs Used for Urban Drilling Activities

Any type of drilling rig that is not conforming to state-of-the-art conventional systems can be classified as unconventional. As new technology becomes available, unconventional rigs evolve further until today's unconventional systems become the conventional rigs of tomorrow.

The current unconventional drilling rigs are characterized chiefly by new designs for the hoisting systems to allow very high load capacity within small structures. Other key features of these rigs are:

- Electrical hydraulic drives
- Ability to use the AC electric supply from a city network
- Low height (single derrick)
- High load capacity
- Partially or fully automated control systems
- Modular construction

To the knowledge of the authors, only two companies, Drilltec and Herrenknecht Vertical, have published information about drilling rigs specifically designed for deep geothermal applications. The main design features that make these rigs appropriate for urban drilling are briefly described below.

Figure 13. Drilltec's Super Single Drilling Rig With Automatic Pipe Handling System
Source: Drilltec (2006). Copyright of Drilltec GUT.

The Drilltec Rig VDD370

The maximum hook load of 3.700 kN makes this rig suitable for deep drilling applications (oil and gas and geothermal). The major components of the Drilltec System (topdrive, pipehandling system) are hydraulically driven. The power packs, that are electrically driven, supply aggregates for hydraulic energy, provide the flexibility to use prime energy supply from a city network or—if there is not enough electrical power available—a diesel motor-driven generator set (standard version) can be used instead. Figure 13 shows the Drilltec rig and the driller's cabin (Drilltec, 2006) from where all operations can be controlled. Both, the small footprint and the low height of total 31 meters, advantage the application of the super single rig in urban areas. The rack and pinion type rig is noise protected in many components. To absorb the sounds of the topdrive (equipped with six hydraulic motors for traveling and four hydraulic motors for rotation) the gears are covered completely. In addition, most of the noise generating equipment (e.g., pumps, generators, power packs) is mounted in insulated containers.

The Herrenknecht Vertical Terra Invader 350 (TI-350) Rig

In response to the worldwide increase in drilling activity and the lack of drilling capacity in the German market, a new versatile drilling rig has been developed with direct application to geothermal deep drilling projects. The Federal Ministry for the Environment, Nature Conservation and Nuclear Safety has promoted the development of new a deep drilling rig as part of its energy research program.

Figure 14. Herrenknecht Vertical Terra Invader 350 Drilling Rig
Source: Herrenknecht (2006). Copyright Herrenknecht.

Being built for urban drilling activities, the new rig, shown in Figure 14, has a marked improvement in noise reduction. The main innovation of this drilling rig design is its hydraulically driven hoist system (linear hydraulic cylinders) and noise insulated containers for prime drivers and mud pumps. It has been reported that the expected noise pressure level at a distance of approximately 150 m from the rig is about the same as a domestic TV or radio at normal listening volume (Herrenknecht, 2006).

To achieve maximum drilling performance and safety, the new rig design uses extensive integration of the automated processes (hands off technology).

After final testing, this new deep drilling rig will be employed in the commercial zone of the municipality of Duembaar (southern Germany). The planned geothermal power plant is expected to generate 5 to 6 MW of electric power and 25 MW thermal.

Future Needs of Drilling in Urban Environments

To accommodate the future needs of drilling in urban environments, the new breed of drilling rigs will have the following design characteristics:

- Modular construction for easier mobilization and transportation through narrow city streets. Being modular will mean that most of the rig equipment will be mounted in small containers of small size, which has the added benefit of reducing noise emission by sound insulation of the containers' walls.
- Low noise emissions outside the drill site. One of the mandatory changes to rig design to reduce noise levels is to lower the rig's height by using single drilling rigs instead of triple rigs. Noise reduction is also obtained by using unconventional hoist systems (e.g., rack and pinion system, linear hydraulic motors)
- High hook load capacity, despite the small size of the drilling rig, which can be achieved by means of unconventional technologies
- Easily camouflaged for long-term drilling projects
- Smart power supply, using on-site diesel generators or tapping into the city electrical power grid, and having low emissions of noise, vibrations, and exhaust gases
- Closed-loop spill and mud processing unit to avoid any contamination of the rig site
- Small size of drilling rig, which will be achieved through integrating the automated processes and computer controlled rig floor equipment

Conclusions

The urban environment forces rig design to evolve to accommodate in-city drilling operations.

A review of international projects that aim to integrate drilling with urban infrastructures has been presented in this article. The new trends in harmonizing urban architecture with drilling rig design have been discussed.

With a rising number of the geothermal deep heat mining projects around the world, there is a slowly increasing need for drilling rigs to operate in an urban environment, with all the problems that entails.

Although the market is small in comparison with the oil and gas industry, the future energy trends may radically change the demand for "urbanized drilling rigs."

References

American Ground Water Trust. (2007). *How wells are drilled*. Retrieved March 15, 2007, from http://www.agwt.org/info/pdfs/welldrilling.pdf

Arabas, I. (2005). The founder of the Polish and world oil industry: Polish pharmacists Ignacy Lukasiewicz and the 150th anniversary of the lighting of the first kerosene lamp. *Pharmaceutical History*, *35*(1), 8-10.

Baker, R. (1996). *A primer of oilwell drilling* (5th ed.). Austin, TX: Petroleum Extension Service and International Association of Drilling Contractors.

Bussmann, W. (2007). *German geothermal trends and developments*. Retrieved March 15, 2007, from http://www.geothermie.de

California Department of Conservation. (2007). *Home*. Retrieved March 15, 2007, from http://conservation.ca.gov/

Drilltec. (2006). *Large scale drillings—Worldwide*. Retrieved December 15, 2006, from http://www.Drilltec.de

Gutsche, W. (2005, June). *A new generation of AC-driven light land rigs*. Paper presented at the Institute of Petroleum Engineering, TU Clausthal, Clausthal, Germany.

Haering, M., & Hopkirk, R. (2002, March). *The Swiss deep heat mining project: The Basel exploration drilling*. Paper presented at the proceedings of the International Summer School Conference: International Geothermal Days, Germany 2001, Bad Urach, Germany.

Herrenknecht. (2006). *Technology going deep*. Retrieved December 15, 2006, from http://www.herrenknecht-vertical.de

Lungonelli, M., & Migliorini, M. (2003). *Piero ginori conti*. Laterza, Italy: Collana Cultura e Industria.

Occidental Petroleum Corporation. (2007). *California-THUMS*. Retrieved March 15, 2007, from http://www.oxy.com/OIL_GAS/world_ops/usa/thums.htm

Oxy Long Beach Inc. (2000, December). *THUMS Long Beach company overview*. Presented at the West Coast PTTC Workshop, Los Angeles.

Reinicke, K. M., & Teodoriu, C. (2005). *Neue entwicklungen in der bohrtechnik*. Heft, Germany: Akademie der Geowissenschaften zu Hannover Veroefentlichungen.

Sanner, B. (2005, April). Geothermal energy—Country profile for Germany. Workshop on Regulatory and Economic Tools Governing the Enhanced Exploitation of Geothermal Energy in the European Union, Kistelek, Hungary.

SuperC. (2006). *The geoscientific research*. Retrieved December 15, 2006, from http://www.superc.rwth-aachen.de

Talwan, M., Belopolsky, A., & Berry, D. L. (1998). *Geology and petroleum potential of central Asia*. Houston, TX: Rice University, Baker Institute.

U.S. Department of Energy. (2006). *A history of geothermal energy in the United States: Energy efficiency and renewable energy*. Retrieved December 15, 2006, from http://www1.eere.energy.gov/geothermal/history.html

World Energy Assessment. (2004). *Energy and the challenge of sustainability*. New York: Author.

Catalin Teodoriu is an assistant professor in the Harold Vance Department of Petroleum Engineering at Texas A&M University. He has an equivalent MS (1996) from "Oil and

Gas" University of Ploiesti and two PhDs (2003, Technical University of Clausthal; 2005, "Oil and Gas" University of Ploiesti). He has worked as a R&D engineer for 2 years with R&D Center of Petrom (actually OMVRomania) Company, more than 6 years as researcher, and later on as research supervisor and equivalent associate professor with the technical University of Clausthal. At technical University of Clausthal, he was involved in teaching graduate and undergraduate drilling and completion courses and in drilling, well integrity, and drilling fluids research for more than 5 years. At Texas A&M University, he is involved in teaching undergraduate drilling courses and in drilling and well integrity research. Related research activities that he has been involved with include casing resistance under extreme loads, swelling cements for gas wells, drillstring components makeup procedures, underbalanced drilling and formation damage, evaluation of the casing fatigue and fatigue of casing connectors, and development of laboratory testing devices and facilities.

Gioia Falcone is an assistant professor in the Harold Vance Department of Petroleum Engineering at Texas A&M University. She holds a first degree in petroleum engineering from the University "La Sapienza" of Rome, an MSc degree in petroleum engineering from Imperial College London, and a PhD in chemical engineering from Imperial College London. Prior to joining Texas A&M, she worked with ENI-Agip, Enterprise Oil UK, Shell E&P UK, and TOTAL E&P UK, covering both offshore and onshore assignments. She has served on the SPE ATCE Technical Programme Committee and, on several occasions, on the SPE ATCE Well Operations Subcommittee. She is a technical editor for the SPE Projects, Facilities & Construction Journal*, memberships chairperson for the SPE Research and Development Technical Section, and a member of the Editorial Advisory Board for Scientific Journals International. Her main research interests are in the areas of integrated production systems and multiphase flow.*

AKADEMIE DER GEOWISSENSCHAFTEN ZU HANNOVER
VERÖFFENTLICHUNGEN HEFT 25

Akad. Geowiss. Hannover, Veröffentl., Heft 25, Die Zukunft von Erdöl und Erdgas

Die Zukunft von Erdöl und Erdgas

Akad. Geowiss. Hannover, Veröffentl., **25** (2005): 24 - 32

Akademie der Geowissenschaften zu Hannover e.V.

Neue Entwicklungen in der Bohrtechnik

KURT M. REINICKE & CATALIN TEODORIU

Kurzfassung: Die Bereitstellung der Energie zur Deckung des ständig zunehmenden Energiebedarfes stellt die Industrie vor steigende Herausforderungen. Der Weiterentwicklung der Bohrtechnik kommt dabei eine besondere Bedeutung zu. Die Vorkommen müssen erbohrt werden, um sie produzieren zu können. Die hierzu erforderlichen Bohrkosten betragen in Deutschland für eine typische Festlandbohrung von 5.000 m Tiefe derzeit 7 bis 12 Millionen Euro und können bis zu 80% der Gesamt-Entwicklungsaufwendungen betragen.

Die Herausforderungen ergeben sich aus einem gestiegenen Bewusstsein für ökologische und ökonomische Belange sowie neuen Lagerstätten, die zunehmend schwieriger zu entwickeln sind.

Ökologischen Interessen wird Rechnung getragen durch Reduzierung der Störung von Umwelt und Umfeld, zum Beispiel durch Verkleinerung des Platzbedarfes, durch Verringerung von Emissionen sowie Aussparen ökologisch besonders sensibler Bereiche.

Ökonomischen Interessen wird Rechnung getragen durch Verringerung der Kosten und Verbesserung des Bohrergebnisses in Sinne von Produktionskapazität pro eingesetztem Kapital, diese Kapazität zu erstellen. Die Kostenreduktion wird erreicht durch geringere Bohrzeiten und Materialaufwendungen. Ermöglicht wird dies durch Mechanisierung und Automatisierung des Bohrgeräteparks, durch Einsatz von Informationstechnologie, um den Bohrvorgang zu überwachen, zu analysieren und steuernd einzugreifen, durch neue Bohrtechnologien, um den Bohrfortschritt zu vergrößern und neue Verrohrungskonzepte, um Materialausgaben zu verringern.

Die Verbesserung des Bohrergebnisses wird erreicht durch Anwendung neuer Bohrkonzepte. Richtbohrverfahren und „Measurement While Drilling (MWD)"-Technologien erlauben heute eine punktgenaue Steuerung des Bohrungsverlaufes und Ablenkungen aus der Vertikalen in jede beliebige Richtung mit Bohrlochlängen von bis zu 10.000 m - bis hin zur Horizontalbohrung mit Horizontalbohrstrecken von 1.000 m und mehr. Geosteering und „Logging While Drilling (LWD)" ermöglichen den verbesserten Aufschluss des Trägergesteins durch optimale Platzierung des Bohrlochverlaufes im Trägergestein. Die Entwicklungen werden an Beispielen erläutert.

1 Einleitung

Die „Essenz des Lebens", wie ein Bohrunternehmer Erdöl und Erdgas einmal genannt hat, ist aus dem heutigen Alltag nicht wegzudenken. Ein kurzer Blick in den Verbrauch Deutschlands zeigt, dass Erdöl die wichtigste Primärenergiequelle ist. Erdgas ist inzwischen unbestritten die Nummer 2 und wird vielleicht der sanfte Übergang zu der Wasserstoffära. Für den weltweiten Verbrauch sind ausreichend Erdöl- und Erdgasreserven für die nächsten 40 bis 60 Jahre vorhanden. Zu diesen Reserven kommen die Ressourcen aus Neufunden und den mit heutiger Technologie, bei heutigen Preises wirtschaftlich noch nicht förderbaren Kohlenwasserstoffen in den nicht konventionellen Vorkommen. Die statistische Reichweite dieser Vorkommen beträgt im Falle von Erdgas mehrere hundert Jahre.

2 Zur Situation in Deutschland

Nach dem Verlust fast des gesamten Geräteparks durch den Krieg wurde der Wiederaufbau der Erdölindustrie durch ein Hilfsprogramm der Regierung gefördert. 1951 waren insgesamt 130 Bohranlagen

Anschrift der Autoren: DR. KURT M. REINICKE, DR. CATALIN TEODORIU
Institut für Erdöl- und Erdgastechnik, TU Clausthal,
Agricolastr. 10, D-38678 Clausthal-Zellerfeld

im Einsatz, die meist im Besitz der Erdölunternehmen waren. Die damaligen Bohrziele in Deutschland waren Erdöllagerstätten in Norddeutschland, dem Rheintalgraben und dem Alpenvorland. Typische Bohrtiefen lagen zwischen 800 und 1500 m (Marx 2001). 50 Jahre später (2001) operierten auf dem Gebiet der Bundesrepublik Deutschland nur noch acht Bohranlagen. Davon wurde nur eine Anlage von einem Erdöl- und Erdgasunternehmen selbst betrieben. Die Bohrziele waren fast ausschließlich tiefe Erdgaslagerstätten, in Teufen von etwa 5000 m. Außer Erdöl- und Erdgasbohrungen wurden im Jahr 2004 auch Geothermalbohrungen niedergebracht, die Deutschlandweit zunehmend an Bedeutung gewinnen.

Abb. 1 zeigt die weltweite Verteilung der Erdöl-

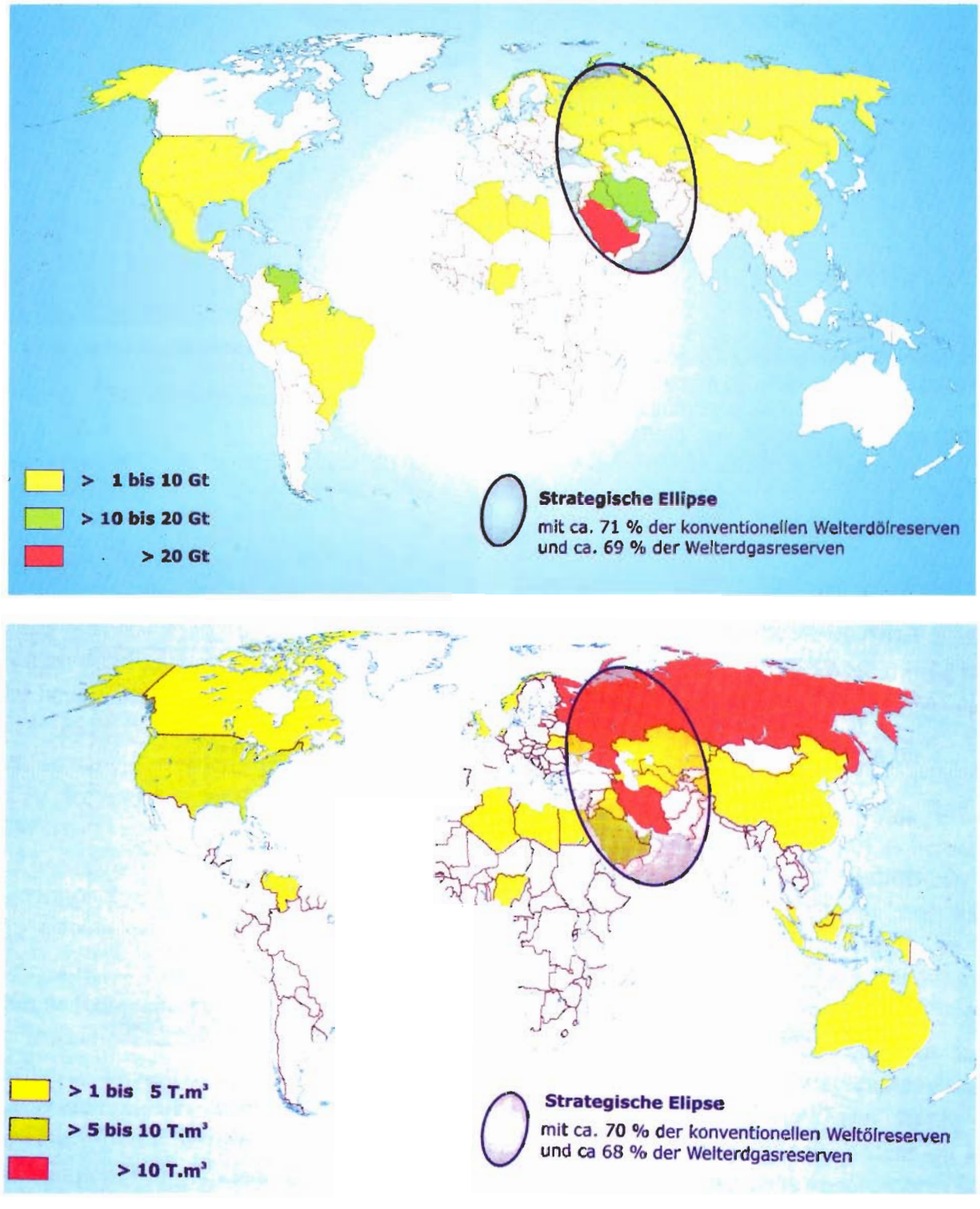

Abb.1: Erdöl- (oben) und Erdgasreserven (unten) weltweit (aus Bundesanstalt für Geowissenschaften und Rohstoffe 2003)

und Erdgasreserven (Bundesanstalt für Geowissenschaften und Rohstoffe 2003). Der Anteil Deutschland's an den weltweiten Reserven liegt im Promillebereich. Die größten Reserven liegen in der so genannten strategischen Ellipse zwischen der arabischen Halbinsel im Süden und dem östlichen Europa bzw. westlichen Sibirien im Norden. Die immer geringer werdenden Erdöl- und Erdgasreserven in Westeuropa und insbesondere in Deutschland führten zu einer sehr starken Reduzierung des Anlagenparks an Bohrgeräten in Europa und Deutschland. Die Erdöl- und Erdgas- Explorations- und Produktionsunternehmen (E&P) haben ihre Anlagen meist abgegeben und sich auf ihr Kerngeschäft – die Suche und Ausbeute von Kohlenwasserstoffvorkommen – beschränkt. Gleichwohl nehmen sie Einfluss auf das Bohrgeschäft, um durch neue Entwicklungen den Bohrbetrieb sicherer und umweltverträglicher zu machen, die Bohrkosten zu senken und das Bohrergebnis (Produktionskapazität/Bohrkosten) zu verbessern. Diese Bemühungen werden ergänzt durch Beiträge der E&P Unternehmen, die großen nichtkonventionellen Ressourcen durch Einsatz von High Technology (Hi-Tech) in wirtschaftlich förderbare Reserven umzuwandeln. So werden gezielt erhebliche Anstrengungen unternommen, um die in Deutschland nachgewiesenen großen Tight Gas Vorkommen in Höhe von etwa 50 – 150 Milliarden Kubikmeter Erdgas wirtschaftlich zu entwickeln und dem Energiemarkt zur Verfügung zu stellen.

3 Bohrtechnik in Deutschland: Umweltverträgliches Hi-Tech Bohren

Laut Baker Hughes Rig Count (2004) waren 2004 Deutschlandweit nur 5 Bohranlagen tätig. Andere deutsche Bohranlagen waren im Ausland beschäftigt. Der heutige Entwicklungsstand bei Bohranlagen wird am Beispiel von drei deutschen Bohranlagen veranschaulicht, von denen zwei in der zweiten Hälfte des vergangenen Jahrzehnts und eine in 2004 in Dienst gestellt wurden.

1. Prostar 2000 von Deutag

Die Anlage Prostar 2000 (Abb. 2) wurde auf Basis eines Anforderungskataloges der Nederlandes Aardolie Maatschappij (NAM) in den Niederlanden gebaut (Deutag 1995) und 1996 in den Dienst gestellt. An der Konzeption haben neben der NAM und KCA-Deutag auch drei Servicefirmen mitgearbeitet.

Der Mast der Anlage hat eine Kapazität von 450t und steht auf einem 9 m hohen Unterbau. Die Anlage verfügt über ein 2000 PS Hebewerk mit der Bezeichnung „Wirth GH 2000 EG", mit einem dieselelektrischen Antrieb mit SCR-Technik *(Silicon-Controlled Rectifier)* (AC-DC). Zwei Wirth Triplex-

Abb. 2: Bohranlage Prostar 2000

pumpen 7½" x 12" ermöglichen die Aufrechterhaltung des Spülungskreislaufes bis zu einem maximalen Betriebsdruck von 500 bar. Für den Antrieb und die Handhabung des Bohrgestänges ist die Anlage mit einem Top-drive-System und einem so genannten Pipe Racker der Firma Varco ausgerüstet. Für Gestängeaufnahme und Verschraubung werden ein Gestänge Pick-up-System und ein so genannter Iron Roughneck der Firma Wallmite (Abb. 3) eingesetzt. Gesteuert wird die gesamte Bohranlage von einem modernen Fahrstand, der Firma Martin Decker/Totco (Abb. 4), in den einen Computer zu den Anlagesystemen integriert wurde.

2. T-160 der RWE-DEA

Im Jahre 1997 wurde die neue Bohranlage T-160 (Abb. 5) der RWE-DEA in Betrieb genommen (Pristouschek 1997). Sie bietet optimale Möglichkeiten für typisch deutsche Bohrverhältnisse bis hin zur Formation des Rotliegenden mit Vertikaltiefen bis 6000 m und zum Abteufen von stark abgelenkten bzw. horizontale Bohrungen, um den Zielhorizont zu erschließen.

Der 51 m hohe Bohrmast hat eine Kronenregellast von 600 t und einen Unterbau von 11 m Höhe. Die diesel-elektrische Anlage arbeitet mit einem Bentec-SCR-System. Das 3-Gang-Getriebehebewerk wurde von der Firma Wirth hergestellt und hat die Bezeichnung GH-2500-EG. Die Spülpumpen arbeiten mit einem maximalen Betriebsdruck von 500 bar. Für den Antrieb des Bohrgestänges wurde auf einen Top-Drive der Firma Maritime Hydraulics zu-

Abb. 3: Wallmite – Pipe Handling System

Abb. 4. Fahrstand MD/Totco

rückgegriffen, von der auch das Iron Roughneck System stammt. Zur Reduzierung von Unfallquellen wurde das Iron Roughneck System fern bedienbar ausgelegt. Der Fahrstand der Firma Martin Decker/ Totco entspricht dem der Pro-Star 2000. Diverse Hilfseinrichtungen auf der Arbeitsbühne, wie hydraulische Hebezeuge, Bentec Antikollisionssystem und Kick Bekämpfungsanlage gehören zur Standardausrüstung dieser neuen schweren Bohranlage.

3. Rig 40 von ITAG

Der letzte Stand der Technik spiegelt sich in der 2004 entwickelten Bohr- und Workoveranlage Rig 40 des Bohrunternehmens ITAG wieder (Abb. 6).

Der Bohrmast ist 32 m hoch und hat eine Haken-

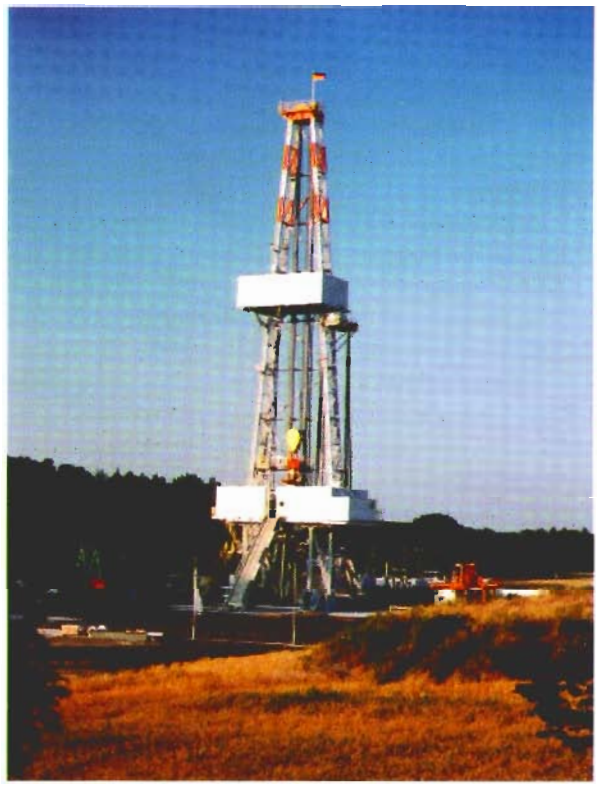

Abb. 5: Bohranlage RWE-DEA T-160

Abb. 6: Bohranlage ITAG Rig 40

regellast von 200 t. Die Höhe des Unterbaus beträgt 5,8 m. Die Anlage verfügt über eine Ausrüstung, die dem neusten Stand der Technik entspricht für Top Drive, Antrieb, „Fail-Safe" Hebewerk, Spülpumpen sowie Systeme zur Handhabung und Verschraubung des Bohrstranges.

Der modulare Aufbau der Anlage vereinfacht den Transport, ermöglicht einen flexiblen Aufbau bei geringem Platzbedarf und verkürzt Auf- und Abbauzeiten. Das diesel-elektrische Antriebssystem mit AC-AC Motoren, die der neusten Generation entsprechen, verringert die Lärmemissionen und verbessert die Energieeffizienz. Durch das besonders hohe Maß an Mechanisierung mit der Möglichkeit praktisch alle Maschinen und Geräte vom Fahrstand bzw. anderen sicheren Arbeitsplätzen aus fernzusteuern, werden Unfallquellen beseitigt.

Die Beispiele sind Beleg für die Bemühungen der Bohrunternehmen, ihren Gerätepark zu modernisieren und sich an die gestiegenen Anforderungen anzupassen. Im Vergleich zu den älteren Anlagen haben die neuen Geräte einen geringeren Platzbedarf (Low Footprint). Sie werden auf Bohrplätzen aufgestellt (Abb. 7) für die sich in Zentraleuropa ein Standard entwickelt hat, auf Grund dessen Umwelt-

Abb. 7: Platzbedarf einer modernen Bohranlage und ihre Integration in das Umfeld

schädigungen ausgeschlossen werden können. Zur Abdichtung gegenüber dem Grundwasser werden die Plätze versiegelt. Anfallende Flüssigkeiten werden gesammelt und gesondert entsorgt. Im Rahmen der Entwicklung des Standards haben sich die Kosten für die Herrichtung eines Bohrplatzes seit Anfang der siebziger Jahre mehr als versechsfacht (Abb. 8) (Schaumberg 2001). Die Ausrüstung der Bohrgeräte ermöglicht die Einhaltung der Immissionsrichtwerte der TA-Luft und TA-Lärm auch in der Nähe bebauter

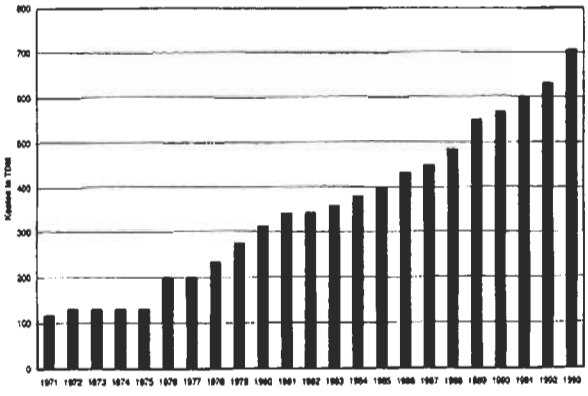

Abb. 8: Bohrplatzkosten (aus Schaumberg 2001)

Gebiete. Durch weitgehende Mechanisierung der Abläufe und die Möglichkeit der Fernbedienung von Anlagen und Geräten werden Arbeiten beschleunigt sowie Unfallquellen reduziert. Der Einfluss der Mechanisierung auf die Rate der meldepflichtigen Unfälle (Total Recordable Incident Rate, TRIR) ist in Abb. 9 erkennbar, die TRIR und fortschreitende

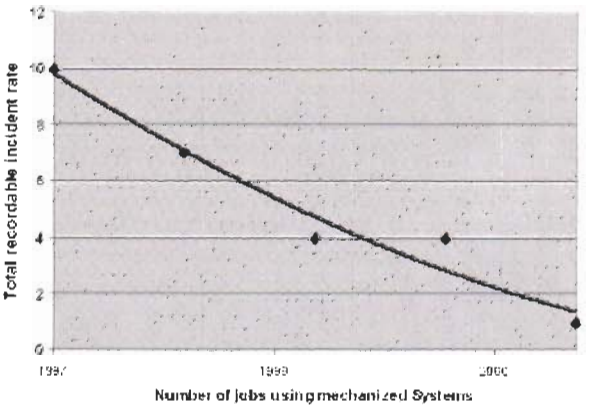

Abb. 9: Meldepflichtige Unfälle im Golf von Mexiko

Mechanisierung zeigt (Kinzel 2002). Danach sank die Unfallfallrate in dem betrachteten Gebiet der USA über den Zeitraum von 1997 bis 2001 von 11 auf unter zwei bei einem gleichzeitigen Anstieg des Mechanisierungsgrades von unter 20% auf 47%. Der Mechanisierungsgrad wird weiter steigen wie zum Beispiel durch Einsatz des StabMaster-Systems von Weatherford, das zusammen mit intelligenten Elevatoren die gefahrenträchtige Arbeit des so genannten Stabbers auf der Bohranlage komplett übernehmen kann (Abb. 10). Die Nutzung von Informationstechnologie für die Verfolgung und Analyse des Bohrvorganges ermöglicht die Reduktion von Ausfallzeiten (Downtime) durch die frühzeitige Erkennung und (automatische) Gegensteuerung von Kicks und Stuck Pipe Situation. Voraussetzung hierfür ist die Verfügbarkeit von Untertage-Daten, die über die Spülung übertragen werden. Durch Einsatz von computer-

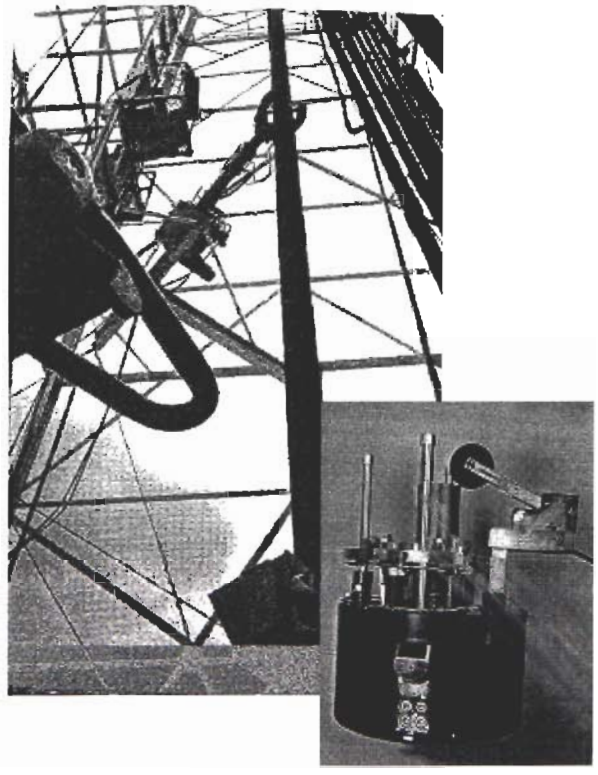

Abb. 10: StabMaster und ferngesteuerter Elevator

gesteuerten Pumpen, die eine vibrationsfreie Verpumpung der Spülung zum Ziel haben und störende Druckwellen (Mud Noise) unterdrücken, lässt sich die Qualität der Datenübertragung erheblich verbessern. Darüber hinaus ermöglichen neue Software Tools die Erzeugung von Berichten in Echtzeit und die gemeinsame Nutzung durch alle an einer Bohrung beteiligten Disziplinen. Auch das Internet wird inzwischen genutzt, um die „Rig Reliability" zu verbessern. So bietet der Gerätehersteller Firma Varco z.B. als „Technology of the Future" das so genannte „Varco e-drill Operation Control System", das eine Fernsteuerung der Teile oder der gesamten Bohranlage ermöglicht.

4 Beherrschung des Bohrlochverlaufs: Navigation und Steuerung langer Bohrstränge

Die Beherrschung des Bohrlochsverlaufs gilt als Kunst der heutigen Bohrtechnik. Es gibt zwei bewährte Verfahren, die eine Steuerung langer Bohrstränge ermöglichen. Beide beruhen darauf, unmittelbar im Meißelbereich eine Meißelseitenkraft zu erzeugen, die eine gewünschte Kursänderung hinsichtlich Neigung und/oder Azimut hervorruft. Diese steuernde Seitenkraft am Meißel wird entweder durch ein Knickstück oder über eine elastische Verformung des Bohrstranges (Auslenkung aus der Bohrlochachse) oberhalb des Meißels erzwungen.

Während das erste Verfahren den Einsatz eines Bohrmotors erfordert, wird im zweiten Verfahren ein Stabilisator mit ausfahrbaren Rippen, die in einer nicht rotierenden Hülse angeordnet sind, verwendet. Diese Entwicklung fußt auf dem Prinzip der Zielbohrstange der Bergbauforschung (DMT) (Marx et al.1985) und des Vertikalbohrsystems der Kontinentalen Tiefbohrung (KTB) (Engeser et al. 1995). Durch Verfahren einzelner Stabilisatorrippen, was während des Bohrvorganges möglich ist, lässt sich der Kippwinkel des Bohrstranges in jede beliebige Richtung einstellen und so der Neigungsaufbau des Bohrloches und die Richtung des Neigungsaufbaus beeinflussen. Bei Verwendung eines Knickstückes lässt sich während es Bohrvorganges nur die Richtung des Neigungsaufbaus durch eine Drehbewegung des nicht rotierenden Bohrstranges und damit Veränderung der Knickrichtung beeinflussen. Die Rate des Neigungsaufbaus ist durch die Größe des Knicks vorbestimmt. Für eine Veränderung des Neigungsaufbaus muss der Bohrvorgang unterbrochen werden, um das Knickstück auszutauschen. Für beide Verfahren genügt ein Kippwinkel im Meißelbereich von ca. 0,5 Grad zur Bohrlochachse, um dem Meißel eine Kurskorrektur mit einem Krümmungswert von 1°/10m zu bewirken.

Soll nach vollzogener Kursänderung wieder richtungsstabil gebohrt werden, so wird bei Einsatz eines Knickstückes der Bohrstrang von Übertage mit etwa 10 U/min rotiert. Beim Steuern mit Stabilisatorrippen werden alle Steuerrippen in eine konzentrische Position zum Bohrloch gebracht.

Durch die Beherrschung des Bohrlochverlaufs durch Navigation und Steuerung, ist der Meißel gleichsam zu einem „Litho-Mobil" geworden.

Navigation

Navigation ist die permanente Ortsbestimmung des Bohrwerkzeuges im dreidimensionalen Raum und der momentanen Bewegungsrichtung. Navigation umfasst die präzise Bestimmung der drei Richtungsgrößen Neigung, Azimut und Toolface (z. B. Ausrichtung des Knickstücks bzw. der richtungsbestimmenden Kraft am Meißel) und die Übertragung dieser Informationen nach Übertage (Schlumberger 1993) Das Messen von meißelnahen Informationen während des Bohrens wird MWD-Technik genannt. (Measuring While Drilling). Für den Messvorgang muss also der Bohrprozess nicht unterbrochen werden (Abb. 11).

Steuern

Steuern ist das aktive oder automatisierte Eingreifen mit dem Ziel, den Bohrlochverlauf zu ändern. Erfolgt die Kursbestimmung einer programmierten Vorgabe, so handelt es sich um selbststeuernde Bohrsysteme wie z. B. das AutoTrackSystem der Firma Baker Hughes Inteq (BHI). Man spricht von Geosteering (Abb. 12) wenn als richtungsbestim-

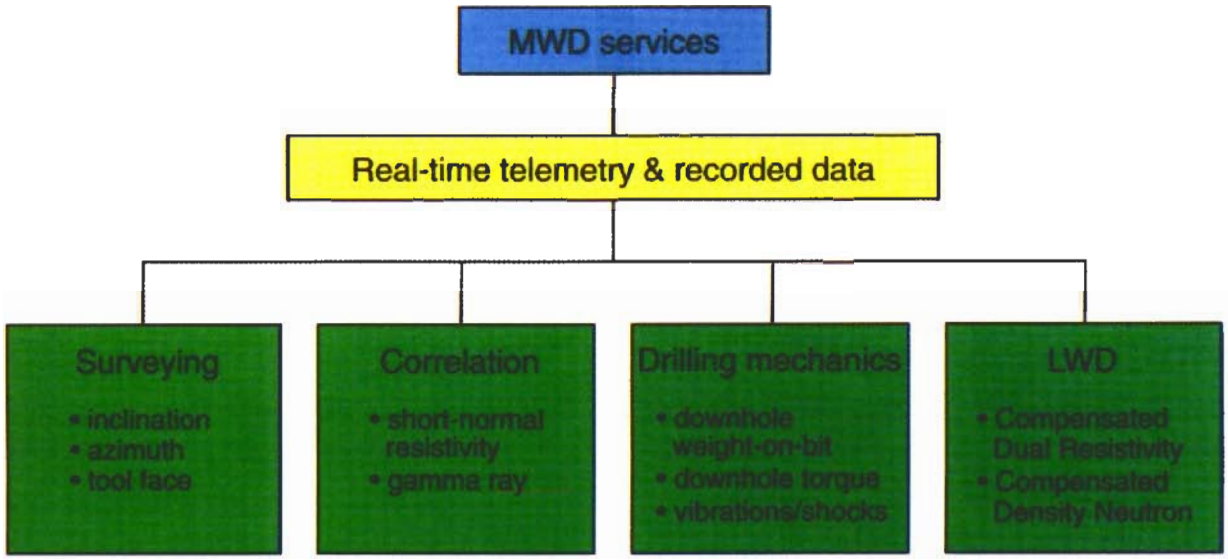

The relationship between MWD and LWD measurements. In this document, LWD is used to denote wireline-quality petrophysical measurements made while drilling—resistivity, gamma ray, density and neutron porosities, calipers and photoelectric effect (P_e). LWD is a subset of MWD services, which also include sensors for drilling-related measurements such as direction and inclination and equipment for data recording and telemetry.

Abb. 11. Messen während des Bohrens (aus: Schlumberger 1993)

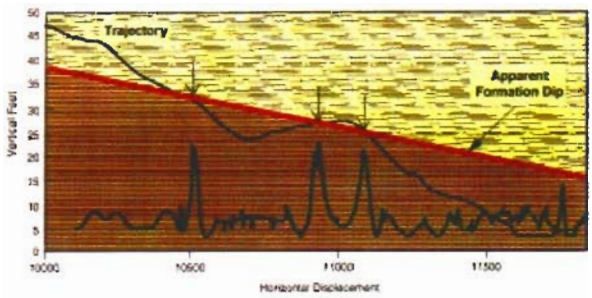

Abb. 12. Geosteering (aus Burgess & Decker 1996)

mende Vorgabe ein Abstand zu einer geologischen Schichtgrenze, zum Beispiel der oberen Begrenzung der Lagerstätte einzuhalten ist (Burgess & Decker 1996). Geosteering wird beim Horizontalbohren in der Lagerstätte angewendet. Es wird vorgenommen auf der Basis der Eigenschaften der durchteuften Formation, die während des Bohrens durch ein Logging While Drilling (LWD) gemessen werden. Diese Messungen ermöglichen eine Bestimmung der Lithologie, der Speichereigenschaften und der Sättigungsverhältnisse der Formation.

Mit der MWD-Technik können optional weitere Messungen durchgeführt werden, wie Meißelandruck, Drehmoment, Schwingungen des Bohrstranges in axialer, torsionaler und lateraler Richtung, Druck über dem Meißel und im Ringraum, Spülungsdichte und Temperatur. Im Laufe der Entwicklung von MWD und LWD Geräten konnte erreicht werden, dass die Messsensoren immer näher an den Meißel verlegt wurden. Das zusätzliche Verfahren Seismik während des Bohrens (SWD) ist noch in der Entwicklung.

5 Neue Verfahren zur Entwicklung von Lagerstätten brauchen neue Geräte

Die Entwicklung von besseren Bohranlagen führt nicht nur zu kürzeren Bohrzeiten, sondern bietet auch die Möglichkeit, neue Verfahren einzusetzen, um Lagerstätten besser aufzuschließen. Es werden in folgendem zwei Bohrkonzepte dargestellt, die in Deutschland und für die deutsche Geologie entwickelt worden sind: die Tight Gas Entwicklung und das Extended Reach Drilling durch Salzformationen.

Tight Gas Erschließung

Die zunehmende Erschöpfung der Erdgas- und Erdölfelder in Deutschland stellt eine besondere Herausforderung dar, die in Deutschland nachgewiesen erheblichen nicht-konventionellen Vorkommen wirtschaftlich zu entwickeln, allen voran die Tight Gas Vorkommen. Tight Gas ist Erdgas, das außerordentlich schwer zu fördern ist, da die Porenräume der Lagerstätten mit Tonmineralen verstopft sind (http://www.exxonmobil.de/produktion/erdgasproduktion/produktion/) Hierdurch ist die Gesteinsdurchlässigkeit (Permeabilität) extrem klein: sie ist um bis zu 1000-mal niedriger als in herkömmlichen Lagerstätten. Mit den traditionellen Bohr- und För-

dermethoden kann Tight Gas kaum gefördert werden. Eine wirtschaftliche Entwicklung erfordert ein gezieltes Erbohren der am besten ausgebildeten Lagerstättenbereiche, ein schonendes Erbohren dieser Bereiche mit Ablenk- und Horizontalbohrungen in der richtigen Richtung sowie ihre Stimulation. ExxonMobil Production Deutschland GmbH hat mit neuen, innovativen Technologien beachtliche Erfolge erzielt: die Horizontalbohrungen mit Multi-Fracs, wie sie im Erdgasfeld Söhlingen zum Einsatz kommen, erschließen das Potenzial der beachtlichen deutschen Tight Gas-Lagerstätten für eine sichere Energieversorgung (Abb. 13).

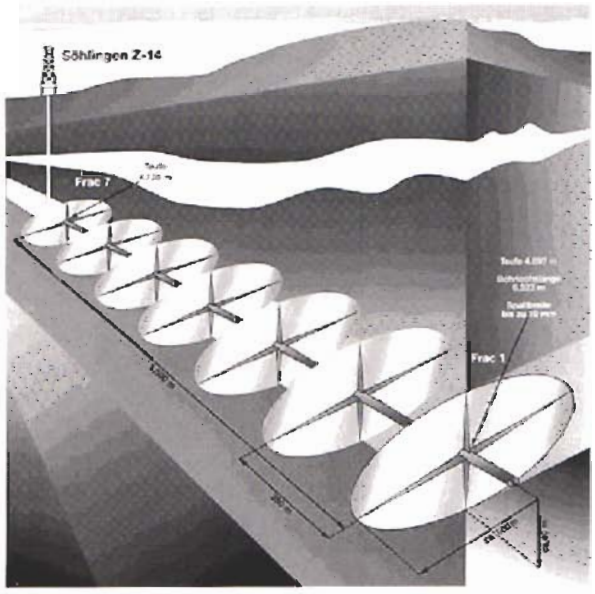

Abb. 13. Multi-Frac-Verfahren zur Erschließung von Tight Gas Reserven

Extended Reach Bohrungen durch Salzformationen

Die zügige Entwicklung des größten deutschen Erdölfeldes Mittelplate des Konsortiums RWE-DEA und Wintershall im Wattbereich vor der westlichen Küste Schleswig Holsteins führte zum Einsatz und zur Weiterentwicklung des Extended Reach Bohrtechnologie. Zusätzlich zu Bohrungen von einer künstlichen Insel im Wattbereich konnten Teile der Lagerstätte mit Extended Reach Bohrungen erschlossen werden. Dabei wurden Bohrungen vom schleswig-holsteinischen Festland schräg unter das Wattenmeer gebohrt, um Bohrziele in einer Tiefe von 2.500 – 3.000 m etwa 8.000 m westlich vom Bohrplatz zu erreichen. Die Herausforderung beim Abteufen der Extended Reach Bohrungen lagen nicht nur im Bohren über 9000 m, sondern auch in dem komplexen Zusammenspiel von verschiedenen Auforderungen, wie Säuberung der Bohrlochsohle, Horizontalbohren in Salz Formationen, etc. Abb.14 zeigt einen Schnitt durch das geologische Profil einer der Bohrungen, Dieksand 2. Für das Durchteufen des Salzgebirges wurde eine speziell entwickelte Spülung benutzt. Für die Komplettierung wurden 7 5/8" Dickwand Rohr verwendet, um dem hohen Druck des Salzes standzuhalten.

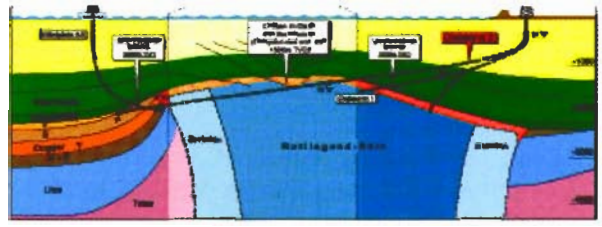

Abb. 14. Dieksand – Extended Reach Bohrung und Geologie

Durch Verwendung der Extended Reach Bohrtechnik konnte die Förderrate des Feldes in etwa verdoppelt werden ohne dass weitere Eingriffe im sensiblen Wattbereich notwendig waren und so ein Ausgleich zwischen ökologischen und ökonomischen Interessen geschaffen werden.

6 Literatur

Baker Hughes (2004): Baker Hughes Rig Count.- www.baker-hughes.com

Bundesanstalt für Geowissenschaften und Rohstoffe (2003): Reserven, Resourcen und Verfügbarkeit von Energierohstoffen 2002. – Rohstoffwirtschaftliche Länderstudien, Bd. XXVIII, 400 S., 128 Abb., 98 Tab, 1 CD; Hannover.

Burgess, T. M., & Decker, D. (1996): Measurements at the bit – the ideal way to geosteer.-Vortragsmanuskript der Schlumberger-Anadrill.

Deutag (1995): Pro-Star 2000, A new generation rig.- Deutag-Post,. **15**,

Engeser, B. et al (1995): Aus der Durchführung des KTB-Projektes ableitbare Erfahrungen zur Nutzung in der Tiefbohrtechnik.- DGMK-Tagung in Celle, 27.- 28.April 1995.

http://www.exxonmobil.de/produktion/erdgas-produktion/produktion/

Kinzel, H. (2002):Mechanisierte Handhabung von Gestänge und Rohren – Sicherheitstechnische und wirtschaftliche Überlegungen.- DGMK Frühjahrskonferenz Celle.

Marx, C (2001): Entwicklungsschwerpunkte auf dem Gebiet der Bohrtechnik (1951-2001).- 52. Berg- und Hüttenmännischer Tag, Juni 2001.

MARX, C., JÜRGENS, R. & ROHDE, H. (1985): Special developments in drilling technology.- Oil Gas-International of EEK, Vol. 7:29 – 35.

PRISTOUSCHEK, F. (1997):RWE-DEA nimmt neue schwere Bohranlage in Betrieb.- EEK, **113**, H. 10: 413 – 416.

SCHAUMBERG, G. (2001): Bohrgeräte Handbuch.- Bohrmeisterschule Celle.

Schlumberger (1993):Logging while drilling.- Schlumberger Educational Services.

SPE 122786-PP

Design of a High-Pressure Research Flow Loop for the Experimental Investigation of Liquid Loading in Gas Wells

J. Fernandez(*), SPE, G. Falcone, SPE and C. Teodoriu, SPE, Texas A&M University

This paper was prepared for presentation at the 2009 SPE Latin American and Caribbean Petroleum Engineering Conference held in Cartagena, Colombia, 31 May–3 June 2009.

Abstract

Existing models to predict and analyze liquid loading in gas wells are based on steady-state flow. Even when transient multiphase wellbore models are employed, steady-state or pseudo steady-state inflow performance relationships are used to characterize the reservoir. A more reliable approach consists of modeling the dynamics in the near-wellbore region with its transient boundary conditions for the wellbore. The development of new models to mimic these dynamics requires a purpose-built flow loop. We have developed a design to construct such a facility.

This new facility will be the first to integrate pipe representing the wellbore with a porous medium that will fully mimic the formation surrounding the wellbore. This design will account not only for flow into the wellbore, but any reverse flow from the pipe into the medium.

We used integrated wellbore/reservoir system analysis to screen the parameters required to recreate liquid loading under laboratory conditions. Once the range in operating conditions was defined, the equipment and mechanical components for the facility were selected and designed.

Our results showed that three reciprocating compressors working in parallel provide the smallest, most economic, and most flexible configuration for the Tower Lab facility at Texas A&M University. The design of the pressure vessel hosting the porous medium will require a cylindrical body with top- and bottom-welded flathead covers with multiple openings to minimize weight. The required superficial velocities for air and water indicate that the system will need independent injection into the porous medium through two manifolds. Optimally, the system will use digital pressure gauges, coriolis or vortex technology to measure air flow and turbine meters for water flow.

The new facility will significantly improve our ability to mimic the physics of multiple phase flow for the development of liquid loading models and lead to better optimization of gas fields.

Introduction

Natural gas is one of the principle sources of energy for many of our day-to-day needs and activities. It is a vital component of the world's supply of energy as it is one of the cleanest, safest, and most useful of all energy sources. Strong domestic and international demand has made it commercially attractive since the 1950s (Yamamoto and Christiansen, 1999). However, the deliverability from existing gas reservoirs continues to decline and the scarcity of promising prospects has increased the need to maximize gas recovery from every gas well.

As natural gas is produced from a reservoir, the simultaneous flow of gas, liquid hydrocarbons, and water is a common situation for both land and offshore production systems (Toma *et al.*, 2006). In vertical wells, water and intermediate hydrocarbons can condense in liquids in the wellbore, depending on the current composition of the gas during production. In depletion-drive reservoirs, the energy available to remove the produced/accumulated liquids, condensates, and formation water to the surface declines. This energy eventually becomes so low that flow rates decrease below a certain critical velocity, and fluids produced with the gas flow stream begin to fall back, no longer being carried to the surface. Where the flow stream is insufficient to continuously transport the well liquids upward in the wellbore, a wellbore liquid loading condition begins.

Loading up of liquid in the wellbore has been recognized as one of the most severe problems in gas production. Accurate prediction is of critical importance to efficiently take the optimal approach to deal with this situation. Although several investigators (Turner *et al.*, 1969; Coleman and McCurdy, 1991; Guo *et al.*, 2005; Dousi *et al.*, 2005; Gool and Currie, 2007) have suggested methods to predict the onset of liquid loading, results from these models are only applicable to steady-state flow; however, liquid loading corresponds to unsteady-state flow conditions, both in the well and in the near-wellbore region of the reservoir.

(*) Now with Anadarko Petroleum Corporation

A more reliable approach would be to use a transient multiphase flow wellbore model that accounts for the dynamics in the near-wellbore region via transient boundary conditions. A dynamic, integrated (reservoir/wellbore) system modeling approach would predict conditions for transition from an acceptable production flow regime (annular or mist flow) to an unacceptable regime (churn flow) that triggers liquid loading in the wellbore (Solomon and Fernandez, 2007). Achieving these objectives, requires rigorous empirical studies of transient multiphase flow under laboratory conditions that attempt to mimic well behavior under liquid loading.

A review of existing flow loops worldwide revealed some specialized areas of research such as liquid loading in gas wells are still lacking dedicated test facilities (Falcone *et al.*, 2007). Having an experimental facility with adequate vertical height and diameter of the test section to reproduce the flow regimes encountered prior to and after onset of liquid loading in gas wells is necessary to conduct experimental studies to mimic the dynamic boundary conditions that exist between the reservoir and wellbore during liquid loading. This requires a compression and boosting system capable of circulating fluids at flow rates, pressures and high gas volume fractions (GVF) similar to real gas-field production situations, as well as, technology and instrumentation for controlling and monitoring key two-phase flow parameters such as pressure, temperature, and flow rates among others.

Additionally, the facility will allow the creation of the flow resistance represented by the reservoir, for which the common practice has been to use a series of valves to simulate permeability variations. However, flow from a real reservoir to the wellbore goes through a porous medium, and in the case of multiphase flow, relative permeability must be taken into consideration.

To recreate the effect of the near-wellbore region, our new facility (TAMU Tower Lab) will allow us to attach a cylindrical pressure vessel containing tightly packed spherical glass beads to the base of a vertical multiphase flow loop. Flow of fluids into the porous medium will be provided by entry points symmetrically aligned at the pressure vessel using an injection manifold with adequate geometry to ensure proper dispersion of the fluids.

Liquid Loading in Gas Wells

The process of liquid loading can be summarized in four stages (Neves and Brimhall, 1989):

1. After the well has been completed and production begins, a gas well has enough energy from its high initial reservoir pressure and gas flow rates, to carry the liquids all the way to the surface (**Fig. 1(a)**). At this stage the gas velocity is greater than or equal to the critical velocity required to continuously remove the liquids in the gas stream.
2. As production continues, natural reservoir pressure declines, producing a decrease in gas flow rate that directly induces a decrease in gas velocity until reaching and falling below the critical gas velocity value. Consequently, liquid droplets suspended in the gaseous phase will begin to move downward and start accumulating at the wellbore, restricting the effective flow area for the gas and impeding its continuous production (**Fig. 1(b)**).

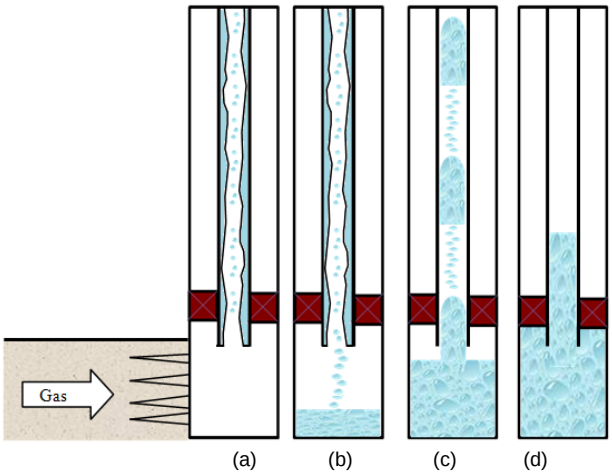

Fig. 1 – During gas production, flow regime changes from mist (a) to annular (b) to slug/churn flow (c), which causes the well to load up and die

3. Followed by the accumulation of the liquids, gas flow rate initially increases because of the reduction of the effective area, which results in a larger pressure drop across the accumulated liquids downhole. The pressure drop increases until the downstream pressure reaches the pressure necessary to transport the liquids up the tubing (**Fig. 1(c)**).
4. As a well cycles back and forth between the last two stages, the time differential between produced liquid slugs at the surface becomes greater as a consequence of the time required by the reservoir to reach a pressure high enough to blow the liquid slugs up the string. Eventually, the backpressure at the sand face originated by the liquids that have accumulated at the bottom overcomes the available reservoir energy, causing the well to load up and die (**Fig. 1(d)**).

The well-established techniques to alleviate the effects of liquid loading have been described by several authors (Stephenson *et al.*, 2000; Lea *et al.*, 2003). Foaming the liquid water can enable the gas to lift water from the well. Using smaller tubing or creating a lower wellhead pressure sometimes can extend mist flow. The well can be unloaded by gas lifting or pumping the liquids out of the well. Heating the wellbore can prevent liquid condensation. Downhole injection of water into an underlying disposal zone could be another option. Each of these technologies has its niche, but choosing the optimal strategy depends on a collection of factors including composition of reservoir fluid, operating pressures and temperatures, and of course economics (Yamamoto and Christiansen, 1999).

Comparison of Major Equipment and Operating Conditions of Multiphase Research Flow Loops

Table 1 illustrates the maximum pressure and the equipment used to handle the liquid and gas phase for the flow loops described in this investigation.

Table 1 – Major equipment used in research loops for liquid injection and gas compression

Flow loop	Maximum Pressure, psi	Liquid phase	Gaseous phase
South West RI (Hart, 2007)	3,600	Centrifugal pumps	Centrifugal compressor
NORSK HYDRO (Robole, 2006)	1,595	Centrifugal pumps + twin screw pump (for oil)	Centrifugal compressor
CEESI (Kegel and Kinney)	1,500	Positive displacement pump	4 stage Recips + 4 single stage recips
SINTEF LSL (Unander, 2007)	1,305	Centrifugal pump	Reciprocating compressor
TUV NEL (www.tuvnel.com)	910	Centrifugal pump	Centrifugal gas blower
Boussens (Corteville *et al.*, 1983)	725	Centrifugal pumps	Centrifugal compressor
IFP (Vilagines and Hall, 2003)	725	Two-phase pump	
IFE (Langsholt, 2007)	145	Centrifugal + dosage pumps + screw pump	Multiphase pump (twin screw)
SINTEF MSL (Unander, 2007)	117	Centrifugal pumps	Multiphase pump (twin screw)
LOTUS (Falcone *et al.*, 2003)	90	Centrifugal pumps	Compressed tank
TAMU Tower Lab	120	Centrifugal pump	Reciprocating compressor

Fig. 2 shows the vertical height for the multiphase research flow loops mentioned in **Table 1**. The maximum length of a flow loop affects the development of different flow regimes, particularly in transient flow investigations (Falcone *et al.*, 2007). The vertical height of the test section available of our design clearly is competitive when compared to other facilities.

The range of flow regimes that can be reproduced in a flow loop is related to the flow rates that can be circulated in the system. The maximum reported flow rates for gas in the flow loops identified for this study are given in **Fig. 3**. The highlighted portions of the graphs show that the proposed range in pressures and rates in our facility would cover a region where current research flow loops do not operate.

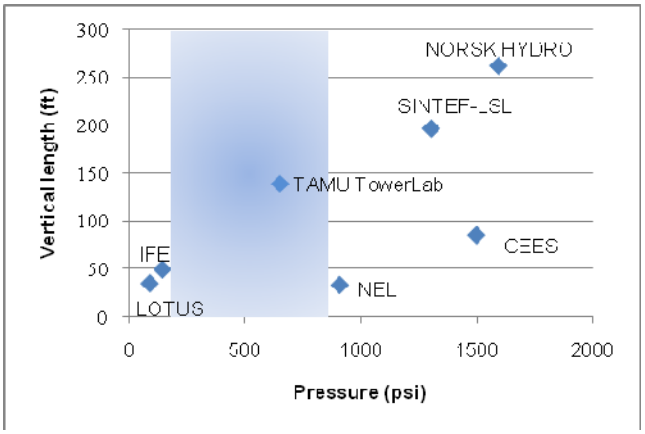

Fig. 2 – Vertical length vs. Pressure

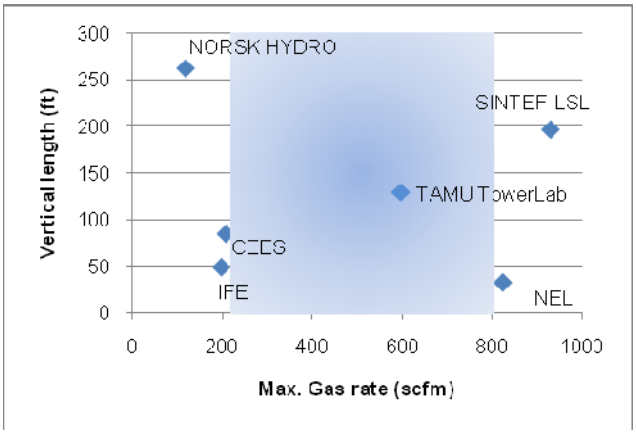

Fig. 3 – Vertical length vs. Max. Gas rate

Results of the extensive review indicate a niche in operating conditions for the TAMU Tower Lab; however, the final values for an experimental facility have to be selected for the type of research to be conducted. Since our facility is intended for the experimental investigation of liquid loading, values of pressure and flow rates including adequate geometry and hardware should allow us to mimic the conditions that precede and follow liquid loading in a gas well.

General Considerations for Flow Loop Design

From a research standpoint the modeling of hydrocarbon processes in a laboratory environment and the existing operating conditions encountered in real oil and gas fields is significant. However, this breach can be narrowed by designing a state-of-

the-art facility operating under more realistic conditions of pressure, flow rates, and temperatures found in real gas wells. Nevertheless, the exact representation of an existing field is difficult to accomplish entirely.

Flexibility is an important characteristic the multiphase flow loop should incorporate at an early stage of the design; however, as a result of the high capital investment needed to build a facility to study multiple problems within the area of multiphase flow, making a flow loop 100% flexible is neither technical nor economically feasible. The approach by most laboratories is to design and build their facilities to accommodate a range in operation and fluids to be handled by their flow loops.

Current models used to study multiphase flow have been obtained and validated via research flow loops. However, new investigations are continuously being carried to out to improve existing correlations or to propose new methods. This creates a need for more problem-oriented research flow loops.

For our facility, we identified the range in operating conditions through a review of multiphase flow loops around the world. We validated these values throughout this study to guarantee that conditions that precede and follow liquid loading can be achieved. **Fig. 4** shows the proposed downscaling of a gas well completion for our facility.

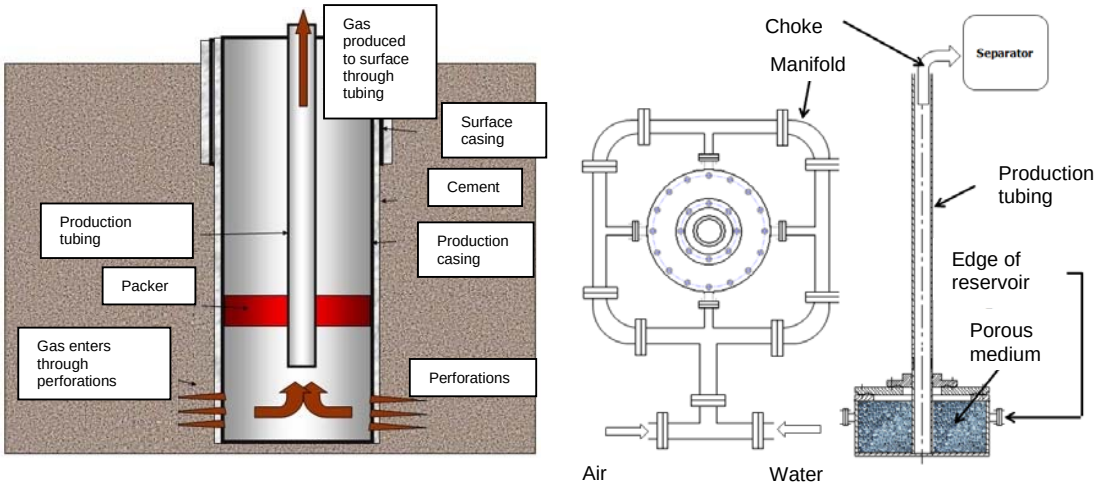

Fig. 4 – Our laboratory will introduce a porous medium to better capture flow behavior in the near wellbore region

The assembly will attempt to mimic the dynamics of the near-wellbore region to provide boundary conditions for the development of predictive transient multiphase flow models.

To recreate the pressure effect of the near-wellbore region we will attach a cylindrical pressure vessel containing tightly packed spherical glass beads to the base of the vertical multiphase flow loop. Glass beads, which represent a formation of uniform grain size, are low cost and readily available, and their use in fluid flow experiments is well documented (Alshuraiqui *et al.*, 2003, Costantini, 2005).

Average porosity of a glass bead pack is in the order of 38% with permeability ranging from 1.2 to 29 Darcy, depending on their size and packing. **Fig. 5** is a front view section of the pressure vessel containing glass beads tightly packed.

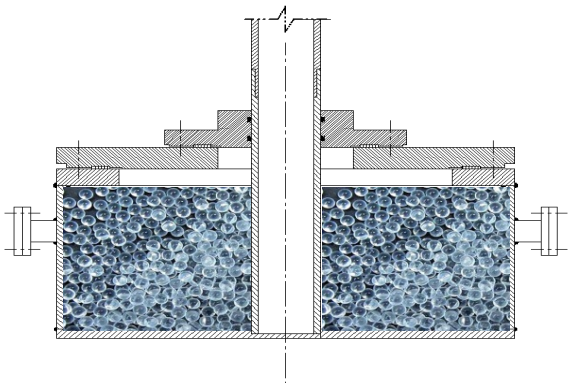

Fig. 5 – Pressure vessel will recreate effects of the near-wellbore region

Flow of fluids into the porous medium may be provided by entry points symmetrically aligned at the pressure vessel by means of a distribution mechanism that ensures proper dispersion of the fluids. **Fig. 6** illustrates the use of a single injection manifold where the testing fluids would mix prior their arrival at the pressure vessel.

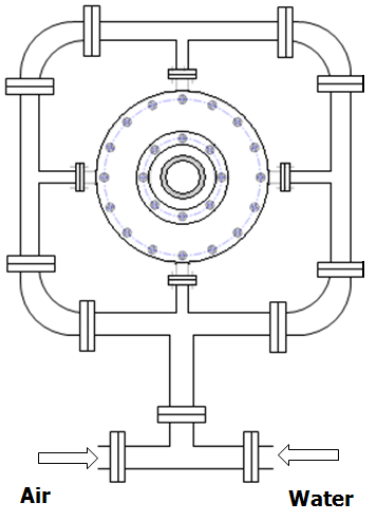

Fig. 6 – A single injection manifold will ensure proper mix of fluids entering the system

The phases initially considered as testing fluids are air and water. This will demand using a compression and boosting system capable of delivering the fluids at the required operating conditions. Control and monitoring will be managed by flow or mass meters. During transient flow periods, measurements of void fraction, temperatures and pressures will be taken at different locations across the flow loop.

Design factors for mimicking liquid loading at TAMU Tower Lab

Solomon and Fernandez (2007) performed a sensitivity analysis using a commercial wellbore/reservoir simulator and a response surface methodology to minimize cost and investigate different design parameter settings for the facility. Table 2 presents the design variables investigated, which included tubing diameter sizes, glass beads' packing permeability, cylindrical pressure vessel dimensions, and operating pressures.

Table 2 – Design factors (Solomon 2007)

Factor	Numerical range
Permeability, Darcy	0.01 to 6,000
Tubing diameter, in.	2.72 to 4.5
Compressor discharge pressure, psia	470 to 650
Pressure vessel radius, ft	1 to 6
Pressure vessel height, ft	0.7 to 3
Water Gas ratio, STB/MMscf (constant)	3,300
Surface choke pressure, psia	20 to 400

Published literature suggests that the typical diameter of glass beads used to perform fluid flow experiments typically ranges from 250 μm to 3mm, with permeability and porosity values of 29 to 1,200 Darcy and 38 to 46%, respectively. However, we will conduct laboratory experiments with glass beads to determine values of permeability and porosities that are apropriate for the artificial porous medium.

Tubing size diameters must be typical for gas-producing wells, which required analysis of the effect of the deliverability of the system, considering other variables. The range given in Table 2 considers diameters found in most gas well completions in the US.

A compressed air system, providing a discharge pressure between 470 to 650 psi with gas rates between 400 to 650 scf/m, was considered necessary to evaluate the impact on the flow potential of the system. We plan to use a compressor capable of delivering operating conditions that can mimick liquid loading. In addition, the analysis assumes a constant water gas ratio of 3,300 STB/MMscf and takes into consideration the operating conditions (pressure and flowrates) that exist at the nozzle ports located on the external entry points of the pressurized vessel. **Fig. 7** shows the location of the four nozzle ports.

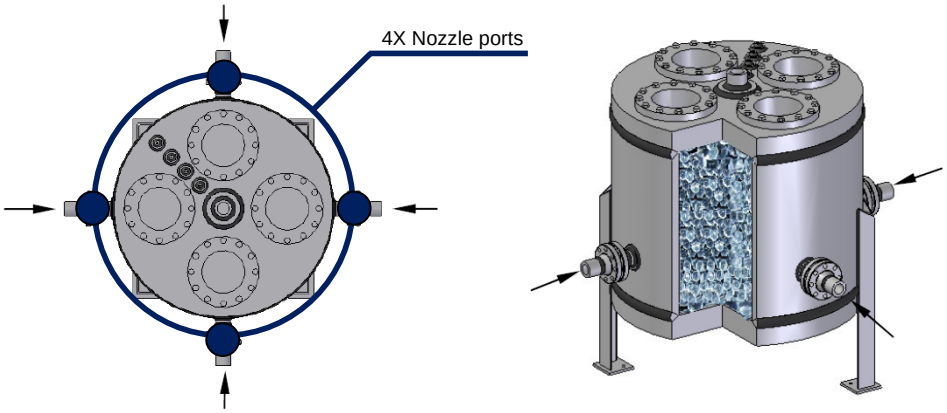

Fig. 7 – Operating conditions are supplied at the 4 nozzle ports surrounding the pressure vessel

For the design of the pressure vessel we plan to make optimal use of the available area in the basement (56 ft^2). The dimensions of the vessel must guarantee safe operations with adequate space for the installation of flow metering and pressure monitoring devices. As for the surface chokes, we investigated a range of 20 to 400 psi.

A multiple response optimization (Solomon and Fernandez, 2007) identified options to minimize cost and maximize system performance. The recommended design factor combination was to use 3 in. tubing with a 500 psi compressor and cylindrical pressure vessel dimensions of radius 4.85 ft and height of 2 ft. System calculations using the wellbore/reservoir simulator with these parameters validated their applicability to simulate liquid loading in our facility. Our results from generating IPR and VLP curves confirmed the feasibility of using the parameters considered in the optimization process.

Design Option for the Boosting System

Three possible arrangements for compression and boosting include a compressor with a water pump, a multiphase pump, or a pressure vessel storing compressed air. Our analysis showed that the pressure vessel option was not feasible, as it would not be capable of delivering the required flow rate and pressure for the time required to run the experiments. The compressor plus pump option proved to be cheaper than the multiphase pump.

Fig. 8 illustrates the system where a compressor and pump deliver independent or commingled injection at the manifold. In addition, two manifolds allow flexibility for single fluid injection or for mixture of the phases prior to entering the bottom section of the tubing.

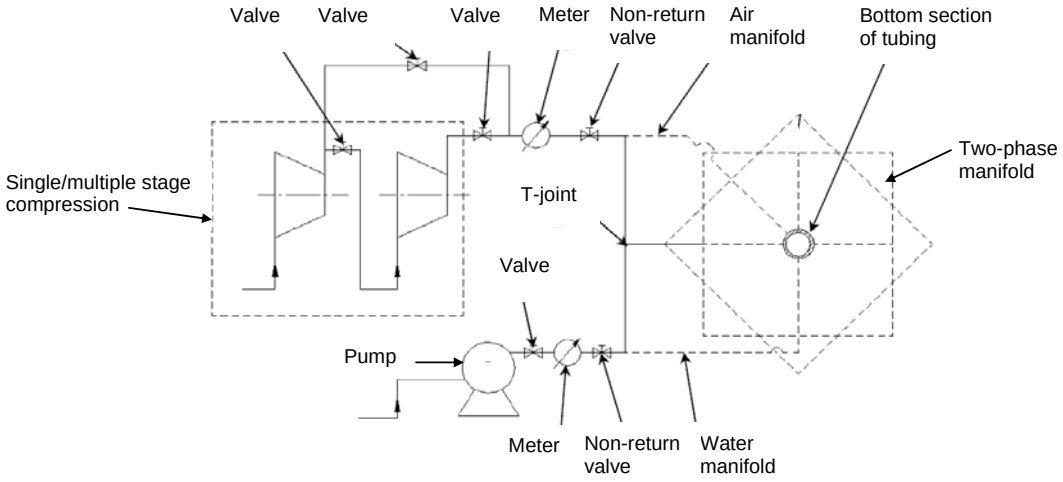

Fig. 8 – Compressor and water pump will allow independent or commingled injection of fluids

This design is practical, and it allows for both single and multiphase flow through the system. Additionally, cost reductions are achieved by eliminating the use of a multiphase pump, which costs more than any other pump and also imposes a challenge from a system-control standpoint. An initial stage of compression given by a small unit, followed by a booster (such as a multiphase pump) would add higher control complexity to the overall compressed air and water system as compared to the

system shown in **Fig. 8**. Furthermore, our design option involves less equipment and so minimizes maintenance complexity and cost. Although larger equipment may be desirable to provide the complete operational envelope, it costs more and must fit into the physical space available.

Facility Design

The approach to designing the facility that will accommodate all the major equipment and components for the operation of the multiphase flow loop at Tower Lab began by establishing the operating conditions. Since one of the main challenges of this project was to properly size the compressed air system, our design set out with the design of the pressure vessel, then progressed upstream, through the injection manifold, pipe lines, instrumentation and compressed air package.

Flow Loop

The pressure vessel will be located at the basement of the Joe C. Richardson Building on the Texas A&M University campus. The first task was to identify the space available for the proper installation and operation of the equipment. **Fig 9(a)** is a top view of the building basement, and **Fig. 9(b)** highlights the possible location for the pressure vessel.

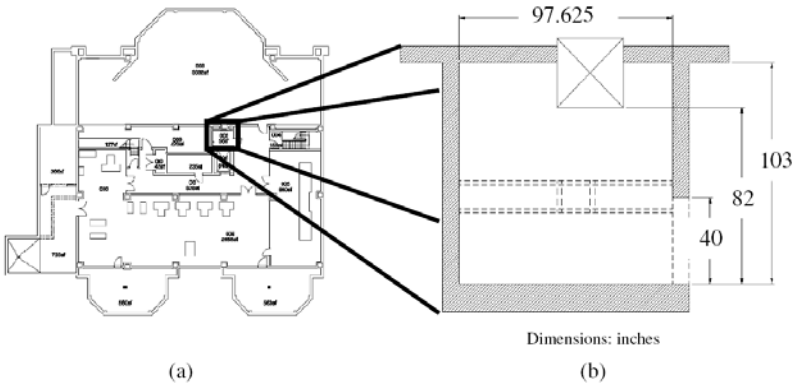

Fig. 9 – Basement at Richardson building and location of pressure vessel

However, it is important to mention that the area in the basement does not extend throughout the height of the building therefore, measurements of every floor were taken to guarantee a free path for the tubing. **Fig. 10** is a top view of the Tower Lab from 2nd to10th floor.

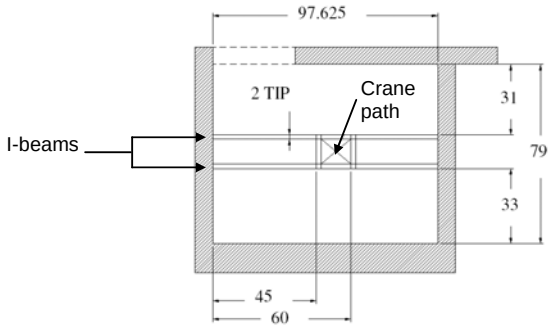

Fig. 10 – Tower Lab main dimensions from 2nd to 10th floor

Three openings can be allocated to support the vertical tubing; however, the central opening is used by a crane, which is installed at the roof of the building. This left only two possible locations for the pressure vessel and of these, the one closest to the wall had to be eliminated as it would limit the radius of the vessel. As **Fig. 10** shows, these openings have "I" beams installed at both sides (on every floor), which are useful for holding and maintaining the verticality of the pipe sections.

Pressure Vessel

By placing the tubing as indicated in **Fig. 11**, and having the geometrical center shared by both the pressure vessel and the tubing, we used the maximum internal diameter of the container to optimize its location with respect to the space available, at every floor and in the basement.

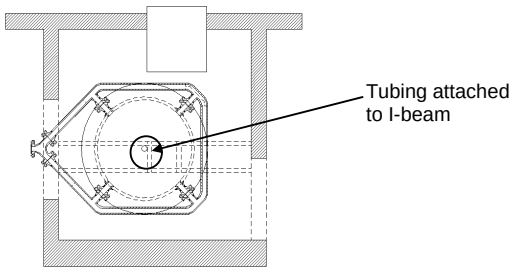

Fig. 11 – Proposed location of pressure vessel

Geometrical parameters (Solomon and Fernandez, 2007) indicated an internal radius of 5 ft (60 in.) and uniform height of 3 ft (36 in.); however, in our facility the internal diameter had to be modified because of lack of space. We designed the pressure vessel providing the largest diameter possible within the physical constraints imposed by the system.

We used ASME Code (2007) to design the different parts, including the shell, unstayed flat heads and covers, openings, reinforcements, nozzles, fittings, bolted connections, lifting lugs and support legs. The fabrication materials are also covered by ASME Code for pressure vessels. **Table 3** presents the chosen materials as a function of operating temperature.

Table 3 – Material selection guide

Design Temperature ºF	Material	Plate	Pipe	Forgings	Bolting/Nuts
33 to 775	Carbon Steel	SA-285C	SA-106-B	SA-105	SA-193-B7 with SA-194-2H

We do not anticipate corrosion issues in our facility. We chose carbon steel as the fabrication material; however, as experience has demonstrated, a fully non-corrosive environment is unlikely to be encountered in any process. As a consequence, we added an additional value of 0.125 in. to the required thicknesses to account for corrosion effects.

Several designs were technically and economically evaluated to not only minimize the fabrication costs, but also to facilitate the installation of the equipment. We used a commercial design software to generate different configurations to determine the best option in terms of expected fabrication costs, total weight, and (most importantly) the ease with which experiments could be conducted.

We evaluated having a flat head attached with bolts (options 1, 2, 3 and 4) and openings (options 3 and 4), a flanged and dished plate on the bottom (options 2, 4 and 6), and welded flat heads on top and bottom (options 5 and 6) with openings on top. **Fig. 12** shows the different alternatives.

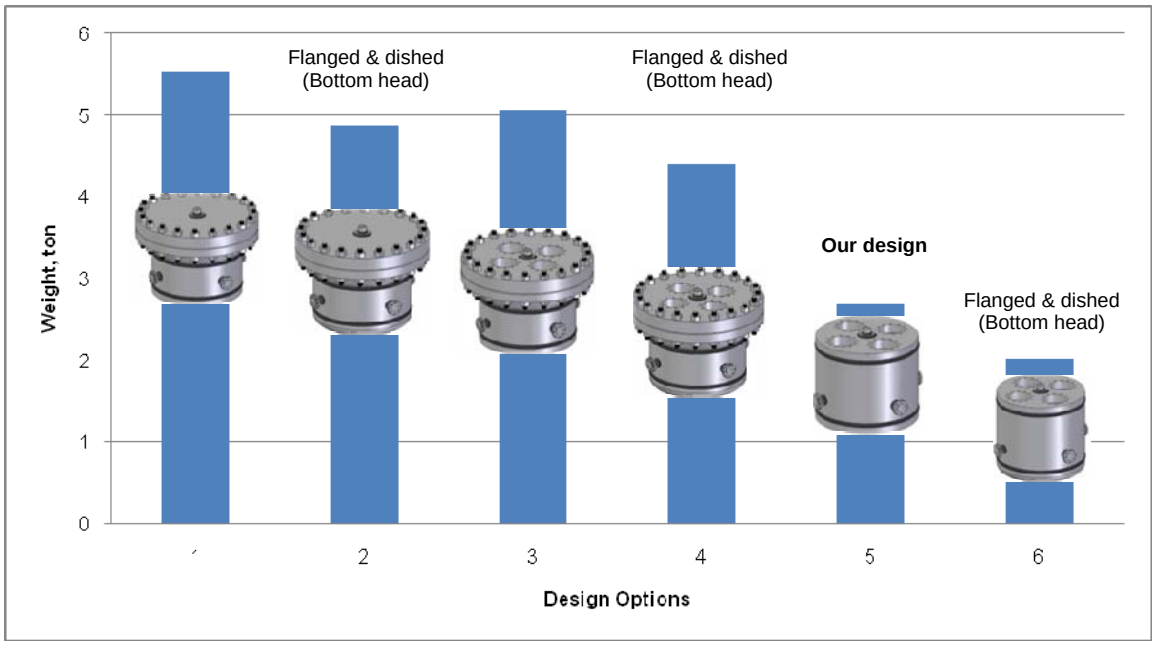

Fig. 12 – Configurations for weight reduction

The chosen option offered outstanding weight reduction, but more importantly, the thickness of the porous medium was kept constant throughout the vessel radius. Additionally, we incorporated leg supports using 4 x 4 x 0.375 in. angle beams of structural steel and 0.625 in. thick base plates. The support system can withstand up to 10 tons, with additional lifting lugs designed to lift up to 14 tons.

Compressed Air System

After identifying the capacity and pressure requirements, we performed an initial screening to select possible technologies for the compressed air system in our facility. **Fig. 13** shows the results.

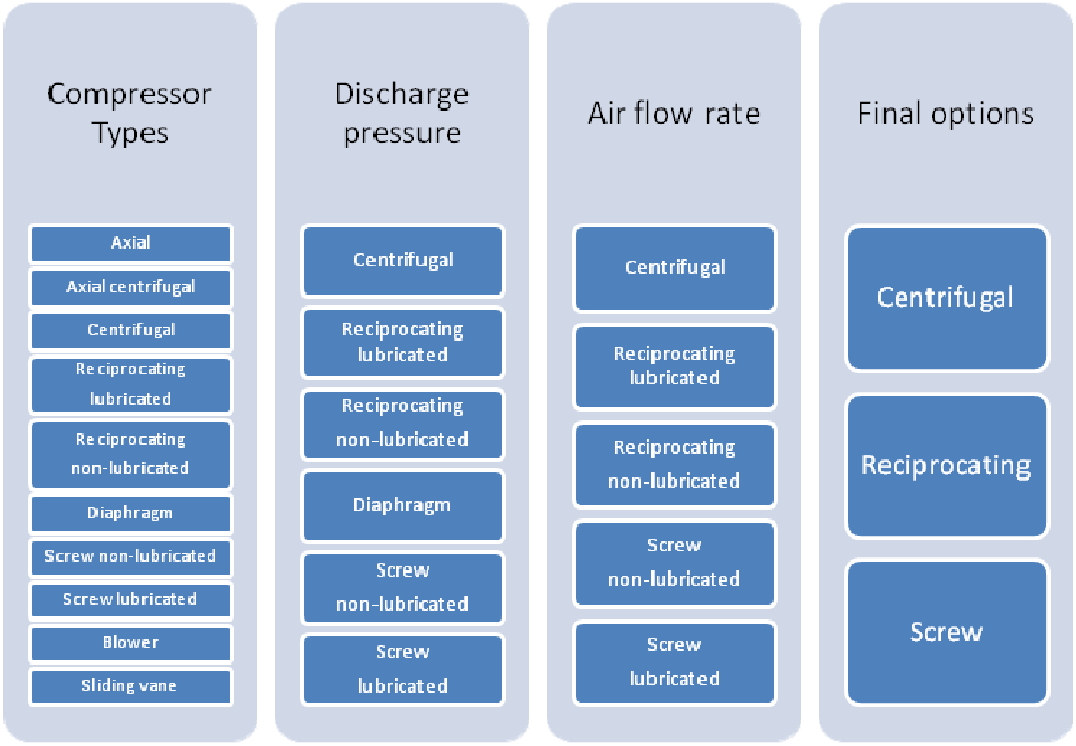

Fig. 13 – Screening of compressor types

According to the literature, air compression is possible using a centrifugal (surge problems might occur with varying flows), reciprocating or screw compressor. However, Snow (2003) showed that a screw compressor by itself is not capable of delivering the discharge pressure required by our system, so one option may be installing a booster to supply the additional increase at the discharge. The proposed solutions are summarized in **Fig. 14**.

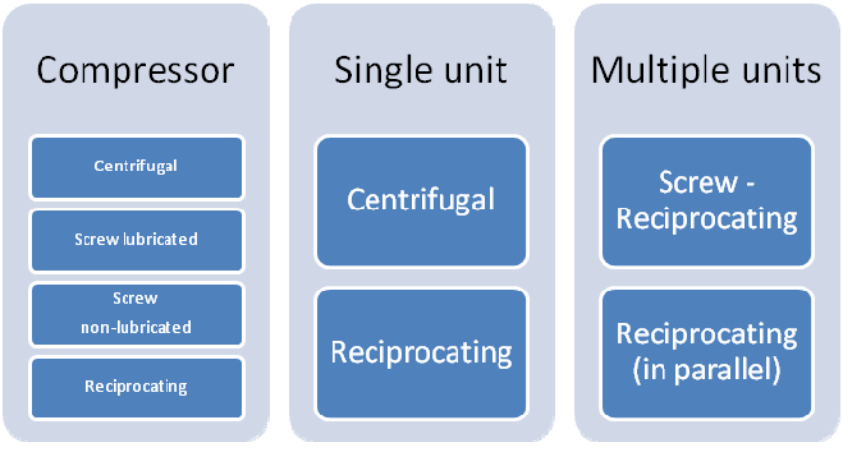

Fig. 14 – Possible solutions for the compressed air system using single or multiple units

The initial approach for this project was to select the appropriate technology (i.e. compressor type) to meet the required operating conditions for the Tower Lab. We contacted 22 manufacturers to get proposals for the facility from which only six qualified in terms of capacity and size. Some of the proposals involved using single or multiple units, all delivering different values of pressure and flow rates within our operating conditions range. **Fig. 15** shows the different combinations.

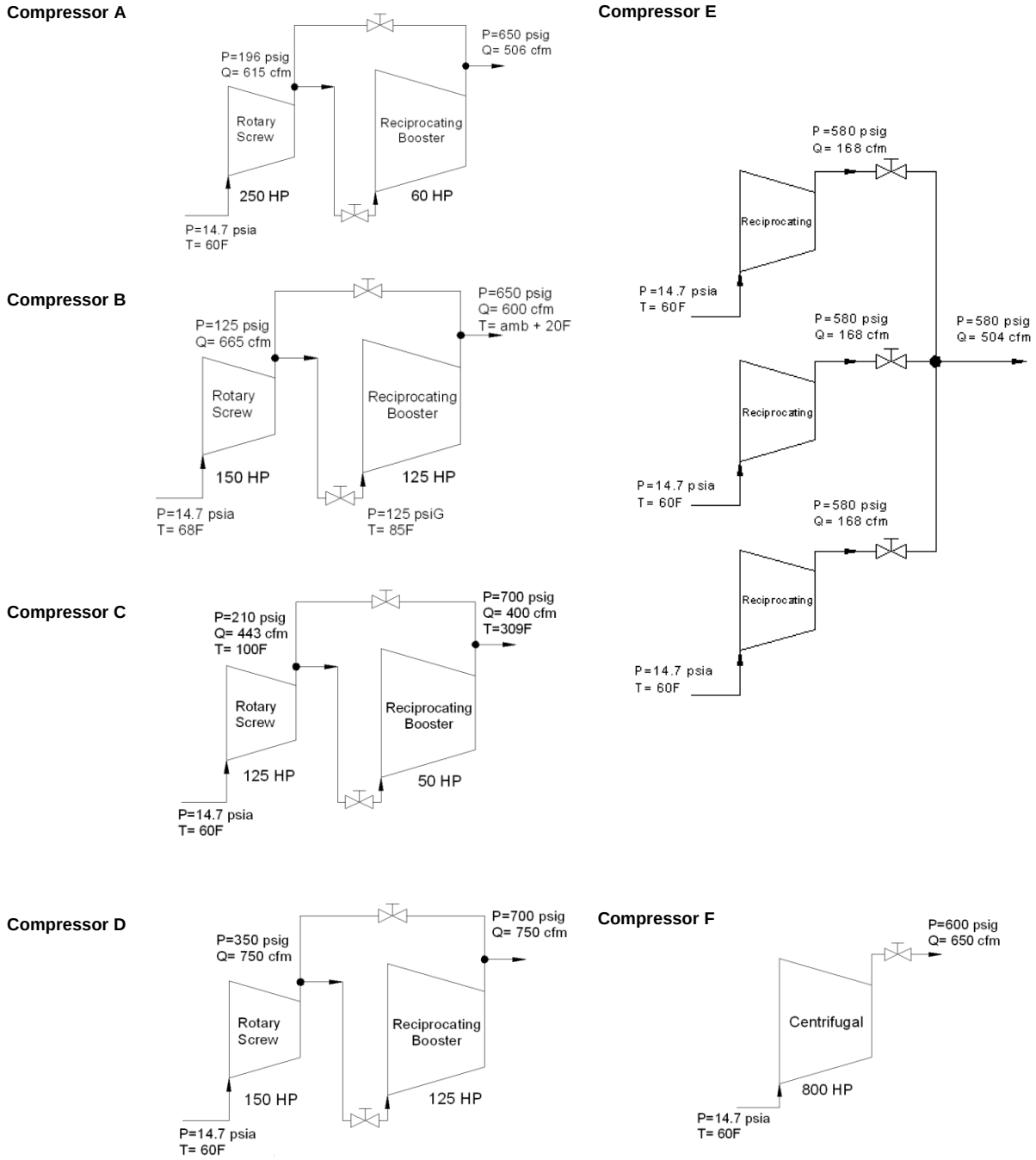

Fig. 15 – Compressor arrangements by different manufacturers

We used a scoring method known as the analytical hierarchy process (Saaty, 1977) to compare not only operating costs but also maintenance, initial and installation costs, footprint, flexibility, foundation requirements and service support (see **Fig. 16**).

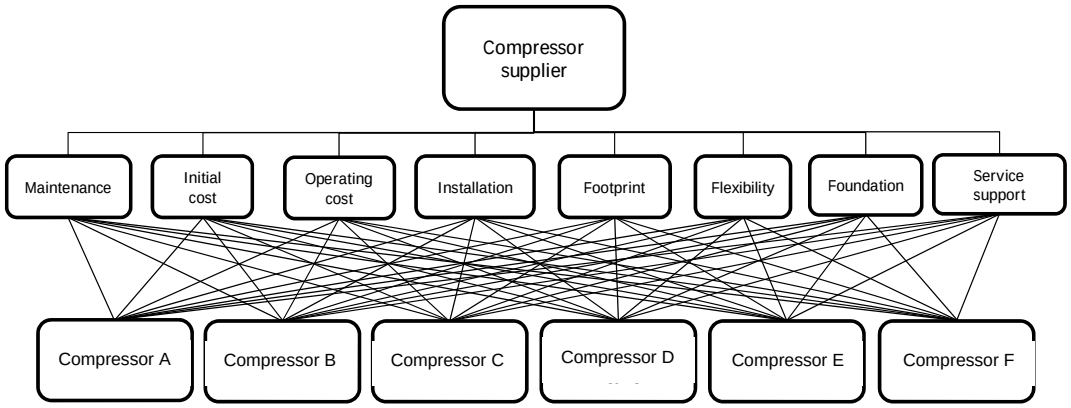

Fig. 16 – Decision hierarchy for choosing a compressed air system supplier

Our analysis showed that Compressor E is the most attractive candidate because of the flexibility of having three units working in parallel, each one providing high pressures and, when powered simultaneously, providing the required flowrate. No special foundations are necessary for the installation of the equipment and the initial operating and maintenance costs are competitive with the other candidates. In addition, the service manufacturers provide adequate support. (**Fig. 17**)

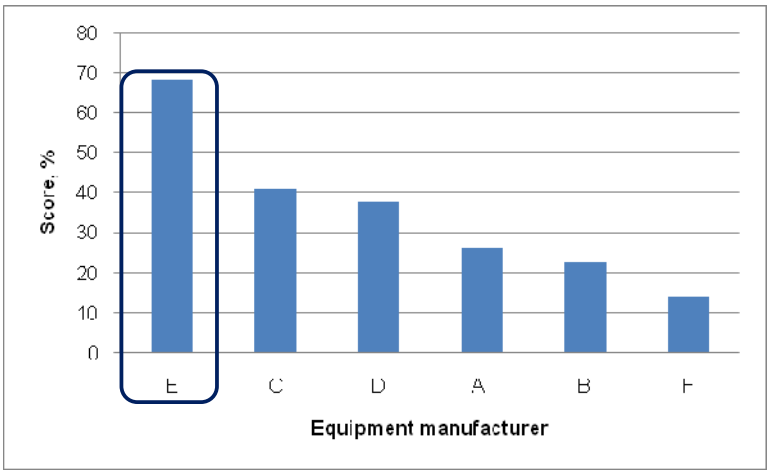

Fig. 17 – Analytic hierarchy process identified Compressor E as the best solution for our facility

Injection Manifold and Piping Design

The manifold is the element in charge of distributing the fluids provided by the compressed air and water systems to the artificial porous medium inside the pressure vessel. It is connected to the container through four equally-spaced entry points to propagate a radial-distributed pressure and flow. During the design phase, we encountered problems as a consequence of the space available to locate the vessel and surrounding it (**Fig. 18**).

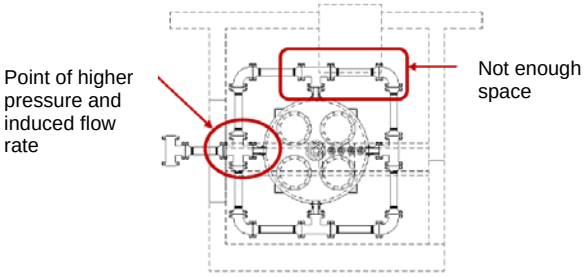

Fig. 18 – Problems with initial design

Alternatively, the options presented in **Fig. 19** allow an adequate installation. Option (a) includes two straight segments of pipe with a circular section, while option (b) has five straight pipes (b), yet both provide uninterrupted flow with lower pressure drops than a system with elbows and tees. However, we need to evaluate the feasibility of their fabrication with pipe

manufacturers.

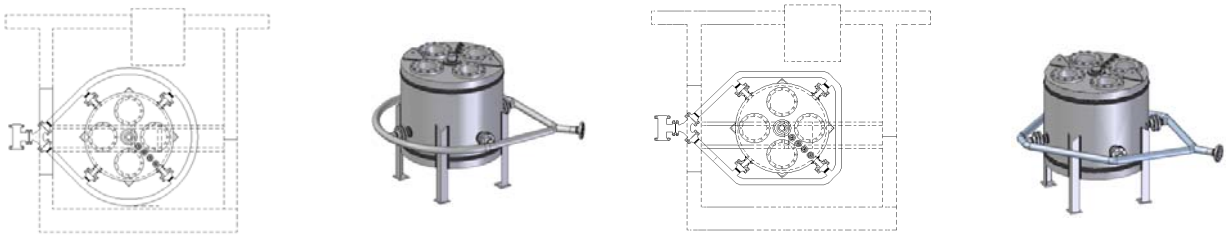

a) **b)**

Fig. 19 – Recommended manifold designs

The injection manifold required selecting an adequate internal diameter for the distribution of both air and water at the entry points. Choosing a line size depends on both pressure drop and flow velocity. The initial design considered a single manifold, but evaluation of the internal diameter, based on the superficial velocities required for both phase,s dictated the need for independent injection. The water and air superficial velocities were obtained from our sensitivity analysis (Solomon and Fernandez, 2007) where parameters such as permeability, tubing size, pressure (at injection points), vessel radius, choke, and water-gas ratio were varied to identify recommended ranges of operation for different scenarios.

Table 5 presents the results for the range in internal diameter required for the water and air pipelines. The difference between sizes for the air and water lines suggested that independent injection, as shown in **Fig. 20,** was necessary to comply with the required superficial velocities. However, to implement a single manifold design, we will need more investigations on how air and water would behave in a shared pipe in order to account for the actual phase distribution in the pipe.

Table 5 – Pipe internal diameter range for air and water

Fluid	Pipe diameter range, in.	
	Min.	Max.
Air	0.532	1.660
Water	2.844	3.030

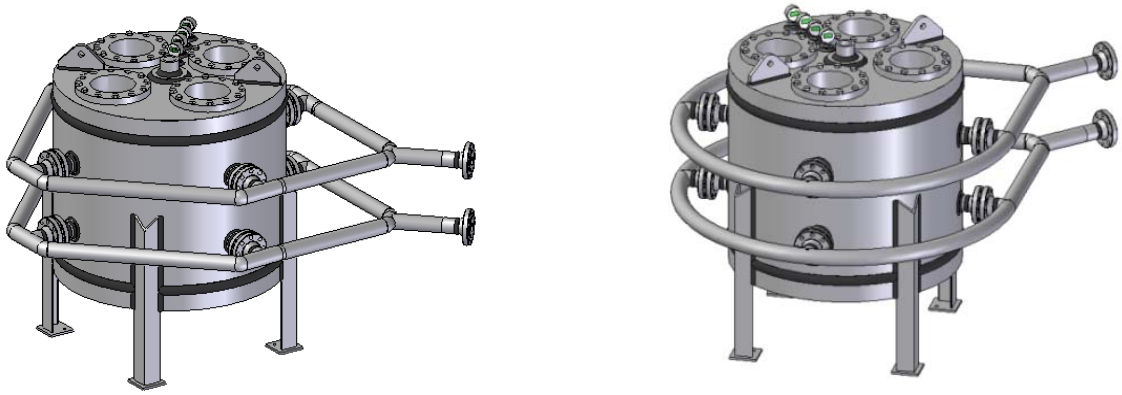

Fig. 20 – Independent injection manifolds for two configurations

We used ANSI B31.3 (2002) to determine the wall thickness of the pipes considering the internal pressure, corrosion and material properties. We selected 1.5 in. and 3 in. nominal pipe size with 1.5 in. and 2.9 in. internal diameter for the air and water lines respectively.

Pressure drops in piping system and manifolds

We calculated pressure drops in the water line system using Darcy's equation Eq. 1. Darcy states that the friction head loss between two points in a completely filled, circular cross section pipe is proportional to the velocity head and the length of pipe and inversely proportional to the pipe diameter.

$$H_L = \frac{fLV^2}{2gd} \quad \text{.....(1)}$$

In most production facility piping systems, the head differences caused by elevation and velocity changes between two points can be neglected. We finally calculated the pressure drop in the water line using equation 2.

$$\Delta p = 11.5 \times 10^{-6} \frac{fLQ_l^2\gamma}{d^5} \quad \text{.....(2)}$$

The estimated distance for the piping network connecting both the compressed air and water system to the pressure vessel is approximately 188 and 190 ft respectively. A schematic of the proposed piping system for water and air flow is depicted in **Fig. 21**.

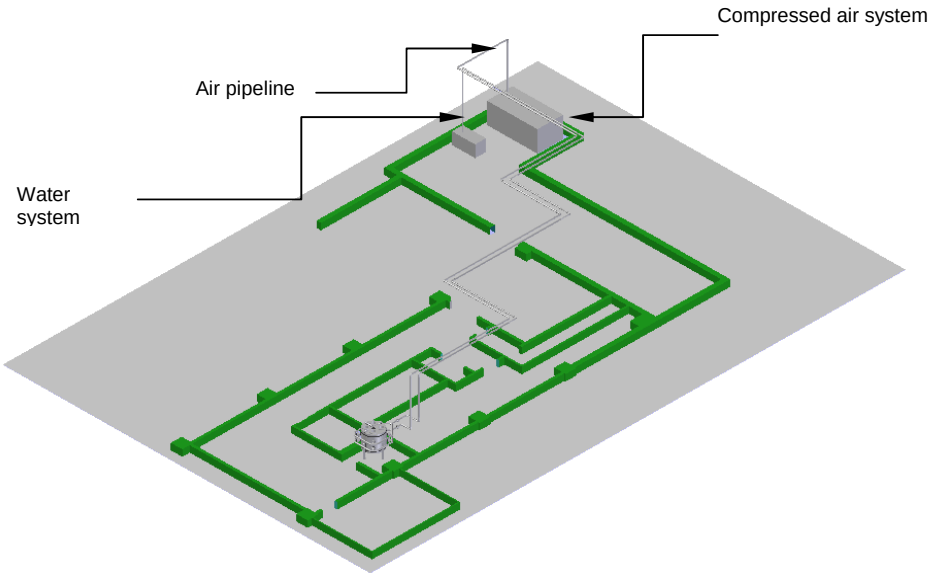

Fig. 21 – Schematic of piping system

Our approach to size the lines was the same as for the manifold. We propose to use 1.5 in. pipe for the two lines allowing for a change equal to 10 times the line diameter of the 3 in. water manifold. The water supply will be provided by a high pressure water pump located in the same area as the compressor (**Fig. 22**).

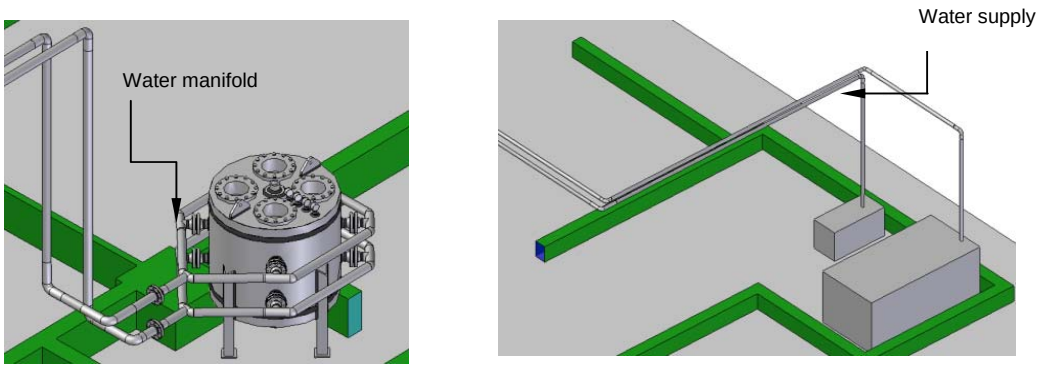

Fig. 22 – Water supply system

For the water line, the total length of straight pipeline is approximately 157 ft, but the minor losses from the installation of 8 long radius elbows increase the total equivalent length to 190 ft. Thus, the total pressure drop in the water line, including the manifold, is ~ 2.6 psi.

For gas pipelines, several empirical equations have been developed, using various coefficients and exponents to account for efficiency and friction factors. We used the Darcy-Weisbach general gas flow equation to calculate pressure drops in the gas line, considering less than a 10% change in the inlet pressure.

$$\Delta p = 12.6\frac{SfLq_g^2ZT}{p_1 d^5} \quad \text{.....(8)}$$

The total length in straight pipes is expected to be 170 ft, increasing to 1885 ft with the installation of long elbows. Additionally, a 1 in. enlargement will be located at the exit of the compressed air system, but the pressure drop at this point can be considered negligible. The final estimated pressure drop is ~ 1.685 psia. (**Fig. 22**)

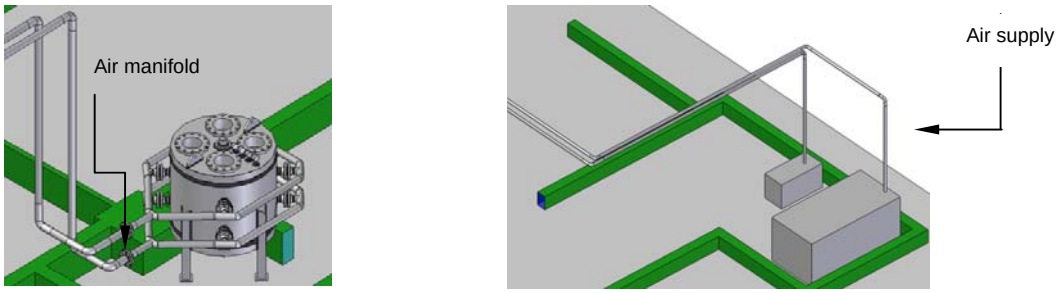

Fig. 23 – Air supply system

Monitoring and Instrumentation – Pressure gauges and Flowmeters

The installation of pressure gauges in a research flow loop is of vital importance, not only to monitor the pressure at which experiments are conducted, but also to evaluate and assess pressure drops in the system and equipment performance. **Table 6** presents the location and number of gauges to be installed at the Tower Lab:

Table 6 – Location and Quantity of Pressure Gauges for Tower Lab

Location	Quantity
Air line prior arrival at injection manifold	1
Entry points of injection manifold	4
Water line prior arrival at injection manifold	1
Top surface of pressure vessel	4

Since the accuracy of most pressure gauges is better in the middle portion of a gauge, the range should be about twice the maximum anticipated pressure. Furthermore, the maximum operating pressure should not exceed 80% of the full pressure range of the gauge. Using the maximum operating pressure of 580 psi given by the Compressor E system, the range for the pressure gauge should be 0 – 1,000 psi. The pressure gauges to be selected for the Tower Lab will be digital, and the accuracy should be at least be 0.25%, but we intend to evaluate the installation of gauges with 0.1 or 0.05% accuracy if costs are comparable. To this end, we reviewed initial costs and accuracy for 0.125 in. socket size, battery charged gauges with capacities from 0-1000 psi and the results are shown in **Fig. 24**.

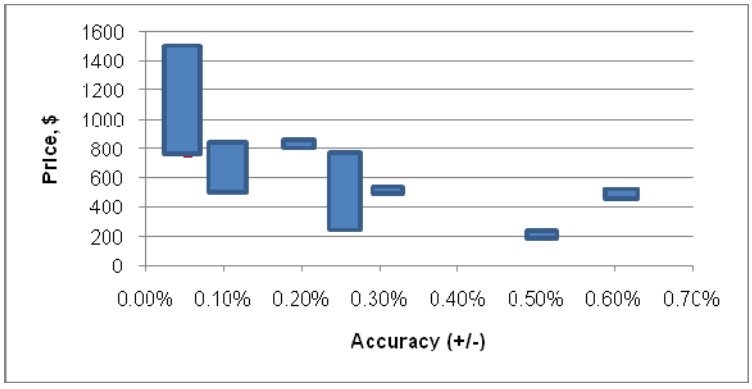

Fig. 24 – Cost of Pressure gauges to be installed at Tower Lab will range from USD 750 to USD 1,500

As expected, the higher the accuracy, the higher the cost, so if we decide to install gauges with 0.05% accuracy we are looking at an initial cost of USD 750 to USD 1,500. In addition, gauges dimensions will be considered due to the limited space

on fittings located on top of the vessel. An example of installation of a model gauge with accuracy of 0.05% on the vessel shows no major issues with space availability is shown in **Fig. 25**.

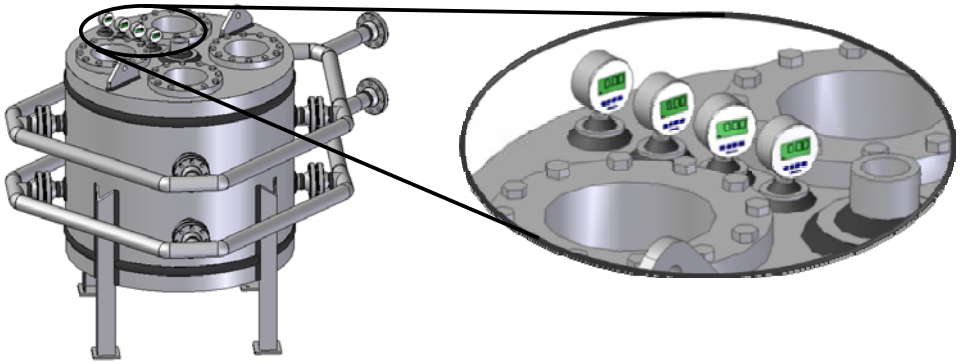

Fig. 25 – Installation of model gauge on pressure vessel

Flow measurement is another "need to know" process parameter besides temperature and pressure, so accurate measurement of both air and water is critical in the operation of a research flow loop. Numerous types of flowmeters are available for closed-piping systems and these can be classified as differential pressure, positive displacement, velocity, and mass meters. Furthermore, they can be grouped into general categories, some of which may overlap with one another, but are still useful in describing some of the factors involved in flowmeter selection. These categories are: I) Flowmeters with wetted moving parts, II) Flowmeters with no wetted parts, III) Obstructionless flowmeters and IV) Flowmeters with sensors mounted external to the pipe.

Flowmeters selection is generally a process of elimination based on technical criteria such as pressure, temperature, specific gravity or density, viscosity and flow range, but specific technologies have been recognized as more appropriate for research facilities. Literature shows a tendency for using coriolis, vortex, and turbine meters. In particular, the coriolis technique has often been described as the near-perfect approach to for gas measurement, but at an average selling price of between USD 5,000 and USD 6,000, it is relativelyI more expensive technology. **Table 7** presents a general comparison between the different technologies used in metering.

Table 7 – Comparison between different flowmeter elements

Flowmeter Element	Recommended Service	Range	Pressure Loss	Typical Accuracy (%)	Relative Cost
Mass (Coriolis)	Clean, dirty viscous liquids; some slurries	10 to 1	Low	±0.4 of rate	High
Mass (Thermal)		10 to 1	Low	±1 of full scale	High
Turbine	Clean, viscous liquids	20 to 1	High	±0.25 of rate	High
Vortex	Clean, dirty liquids	10 to 1	Medium	±1 of rate	High
Electromagnetic	Clean, dirty, viscous conductive liquids and slurries	40 to 1	None	±0.5 of rate	High
Ultrasonic(Doppler)	Dirty, viscous liquids and slurries	10 to 1	None	±5 of full scale	High
Venturi tube	Clean, dirty and viscous liquids; some slurries	4 to 1	Low	±1 of full scale	Medium
Flow nozzle	Clean and dirty liquids	4 to 1	Medium	±1 to ±2 of full scale	Medium
Target meter	Clean, dirty viscous liquids; some slurries	10 to 1	Medium	±1 to ±5 of full scale	Medium
Positive Displacement	Clean, viscous liquids	10 to 1	High	±0.5 of rate	Medium
Pitot tube	Clean liquids	3 to 1	Very low	±3 to ±5 of full scale	Low

Initially, two flowmeters will be required for the air and water lines before the arrival of fluids at the independent manifolds. Regardless of economic issues, we decided to install a coriolis meter for the air line because of its high accuracy and low maintenance; as for the water line, we chose a turbine meter. With a coriolis meter, the estimated cost will be USD 7,000 with pressure drops varying from 0.043 to 13.2 psi, the turbine meter will cost around USD 2,000 with an expected pressure drop of 2 psi.

Conclusions

A new dedicated facility to be located at Texas A&M University will house experimental investigations of liquid loading in gas wells. A technical and economic analysis of the design options considered for the compression and pumping system showed that using a compressor and a water pump is the most feasible option for the Tower Lab.

For the compressed air system, a technical and economic evaluation identified the most attractive candidate as one with three-reciprocating units working in parallel. Each machine provides 580 psig and 168 scf/m and they are conveniently balanced with minimal vibration and low structure and air-borne noise.

The pressure vessel located at the bottom of the vertical section of the tubing was designed not only to minimize costs and weight, but also to facilitate its installation in the laboratory. The vessel will have a top and bottom flat head cover with multiple openings welded to the cylindrical shell body. These openings will allow access to the internal space in the vessel to accommodate glass beads representing the porous medium. The vessel also incorporates eight openings to attach the injection manifolds, fittings to install pressure gauges, and lugs for lifting and installation purposes.

The required superficial velocities for air and water showed the need for independent manifolds to be connected to the pressure vessel. Two options are recommended for the geometry of the device, but costs and ease for fabrication need to be addressed. We chose 3 in. and 1.5 in. schedule 80 for water and air, respectively.

The air and water pipelines were selected based on the superficial velocities required at the entry points at the pressure vessel. They will accommodate different types of fittings, such as long radius elbows and reduction/expansion joints, as well as pressure gauges and flow metering devices. The total pressure drop in the system was estimated to be below 6 psi for both lines including their respective manifolds.

Digital pressure gauges with a minimum range in accuracy from 0.05 to 0.1% are to be installed on the fittings located at the top of the pressure vessel, as well as the eight entry points in the injection manifold. In addition, two flowmeters will measure the flowrate of air and water. The selected metering technologies are coriolis for the air line and turbine for the water line.

Acknowledgments

We would like to express our sincere gratitude to the Crisman Institute at the Harold Vance Department of Petroleum Engineering at Texas A&M University for funding this project.

Nomenclature

d	=	Pipe internal diameter, in
f	=	Moody friction factor, dimensionless
g	=	Gravitation constant, ft/s^2
H_L	=	Friction head loss, ft
L	=	Length of pipe, ft
p	=	Internal pipe pressure, psi
p_1	=	Upstream internal pipe pressure, psia
Δp	=	Pressure drop, psi (liquid) psia (gas)
Q_g	=	Gas flow rate, MMscf/d
Q_l	=	Liquid flow rate, bpd
S	=	Allowable stress for pipe material, psi
T	=	Flowing temperature, ^{o}R
V	=	Velocity, ft/s
Z	=	Compressibility factor for gas, dimensionless
γ	=	Specific gravity, dimensionless

References

1. Alshuraiqui, H., Grattoni, C., and Muggeridge. A: 2003 Laboratory and Numerical Studies of First Contact Miscible WAG Displacement: The Effects of WAG Ratio and Flowrate. Paper presented at the 12th European Symposium on Improved Oil Recovery, Kazan, Russia, 8-10 September.
2. American Society of Mechanical Engineers, Boiler and Pressure Vessel Code, ASME, Section VIII. 2007: *Rules for Construction of Pressure Vessels*, Division 1, New York. 15-364.
3. American Society of Mechanical Engineers. 2004. *Chemical Plant and Petroleum Refinery Piping.* New York.
4. Coleman, S., Clay, H., McCurdy, D., and Norris, L. III. 1991: Understanding Gas-Well Load-Up Behavior. Paper SPE 20281, *JPT*.
5. Coleman, S. and McCurdy D.: "A New Look at Predicting Gas-Well Load-Up," paper SPE 20280, *JPT* March 1991.
6. Costantini, A. 2005: Dynamic Interaction Between the Resevoir and the Well During Well Testing, Dip. Ing. thesis, University La Sapienza of Rome and Imperial College.
7. Corteville, J., Grouvel, M., and Lagiere, M. 1983: Experimentation des Ecoulements Diphasiques en Conduuites Petrolieres: Boucles d'essais de Boussens," *Revue de l'Institute Francaise du Petrole.* 38 **:** 143-151.
8. Dousi, N., Veeken, C.A.M., and Currie P.K. 2005: Modeling the Gas Well Liquid Loading Process. Paper SPE 95282-MS presented at the Offshore Europe Conference, Aberdeen, 6-9 September.
9. Falcone, G., Teodoriu, C., Reinicke, K., and Bello, O. 2007: Multiphase Flow Modeling Based on Experimental Testing: A Comprehensive Overview of Research Facilities Worldwide and the Need for Future Developments. Paper SPE 110116 presented at the SPE Annual Technical Conference and Exhibition, Anaheim, California, 11-14, November.
10. Falcone, G., Hewitt, G., and Richardson, L. 2003: ANUMET: A Novel Wet Gas Flowmeter. Paper SPE 84504-MS presented at the SPE Annual Technical Conference and Exhibition, Denver, Colorado, 5-8 October.
11. Gool, F., and Currie, P. 2007: An Improved Model for the Liquid Loading Process in Gas Wells. Paper SPE 106699-MS presented at the Production Operations Symposium. Oklahoma City, Oklahoma, March 31 – April 3.
12. Guo, B., Ghalambor, A., and Xu, C. 2005: A Systematic Approach to Predicting Liquid Loading in Gas Wells. Paper SPE 94081-MS presented at the SPE Production Operations Symposium. Oklahoma City, Oklahoma, 17-19.

13. Hart, R. 2007. http://www.swri.org/4org/d18/mechflu/fluiddyn/pdfs/flowloop.pdf. November 2007.
14. Kegel, T., and Kinney, J.: "Wet Gas Metering Facility at CEESI," Nunn, Colorado, Internal Report.
15. Langsholt, M. 2007. http://www.ife.no/laboratories/well_flow_loop/index_html-en/view. November 2007.
16. Lea, J.F., Nickens, H.V., and Wells, M.: *Gas Well De-Liquefaction*, first edition, Elsevier Press, Cambridge, MA (2003).
17. Neves, T. and Brimhall R.: "Elimination of Liquid Loading in Low-Productivity Gas Wells," paper SPE 18833 presented at the SPE Production Operations Symposium held in Oklahoma City, Oklahoma, 13-14 March 1989.
18. Robole, B., Kvandal, H. And Chuller, R.: "The Norsk Hydro Multiphase Flow Loop. A high pressure flow loop for real three-phase hydrocarbon systems," *Flow Measurement and Instrumentation* **17** (2006) 163-170.
19. Saaty, T.: "A Scaling Method for Priorities in Hierarchical Structures," Journal of Mathematical Psychology, 15, 234-281 (1977).
20. Sintef. 2007. http://www.sintef.no/Home/Petroleum-and-Energy/SINTEF-Petroleum-Research/Wellstream-Technology/Laboratories/. November 2007.
21. Snow, D.: *Plant Engineer's Reference Book*, Elsevier, Second Edition, Burlington, Massachusetts (2003), 26.
22. Solomon, F. and Fernandez, J.: "Design and Construction of a Dedicated Facility for the Experimental Study of Liquid Loading in Gas Wells," Interim report for the Crisman Institute, College Station, Texas, 5, November 2007.
23. Stephenson, G., Rouen, R., and Rosenzweig, M.: "Gas-Well Dewatering: A Coordinated Approach," paper SPE 58984 presented at the International Petroleum Conference and Exhibition held in Villahermosa, Mexico, 1-3 February 2000.
24. Toma, P., Vargas, E. and Kuru, E.: "Predicting Slug to Annular Flow Pattern Transitions for Reducing Risks of Gas Lift Instabilities and Effective Gas/Liquid Transport from Low Pressure Reservoirs," paper SPE 100615 presented at the Gas Technology Symposium held in Calgary, Alberta, Canada 15-17 May 2006.
25. Turner, R., Hubbard, M. and Dukler A.: "Analysis and Prediction of Minimum Flow Rate for the Continuous Removal of Liquids from Gas Wells," paper 2198, *JPT*, November 1969.
26. TUV NEL. 2008. http://www.tuvnel.com/content/pdfs/wet_gas_facility.pdf. November 2007.
27. Unander, T. E. Sintef. 2007. http://www.sintef.no/Home/Petroleum-and-Energy/SINTEF-Petroleum-Research/Wellstream-Technology/Laboratories/
28. Vilagines, R. and Hall, A. "A comparative Behavior of Multiphase Flowmeter Test Facilities," *Oil and Gas Science and Technology* – Rev. IFP, (2003) **58**, No.6, 647-657.
29. Yamamoto, H. and Christiansen R.: "Enhancing Liquid Lift from Low Pressure Gas Reservoirs," paper SPE 55625 presented at the Rocky Mountain Regional Meeting held in Gillette, Wyoming 15-18 May 1999.

Particle Holdup Profiles in Horizontal Gas-liquid-solid Multiphase Flow Pipeline

By *Oladele O. Bello*,* *Kurt M. Reinicke*, and *Catalin Teodoriu*

Sand holdup is one of the most important hydrodynamic parameters that is needed for performance estimation, design, operation and control of oil-gas-sand multiphase production and pipeline transportation systems. The performance of oil-gas-sand multiphase flow can be reliably evaluated by measuring the sand holdup in such oil-gas-sand multiphase production and pipeline transportation systems. In the present work, a local sand holdup has been measured under conditions analogous to the horizontal oil-gas-sand three-phase slug flow in pipelines. Accurate local sand particle holdup measurements were performed by the digital imaging technique. The results revealed the influence of operating conditions such as gas and liquid velocities and sand particle loading on the distribution of the local sand particle holdup in the horizontal air-water-sand multiphase slug flow pipe. Explanations for the observed trends are provided, shedding light on the general structures and mechanisms of the distribution of the local sand holdup in a horizontal oil-gas-sand three-phase slug flow. Such information on the horizontal air-water-sand three-phase slug flow mechanisms are essential to advance the mechanistic approach for predicting local sand holdup distribution and the subsequent effect on sand deposition during multiphase petroleum production and transfer operations.

1 Introduction

Gas-liquid-solid multiphase production and pipeline transportation has become a key technological feature of producing oil and gas reserves contained in unconsolidated formations and situated in deep water and marginal fields [1–7]. Local sand holdup is one of the most important hydrodynamic characteristics that is needed for the performance estimation, design, and detailed analysis of the oil-gas-sand multiphase flow and pipeline transportation systems.

A scrutinizing look at the literature with regards to gas-liquid-solid multiphase flows shows a scanty interest by the researchers. Most of the reported investigations have been mainly focused on measurement of pressure drops and sand transport rate, which is independent of flow patterns [8–17]. The team of Stevenson and Thorpe [18–24] conducted detailed studies on solid particle behavior in gas-liquid-solid three phase flows at low particle loading in intermittent and stratified flow through horizontal and near horizontal pipes. A high-speed video system was used for flow visualization of suspended and entrained sand particle dynamics in gas-liquid-solid intermittent and stratified flows. The time-averaged sand particle velocities were measured using a visual particle tracking technique. Empirical models were developed to predict sand particle velocities in the slug and stratified flows. The models seem to give acceptable results when compared to experimental and hydraulic conveying data. Criteria to determine the average sand holdup were also proposed. However, these measurements were limited because the local sand holdup in a gas-liquid-solid three-phase flow were neither studied nor measured.

Sakaguchi et al. [25–29] carried out detailed studies on production of manganese nodules from the seabed to the floating ship using vertical pipes of different sizes. Both bubble and slug gas-liquid-solid three-phase flows were investigated. They measured axial large bubble and solid particle rising velocities using a high-speed video system, but only average values of the velocities were reported. Information on the velocity profiles of the solid phase was not presented. The holdup of gas, liquid and solid phase was measured according to the quick-closing value method. Four valves were used to trap the heights of the solid particles and water in the test section. This invasive method suffers from its inability to be applied to a continuous gas-liquid-solid multiphase system coupled with the fact that these studies only report on an average solid holdup.

In order to design the oil-gas-sand multiphase flow and pipeline transportation systems on a rational basis, it would be highly desirable to know the local values of the sand holdup and how these change with operating conditions. With this information and the local particle velocity distribution, the mass flux can be estimated at different locations in multiphase pipelines, the local rate of sand deposition buildup can be predicted, and in turn the pressure drop and overall performance of oil-gas-sand multiphase pipeline transportation systems can be estimated. Local sand holdup in gas-liquid-solid multiphase slug flow systems analogous to multiphase petroleum production and transfer operations has not been reported in the open literature. The absence of information in literature dealing with the measurement of local sand holdup profiles in a gas-liquid-solid multiphase pipeline system, suggests the need for laboratory measurements with a reliable technique to capture and analyze local sand holdup distributions in the multiphase pipeline system. De-

[*] Dipl.-Ing. O. O. Bello (booladele@spemail.org), Dr.-Ing. K. M. Reinicke, Dr.-Ing. C. Teodoriu, Institute of Petroleum Engineering, Technische Universität Clausthal, Agricolastraße 10, D-38678 Clausthal-Zellerfeld, Germany.

  DOI: 10.1002/ceat.200500195

velopment and application of non-invasive digital imaging technique capable of measuring local sand holdup distributions in horizontal multiphase flows through pipelines will greatly facilitate current efforts to predict and improve oil-gas-sand multiphase production and pipeline transport systems.

Digital imaging technique is an established method for multiphase flow visualization and analysis [30–36]. It has the advantage over the existing methods of solid phase holdup measurements because of its non-invasive character. The fast response of the technique justifies its likely application to multiphase process control. Hence, development of a non-intrusive measuring technique, which can provide good information about the solid phase flow structure and holdup profiles appears to be essential to advance a mechanistic and hydrodynamic approach to sand transport phenomena in multiphase production and pipeline transportation. These experimental results can be used as a basis for comparison with the prediction using existing three-phase solid phase holdup models. The sand holdup profiles also provide a good basis for comparison with the performance of multiphase petroleum pipeline transportation systems and may allow improving operations, safety and reducing capital cost.

Oil and gas mixtures from several wells are often transported long distances to a processing platform. In these multiphase pipelines, several flow regimes exist including stratified, slug and annular flow as shown in Fig. 1. Most commercial multiphase pipelines running over long distances operate at high throughputs and, hence, hydrodynamically turbulent slug flow conditions. High turbulence and mixing vortex in slug flow have been extensively reported in the literature [37–38]. The aim of the present work was to employ digital imaging technique for the measurement of the local sand holdup in a gas-liquid-solid three-phase slug flow. The effects of the gas and liquid superficial velocities and sand particle loading on the local sand holdup profiles were also investigated and discussed.

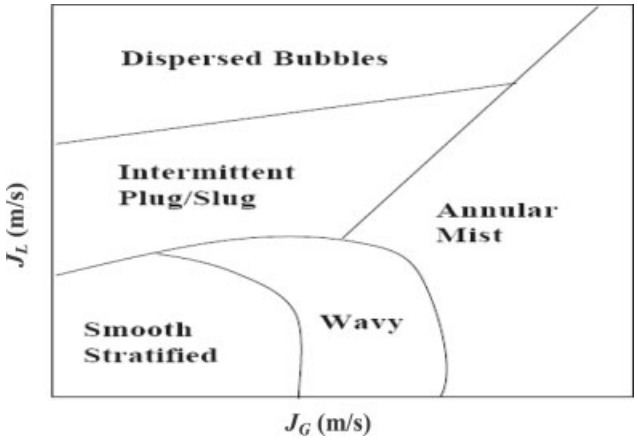

Figure 1. A typical flow regime map for gas-liquid two-phase flow in horizontal pipes [36].

2 Experimental

2.1 Loop Design

Gas-liquid-solid three-phase flow tests were performed in a 40 mm internal diameter (ID) plexiglass pipe fed concurrently with air, water, and sand. The facility (see Fig. 2) consisted of a 6.0 m long inclinable bench, the slope of which can be varied continuously between horizontal and vertical sections by means of a motorized support. The test section is a transparent plexiglass pipe of 40 mm internal diameter and 6.5 m length. The pipe was made of carefully flanged, 2 m long, interchangeable sections mounted on the bench by precision supports.

Measurements were performed at a distance of 5 m from the test section inlet, to avoid entrance effects and to assure a stabilized flow. At the measuring station the pipe was surrounded by a rectangular opaque paper box in order to reduce image distortion. Water, oil-free air, and sand are used as liquid, gas and solid phases, respectively. The water was supplied by a 6.0 KW stainless steel centrifugal slurry pump from a 0.4 m^3 stainless steel slurry tank into a 25 mm ID stainless steel pipe, where its flow rate was measured using an electromagnetic induction flow meter. The flow rate of the water was controlled by the rotational speed of the centrifugal pump. Air from the compressor was fed to the mixing chamber through the cooler, filter, the regulating valve, and the porous pipe. The flow rate of the air was measured by an orifice meter and controlled by a regulating valve.

The solid phase used is black sand particles supplied by Erich Friedrich Handel GmbH, Germany, with a normal mean diameter of 0.6 mm and a density of 2600 kg/m^3. The sand particles in the hopper are supplied to the water tank by an electromagnetic feeder and then fed with water into the test section by the centrifugal pump. The particle loading of the sand was controlled by the vibration frequency of the electromagnetic feeder. The sand loadings were determined by sampling. The loop was sampled several times during the gas-liquid-solid slug flow experiments to determine the concentration of particles suspended in the water. Samples of transported sand particles were collected by discharging the air-water-sand mixture into a calibrated collecting tube through a three-way valve. When the three-way valve was opened, an air-water-sand mixture was discharged into the collecting tube. Previous tests on dredging pipelines [39] suggested that a sample collected this way would realistically represent all fractions in transported solids. The discharged solid particles collected were measured by a weighing scale, after the discharged wet particles were dried using a hot air-dryer. In addition, the discharged water was measured by a graduated cylinder and the sand particle loading was determined. The uncertainties of the sand particle loading measurement are within ± 0.002 kg/m^3.

The air, water and sand mixture introduced was allowed to flow into the 0.04 m × 6.5 m transparent plexiglass test pipe. The mixture flows back into the slurry tank and the air vented

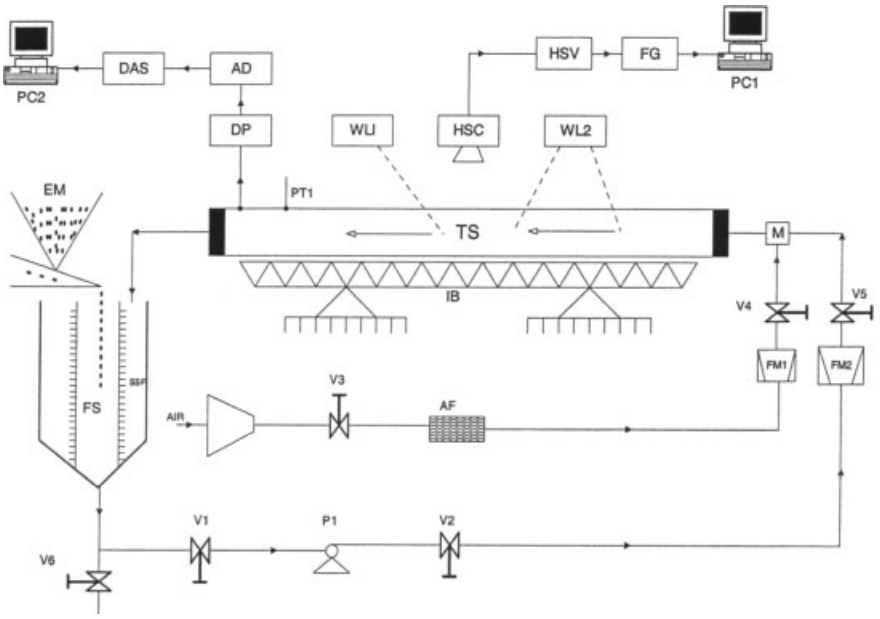

Figure 2. Schematic diagram of the experimental setup. EM: Electromagnetic feeder; FS: Feed slurry tank; SSF: Sand screen filter; FM1: Flow meter (gas) ; FM2: Flow meter (liquid); IB: Inclinable bench; V1: Slurry valve 1; V2: Slurry valve 2; V3: Gas valve 1; V4: Gas valve 2; V5: Gas valve 3; M: Gas-slurry mixer; PI: Pump; C: Compressor; V6: Discharge valve; AF: Air filter; TS: Test section; PT: Pressure taps; DP: Differential pressure transducer; AD: AID Converter; DB: Data acquisition system; WL1: White light illumination; WL2: White light illumination; HSC: High-speed camera; HSV: High-speed video system; FG: Frame grabber; PC1: Personal computer for imaging acquisition; PC2: Personal computer for differential pressure fluctuation acquisition.

to the atmosphere. The sand particles were separated from the water by means of a sand screen filter and the water recirculated into the system. Nine pressure taps were installed on the test pipe to measure the static and dynamic pressure distributions along the test section. Tab. 1 gives the range of the experimental conditions investigated in this study.

2.2 Digital Image Measurement and Visualization System

Images on the gas-liquid-solid three phase slug flows were captured using a VDS Vosskühler high-speed CMOS HCC-1000 camera with a mega pixel resolution and features for high-speed motion analysis. The VDS Vosskühler system consists of a high-speed camera, full size single slot HCC camera control and frame storage, user interface, and easy to use analysis software. An image resolution of 1024 × 512 was used, which allows the features of gas-liquid-solid slug flow to be viewed and to obtain detailed data regarding the sand particle flow structure and holdup characteristics in the three-phase slug flow. The test pipe was illuminated by a 1000 Watt fluorescent lamp. The high speed camera was mounted and fixed at a right angle to the flow. The camera

Table 1. Experimental conditions employed during the experiments.

pipe diameter (m)	0.04
pipe length (m)	6.50
pipe configuration	horizontal
particle size range (mm)	0.60–0.80
particle mean diameter (mm)	0.60
particle density (kg/m^3)	2600
particle loading (kg/m^3)	0.10–0.80
terminal particle settling velocity (m/s)	0.09
hindered particle settling velocity (m/s)	0.14
particle Reynolds number	84.00
particle response time (dimensionless)	23.00
water density (kg/m^3)	998
water kinematic viscosity ($1 \cdot 10^{-6}$ m^2/s)	1.02
superficial gas velocity (m/s)	0.40–1.60
superficial liquid velocity (m/s)	0.50–1.50
gas kinematic viscosity ($1 \cdot 10^{-6}$ m^2/s)	15.10
water surface tension (N/m)	0.070

high buffer memory allowed 128 images to be obtained in each second. The films were recorded in the grey format and the video signal from the CMOS camera was sent to a 17 inches high resolution computer monitor. This allowed direct viewing of the image quality and enhancement. All image analysis was performed on digital video of water-air-sand slugs due to the need for high-resolution, clear images that would lend themselves to this type of analysis.

For calibration purpose, a graph paper was also recorded with each video film. This allowed the pixel coordinates obtained from subsequent image analysis to be converted to centimetres. In this manner, all screen resolutions (magnification) in the video could be scaled to real-world values. The camera lens produces a magnification factor of approximately 37. Some images were recorded covering two minutes to obtain transient information on sand particles velocity and holdup distribution profiles. The features of the high-speed video recording camera system used are given in Tab. 2.

2.3 Digital Image Analysis

The analysis of the sand particle flow structure and of their characteristics in the air-water-sand three-phase slug flow requires quantitative local sand particle holdup distribution data. Extraction of these data from the digital images was done manually in most of the cases, although an automatic particle counting algorithm provided by VDS Vosskühler software was used in some cases.

Measurement of Sand Holdup Profile

No information regarding the sand holdup distribution in moving gas-liquid-solid slug flow is currently available. Hence, a detailed particle holdup profile across the cross section of the pipe throughout the slug unit was generated using a grid system. To accurately analyze the local sand particle holdup in the horizontal air-water-sand three-phase slug flow, a two-dimensional mesh was created, as shown in Fig. 3 and superimposed on the three-phase slug flow image.

Since most of the sand particles are approximately spherical, the volumes of sand particles in each section were calculated using the formula for the volume of a sphere multiplied with the counted numbers of solid particles in that section of the pipe. Next, the volume of each section of the grid was calculated. The sand holdup of any section of

Table 2. Features of the VDS Vosskühler high-speed CMOS HCC-1000 system used.

image resolution	up to 1024×1024
frame rate	923 fps
number of images	128 images
pixel size	$10 \cdot 10^{-6}$ m $\times$ $10 \cdot 10^{-6}$ m
active sensor size	2.56 (H) mm $\times$ 2.56 (V) mm
sensor array	linear CMOS-sensor
memory	512 Mbytes
shutter	global electronic shutter with exposure time from 2 ms
particle	pixel coordinates of the particle position are always displayed on the screen
digital output	8-bit (mono)
computer control	RS-232 interface
output frame rate	up to 4000 frames per second
output pixel clock	33 MHz
power supply	12 V DC, 500 mA
playback rates	user selectable variable playback
lens mount	standard C-mount
camera control software	matrix vision frame grabber
images recording file format	bmp, jpeg, tif, and avi
analysis features	Microsoft excel compatible features include linear and angular velocity measurement. Track multiple points over multiple frames.

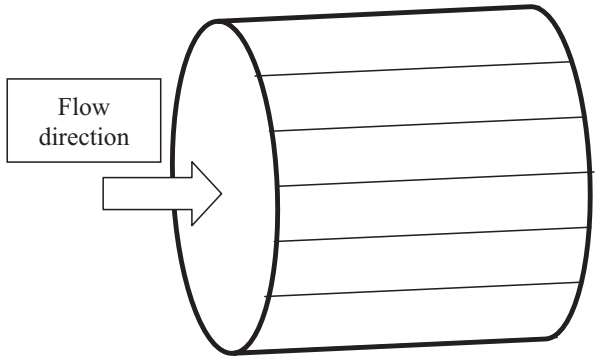

Figure 3. Two-dimensional view of the 6-section mesh drawn over the pipe for image analysis.

the pipe at height h from the bottom can be calculated as follows:[1)]

$$E_s = \frac{V_s}{V_g} \tag{1}$$

$$V_s = \frac{\pi}{6} \cdot d_p^3 \cdot N \tag{2}$$

$$V_g = d_x A \tag{3}$$

$$A = \frac{D^2}{4} \cdot \left[\pi - \cos^{-1}(2 \cdot \bar{h} - 1) + (2 \cdot \bar{h} - 1) \cdot \sqrt{1 - (2 \cdot \bar{h} - 1)^2}\right] \tag{4}$$

The face area of section 1 at height h_1 and the cumulative areas of sections 1 and 2 (height h_2) can be calculated using Eq. (4). The area of section 2 is then obtained by subtracting the area of section 1 from the cumulative area. The areas of all the six sections of the grid can be obtained in this manner. The volume of each section is then given by the product of its area and the length of the image. Knowing the volume of each section of the grid and the solid particle volume in each section, the sand holdup profile can be calculated: The average sand holdup is then simply the ratio of the total sand volume and the total volume of the cylindrical grid.

3 Results and Discussion

3.1 Visual Observations

Sand particle characteristics in the pipeline are investigated by direct visualization of the local flow behavior in the air-water-sand three-phase slug flow regime. An example of the images used for the analysis is given in Fig. 4. Three types of interactions have been suggested for the flow visualization of sand particles moving in a gas-liquid slug flow through a pipe: a sand particle interacting with gas bubbles, other sand particles, or a slug turbulent flow structure. The latter can be a direct momentum transfer or an additional momentum transfer with the liquid phase resulting from a velocity gradient generated by the motion of the gas bubbles and the slug motion.

Figure 4. Images showing sand particle distribution characteristics in air-water two-phase slug flow at d = 0.60 mm, J_g = 0.6 m/s, and J_L = 1.0 m/s (e_s = 0.03, 0.05, 0.07, 0.09, 0.2, and 0.35 kg/m^3 for image (a) to (f), respectively).

The first and second mechanisms were indicated by the observed change in the local velocity of the sand particle after collision with gas bubbles or other particles. The third mechanism can be described as a lifting of sand particles due to the mixing process related to gas bubbles and the vortex motion of the slug. The collision of gas bubbles with gas bubbles and sand particles was observed regularly. This collision changes the trajectory of the sand particles to the right and left. The number of gas bubbles which moved towards the axial part of the pipe is great because of the effect of buoyancy forces. This tends to reduce the thickness of the boundary layer and reduces the settling velocities of the suspended sand particles flowing near the axis of the pipe. This is a well recognized phenomenon observed among previous investigators [25, 31].

At the tail end of the Taylor bubble or the liquid slug nose, violent mixing and eddies were observed leading to a generation of vortices. These vortices create a pumping effect, which produces ejection of low-momentum fluid away from the wall on one side of the vortex and in-rush of high-momentum fluid towards the wall on the other side. The vor-

1) List of symbols at the end of the paper.

tices rotate around the axis of the sand particles and according to this rotating motion, the sand particles also rotate. The pumping effect also strongly influences the sand particle distribution in the air-water-sand slug flow.

3.2 Local Instantaneous Sand Holdup Profiles

The non-invasive nature of the digital image analysis technique permits continuous recording of sand holdup profiles in the air-water-sand three-phase slug flow, without disturbing the operation. The instantaneous local sand holdup in the air-water-sand three-phase slug flow for different superficial gas velocities shows rapid fluctuations. Axial profiles of the dynamic response of the sand holdup for different superficial gas velocities at a constant superficial liquid velocity and sand loading values is shown in Fig. 5. For the 0.505 and 0.606 ms^{-1} gas velocities, the profiles are w-shaped, the sand holdup being highest at the walls and with a peak at the center. Another important feature of Fig. 5 is the sudden increase in the sand holdup value observed particularly at the h/D 0.4 location. It is seen that the sand holdup profile increases in a non-linear manner across the sections of the pipe. The following general observations were made:

- Depending on the superficial gas velocities, the cross-sectional variation is quite large; the difference in the local sand holdup can be about 25 %.
- The profiles do change significantly with respect to location. These data are suitable for analyzing the dynamic variations of the sand holdup in the air-water-sand three-phase slug flow.

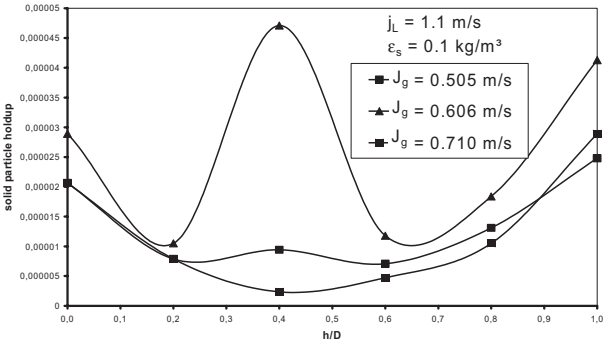

Figure 5. Effect of superficial gas velocity on axial distribution of sand holdup.

Fig. 6 also shows the dynamic response of the sand holdup to changes in superficial liquid velocity. Three superficial liquid velocities were compared at different values. The variation of sand holdup in distance is not uniform for all the superficial liquid velocities values investigated. Fig. 6 also shows that the smaller superficial liquid velocity gave a slightly higher sand holdup.

Fig. 7 shows the dependence of the sand holdup from the sand loading. At sand loadings of 0.3 and 0.4 kg/m^3, the sand

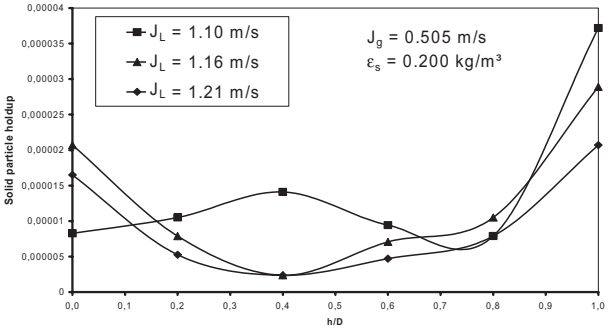

Figure 6. Effect of superficial liquid velocity on axial distribution of sand holdup.

holdup in the air-water-sand three-phase slug flow was lowered compared to the sand loading at 0.10. Fig. 7 illustrates the complex interaction between the sand loading and all other parameters. The increase in percentage of the local sand holdup is caused by the slip velocity between the sand and the liquid phase of the multiphase mixtures and the increase rate of particle-particle collision. This observation has been noted experimentally by several researchers [26, 28, 29]. The capability to observe these strong non-uniformities in sand holdup profiles permits one to develop a more rigorous definition of the onset of deposition, which requires knowledge of the distributed nature of the sand holdup profile.

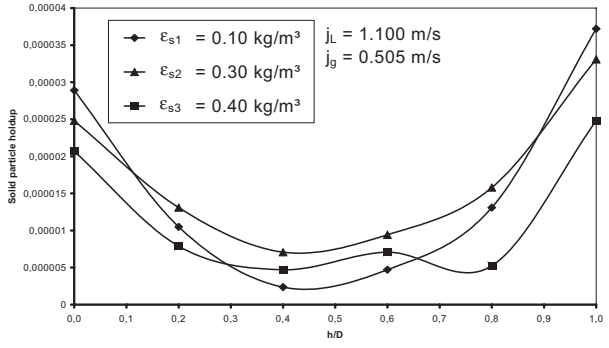

Figure 7. Effect of sand loading on axial distribution of sand holdup.

3.3 Local Mean Sand Holdup Profiles

Fig. 8 presents the local time-mean sand holdup as a function of superficial gas velocity for different axial positions. In every case, the sand holdup profile decreases with increasing superficial gas velocity across the entire cross-section of the pipe. The sand holdup profile equals the volumetric fraction of the solid phase found by Sakaguchi et al. [25], Sakaguchi et al. [28], and Minagawa and Sakaguchi [30] who reported averaged overall solid phase volumetric fractions. The trend observed can be attributed to the passage of the successive long Taylor bubble wake, which is highly tur-

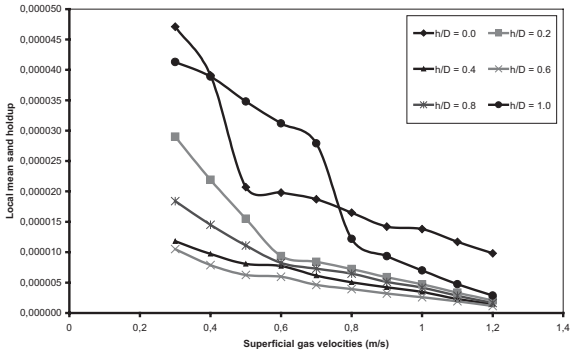

Figure 8. Local mean sand holdup at different superficial gas velocities and different axial positions in the slug flow.

bulent with an intense mixing. The bubble wake has been identified as a major factor in such phenomena as solids mixing by previous investigators [40–41]. The slug flow, being an efficient flow enhancer improves the flow structure of the solid phase and, thereby, reduces the amount of sand particle that is held up in the boundary layer of the pipe wall. An increase in axial variation of the sand holdup reduces the average sand holdup.

A comparison of the Figs. 5–8 appears to indicate that the transient sand flow structures are significantly different from the sand phase structure observed in the local time-averaged flow measurement. It was seen that for any instantaneous flow field, a significant position portion of the air-water-sand slug flow has much larger velocities than those observed for the time-averaged flow field. This observation compliments the computational results of Bernard and Fitremann [42], which showed that the solid and liquid velocity distributions in the gas-liquid-solid three-phase pipeline flows for time-averaged flow and instantaneous transient flow is significantly different.

4 Conclusions

The behavior of the sand particles in a horizontal air-water-sand slug flow was studied using digital imaging technique for design and analysis of oil-gas-sand three-phase slug flow in pipelines connected to sand management wells (low to moderately high sand loading). Digital image analysis technique proved to be a powerful tool at visualizing the movement and determining the local sand holdup profile under conditions analogous to oil-gas-sand three-phase slug flow in pipelines. An equation has been developed to estimate the local sand holdup.

Although in this work only spatial cross-sectional distributions were investigated, the method may be applied to a real-time imaging of sand phase systems by developing a better transducer array for data acquisition [43] and a better image reconstruction algorithm [44].

The results obtained from the continuous air-water-sand three-phase slug flow system in the horizontally 40 mm pipeline are summarized as follows:

- The axial distribution of the local sand holdup profiles shows the existence of strong non-uniformities at any location in the pipe cross-section under the various operating conditions such as sand particle loading, superficial gas and liquid velocities.
- The profile changed from w- to saddle-shaped as superficial gas and liquid velocities as well as the sand loading increased.
- Analysis of the results from sand holdup distribution profiles indicates that convective and dispersive mixing due to gas bubble wakes and liquid slug length are important parameters for the sand particle distribution.
- The local mean sand holdup profile changes with the appearance of large bubbles in the air-water-sand three-phase slug flow.
- The influence of the convective and dispersive mixing on the sand holdup appears to be large.

Many more experiments are to be conducted to determine if the sand particles in oil-gas-sand multiphase pipelines behave much differently than accounted for by correlations presently in literature. Work is in progress to simulate the dynamic behavior of sand holdup profiles in gas-liquid-solid three-phase slug flow and to couple the digital image analysis technique with appropriate instrumentation in order to demonstrate the effect of the gas-liquid slug flow hydrodynamic parameters on the sand transport.

Acknowledgements

The authors would like to thank Professor Reiner Weichert (Technical University of Clausthal, Germany) for many helpful discussions and his great interest in our work. The assistance of Messrs. E. Winter, M. Dietrich, S. Klose, Z. Pisarski, and P. Patil in the construction of the experimental facility and data reduction is gratefully appreciated. The first author gratefully acknowledges the financial support of the German Academic Exchange Service (DAAD) through a fellowship.

Received: June 12, 2005 [CET 0195]

Symbols used

A	[m]	area of each section drawn over the pipe for image analysis
D	[m]	pipe diameter
d	[m]	characteristic particle diameter
d_x	[m]	x-direction length of the image
d_x	[m]	axial direction length of the image
d_p	[m]	mean particle diameter
E_s	[–]	local instantaneous sand holdup
E_p	[–]	local mean sand holdup
h	[m]	height of pipe from bottom to the top
$\bar{h}$	[m]	average height of two sections of the mesh

J_L	[m/s]	superficial liquid velocity
J_g	[m/s]	superficial gas velocity
M	[–]	image magnification factor
N	[–]	number of spherical sand particles found in v_g
Δt	[s]	time for collecting each frame data
V_g	[m^3]	volume of each-section of the mesh
v_s	[m^3]	volume of a sphere
v_g	[m^3]	volume of a section in the mesh

Greek symbols

e_s	[kg/m^3]	sand loading
ρ_l	[kg/m^3]	liquid density
ρ_p	[kg/m^3]	sand particle density

References

[1] M. M. Salama, *Offshore Technology Conf. 8900*, Houston, TX, May **1998**.
[2] J. Tronvoll, M. B. Dusseault, F. Sanfilippo, F. J. Santarelli, *SPE Annual Tech. Conf. and Exhib.*, New Orleans, Sept./Oct. **2001**.
[3] M. B. Dusseault, S. El-Sayed, in *Proc. 2001 SPE/DOE Improved Oil Recovery Sym.*, Tulsa, OK **2001**.
[4] M. B. Dusseault, J. Tronvolli, F. Sanfilippo, F. J. Santarelli, *Int. Conf. on Formation Damage, SPE 58786*, LA **2000**.
[5] M. B. Geilikman, M. B. Dusseault, *J. Pet. Sci. Eng.* **1997**, *17*, 5. (Special Issue: Near Well bore Formation Damage and Remediation)
[6] R. K. Bratli, M. B. Dusseault, F. J. Santarelli, J. Tronvoll, in *Proc. Trinidad and Tobago Biennial SPE Conf.*, Port-of-Spain **2000**.
[7] O. O. Bello, S. O. Fasesan, in *Proc. of the 33rd Annual Conf. and Meeting of Nigerian Soc. Chem. Eng.*, Abeokuta, Nigeria, 19/20 Nov. **2003**.
[8] M. Wicks, in *Advances in Solid-Liquid Flow in Pipes and its Application* (Ed: I. Zandi), Pergamon Press, Oxford **1971**.
[9] S. Angelson, O. Kvernvold, M. Linglem, S. Oslen, in *Proc. 4th Int. Conf. on Multiphase Flow*, BHRA, Nice, **1989**.
[10] M. Linglem, S. Nuland, *Offshore Technol. Conf.*, Houston, TX, USA **1990**.
[11] C. A. Shook, R. G. Gillies, B. J. Kristoff, M. H. Small, in *Proc. 4th Petroleum Conf. of the South Saskatchewan Section*, The Petroleum Society of CIM, Canmet, Regina, Canada, October **1991**.
[12] P. Oudeman, *Conf. SPE Production and Facilities, SPE 25142*, Nov. **1993**.
[13] R. G. Gillies, M. J. Mckibben, C. Shook, *J. Can. Pet. Technol.* **1995**, *34 (9)*, 56.
[14] R. G. Gillies, M. J. Mckibben, C. Shook, *J. Can. Pet. Technol.* **1997**, *36*, 36.
[15] R. G. Gillies, K. B. Hill, M. J. Mckibben, C. Shook, *Powder Technol.* **1999**, *104*, 269.
[16] J. R. Tippetts, G. H. Priestman, in *Proc. 8rd Int. Conf. on Multiphase Flow*, B. H. R. Group, Cannes, France **1997**.
[17] M. J. J. King, C. P. Fairhurst, T. J. Hill, *J. Energy Resour. Technol.* **2001**, *123*, 200.
[18] P. Stevenson, R. B. Thorpe, in *Proc. 9th Int. Conf. on Multiphase Flow*, B. H. R. Group, Cannes, France, June **1999**.
[19] P. Stevenson, Particle Transport in Pipes by Two-phase Flows, *Ph.D. Thesis*, University of Cambridge **2000**.
[20] P. Stevenson, R. B. Thorpe, *Oil Gas J.* **2002**, *100 (30)*, 47.
[21] P. Stevenson, R. B. Thorpe, *Can. J. Chem. Eng.* **2003**, *81*, 271.
[22] P. Stevenson, J. E. Kennedy, R. B. Thorpe, in *Proc. 12th Int. Conf. on Multiphase Technol.*, B. H. R. Group, Bantif, Canada **2002**.
[23] P. Stevenson, R. B. Thorpe, J. E. Kennedy, C. McDermott, *Chem. Eng. Sci.* **2001**, *56*, 2149.
[24] P. Stevenson, R. B. Thorpe, J. E. Kennedy, C. McDermott, in *Proc. 10th Int. Conf. on Multiphase Flow*, B. H. R. Group, Cannes, France **2001**.
[25] T. Sakaguchi, H. Minagawa, A. Tomiyama, in *Proc. of the Exp. Heat Transfer, Fluid Mechanics and Thermodynamics* (Eds: M. Giot, F. Mayinger, G. P. Celata), Brussel, Belgium **1997**, pp. 1137–1144.
[26] T. Sakaguchi, H. Minagawa, K. Sahara, Y. Kato, N. Kuroda, T. Matsumoto, in *Proc. of the JSME/ASME Thermal Eng. Joint Int. Conf.*, Honolulu, Hawaii **1987**.
[27] T. Sakaguchi, H. Minagawa, T. Saibe, K. Sahara, in *Proc. of the Japan-US Seminar on Two-phase Flow Dynamics*, Ohtsu, Japan **1988**.
[28] T. Sakaguchi, H. Minagawa, A. Tomiyama, H. Shakutshi, *Int. Video J. Eng. Res.* **1992**, *2*, 37.
[29] T. Sakaguchi, H. Shakutsui, A. Tomiyama, H. Minagawa, H. Takahashi, in *Proc. of the 1st JSME/ASME Joint Int. Conf. on Nuclear Eng.*, Tokyo, Japan, November **1991**.
[30] H. Minagawa, T. Sakaguchi, in *Proc. of the 3rd Int. Conf. on Multiphase Flow, ICMF '98*, Lyon, France **1998**.
[31] L. Kundakovic, G. Vunjak-Novaakovie, *Chem. Eng. Sci.* 1995, *50 (20)*, 3285.
[32] B. Meza-diaz, Q. Doan, B. Tremblay, *Can. J. Petroleum Technol.* **2004**, *43 (12)*, 30.
[33] Y. Nino, M. H. Garcia, *J. Fluid Mechanics* **1996**, *326*, 285.
[34] D. Kaftori, G. Hetstroni, S. Banerjee, *Phys. Fluids* **1995**, *7 (5)*, 1095.
[35] D. Kaftori, G. Hetstroni, S. Banerjee, *Phys. Fluids* **1995**, *7 (5)*, 1107.
[36] Y. Taitel, A. E. Dukler, *AIChE J.* **1976**, *22 (1)*, 47.
[37] M. Gopal, W. P. Jepson, *Int. J. Multiphase Flow* **1997**, *23 (5)*, 945.
[38] M. Nadler, D. Mewes, *Int. J. Multiphase Flow* **1995**, *21 (2)*, 253.
[39] V. Matousek, Flow Mechanism of Sand-water Mixtures in Pipelines, *Ph.D. Thesis*, Technical University of Delft **1997**.
[40] M. Casssanello, F. Larachi, M. N. Marie, C. Guy, J. Chaouki, *Ind. Eng. Chem. Res.* **1995**, *34*, 2971.
[41] M. Casssanello, F. Larachi, C. Guy, J. Chaouki, *Chem. Eng. Sci.* **1996**, *51 (10)*, 2011.
[42] J. Bernard, J.-M. Fitremann, *3rd Int. Conf. on Multiphase Flow*, B. H. R. Group, The Hague, Netherlands, May **1987**.
[43] M. Kamiwano, M. Kaminoyama, K. Nishi, D. Shirota, *J. Chem. Eng. Jpn.* **1998**, *13 (3)*, 366.
[44] M. Kamiwano, M. Kaminoyama, K. Nishi, *Proc. 3rd. Int. Symp. Mixing in Ind. Processes*, Japan, 19/22 Sept. **1999**.

Journal of
Physical and Natural Sciences
Volume 1, Issue 2, 2007

Can We Be More Efficient in Oil and Gas Exploitation? A Review of the Shortcomings of Recovery Factor and the Need for an Open Worldwide Production Database.

Gioia Falcone, Assistant Professor, Texas A&M University, gioia.falcone@pe.tamu.edu
Bob Harrison, Director, Soluzioni Idrocarburi s.r.l., bh@si-srl.com
Catalin Teodoriu, Assistant Professor, Texas A&M University, catalin.teodoriu@pe.tamu.edu

Abstract

This paper critically reviews the concept of recovery factor (RF) of oil and gas fields. Although this simple parameter is used throughout the oil and gas industry, it is subject to misunderstanding and misuse. Besides changing continually through the producing life of a field, the estimate of RF is affected by geological uncertainty, inappropriate reserves reporting, technological shortcomings, commercial practices and political decisions. At present, the information necessary to fully evaluate RF is not unequivocally determined, audited or reported, which makes it impossible to produce consistent global field statistics. Based on the authors' experience, the paper outlines the shortcomings of RF and suggests how they may be overcome. To promote clarity and transparency in RF calculations, a template for an open worldwide production database is proposed.

Introduction

Accepted wisdom suggests that the higher an oil or gas fields' value of RF, the more efficient the hydrocarbons have been produced from the reservoir. Optimising the recovery from a hydrocarbon field should be the common goal of both Governments and Operators, although increasing production levels at the right economic and political moment may prove too tempting to some. Hence, the use of RF as a yardstick to measure the performance of a reservoir (or the management of that reservoir) has some serious shortcomings. In order to use RF appropriately, it is important to understand what it is, how it is calculated and the uncertainty inherent to the parameters from which it is derived.

The value of RF is defined as the ratio of the recoverable volume to the hydrocarbons originally in place (HOIP) over the course of a field's economic life. Yet this seemingly trivial calculation has inherent uncertainty and can vary due to many reasons.

Among the many factors that impact on the ultimate recovery from a field are: the geology of the reservoir; the properties of the reservoir fluids; the drive mechanism; the technology used to drill, complete and produce the field; the oil and gas prices. The RF of "tight" hydrocarbons reservoirs can be as low as 1%, but it can be as high as 80% for reservoirs of excellent porosity and permeability. In addition, for a given geology, enhanced oil recovery (EOR) methods can recover more oil from the same reservoir. It is common practice to differentiate between primary, secondary, and tertiary (or enhanced) oil recovery. With primary recovery, the natural potential of the reservoir drives the oil to the surface and this can be combined with well-bore artificial lift techniques, but only a small amount (~10%) of the HOIP can be recovered by this method. Injecting water or gas to displace oil is referred to as secondary recovery and this usually allows a recovery of 20-40%. The field characteristics that lead to high primary and secondary recovery are summarised in Table 1.

Tertiary recovery may lead to recovering ~60% or more of HOIP, using methods such as:

- Thermal recovery, by adding heat to the reservoir fluids to make them more mobile.

- Gas injection for miscible sweep of the oil, is achieved by injecting flue gases or CO_2, which dissolve in the oil, reducing its viscosity and increasing its mobility.
- Chemical injection, either using polymers to "thicken" the injected water to increase its viscosity and so improve water-flood efficiency, or using surfactants, to improve the mobility of the oil droplets by reducing the surface tension.

• Homogeneous at all scales • Good connectivity • Good (induced) fluid mobility • Gravity stable at reasonable rates • Appropriate natural drive • Non-fractured or homogeneous, densely fractured • Clean, sweet oil • Thick oil column, large areal extend • Good, cheap accessibility • Good monitoring (seismic, etc) ability • Consolidated sands • Low residual Hydrocarbon saturation

Table 1: Main features of high-recovery fields. (Schulte, 2005).

The RF values quoted above are suggested by the U.S. Department of Energy and reflect the USA experience. The numbers do change for different geographical areas, e.g. the average RF in the UK North Sea for a water-flood oil field is around 45% and may be up to 60% in some fields. However, care must be taken before applying average RF values to all fields as heavy oil, tight gas, HP/HT fractured and deepwater reservoirs present special challenges and, therefore, different levels of recovery should be expected.

The estimate of RF has an element of time dependency. When considering hydrocarbon reserves, it is important to distinguish between the reserves of fields that have already been abandoned and the reserves of fields that are either about to come on stream or in the early years of production. The evolution of uncertainty for reserves estimation for a generic field is shown in figure 1, where the uncertainty reduces as more information is gathered from the field, from the exploration and appraisal stage to abandonment.

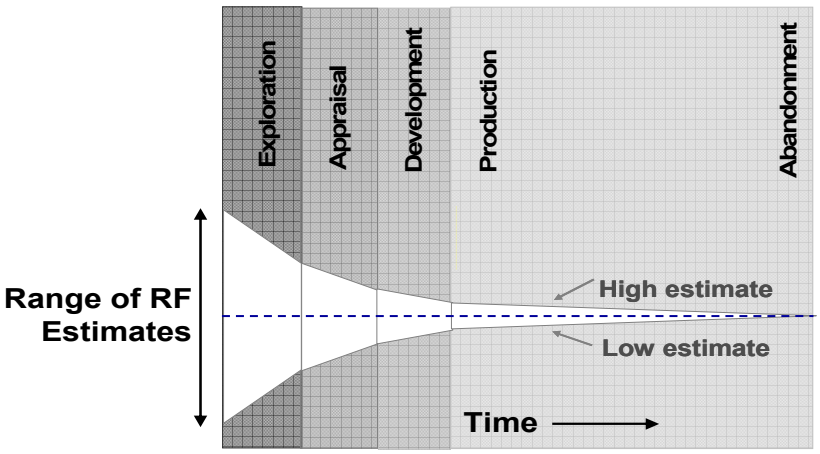

Figure 1: Uncertainty of reserves estimation decreases as field life progresses

Hence, reserves do change over an asset's life as does HOIP as more reservoir data is gathered during development drilling and production history is matched. Some analysts claim that RF does not change over time, but the authors disagree with this statement.

Not only do the reserves change over the life of a field, the method used to compute reserves also changes. Figure 2 illustrates that different reserves determination methods (use of results from analogue fields, volumetric calculations, decline curve analysis, material balance and numerical simulation) are used at different stages of a field's life.

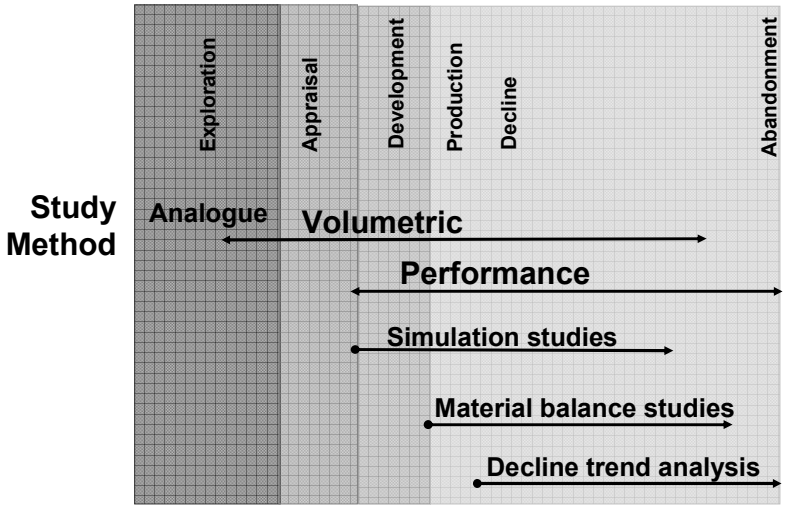

Figure 2: Reserves determination methods change through field life

As mentioned earlier, besides time dependency, there are many other factors affect the RF, which reflect geological risk, regulatory guidelines, technological shortcomings, commercial practices or political stances. Some of the more important factors are:

- Uncertainty in value of HOIP.
- Definition of reserves and reporting standards.
- Metering error(s) when measuring produced volumes.
- Application of new technology to enhance well productivity.
- Change in operatorship of the asset.
- Change in business model used by operator.
- Paucity of verified field and well data in the public domain.

The above factors, their effect on RF estimates and how their impact may be lessened are discussed in detail below.

Factors Affecting Estimation of RF

The following factors influence RF; some implicitly, some explicitly, but they can all have a major impact on its estimate.

Uncertainty in HOIP.

The recoverable volume will only be known when all the reserves from that field have all been produced, but the HOIP will probably never be known for certain. This is because the cumulative produced volume can be metered, but the HOIP must be estimated from seismic surveys, well

logs, geological models and hydrocarbon samples. Thus, even after all reserves have been produced, the actual RF will have inherent uncertainty as the HOIP is estimated, not measured. Hence, the HOIP of a field can go up or down, depending on revisions of the original numbers and/or field extensions. In the case of field extensions, the extra reservoir volume may be of a better or worse quality than the original discovery, therefore the overall RF may be lower or higher than that originally predicted.

Definition of Reserves.

There is currently no unique way of defining and assessing reserves, although the Society of Petroleum Engineers (SPE) and the World Petroleum Congress (WPC) have jointly published a guideline (SPE-WPC, 2007) that purports to do just that. Neither is there a global standard for financial reporting purposes. The reserves may be reported in different ways, more conservative or more likely, and the RF will reflect the choice of reserves reporting. Some of the reserves databases that are available in the public domain will be discussed later in the paper.

Reserves are usually estimated according to a probabilistic approach, where a differentiation is made between proven, probable and possible reserves. In some parts of the world, companies only have to report proved reserves (referred to as 1P or P90). In other countries, the probable reserves (2P or P50) are issued. Finally, some classification systems are extended to include possible reserves (3P or P10). As the value of an oil and gas company is a direct function of its forecast reserves base, the same company may show completely different results depending on whether 1P, 2P or 3P numbers are used.

Production profiles that are based on 2P reserves are more optimistic than the 1P, yet more conservative than the 3P. In asset sales, the 3P or upside reserves of a field development may be taken into consideration. Different available databases report different types of reserves. This will be covered later in the paper.

Figure 3 shows how reserve growth occurs when reserves are reported as proven, but does not statistically occur when the reserves are reported as probable (2P). The figure highlights the possible confusion that may arise in quantifying reserves when using 1P numbers only.

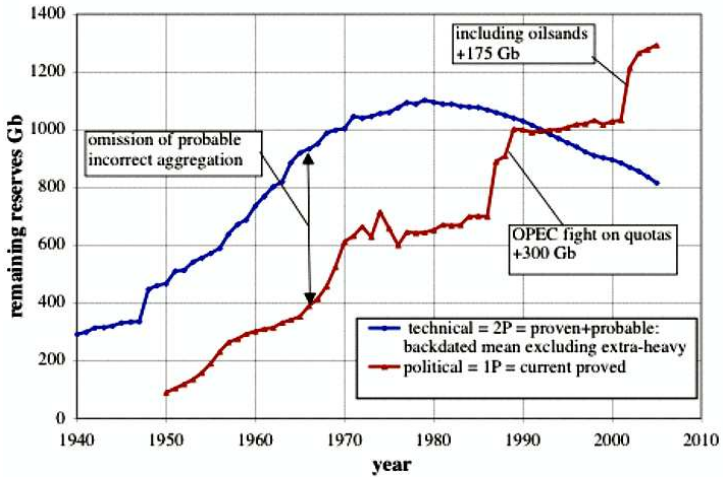

Figure 3: World remaining conventional oil & gas reserves from “political” & “technical” sources (Laherrère, 2006)

When aggregating the reserves of a company, two common practices exist. The first is based on the arithmetic summation of deterministic estimates, whilst the second performs a probabilistic (or statistical) aggregation of probabilistic distributions. The difference between these two methods is illustrated in Figure 4, which is taken from the guideline (SPE-WPC, 2007).

In order to correctly add together the ranges of reserves from a number of fields, the second method of probabilistic aggregation must be used. Reserves distributions tend to be skewed log-normal, as they are based on permeability variations. The only point where the deterministic and probabilistic results coincide is at the mean or average value of the aggregated distribution. Thus, when working out the overall reserves distribution curve of several fields, the P50 of the total curve does not correspond to the sum of the individual P50s. The log normal distribution ensures that the computed mean is always higher than the P50 value. The larger the skew of the resultant reserves distribution, the bigger the difference between the computed mean and the P50 value. Traditionally, companies have quoted reserves ranges as 1P-2P-3P (P90-P50-P10) values. However, the authors have seen many instances where the aggregated reserves of a number of fields have been incorrectly determined. It is the authors' opinion that reporting a field or aggregated fields' mean reserves over time are the best estimate for ultimate recovery. From the discussions above it follows that a unique definition of reserves is needed prior to defining the RF.

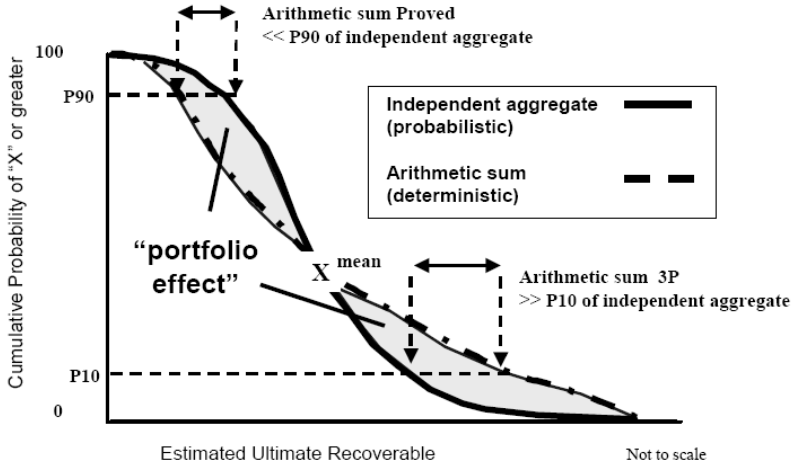

Figure 4: Deterministic versus Probabilistic Aggregation of Reserves (SPE-WPC, 2007).

Metering Error(s).

When using reservoir modelling techniques to forecast oil and gas production, from which the ultimate field recovery can be predicted, the volumes and flow rates of fluids produced from a reservoir are used to tune the models. However, the metering of the produced fluids is not error free; the measurements may be taken with different levels of accuracy, depending on whether they are required for fiscal, allocation or reservoir management purposes. In the latter case, an accuracy of ±10% for the measurement of the produced hydrocarbons is generally considered to be acceptable. The metering uncertainty is particularly important for small discoveries or marginal fields, where the effect of wrongly predicting the ultimate reserves and RF can severely impact the overall field economics. Since the results from production measurements are implemented in the reservoir modelling or production optimisation processes, it is clear that the accuracy of such measurements will affect the prediction of ultimate recovery from a reservoir. More accurate measurements imply that this uncertainty can be reduced. It is also clear that different levels of uncertainty may be acceptable, depending on overall field reserves, oil price, production lifetime, etc.

Application of New Technology.

It is often suggested that new technology can enhance the produced volumes and therefore accelerate and, in many cases, increase the recovery from a field. In the last decade, some fundamental technological advances have been made in remote detection (higher definition and

4D seismic, controlled source electro magnetic surveys (CSEM)), drilling and completions (e.g. geo-steering, multilateral producers, under-balanced drilling, smart wells), well logging, real time reservoir monitoring (including multiphase flow metering and fibre optics), sub-sea and down-hole technology (e.g. water shut-offs, water separation), multiphase transport (including multiphase pumps and wet gas compressors) and flow assurance.

An example of where new technology has enhanced recoverable reserves is represented by tight gas reservoirs. These formations, which are classified as having permeability less than 0.1 md, may contain at least 1,300 x10^9 m^3 of gas worldwide (BGR, 1999). Many tight gas reservoirs were discovered years ago, but their potential has still to be fully realised due to their low productivity when developed with "conventional" completions and reservoir management techniques. However, this situation is already changing, as new technology improvements and the recent gas price hikes have seen a rapid development of tight gas sands worldwide, and particularly in the US. Table 2 summarises the quantitative impact of new technologies on tight gas resources (Perry *et al*., 1998). The cumulative impact of new technology results in an average tight gas producer with an increased recovery of 25% and a cost reduction of 17%.

New Technology	Impact	Well Cost Impact
Geo-steering for zone selection	Keep well in higher quality pay zones	+ 5 %
Under Balanced Drilling (UBD)	Less fluid loss, minimise formation damage	+ 5 %
Drill multiple wells from a single location	Smaller footprint, quicker rig up/down	- 5 %
All waste disposed of on-site	Cuttings, drill fluids, produced water re-injected	- 5 %
Better fracture materials management	Bulk purchasing & handling, cheaper treatment	- 25 %
High angle drilling	Maximises reservoir interval penetrated	+ 5 %
Coiled Tubing drilling,	CT also be used as production tubing	- 10 %
Improved hydraulic fracture conductivity	More complete clean-up	+ 40 %
Monthly operating costs		- 20%

Table 2: Impact of new technology on tight gas recovery (after Perry et al, 1998)

With conventional technology, the RF for tight gas reservoirs is very low, up to 10%, which makes the majority of them uneconomic. However, new technology can increase tight gas RF to between 30 and 50% (Friedel, 2004). Combining several new technologies together has proved particularly successful in unlocking extra reserves from tight gas reservoirs such. One example of "combo-technology" is to geo-steer horizontal wellbores into better quality reservoir units, while avoiding depleted zones or aquifers, and subsequently completing them with multiple fracturing techniques (Bencic, 2005). The combined benefits are illustrated in Figure 5, which shows an increase in recovery of an additional 1000 million cubic metres of gas (at normal conditions) from a tight Permian sandstone.

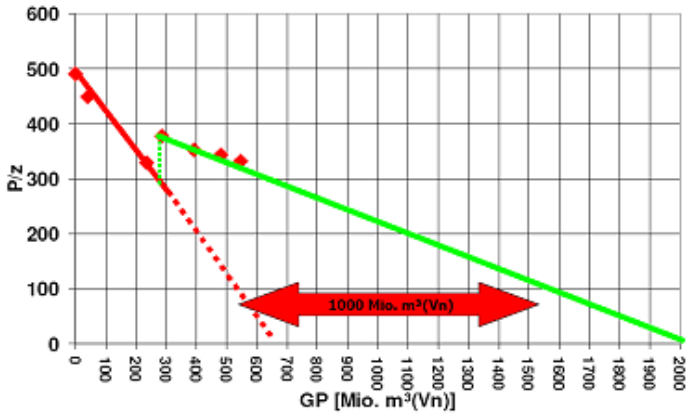

Figure 5. Unlocking gas well reserves by using combined drilling and fracturing techniques. (Bencic, 2005)
[GP=Gas Produced; P/z=Reservoir pressure/gas compressibility factor]

However, while it is true to say that advances in key technologies may allow more recovery from a field, it is also true that novel technology may sometimes only accelerate the production of oil and gas volumes that would be equally produced using older techniques.

There also seems to be a correlation between RF values and oil and gas prices, and the higher the price, the more likely it is that new techniques are implemented in the field. There tends to be a lag time between when the oil and gas prices rise and when more expensive field development methods are adopted. An example of how the RF and the oil and gas prices are related is given by Canada's tar sands. Canada was not a significant player in the oil reserves charts until the oil prices jumped to over 50 $/barrel. At that point, the investors felt more confident in trying new exploration and production techniques to increase the recovery factor of tar sands and, since then, the World Oil Statistics position Canada in second place after Saudi Arabia for reserves.

Such dependencies of the RF could be easily proved (or not) if the appropriate data were made available by government agencies, as will be discussed later.

Change of Asset Ownership.

In order to quickly and efficiently implement field development opportunities, it is important to guarantee that the asset is always in good hands. Asset sales imply that a new study is carried out to evaluate the asset value, resulting in new investment and additional production. This is illustrated by an example in Figure 6, which shows the production profile for the Forties field in the UK. The observed increase in production resulted from the transfer of the asset from the previous operator to a new one, from BP to Apache in this case. Prior to its sale in 2003, the Forties field was stated to have HOIP of 4.2 billion barrels, but this was increased, after re-processing of 3D seismic and an aggressive infill drilling programme, to 5 billion barrels. The subsequent RF fell from the 2003 figure of 62% to 53%. Although the Forties field is a success case for change of asset ownership, such mature asset transfers can be financially complex due to decommissioning costs and liabilities (PILOT, 2005).

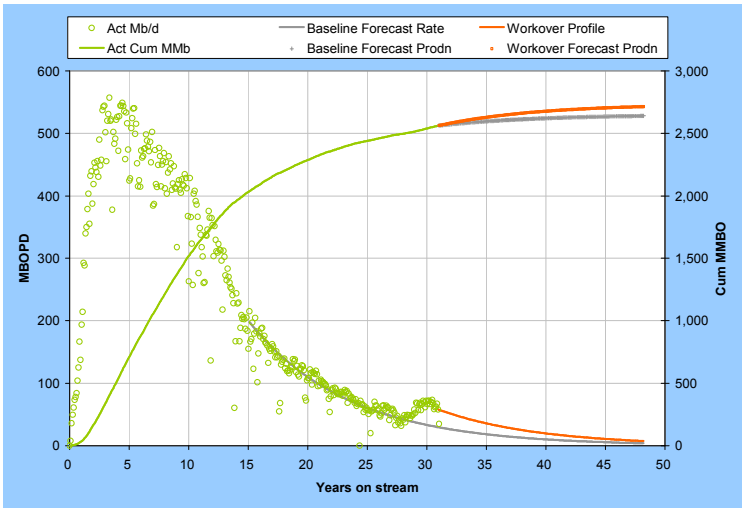

Figure 6: Forties field production, showing improvement (actual and forecast) over baseline by infill drilling programme by new operator (UK dti's PPRS online database, 2006).

Change of Business Model.

Another way to ensure the recovery from a field is maximised is to apply new business models and enhance cross-industry partnerships (PILOT, 2005). New start-up companies have appeared on the scene that invest in development projects and take technical control of them. They form

partnerships with field owners to help increase production and earn a share of the incremental revenue. A typical cash flow for such business models is shown schematically in Figure 7.

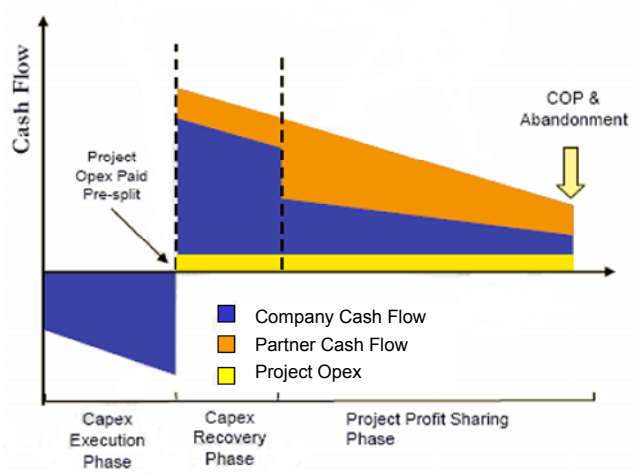

Figure 7: Cash flow of production sharing business model. (EDP 2005)

Paucity of Accessible Production Databases

In order to investigate the values of the RF of hydrocarbon fields worldwide, it is necessary to review historical production data and forecast reserves from available databases. While some countries and states have their own collection of production data by field (or even better, by well), no "official" database exists for all producing fields and/or wells worldwide. In fact, many countries treat their figures as confidential and do not disclose them.
Some of the resources that are available in the public domain include:

- BP Statistical Review of World Energy, summarise the production and consumption figures of hydrocarbon resources by country each year.
- Oil & Gas Journal (OGJ), provides production data down to an oil field level for each country in the world. This annual survey gives each oil field's rate in barrels per day, the oil's API gravity and the depth of the reservoir.
- Official online production databases, maintained and provided by some government and federal agencies. Some examples of these excellent, but limited resources are:
  - Well and field databases of some of the oil and gas producing states in the USA (California, Wyoming, etc.) are exemplary, giving almost everything analysts need to compute RF with some confidence.
  - Petroleum Production Reporting System (PPRS) of the UK's Department of Trade and Industry (dti), which gives online monthly data for each oil and gas field in the UKCS only three months in arrears. [*PPRS did provide detailed monthly production data on a well-by-well basis, but unfortunately this excellent service was discontinued in 1999 - a serious mistake in the authors' view*].
- Commercial Production & Reserves Databases, which attempt to provide a worldwide dataset, but they can only publish field data for the countries that disclose them. Two of the major providers of this data service are:
  - IHS, whose global database provides both reserves and HOIP figures, allowing RF to be estimated (although its accuracy will depend on the accuracy of the input data, which is provided by the host governments and operating companies). IHS has a tendency to be more exploration focused in its reporting.
  - Wood Mackenzie, whose global database only provides reserves and is less extensive than that of IHS, but covers some regions in greater depth. Wood Mackenzie has a tendency to be more production focused in its reporting.

Because of these inconsistencies in the way production and reserves data are released and published, it is not unusual to discover different databases with different production and reserves figures for the same field.
After discussing the various factors that impact on RF estimates, let us now see how their variability around the world makes it difficult to generate useful RF statistics without the availability of detailed and consistent field data from government agencies.

RF Statistics and their Limitations

A note of caution is warranted for those who analyse and use production and reserves data in the public domain. Because of the inconsistencies in the way production and reserves data are released and published, it is very difficult to generate valid and consistent RF statistics across the world. There is also missing information from published databases, which is not being released by all countries and/or field owners worldwide.
Nevertheless, several researchers have studied the published global data in an attempt to determine the range and average value of RF. Schulte (2005) reports a global average RF value of 34%; the results of his analysis are shown in Figure 8.

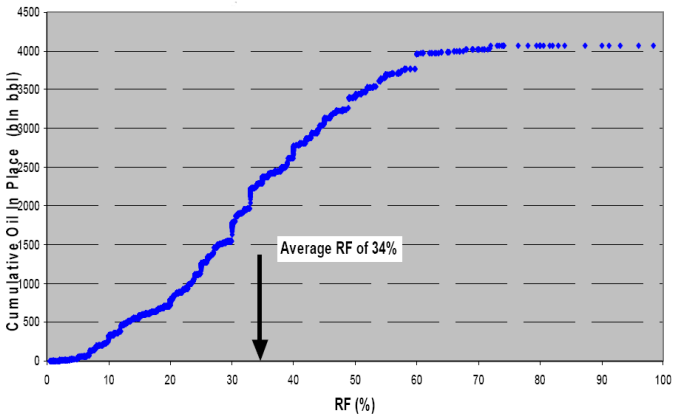

Figure 8: Global cumulative oil in place ordered for RF (data from IHS, no year specified). Schulte (2005).

Laherrère (2006) reports a slightly lower global average value of RF of 27%, as shown in Figure 9. It is unfortunate that this analysis does not provide the average field RF for 2001 and 2006 using the same fields, which would have been a better indicator of whether technology had improved RF over time.

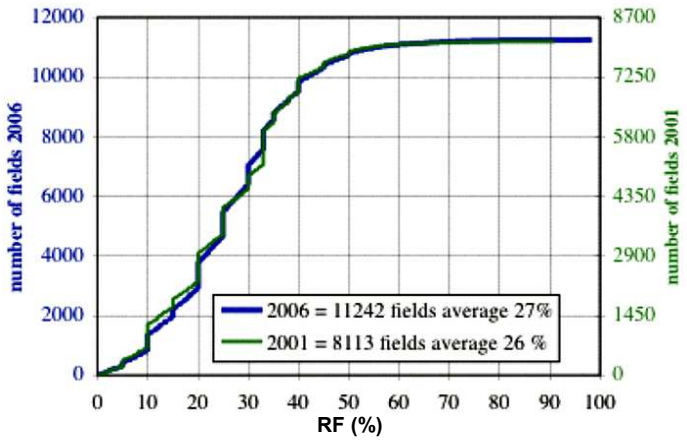

Figure 9: Cumulative number of oil fields worldwide (less US onshore) ordered by their RF (data reported in IHS database for 2001 and 2006) (Laherrère, 2006).

Figures 8 and 9 indicate an average oil RF of around 30%, but it must be noted that such plots do not make any differentiation by oil quality (heavy vs. light), reservoir depth, location, water depth (if offshore), geology, drive mechanism, etc. Also, the information displayed does not touch on the technology used (if any) to improve the recovery.

Another word of caution about statistics of the type shown in Figures 8 and 9: the stated RF could actually be higher if the oil originally in place has been overestimated and vice versa. In other words, it is impossible to separate the concept of recovery from that of resources originally in place, yet the latter are rarely published by government agencies.

Template for an Open Access Worldwide Production Database

As shown above, there is an inherent inaccuracy in estimating, measuring and reporting all the information necessary to determine the RF of a field. Also, depending on whether the RF is being estimated at the pre-development stage of a field or during its producing life, different data are needed to evaluate the RF. For pre-development, analogue fields help with the estimate of the new discovery's performance. In this case, the main criteria for screening analogue fields are the reservoir geology and fluid properties and the technology to be implemented. After field start-up, production data will become available and so allow the use of more sophisticated techniques such as decline curve analysis, material balance and/or numerical modelling to predict the field's recovery.

Accessibility to information on wells' performance, field behaviour, HOIP, geology, fluid properties and technology adopted is essential when estimating the RF of a field. This is true whether the field is a new discovery or on production. The data required to determine the RF through a cascade of input and output variables are summarised in Table 3.

	Item to be Reported	**Reported Variables for Item**	**Outputs Derived from Variables**
1a	Monthly well producer records	gas-oil-water volumes, days online, WHP, WHT, choke %	Producer Uptime, Well producing GOR-WOR-Water Cut, Well Decline Curve, Reserves per well, Field Reserves
1b	Monthly well injector records	gas, water volumes, days online, WHP, WHT	Injector Uptime, Injectivity model, Producer:Injector Ratio
1c	Well Technology	Artificially lifted? Stimulated? Water shut-offs? Horizontal or vertical? Completion details	Aids selection of appropriate analogue fields
3a	Monthly Field production records	gas-oil-water volumes	Field producing GOR-WOR-Water Cut, Field Decline Curve, Field Reserves
3b	Monthly Field injection records	gas, water volumes	Field Injectivity model (aquifer strength)
3c	Field Technology	Gas compression? Multiphase pumping? EOR?	Aids selection of appropriate analogue fields
4	Bottom hole Surveys	average reservoir pressure & temperature history (date and depth datum)	Material balance for HOIP
5	Top & Base reservoir structure maps	depth contours, scale, well locations, fluid contacts, major faults	Gross rock volume, Field area, Hydrocarbon fill factor
6	Field Geological description	sandstone or carbonate, matrix porosity or naturally fractured, massive or thin-bedded	Aids selection of appropriate analogue fields
7	Field Petrophysical parameters	porosity, water saturation, gross thickness, net-to-gross	Hydrocarbon pore volume (at reservoir conditions) [Combining Items 5 & 7]
8	Field PVT properties (Oil)	API gravity, solution GOR, viscosity, bubble point, FVF	STOIIP (at surface conditions) [Combining Items 5, 7 & 8]
9	Field PVT properties (Gas)	Gas gravity, condensate gravity, CGR, viscosity, dew point, H2S-CO2-N2, FVF	GIIP (at reservoir conditions) [Combining Items 5, 7 & 9]
10	**Recovery Factor**	**Field Reserves (from 1a or 3a), HOIP (from 8 or 9), with date reference**	

Table 3: Template for what production data should be provided by government agencies.
[WHP=Well Head Pressure; WHT=Well Head Temperature; GOR=Gas-Oil Ratio; WOR=Water-Oil Ratio; EOR=Enhanced Oil Recovery; PVT=Pressure-Volume-Temperature; FVF=Formation Volume Factor; CGR=Condensate-Gas Ratio; STOIIP=Stock Tank Oil Initially In Place]

Table 3 shows that field production data, injection data and reserves alone (which are the only data published in the majority of the available databases) are insufficient to estimate the RF from an engineering standpoint. Many more data are required, without which the published RF estimates must be treated with caution.

Conclusions

- This paper has highlighted the uncertainty in RF determination for hydrocarbon fields. This uncertainty is often underestimated and is due to the uncertainty in reserves determination and HOIP estimate.
- The concepts of RF and reserves are directly linked, so it is necessary to refer to the same reserves definition prior to being able to compare the values of RF worldwide in a consistent manner.
- HOIP should be published by government agencies, in order to avoid ambiguities when producing worldwide statistics.
- The publication of reliable HOIP and reserves will allow more confident estimates of RF to be made, which will help with the evaluation of new prospects by comparing them with analogue fields.
- Because of the strong interdependence between RF, reserves and HOIP estimates, it remains impossible to state, on a general basis, that new technology will improve the ultimate recovery from a field. This generalisation is particularly difficult considering that the geology of a reservoir, the properties of the fluids therein and its drive mechanism all impact on the estimate of RF.
- The authors believe that the stated dependencies of the RF could be easily proved (or not) if appropriate data were made available from government agencies. The data should include geology, fluid properties, well-by-well information, HOIP and a description of the type of drive mechanism and technology adopted for each field in the world. Although this may sound ambitious, it is based on the recognition that RF estimates issued without such supporting information may be totally meaningless.

References

Apache Corporation, (2005), Annual Report 2005.

Apache Corporation, (2005), presentation for Merrill Lynch, November 2005.

Bencic, A., (2005) “Hydraulic Fracturing of the Rotliegend Sandstone in N-Germany –Technology, Company History and Strategic Importance”, SPE Technology Transfer Workshop, SUCO 2005.

BGR, (1999) (Bundesanstalt für Geowissenschaften und Rohstoffe): „Reserven, Ressourcen und Verfügbarkeit von Energierohstoffen 1998“, Rohstoffwirtschaftliche Länderstudien, Band XVII: 400 S., Hannover, 1999.

dti, (2005) “Brown Book – UKCS Reserves”, published annually (2005)

EDP, (2005), presentation to PESGB Aberdeen, November 2005.

Friedel, T., (2004), “Numerical Simulation of Production from Tight Gas Reservoirs by Advanced Stimulation Technologies”, PhD thesis, TU Bergakademie Freiberg, 2004.

Laherrère, J., (1997), “Distribution and evolution of Recovery Factor”, Oil reserves conference, Paris, France, 11 November 1997.

Laherrère, J., (2006), “Oil and gas: what future?”, Groningen Annual Energy Convention, 21 November 2006.

Perry, K.F., Cleary, M.P., Curtiss, J.B., (1998), “New technology for tight gas sand”, World Energy Congress, Houston, USA, 13-18 September 1998.

PILOT, (2005), “Maximising Economic Recovery of the UK’s Oil and Gas Reserves”, report of PILOT 204, Brownfields Study, March 2005.

Schulte, W.M., (2005), “Challenges and Strategy for Increased Oil Recovery”, paper IPTC 10146, International Petroleum Technology Conference, Doha, Qatar, 21-23 November 2005.

SPE-WPC, (2007), “Petroleum Reserves and Resources Classification, Definitions, and Guidelines”, DRAFT for Industry Review, September 2006.